Author:
Cathery, William R

Title:
Umbilical cord pericytes provide a viable option for neonatal vascular tissue engineering applications

Umbilical cord pericytes provide a viable option for neonatal vascular tissue engineering applications

William Cathery (MEng)

A dissertation submitted to the University of Bristol in accordance with the requirements of the degree of Doctor of Philosophy in the Department of Translational Health Science, Bristol Medical School

February 2021

Word Count: 54,248

Abstract

Congenital heart disease is an abnormality in the structure of the heart affecting roughly 1% of new-borns. Although prognosis has improved recently, reconstructive surgery remains inadequate due to the inability of prosthetic grafts to replicate the functionality or the somatic growth of native tissue. In malformations such as Tetralogy of Fallot, this results in repeated surgical intervention, which has a substantial impact on quality of life. Tissue engineering may offer a solution to the limitations of current graft technology by generating a biological graft with improved functionality. Indeed, recent evidence has demonstrated the feasibility of using cardiac pericytes engineered vascular grafts for reconstruction of the pulmonary artery; however, isolation of this cell population is reliant upon tissue obtained during initial palliative surgery or an ad hoc invasive cardiac biopsy, which carries elevated risk. In search of a more accessible cell source, this study aimed to explore the prospect of isolating pericytes from the umbilical cord or placenta and using them for neonatal vascular engineering applications.

Different isolation methodologies were explored in parallel resulting in isolation and expansion of three different pericyte populations categorised by their isolation marker, namely NG2 umbilical cord pericytes (UCPs), CD146 UCPs and CD34 placenta pericytes. These populations were characterised to assess their purity and compare therapeutic properties. Of the three populations, NG2 UCPs demonstrated the most consistent antigenic phenotype and a high proliferation rate. After exposure to differentiation medium, they were successfully induced to a vascular smooth muscle cell-like phenotype, as evidenced by the expression of transgelin and smooth muscle myosin heavy chain. Analysis of cell monolayers and conditioned medium revealed production of extracellular matrix proteins and the secretion of major angiocrine factors, which conferred NG2 UCPs with ability to promote endothelial cell migration and tube formation. Decellularized swine-derived grafts were functionalized using UCPs and cultured under static and dynamic flow conditions. UCPs were observed to integrate into the outer layer of the graft and modify the extracellular environment, resulting in improved elasticity and rupture strain in comparison with acellular grafts.

These findings demonstrate that a homogeneous pericyte-like population can be efficiently isolated and expanded from human cords and integrated in acellular grafts currently used for repair of CHD. Functional assays and *in vitro* graft testing suggest that NG2 UCPs may represent a viable option for neonatal tissue engineering applications.

Dedications and Acknowledgements

Firstly, I would like to thank my supervisor Professor Paolo Madeddu for his support and encouragement throughout my PhD. Your door has always been open to discuss new ideas or reassure me when experiments haven't gone the way I hoped. I really appreciate the opportunity you have given me to develop as a researcher. Thanks must also go to my co-supervisors, Professor Massimo Caputo and Dr Elisa Avolio, for their insight and support during my studentship.

In addition, I would like to thank my colleagues Eva and Ashton. You have both been invaluable to me as mentors and friends, and I genuinely think I would have struggled to get to where I am now without your guidance and encouragement when I've doubted myself. Your dedication to science has inspired me and kept me motivated during the last 4 years.

Thank you to all the members of the Madeddu lab for making my experience here in Bristol so enjoyable. Michele, Marco, David and the rest, I will miss our Friday nights spent down the pub, which provided me with a welcome distraction to the frequently frustrating world of science.

Away from the lab, I would like to thank the many people that have supported me throughout this period. To my friends, cousins, and brother, who have provided me with much needed laughs and adventures, and my parents, who have always provided unconditional support and belief in me. I would also like to thank my partner Beth who has put up with me during this roller-coaster of a PhD. The patience you've shown helping me talk through ideas, despite not knowing a thing about science, and evenings spent checking my work for errors has been a tremendous help. This last year during the pandemic would have no doubt been a struggle without you to lift my spirits and provide the encouragement I needed. I truly cannot thank you enough. I would also like to thank my Nain, who always believed in me, but sadly passed away last year.

Finally, I would like to thank Heart Research UK for providing the funding that made this project possible.

Author’s Declaration

I declare that the work in this dissertation was carried out in accordance with the requirements of the University's Regulations and Code of Practice for Research Degree Programmes and that it has not been submitted for any other academic award. Except where indicated by specific reference in the text, the work is the candidate's own work. Work done in collaboration with, or with the assistance of, others, is indicated as such. Any views expressed in the dissertation are those of the author.

SIGNED: ..... DATE: .....

Plagiarism Declaration

I declare that some of the text used in this thesis has been taken from the published review:

Cathery, W., Faulkner, A., Maselli, D., & Madeddu, P. (2018). Concise Review: The Regenerative Journey of Pericytes Toward Clinical Translation. Stem Cells, 36(9), 1295–1310.

The text utilised was written by myself.

SIGNED BY FIRST AUTHOR: ..... DATE: .....

SIGNED BY SENIOR AUTHOR: [redacted] DATE: .....

I declare that some the text in this thesis has been taken from the original research article:

Cathery, W. Faulkner, A. Jover, E. Rodriguez-Arabaolaza, I. Thomas, A. Avolio, E. Caputo, M. & Madeddu, P. Umbilical cord pericytes provide a viable alternative to mesenchymal stem cells for neonatal vascular engineering. Frontiers in Cardiovascular Medicine. (2021) 7:410.

The text utilised was written by myself.

SIGNED BY FIRST AUTHOR: ..... DATE: .....

SIGNED BY SENIOR AUTHOR: [redacted] DATE: .....

Contents

List of Figures

List of Tables

List of Abbreviations

A

AEBSF	4-benzenesulfonyl fluoride hydrochloride
ALP	Alkaline phosphatase
ANGPT-1	Angiopoietin-1
ANGPT-2	Angiopoietin-2
ANOVA	Analysis of variance
APS	Ammonium persulfate

B

BDM	2, 3-Butanedione monoxime
bFGF	basic fibroblast growth factor
BGLAP	Bone gamma-carboxyglutamic acid-containing protein/osteocalcin
BMP2	Bone morphogenetic protein 2
BSA	Bovine serum albumin

C

CD	Cluster of differentiation
CD34 PLP	CD31-/CD34+ placenta pericyte
CD34 UCP	CD31-/CD34+ umbilical cord pericyte
CD146 UCP	CD31-/CD146+ umbilical cord pericyte
cDNA	Complementary DNA
CHD	Congenital heart disease
CNV	Copy number variant

CNS	Central nervous system
CM	Conditioned medium
COOH	Carboxyl group
D	
ddH_2O	Distilled water
DMEM	Dulbecco's modified eagle medium
DMSO	Dimethyl sulphoxide
DPBS	Dulbecco's phosphate-buffered saline
E	
EBM-2	Endothelial cell basal medium-2
EC	Endothelial cell
ECM	Extracellular matrix
EDTA	Ethylenediaminetetraacetic
EGF	Epidermal growth factor
EGM-2	Endothelial cell growth medium-2
ELISA	Enzyme-linked immunosorbent assay
EVG	Verhoeff's Van Geison
F	
FACS	Fluorescence activated cell sorting
FBS	Foetal bovine serum
FDA	Food and drug administration
FMO	Fluorescence minus one control
FSC-A	Forward scatter area

FSC-H	Forward scatter height
G	
GFP	Green fluorescent protein
GAPDH	Glyceraldehyde 3-phosphate dehydrogenase
GATA4	GATA-binding protein 4
H	
HCL	Hydrochloric acid
H&E	Haematoxylin and Eosin
HEK293T	Human embryonic kidney 293T cell
HGF	Hepatocyte growth factor
HP	High phosphate
HPASMC	Human pulmonary artery smooth muscle cell
HRP	Horseradish peroxidase
HUCPV	Human umbilical cord perivascular cell
HUVEC	Human umbilical vein endothelial cell
I	
ICC	Immunocytochemistry
IHC	Immunohistochemistry
iPSC	Induced pluripotent stem cell
L	
LDH	Lactate dehydrogenase
M	
MACS	Magnetic activated cell sorting

MCP-1	Monocyte chemoattractant protein-1
MCS	Multiple cloning site
MHC	Major histocompatibility complex
MKI67	Marker of proliferation Ki-67
MMP	Matrix-metalloproteinase
MRI	Magnetic resonance imaging
MSC	Mesenchymal stem cell
N	
NANOG	Homeobox protein NANOG
NG2	Neural/glial antigen 2
NG2 UCP	CD31-/NG2+ umbilical cord pericyte
NHDF	Normal human dermal fibroblast
NMMyoIIB	Non-muscle myosin IIB
O	
OCT	Optimal cutting temperature compound
OCT4	Octamer binding transcription factor 4
P	
PBS	Phosphate-buffered saline
PCL	Polycaprolactone
PDGFRβ	Platelet-derived growth factor receptor-β
PFA	Paraformaldehyde
PGA	Polyglycolic acid
PLA	Poly-lactic acid

PLLA	Poly-l-lactic acid
PLP	Placenta pericyte
PVDF	Polyvinylidene difluoride

Q

qPCR	Quantitative polymerase chain reaction

R

RGD	Arginine-glycine-aspartate
RT	Room temperature
RT-qPCR	Reverse transcription quantitative polymerase chain reaction
RUNX2	Runt-related transcription factor 2
RVOT	Right ventricular outflow tract

S

SDF-1	Stromal derived factor 1
SDS-PAGE	Sodium dodecyl sulphate-polyacrylamide gel electrophoresis
SEM	Standard error of the mean
SM-MHC	Smooth muscle myosin heavy chain
SOX2	Sex determining region Y-box 2
SOX9	Transcription factor SOX-9
SP7	Transcription factor SP7/Osterix
SSC-a	Side scatter area

T

TA	Tunica adventitia

TBST	Tris-buffered saline with 0.05% Tween-20
TEMED	Tetramethylethylenediamine
TGF-β	Transforming growth factor-beta
TI	Tunica intima
TIMP	Tissue inhibitors of MMPs
TM	Tunica media
ToF	Tetralogy of Fallot
U	
UCP	Umbilical cord pericyte
V	
VECAD	Vascular endothelial cadherin
VEGF(-A)	Vascular endothelial growth factor (-A)
VSD	Ventricular septal defect
VSMC	Vascular smooth muscle cell
W	
WJ	Wharton's Jelly
WJ-MSC	Wharton's Jelly Mesenchymal stem cells
α	
αSMA	alpha-smooth muscle actin

1. Introduction

1.1. Congenital Heart Disease

Congenital heart disease (CHD) is the general term used to describe the group of birth defects affecting the functionality of the heart. The first comprehensive studies of this pathology began in the 1930s after the establishment of Dr Helen Taussig's paediatric cardiology clinic at Johns Hopkins Hospital in Baltimore (Kiess, 2016). Since then, huge progress has been made in the understanding, diagnosis, treatment, and management of the disease, which has resulted in greatly improved prognoses for patients today. However, despite this, CHD remains one of the leading causes of perinatal mortality and substantially increases a patient's risk of cardiovascular disease later in life (Dolk et al., 2011). This has highlighted the need for further improvement, particularly in complex malformations such as tetralogy of Fallot (ToF).

The following section describes the current understanding and impact of CHD. Specifically, it will focus on ToF, the most common form of complex defect (Bjornard et al., 2013), and provide an overview of the current treatment options and shortcomings that indicate further development is required.

1.1.1. Prevalence and Perinatal Mortality

CHD is the most common type of birth defect and accounts for one-third of all major congenital anomalies. Each year on average it is thought that around 1% of new-borns present with CHD; however, it has also been reported in 10% of still births and is presumed to be a significant cause of early foetal death (Bjornard et al., 2013; Dolk et al., 2011; Fahed et al., 2013; Triedman et al., 2016). The actual prevalence is thought to exceed these estimates due to the number of mild lesions that go undiagnosed.

Lui et al recently demonstrated through a meta-analysis of 260 studies that the incidence of CHD has been progressively increasing by an average of 10% every 5 years for the last 5 decades (Liu et al., 2019). The authors suggest this is due to improved postnatal detection of less severe anomalies. Indeed, mild lesions accounted for 93.4% of diagnosed CHD, whilst complex defects remained relatively stable (**Figure 1.1**). Interestingly, the distribution of anomalies varied by geographic location. Of note, Asia demonstrated higher prevalence which suggests a greater genetic or environmental susceptibility. Although further detailed studies are

yet to explore this trend, some initial analysis has identified genetic risk loci in Chinese populations which could be responsible for this higher prevalence (Lin et al., 2015). Despite Africa reporting far fewer CHD cases, it was thought this was due to unmet diagnosis rather than a genetic of environmental factors. Overall, this study signifies that the global burden of CHD only stands to increase, with population based studies in US reporting similar findings (Bjornard et al., 2013).

Despite the described heightened trend in prevalence, CHD-related deaths have decreased in recent years. In 1990, there were an estimated 398,580 global deaths related to CHD, whereas in 2017 this had dropped to 261,247, representing a 34.5% decrease (Zimmerman et al., 2020). Likewise, the mortality of infants under 1 year has dropped (**Figure 1.2**). Various studies have reported more than 90% of children born with CHD in developed regions of the world will now survive to adulthood, which is a vast improvement from the 1930s where survival rate could be as low as 20% (Neidenbach et al., 2018; Zimmerman et al., 2020). In fact, an estimated 96% of children who survive their first year will live until adulthood (Van Der Bom et al., 2011). Regretfully, this increasing survival rate does not extend to the global picture. Mortality has only dropped 6% in patients from a low socio-demographic index compared with more than 50% in higher index groups (Zimmerman et al., 2020). Another interesting result from this study is that, despite decreasing mortality rates, the proportion of total infant deaths due to CHD is rising (**Figure 1.2**). Although advances have reduced infant mortality associated with CHD, it appears progress has lagged behind the general trend in infant survival rates. This demonstrates that CHD must be a primary focus for future research into improved paediatric cardiovascular medicine.

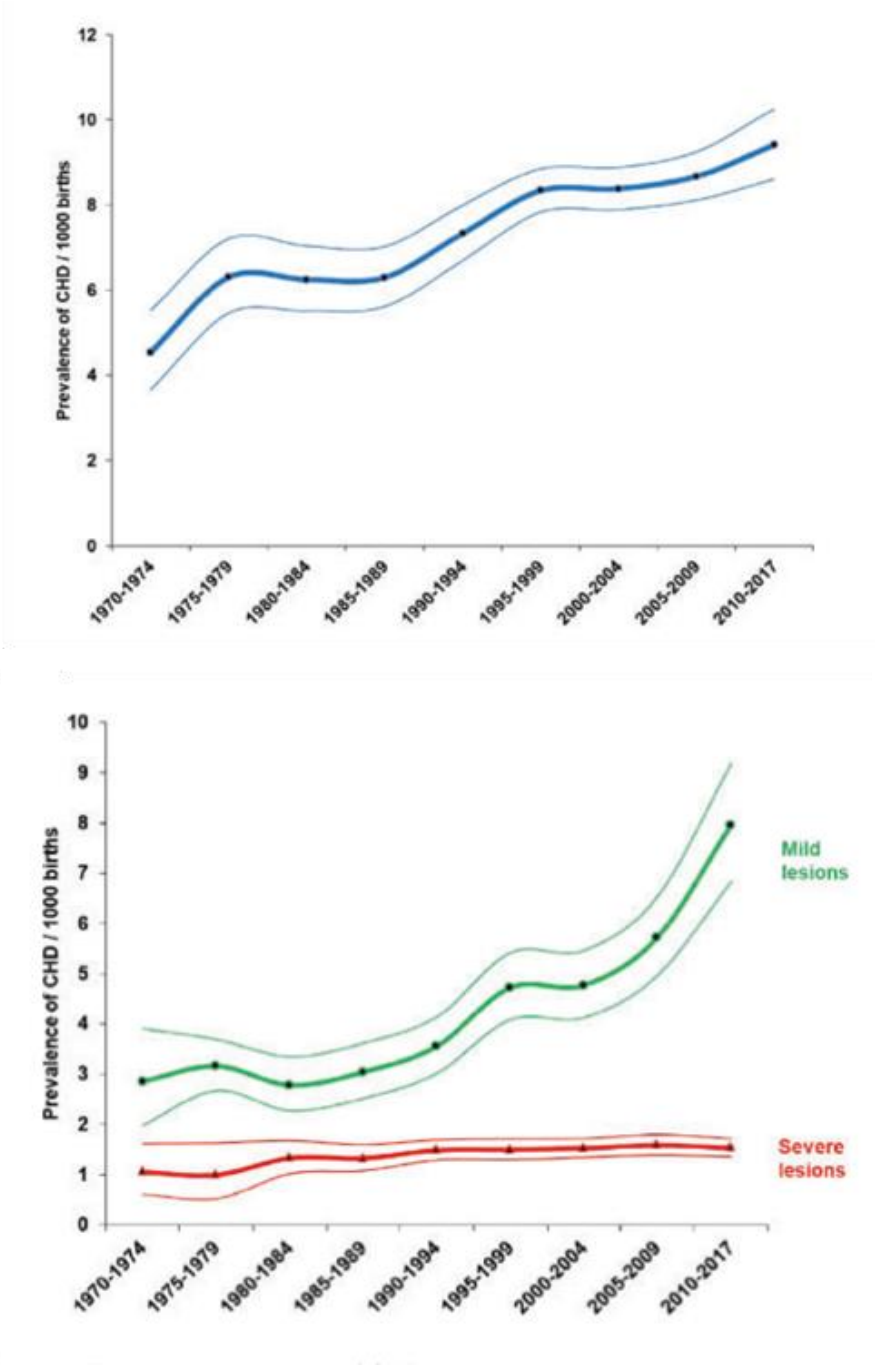

Figure 1.1: Changes in the birth prevalence of congenital heart disease 1970 – 2017. Thick lines represent the estimated prevalence whilst thin lines represent the 95% confidence interval. Figure source: Lui et al., 2019.

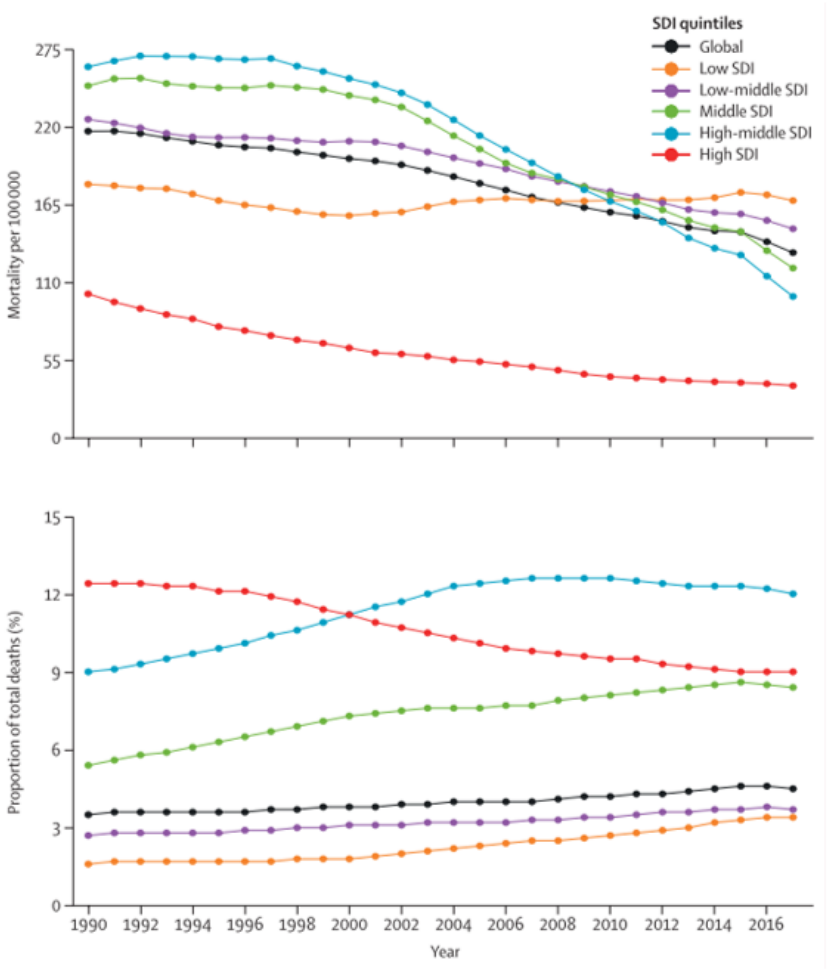

Figure 1.2: Mortality of congenital heart disease in children under 1 year of age, 1990 – 2017. SDI = socio-demographic index. Figure source: Zimmerman et al., 2020.

1.1.2. Aetiology

Our current understanding of the aetiology of CHD has been brilliantly reviewed by Blue et al. and Fahed et al. (Blue et al., 2012; Fahed et al., 2013). Here, I will briefly summarise the key insights.

Although prognosis and treatment of patients with CHD has improved, the causation of CHD is still relatively unknown. As more patients survive to adulthood, our understanding of inherited risks will become increasingly important.

Development of CHD is attributed to both genetic and non-genetic factors. Approximately 20% of CHD cases can be attributed to known genetic disorders or teratogens such as dioxins, polychlorinated biphenyls, and pesticides. The other 80% remains undetermined. The fact that identical gene mutations can induce a spectrum of heart abnormalities provides further complexity to understanding the development of CHD. Consequently, most researchers favour a multifactorial model involving a combination of both environmental and genetic factors.

Of the known causes, chromosomal aneuploidy syndromes have the greatest contribution to CHD, accounting for roughly 8 – 10% of total CHD cases (Roos-Hesselink et al., 2005). In particular, patients with Down syndrome or velocardiofacial syndrome make up a large proportion of these cases. Indeed, up to 50% of Down syndrome patients and 80% of velocardiofacial syndrome present with a form of defect, usually affecting the outflow tract such as ToF. In other less common disorders such as Edwards syndrome, almost all patients are born with a defect. Other chromosomal anomalies such as copy number variations (CNV) have also recently been linked with CHD. These act in a similar manner, causing mutations through their effect on dose-dependent genes. For example, chromosome 22q11 CNVs result in an altered dose of *TBX1*, a transcription factor involved in the development of the right ventricle and outflow tract. Accordingly, 15% of patients presenting with ToF, a complex malformation involving the right ventricular outflow tract, also display chromosome 22q11 CNVs (Fahed et al., 2013). Similarly, CNVs in chromosome 20p12.2 and 9q34.3 alter *JAGI* and *NOTCH1*, which effects the Notch signalling pathway.

Mendelian disorders are thought to account for up to 5% of CHD cases. These disorders are caused by a single gene mutation. For example, patients with Holt-Oram syndrome, which is caused by a mutation in the *TBX5* gene, have an 80% chance of CHD. Additionally, up to 30

non-syndrome gene mutations have now been associated with CHD, including key regulators of cardiac differentiation GATA-binding protein 4 (GATA4) and NK2 Homeobox 5 (Dixit et al., 2018; Kloesel et al., 2016). These gene mutations and corresponding CHD abnormalities have been described comprehensively; however, this level of detail is beyond the context of this thesis (Fahed et al., 2013).

Non-genetic factors are thought to participate in development of CHD; however, the specific contribution of various environmental factors is difficult to define. A major well studied risk factor is pregestational diabetes. This disease has been found to elevate CHD risk 5-fold; however, the mechanism by which this occurs is yet unknown (Wren et al., 2003). Similarly, maternal rubella and phenylketonuria have been associated with a significantly increased risk of CHD, although again further research is needed to determine why this is the case. Other non-genetic factors associated with CHD include obesity, hypercholesterolemia, and maternal exposures such as alcohol and certain medications (Fahed et al., 2013).

Overall, our understanding of the aetiology of CHD is quite limited. Although some genetic and non-genetic factors have been discovered, the mechanism of CHD induction is generally unknown, and the causation of most cases is still ambiguous. Perhaps in the future, developments in techniques such as whole exome and genome sequencing may help to unlock the mechanisms of CHD development and help early diagnosis of the disease.

1.1.3. Diagnosis

As introduced in the previous section, the rise in prevalence of CHD is believed to be driven by the improvement in diagnostic imaging. Over recent years, the accuracy of foetal echocardiography has steadily improved, allowing earlier prenatal diagnosis of cardiac malformations. Just between 2006 and 2012, the rate of foetal diagnosis in patients who require intervention has increased from 26% to 42% (Holst et al., 2017). Early detection of CHD facilitates improved perioperative planning and postnatal care, which is associated with decreased incidence of perinatal adverse events. This improvement in diagnostics has opened the possibility of foetal intervention in the most critical patients.

Improvements in cardiac imaging have also been pivotal for postnatal diagnosis and optimal operative planning and postoperative monitoring. In particular, cardiac magnetic resonance imaging (MRI) is being increasingly used providing excellent resolution cross-sectional imaging without radiation exposure (Holst et al., 2017). More recently, advances in cardiac MRI and computed tomography have led to the development of 3D reconstructions of patient hearts to improve understanding of the defect and assist surgery planning (Batteux et al., 2019).

In parallel with medical imaging, electrocardiography, pulse oximetry and a physical examination are often performed to validate the diagnosis. These techniques can identify the functional implications of a defect by measuring electrical activity of the heart and oxygen levels of the blood.

1.1.4. Intervention

Most defects will not need intervention; however, surgery is required for more severe forms. In the US, approximately 25% of children born with CHD annually require intervention in the first year of life (Triedman et al., 2016). For simple lesions, such as an atrial septal defect, a catheter may be used to deliver a closure device to the site of deformation. Normal tissue will usually grow in on the device within 6 months, providing a permanent solution (Sun et al., 2015). In more complicated malformations it may be necessary to perform open heart corrective surgery. The exact process varies due to the numerous forms of defects and patient heterogeneity; however, the specific aim is to reconstruct the cardiac tissue, valves, and blood vessels so that normal cardiovascular functionality is returned. Surgery may be a one-step or multi-step procedure depending on the complexity of the defect. Furthermore, the initial intervention can either be palliative or reparative. Palliative surgery is used to relieve severe symptoms in patients that are too weak for reparative intervention. For example, in patients with pulmonary stenosis, a shunt might be inserted prior to the repair so that adequate blood is restored, and the infant can recover before further reparative surgery is performed. A more comprehensive view of the general techniques performed for correction of CHD can been found in previously published reviews (Holst et al., 2017; Kenny, 2018).

A major complication in repair of CHD is the rate of reoperation. Reoperation is needed when initial intervention is palliative or when materials used for cardiac reconstruction fail, which is often due to degeneration, calcification or lack of growth potential (Kalfa et al., 2013). To demonstrate the extent of the problem, in a Norwegian study of 2918 patients with complex CHD, 33.8% of the patients required at least one reoperation before the age of 16 (Erikssen et al., 2015). Furthermore, many patients undergo 6 or more operations within their lifetime due to inadequate correction (Jacobs et al., 2014). Freedom from reoperation may be increasing as clinical and surgical practice improves, allowing initial correction rather than palliative intervention; however, the number of reoperations is still worryingly high. Additionally, as the life expectancy of CHD patients increase, the number of reoperations will likely grow. With increased number of reoperations the risk of cardiac injury and mortality rate increase (Holst et al., 2011). It is therefore essential that future developments in therapeutic strategies provide durable solutions that reduce the need for reoperation.

1.1.5. Adults with CHD

Due to advances in congenital cardiology and clinical care, even children born with the most complex malformations now often survive until adulthood. Consequently, the number of people living with CHD has greatly risen. In fact, between 1990 and 2017 this increased by 18.7% from ~10 million to ~12 million (Zimmerman et al., 2020). As a result, adults now represent the highest proportion of CHD-associated deaths (**Figure 1.3**) (Knowles et al., 2012). Whilst improved paediatric care has succeeded in prolonging survival to adulthood, the long-term efficacy of such treatment is now being evaluated. It should be recognised that only rarely does CHD correction result in permanent restoration of cardiac structure and function, free from further treatment (Neidenbach et al., 2018).

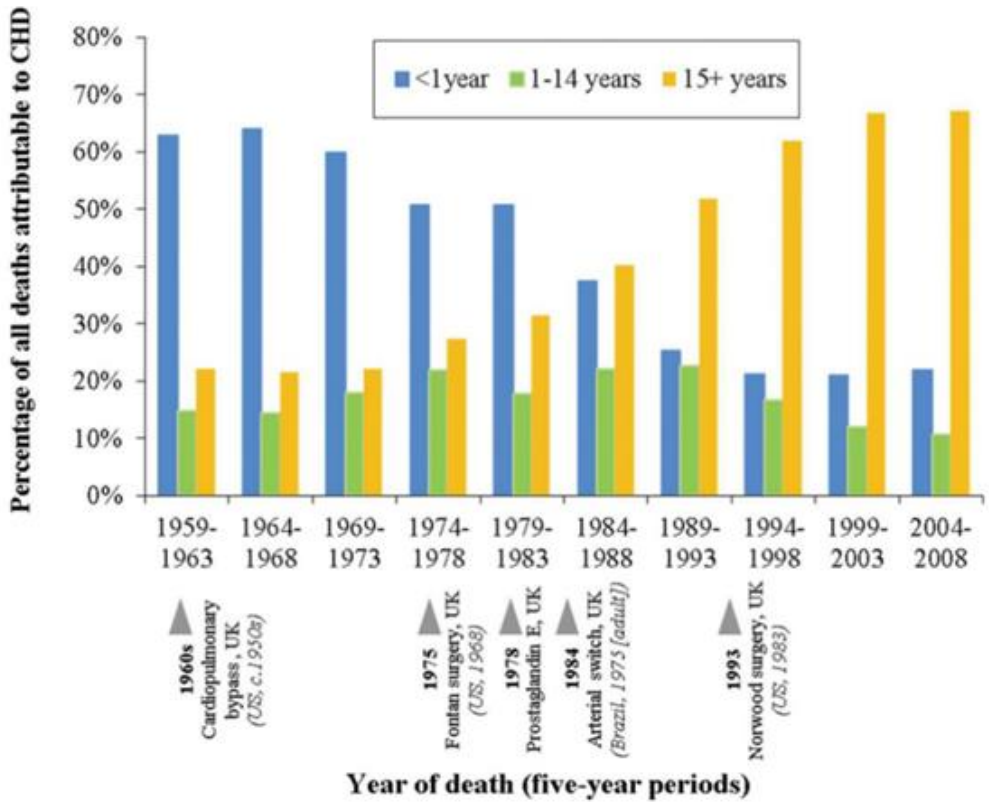

Figure 1.3: Trends in the percentage of all congenital heart defect-related deaths occurring in England and Wales between 1959 and 2009, assessed by age groups. Figure source: Knowles et al., 2012.

Today, mortality in adults with CHD is significantly higher than the general population (Triedman et al., 2016). Indeed, a Dutch study from 2007 demonstrated considerably elevated mortality rate among adults with CHD in all 10-year age groups from 20 years onwards (Verheugt et al., 2010). This is largely due to the presence of comorbidities that arise because of the underlying defect, residual structural issues, and sequelae from cardiac surgery. Indeed, Verheught showed that the vast majority of deaths in adults with CHD were associated with cardiovascular complications (Verheugt et al., 2010). Specifically, risk of heart failure was increased in all forms of CHD, even minor lesions such as ventricular septal defects (VSDs), accounting for 25% of deaths in adults with CHD (Neidenbach et al., 2018). Additionally, cardiac arrhythmia caused by myocardial fibrosis or postoperative scarring was frequently associated with death in long-term care.

Although most patients with CHD now survive to adulthood, significant progress is still needed to address long-term complications. Specifically, this can be addressed in two ways. Firstly, primary correction strategies should look towards the development of definitive solutions, which eliminate the need for reoperations. Currently, surgical practice has achieved success in improving survival to adulthood; however, the long-term patency of grafts used to correct complex defects is limited, with many patients requiring multiple interventions which increase the risk of sequelae and residua. And secondly, there should be greater emphasis on providing specialised CHD care management for adults so that cardiovascular complications are sufficiently monitored.

1.2. Tetralogy of Fallot (ToF)

Tetralogy of Fallot (ToF) is the second most prevalent form of CHD, behind septal defects, with an estimated incidence of 3- 6 infants per 10,000 live births and accounting for one-third of all CHD in patients under 15 years of age (Bjornard et al., 2013; Gerrah et al., 2015; Verheugt et al., 2010). Whilst atrial and septal defects represent simpler malformations that can be repaired with minimal complications, ToF is far more complex and requires significant surgical intervention. Moreover, correction of ToF is often a multistep process with reoperation extremely common due to the limitations of current graft technology (Avolio, Caputo, et al., 2015; Downing et al., 2015). As previously mentioned, reoperation elevates the risk of sequelae and residua, and significantly impacts an infant's lifestyle. Consequently, ToF has been highlighted as a form of defect which could benefit greatly from the development of improved graft technology. In the following sections, we describe the structure and implications of the defect, and provide an evaluation of the current treatment methods and their limitations.

1.2.1. Pathophysiology and Causation

To understand the defects involved in ToF and their impact on circulation, it is useful to provide a basic summary of the functionality of the normal heart (**Figure 1.4**).

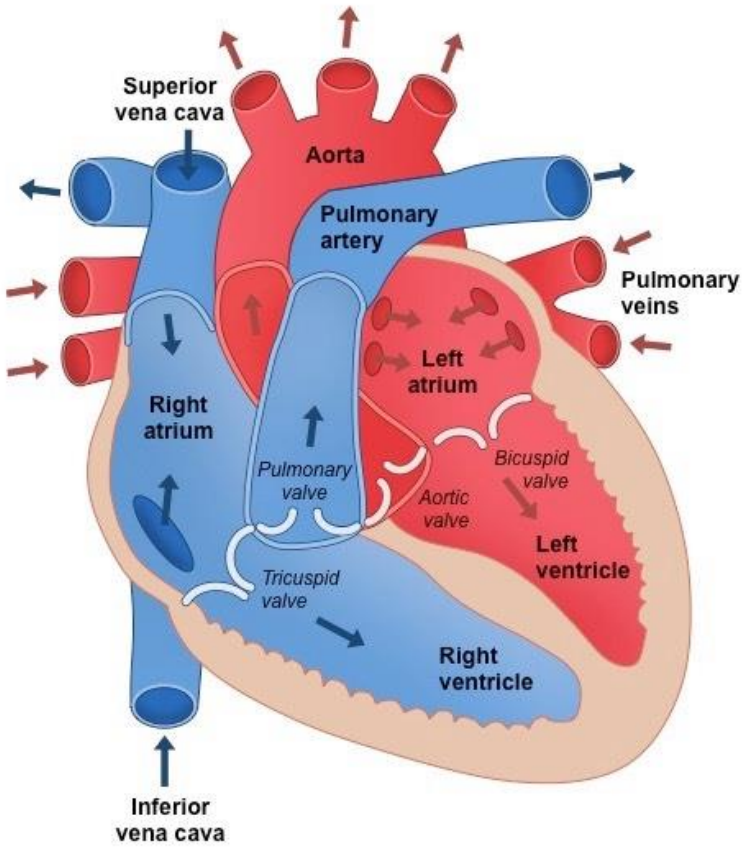

Figure 1.4: Normal heart structure and blood flow. Figure source: https://ib.bioninja.com.au/standard-level/topic-6-human-physiology/62-the-blood-system/heart-structure.html

In a normal heart, oxygen-poor blood enters the right atrium through the inferior and superior vena cava. The right atrium contracts to direct blood flow into the right ventricle through the tricuspid valve. Once the ventricle is full, the valve shuts to stop backflow of blood. As the right ventricle contracts, the ventricle pressure exceeds that of the pulmonary artery and the pulmonary valve opens to allow blood to travel to the lungs. After becoming oxygenated in the lungs, the blood enters the left atrium, which contracts to force blood into the left ventricle. Once the left ventricle is full, the bicuspid valve shuts and ventricle contracts. The pressure inside the left ventricle opens the aortic valve, pumping oxygenated blood to the systemic system (Mesotten et al., 1998).

In patients with ToF, normal circulation is compromised. During development, the infundibular portion of the ventricular septum is displaced towards the right ventricular outflow tract (RVOT), resulting in the presence of four malformations (Lev et al., 1964) (**Figure 1.5**). These consist of the following:

- Pulmonary stenosis: A narrowing of the pulmonary valve and outflow tract which results in a reduction of blood to the lungs. In some more severe cases, the valve may not form at all, termed pulmonary atresia, meaning blood cannot flow to the lungs in the usual way. In this event, surgery is urgently required to promote normal blood flow.
- VSD: a hole exists in the septum between the left and right ventricles. The oxygen-rich blood from the left ventricle mixes with oxygen deficient blood from the right ventricle, reducing the supply of oxygenated blood to the systemic system.
- Overriding Aorta: the aorta is located between the right and left ventricle, directly above the VSD. This results in oxygen deficient blood from the right ventricle mixing with oxygen rich blood from the left ventricle before exiting the heart through the aorta to the systemic system.
- Right Ventricular Hypertrophy: the muscle in the right ventricle is thicker than usual due to the extra effort of the heart to force blood through the narrowed pulmonary outflow tract. If left untreated, over time the muscle may stiffen and fail.

The combination of these four malformations typically means that the blood pumped to the systemic system contains lower than the normal concentration of oxygen. For this reason, ToF is classically defined as a cyanotic defect, which can be recognised by the blue colouring of the skin in patients (McCORD et al., 1957).

A variety of genetic links have been proposed including syndromes with a deletion of chromosome 22q11 or CNVs of genes such as TBX1, NOTCH1, JAG1 and GATA4 (Dixit et al., 2018; Dolk et al., 2011; Fahed et al., 2013; Kloesel et al., 2016). Despite this, as with many congenital heart defects, the cause of most ToF cases remains ambiguous.

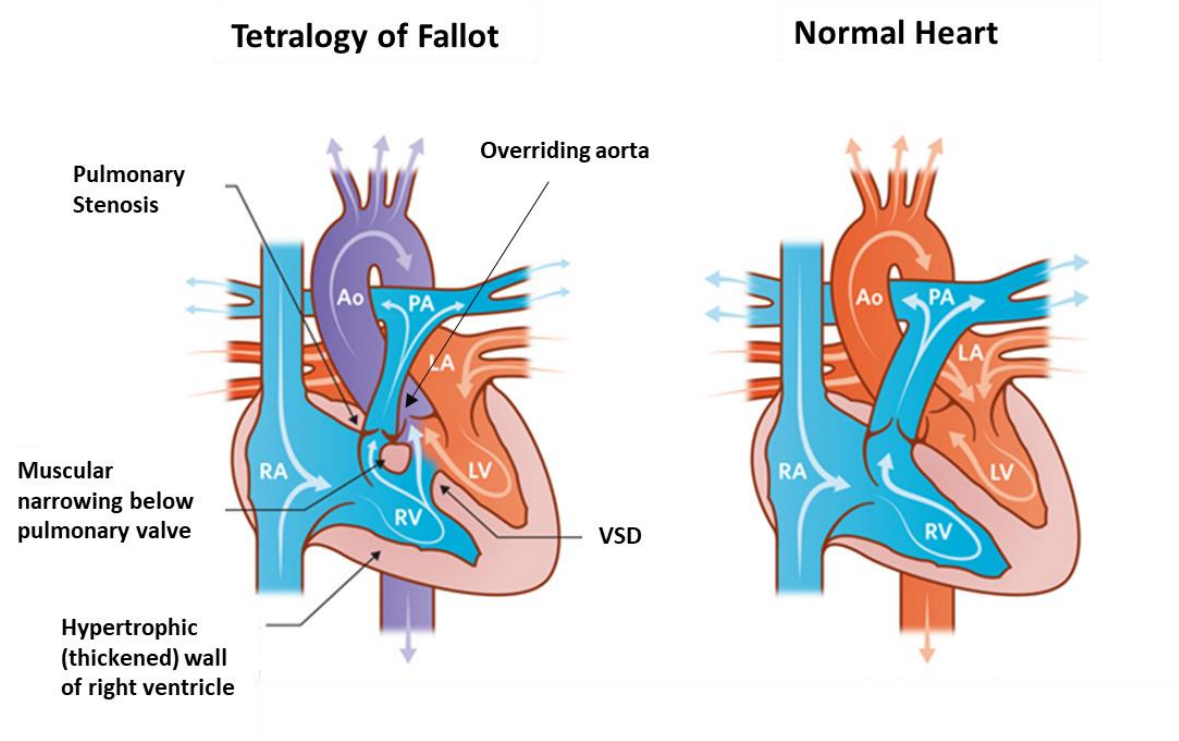

Figure 1.5: Structure and blood flow in the interior of a heart with tetralogy of Fallot compared to a normal heart. Aorta (Ao), pulmonary artery (PA), left atrium (LA), right atrium (RA), left ventricle (LV), right ventricle (RV), ventricular septal defect (VSD). Figure source: https://www.rch.org.au/cardiology/heart_defects/Fallots_Tetralogy/.

1.2.2. Intervention

Surgery is required to definitively repair ToF; however, palliative surgery is typically performed when the infant is not strong enough for a complete repair. Here, a shunt is introduced between the aorta and pulmonary artery, which facilitates oxygenation of the blood by providing an additional route for blood to reach the lungs (**Figure 1.6**). This temporary measure allows the infant time to grow and become strong enough for full corrective surgery; however, palliative surgery is associated with a 3 – 5% early mortality rate, and therefore repair in the first instance is usually preferred (van der Ven et al., 2019). Indeed, Arenz et al. demonstrated that primary repair can be performed effectively in symptomatic neonates and infants less than 6 months with no increase in mortality, suggesting shunting is no longer necessary (Arenz et al., 2013). Furthermore, in a study of ToF repair in children less than 4kg

body weight, those with a shunt instead of primary repair had significantly more surgical procedures and subsequent hospitalisations (Gerrah et al., 2015).

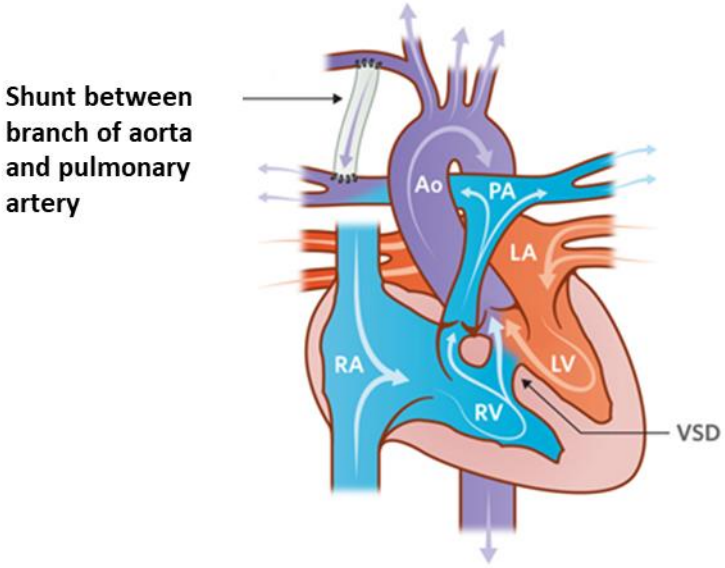

Figure 1.6: Palliative shunt intervention. Aorta (Ao), pulmonary artery (PA), left atrium (LA), right atrium (RA), left ventricle (LV), right ventricle (RV), ventricular septal defect (VSD). Figure source: https://www.rch.org.au/cardiology/heart_defects/Fallots_Tetralogy/.

Following palliative surgery, or preferably in the first instance, full corrective surgery is performed. Full repair requires firstly the closure of the VSD using a patch, followed by reconstruction of the RVOT. This is usually performed via the trans atrial approach, which involves atriotomy to reach the defect. In patients with a mild stenosis, pulmonary valvotomy and enlargement of the infundibulum is used to relieve the obstruction; however, more complex reconstruction is required in those with considerable pulmonary annular hypoplasia or atresia. In these cases, the patient will require a transannular patch or pulmonary conduit, or valved conduit, to alleviate the obstruction (**Figure 1.7**) (Downing et al., 2015).

With the repair of the VSD and RVOT, the other defects resolve by themselves. After widening of the RVOT, the heart does not have to pump as hard to force blood towards the lungs, so the right ventricle returns to normal thickness. Similarly, closing the septal defect ensures only oxygen-rich blood is ejected through the aorta.

In general, early repair of ToF is thought to be optimal as it limits the exposure to increased right ventricle pressure and low oxygen saturation; however, how early this should be is still debated (van der Ven et al., 2019). A study of 227 patients with ToF by Van Arsdell et al, concluded that primary repair should be performed between 3 and 11 months; however, others have suggested early repair in infants less than 90 days of age is desirable (Pigula et al., 1999; Van Arsdell et al., 2000).

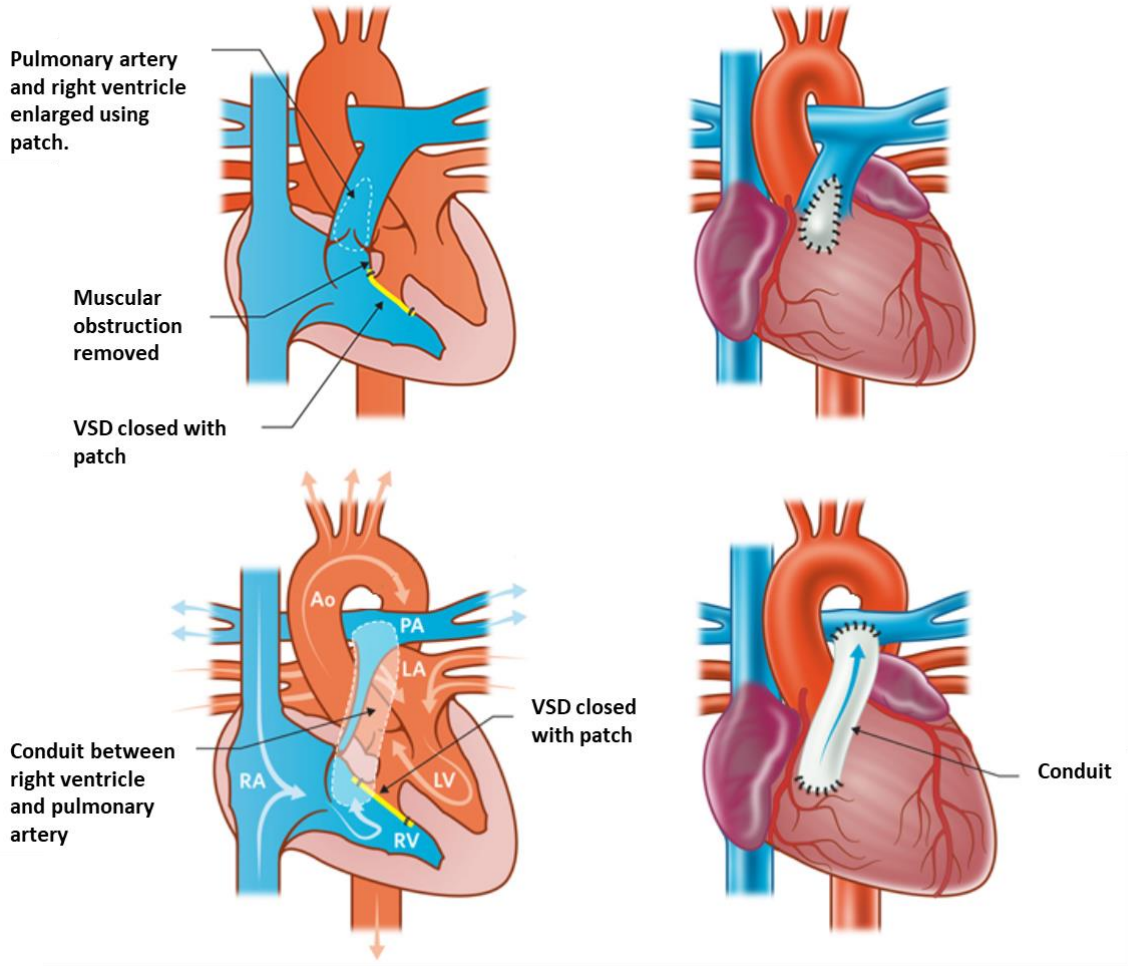

Figure 1.7: Complete repair with transannular patch or conduit. Aorta (Ao), pulmonary artery (PA), left atrium (LA), right atrium (RA), left ventricle (LV), right ventricle (RV), ventricular septal defect (VSD). Figure source: https://www.rch.org.au/cardiology/heart_defects/Fallots_Tetralogy/.

1.2.3. Prognosis

The 30 – 40 year survival can be as high as 90%; however, cardiac morbidities and sequelae from repair are common, resulting in frequent reintervention (Downing et al., 2015). Indeed, ToF reoperation rate can be as high as 50% (Berdat et al., 2004). In particular, a large proportion of ToF patients have residual RVOT disease, which is often a consequence of surgery. For example, patients that require a transannular patch during initial repair often demonstrate pulmonary regurgitation and progressive right ventricle dilation. In fact, moderate to severe pulmonary regurgitation is reported in 40% to 85% of patients five to ten years after repair (van der Ven et al., 2019). Likewise, conduits lack durability and are frequently associated with stenosis recurrent stenosis or regurgitation. This means that pulmonary valves and conduits will need replacing through reintervention to avoid progressive adverse right ventricle remodelling. Indeed, after 35 years, 40% of patients have undergone pulmonary valve replacement, with patients who've received staged repair at even higher risk (van der Ven et al., 2019). Unfortunately, as mentioned previously, each additional surgical procedure places greater risk on the patient. Specifically, patients who have undergone surgery for correction of ToF frequently have a higher risk of heart failure and cardiac arrhythmia as a side effect of reconstruction of the pulmonary valve or VSD (Neidenbach et al., 2018). In fact, atrial arrhythmias have been reported in up to 35% of patients who have undergone reparative surgery for ToF (Downing et al., 2015). Likewise, right ventricle dilation results in vulnerability to ventricular tachyarrhythmia and increased long-term risk of mortality (Henaine et al., 2012).

In summary, the prognosis for patients with ToF is positive, with survival to adulthood high, particularly in patients undergoing initial one-step repair. The major complications for ToF are the high rate of reoperation, such as adulthood pulmonary valve replacement, which increase the probability of sequelae and comorbidities, and can severely affect quality of life. The cause of reoperation is often due to the failure of the grafts that are used to reconstruct the RVOT. In the following section we will explore why graft failure occurs.

1.2.4. Why do Grafts Fail?

Graft failure rates have been reported as high as 70 – 100% after 10 years (Drews et al., 2017). Failure usually occurs due to adverse remodelling, which results in degeneration of the graft. It is also common for grafts to fail in paediatric patients due to the lack of growth potential, which leads to a progressive mismatch between the properties of the graft and native vessel (Pashneh-Tala et al., 2015). Under normal physiological conditions, vascular wall homeostasis and repair is tightly controlled through regulation of reparative processes, namely inflammation and extracellular matrix (ECM) remodelling. These processes require intricate interplay between a myriad of different cells types, such as macrophages, endothelial cells (ECs), and mural cells, and facilitate tissue growth and development. The introduction of prostheses, which are often acellular, disturbs this balance. The foreign material can induce an immunogenic response and the lack of homogenous endothelial layer and provides a site for thrombosis. The absence of a cellular component in some grafts means there is a lack of ECM remodelling, resulting in deterioration. Furthermore, the modified extracellular environment properties may trigger calcium deposition, leading to ectopic calcification and atherosclerosis.

The type of material used for reconstruction plays an essential role in how this remodelling and failure occurs. In the following paragraphs, we provide a brief description of the benefits and limitations of prostheses that are regularly used for CHD repair.

Synthetic Grafts: Mechanical valves and Gore-Tex conduits have been used to reconstruct the RVOT. These are durable, readily available, and the properties can be tailored; however, they have been associated with an increased risk of thrombosis and haemolysis (Mirensky et al., 2008). Patients also require anticoagulants for life, which increases risk of haemorrhagic complications. Furthermore, synthetic grafts lack growth potential, which is critical to avoid reoperation. Although Allen et al. reported promising results using Gore-Tex conduits for RVOT reconstruction, the study lacked long-term follow up and therefore the effect of growth limitation was not assessed (Allen et al., 2002). It is also worth mentioning that mechanical valves are not usually suitable at a young age due to the small patient size and thromboembolism risk. For this reason, these are more commonly used in adults and patients that have undergone multiple previous operations (Henaine et al., 2012).

Xenografts: Xenografts are animal-derived, often originating from porcine tissue due to the similarities in anatomic structure. They are readily available and often used due to the shortage of human substitutes (Avolio, Caputo, et al., 2015). Materials such as CorMatrix, an ECM derived from decellularised porcine small intestinal submucosa that is already widely used in cardiac surgery, provide optimal biological properties; however, used on their own they lack growth potential and previous studies have shown limited recellularization by host cells (Mosala et al., 2016; Woo et al., 2016). The decellularisation process, which is required to reduce the risk of an immune response, results in a weakening of the ECM, meaning crosslinking agents are often added to improve mechanical properties. The reagents used for these processes are toxic and can elicit a response from the host. Furthermore, cross-linking prevent matrix-metalloproteinase (MMP) degradation, which is essential for ECM remodelling (Schmidt et al., 2007). Additionally, the lack of a cellular component, which is responsible for ensuring the ECM is maintained, means some grafts are prone to degeneration. Finally, cell nuclei from incomplete decellularisation can act as a site for ectopic calcification and may also induce an immune response (Avolio, Caputo, et al., 2015; Wolner et al., 2004).

Homografts: These are usually derived from cadavers and exhibit excellent mechanical properties and anatomical structure. Homografts are frequently used for pulmonary valve replacement due to superior haemodynamic results; however, accelerated degeneration is often reported with up to 38.5% of patients developing complications within 18 years (Meijer et al., 2019). Cryopreservation and decellularisation processes increase the risk of degeneration. Indeed, after 10 years up to 87% of patients display signs of valve deterioration (Ruel et al., 2005). Furthermore, they are severely limited in supply, especially sizes suitable for paediatric surgery (Avolio, Caputo, et al., 2015). Interestingly, a high incidence of calcification and degeneration has been reported in paediatric patients (Mirensky et al., 2008).

Autografts: autologous tissue, such as pericardium or valves, is commonly used in CHD repair. For example, during the Ross procedure the pulmonary valve is used to reconstruct the aortic valve, and subsequently the RVOT is reconstructed with an alternative graft. The grafts possess no risk of immune response or thromboembolism, and importantly some studies report grafts match somatic growth (Raja et al., 2004). Despite this, suitable autologous tissue is often not available, and the tissue can be difficult to work with. There have also been reports of shorter durability due to calcific degradation (Kurobe et al., 2012).

Table 1.1: Summary of prostheses used for CHD reconstruction.

Prosthesis	Advantages	Limitations	Examples
Synthetic	Durable Readily available	Thrombotic events Haemolysis Anticoagulant treatment No growth potential	Gore-Tex, Mechanical
Xenograft	Readily available Biological properties Anatomical structure	Harsh decellularisation process Immunogenic Calcification Infection No growth potential	CorMatrix, bovine pericardium
Homograft	Non-thrombotic Good mechanical Properties Anatomical structure	Degeneration Harsh decellularisation process Infection Limited donor availability Calcification No growth potential	Human valves and vessels
Autograft	Non-thrombotic Good mechanical Properties Anatomical structure Non-immunogenic	Limited availability Calcification	Pericardium

In summary, all the current options possess substantial limitations, and frequently result in failure and subsequent replacement (**Table 1.1**). In particular, none of the current options offer the potential to grow and remodel, which is crucial for paediatric patients (Kalfa et al., 2013). It is clear there is demonstrable need for further developments in graft technology for congenital heart surgery.

1.2.5. The Ideal Graft for CHD Correction

Current grafts used for CHD correction, in particular reconstruction of the RVOT during ToF surgery, are inadequate due to various shortcomings that result in a high frequency of replacement. An optimal graft should address these limitations and ideally possess the following properties (Avolio, Caputo, et al., 2015; Mirensky et al., 2008):

- *Availability*: as discussed above, early repair of congenital heart defects such as ToF is beneficial. Graft should be readily available shortly after birth, within the window for primary surgical correction.
- *Calcification resistance:* vascular calcification results in stiffening of tissue/grafts and a subsequent loss of function. The risk of calcification is particularly high in infants. To remain functional and facilitate normal physiological haemodynamics, grafts should not increase the risk of ectopic calcification.
- *Compliance:* grafts must behave like native vascular tissue and elastically deform in response to pulsatile flow.
- *Customisable:* ideally the graft should be modifiable according to patients' requirements, particularly in terms of size.
- *Durability:* grafts should not deteriorate throughout a patient's life, ensuring reoperation events are minimised.
- *Growth potential:* the graft should match the somatic growth rate of the patient so that it does not need replacing periodically throughout a child's life.
- *Mechanical integrity:* the mechanical properties should mimic native tissue to ensure the graft copes with blood flow and pressure.
- *Non-immunogenic:* Grafts should not elicit an immune response, which can trigger inflammation and adverse remodelling of the graft.
- *Non-thrombotic:* the formation of a blood clot obstructs regular blood flow and can cause catastrophic damage. Prostheses that promote thrombosis require anticoagulants for life, which can have problematic side effects for a patient. For this reason, an ideal graft will provide a non-thrombotic luminal surface.

No graft currently exists that can fulfil all these criteria; however, tissue engineering may offer an opportunity to change this.

1.3. Tissue Engineering and Regenerative Medicine

The relatively new and exciting field of tissue engineering may offer the solution to the limitations of current treatments by allowing fabrication of cellularised conduits with the capacity to integrate into the patient's tissue and match the biological growth rate.

Tissue engineering is an interdisciplinary field that combines the principles of biology and engineering to develop functional substitutes that restore, maintain or improve tissue function (Langer et al., 1993). The concept of tissue engineering relies upon the combination of three essential pillars: scaffolds, signals, and cells (**Figure 1.8**). By combining these components, tissue engineering aims to construct biological tissues that more closely mimic native tissue and possesses superior properties to currently used transplant options. To accomplish this, each of these components need to be optimised for the intended tissue application. For example, for vascular tissue engineering a scaffold with elastic properties and vessel-like architecture would be preferred to a porous material with a rigid structure. Similarly, vascular-associated cells and growth factors may be used to functionalise the scaffold, such as ECs and angiopoietins.

It should also be noted that tissue engineering does not necessarily require incorporation of all these components. Indeed, tissue engineered vascular grafts can be broadly categorised into two groups based on their method of fabrication: self-assembled and scaffold based. The self-assembled approach relies on providing cells with a suitable environment to facilitate organisation into complex tissues without the need of a scaffold. Scaffold-based approaches, on the other hand, utilise a support that can be used to tailor physical properties and add further complexity to engineered tissues. In the following sections, we will provide an overview of each component (scaffolds, signals, and cells) with particular focus on vascular tissue engineering and applications for CHD. There are many excellent reviews evaluating the myriad of different tissue engineering techniques and applications; however, this subject is extremely broad and outside the context of this thesis.

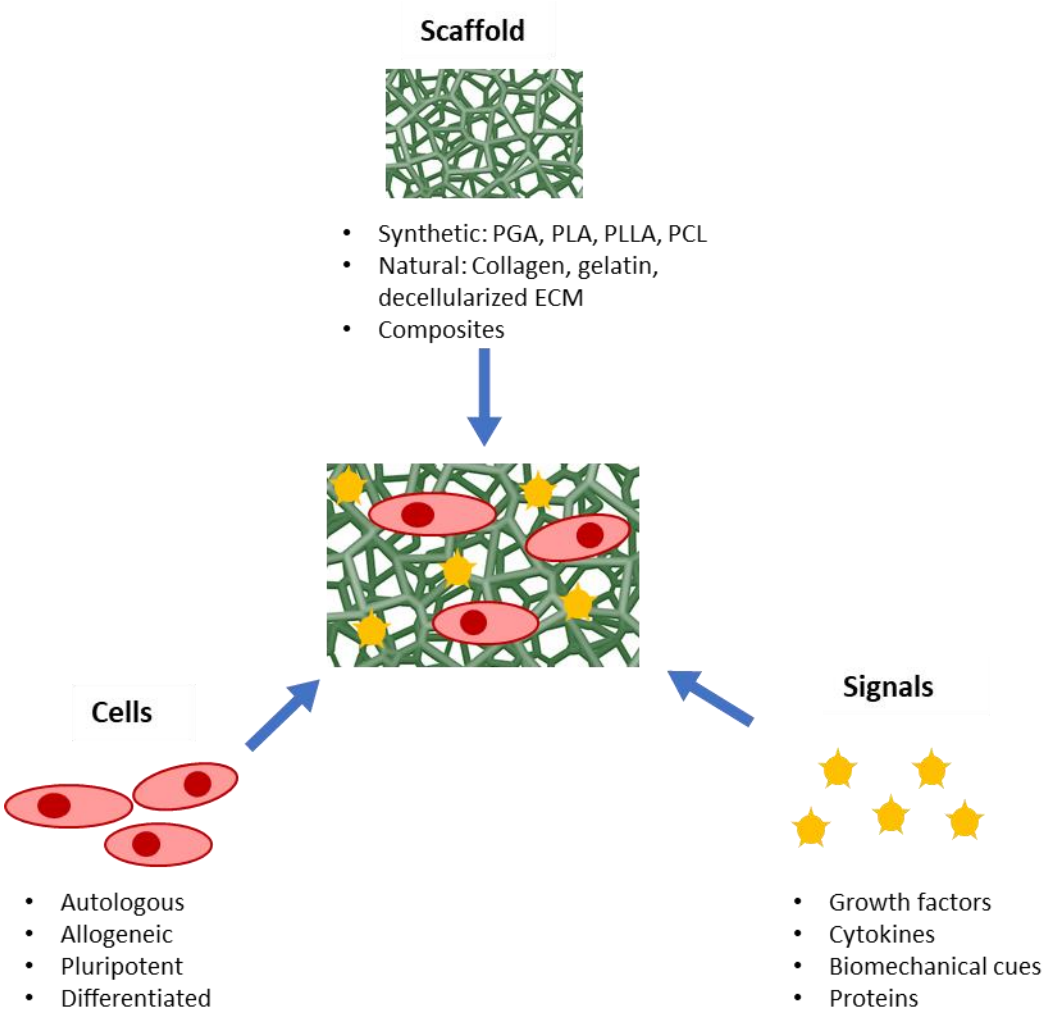

Figure 1.8: The three pillars of tissue engineering: Scaffolds, Cells and Signals. These three components can be used in various combinations to engineer biological constructs that aim to restore, maintain, or improve tissue function. The examples given for each component are just a small sample of the options considered for tissue engineering. Polyglycolic acid (PGA), poly-lactic acid (PLA), poly-l-lactic acid (PLLA), polycaprolactone (PCL) and extracellular matrix (ECM)

1.3.1. Scaffolds

The term ‘scaffold’ is used to describe the supportive 3D or planar material used for the base of engineered tissue. The scaffold must be able to support cell adhesion and proliferation, allowing for the development of 3D tissues. *In vivo,* cells sit within the ECM, which is a dynamic and physiologically active 3D network of macromolecules secreted by cells. Cells receive cues through interactions with the ECM which direct differentiation, migration and proliferation, as well as other key cellular processes (Ross, 1998). Conversely, under normal *in vitro* cell culture the extracellular environment is vastly different, namely the absence of a 3D environment, complex signalling, and abnormal culture surface mechanical properties, which can trigger changes in gene and protein expression. For example, the stiffness of culture plastic is several orders of magnitude greater than most *in vivo* tissues, which results in a change in phenotype and increase in processes such as fibrogenesis and proliferation (Wells, 2008). For this reason, scaffolds are designed to provide a support structure that more closely resembles the *in vivo* environment. For cellularised grafts, the scaffolds may also need to be optimised for the specific cell types used.

The field of scaffold design is incredibly complex with a huge number of variables to consider and optimise in order to provide the perfect environment for cell engraftment. Biocompatibility, biodegradability, mechanical properties, architecture and ease of fabrication have been identified as key criteria to consider when designing a scaffold (O’Brien, 2011).

- *Biocompatibility*: Initially, researchers thought materials should be inert so that no reactions were induced; however, the school of thought has changed. Bioactive materials, or biomaterials, are preferred that allow cells to adhere, proliferate and integrate into the scaffold. Additionally, the material should not elicit an immune reaction, leading to inflammation and implant failure.
- *Biodegradability*: In most applications of tissue engineering the scaffolds are required to degrade over time as the native cells and tissue replace the implant; however, degradation time must be optimised to ensure there is enough time for ECM remodelling and the mechanical properties of the graft are not compromised. The by-products of degradation must also be non-toxic and capable of being easily removed by the body.

- *Mechanical properties:* The scaffold should possess properties comparable to the tissue at the site of implantation. The mechanical properties can alter the phenotype and behaviour of cells, promote migration along stiffness gradients through durotaxis, and provide differentiation cues to stem cells (Whang et al., 2016; Xing et al., 2019). Designing a scaffold to mimic the properties of the in vivo niche can encourage normal cell function and tissue growth. Additionally, the scaffold should be strong enough to withstand the surgical procedure and *in vivo* forces, such as shear stress in blood flow.
- *Architecture:* Ideally scaffolds should possess an interconnected pore structure. These pores facilitate cellular penetration, vascularisation, and diffusion of nutrients and waste products to prevent core degradation. Indeed, creating a scaffold with sufficient pore size and architecture for vascularisation, which is critical for construction of complex tissues, is a major consideration for tissue engineering (Mastrullo et al., 2020). Additionally, the pore size can affect cellular processes and therefore must be optimised according to the cell types used and tissue engineered (Murphy et al., 2010). As well as porosity, the topography of the scaffold should be tightly controlled due to its influence on cellular function (Miyoshi et al., 2014).
- *Fabrication Method:* the manufacturing method is essential for clinical and commercial feasibility. Scaffolds must be scalable and cost effective. Additionally, they should be readily available for clinical use.

A wide range of vascular tissue engineering biomaterial scaffolds have been designed with these requirements in mind, with the majority of focus on decellularized ECM and biodegradable synthetic materials (Drews et al., 2017).

Specifically, biodegradable polymers such as polyglycolic acid (PGA), poly-lactic acid (PLA), poly-l-lactic acid (PLLA) and polycaprolactone (PCL) have been extensively explored for vascular tissue engineering (Carrabba et al., 2018; Kurobe et al., 2012). These materials are readily available and can be printed into complex shapes. Furthermore, the properties can be tailored by adjusting the ratio of copolymers. Despite this, there are still considerable limitations with these scaffolds. Unlike natural scaffolds, they lack cell binding sites, which are required to develop a non-thrombogenic endothelial layer (Carrabba et al., 2018). There have also been issues raised regarding rapid degradation and cytotoxic degradation by products (Avolio, Caputo, et al., 2015).

Although natural polymers lack the mechanical strength and tunability of synthetic alternatives, they offer increased remodelling capacity and biocompatibility due to the presence of native signalling molecules. Indeed, materials such as CorMatrix, decellularized porcine small intestinal submucosa, have already gained food and drug administration (FDA) approval and are routinely used in cardiovascular surgery for reconstruction of cardiac defects (Mosala et al., 2016; Scholl et al., 2010). CorMatrix is an excellent scaffold due to its sufficient mechanical strength, natural biocompatibility and porosity that allows for recruitment and integration of host cells (Avolio, Caputo, et al., 2015). Although there have been a few reports of inflammation, most likely due to the decellularization process, a majority of the studies have reported successful results, with only 10% failure reported (Mosala et al., 2016). Alone, it may possess limited growth potential, but for use as scaffold in a tissue engineering system, there is great potential.

1.3.2. Signals

In vivo, the ECM is a complex structure that not only provides physical support to the cells, but also interacts with cells through an array of chemical, biological and biomechanical cues (Nakayama et al., 2014). These play a crucial role in cell fate and tissue development. Consequently, it is essential for tissue engineering approaches to incorporate these signals.

Scaffolds alone can provide biomechanical cues through properties such as stiffness, topography, and porosity; however, it is often necessary to provide further functionalisation, particularly with synthetic scaffolds which possess lower biocompatibility. Delivery of growth factors is a common approach to influence cell behaviour. For example, acellular scaffolds often utilise patterning of growth factors such as vascular endothelial growth factor (VEGF) and basic fibroblast growth factor (bFGF) to encourage *in situ* cellularisation and tissue development (Alsop et al., 2014; Kuttappan et al., 2018). In tissue engineering approaches that utilise in vitro cell seeding, tissues and cells are provided with growth factor rich media which can direct differentiation and tissue development (Cai et al., 2018). Furthermore, the scaffolds can become functionalised through adsorption of biomolecules from the medium. Alternative biological methods to influence cell adhesion include incorporation of peptides, such as the

arginine-glycine-aspartate (RGD), and coating with matrix proteins such as collagen and fibronectin (Post et al., 2019; F. Wang et al., 2013).

As previously mentioned, design of the scaffold allows incorporation of biomechanical cues; however, additional methods are now being utilised to expose cells and scaffolds to physiological forces. In the vascular niche in vivo, cells are exposed to shear stress and cyclic strain due to being exposed to blood flow. The mean blood flow in the pulmonary artery is 10cm/sec, which induces a cyclic strain and shear stress equivalent to 4 – 15 dynes/cm^2 over the cardiac cycle (Gabe et al., 1969; Golob et al., 2017; Salibe-Filho et al., 2020). These stimuli significantly influence cell processes such as angiogenesis, extracellular protein deposition and differentiation, which are key to creating a mature vascular graft similar to the in vivo vessel (Nakayama et al., 2014). To mimic these stimuli, bioreactors have been developed that create these mechanical cues in an in vitro environment and encourage tissue maturation (Zhao et al., 2016). Indeed, dynamic flow conditioning has been utilised to accelerate maturation of tissue engineered heart valves (Flanagan et al., 2007). For vascular tissue engineering, dynamic flow conditioning involves placing sections of cellularised scaffold or graft into a bioreactor. The bioreactor is a closed system containing cell culture media, a pump, and a tubing circuit. The pump can be set to generate a media flow similar to the physiological flow, which stimulates the cells on the graft to differentiate, mature and produce extracellular proteins in response to the shear stresses the flow generates. Likewise, cyclic strain can induce extracellular remodelling and improve mechanical properties in collagen-based tissue engineered vessel constructs (Seliktar et al., 2000). This can be simulated using periodic stretching of cellularised graft materials, either using a mechanical stretching device or a pulsatile flow bioreactor. An illustration of a basic bioreactor setup can be found in figure 1.9 and further details of the bioreactor setup can be found in chapter 2 section 20.

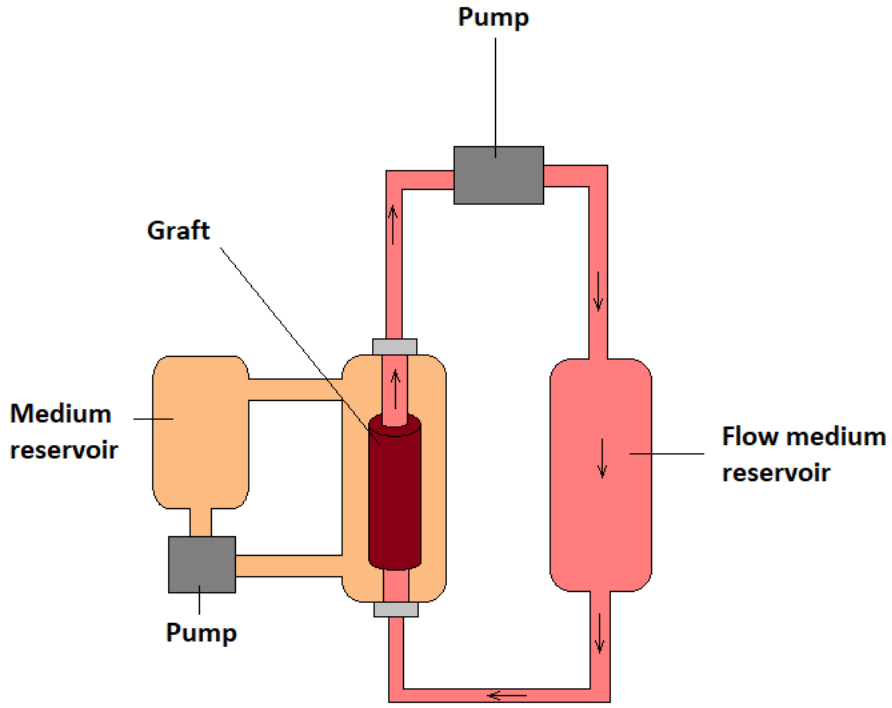

Figure 1.9: Basic bioreactor schematic for dynamic flow conditioning. The cellularised tissue engineered graft is positioned in a bioreactor chamber filled with cell culture media. This is connected to a pump via tubing. The pump can be set to generate the desired flow of medium from the tubing and medium reservoir through the graft. This flow stimulates shear stress and graft strain which the cells respond to, facilitating maturation of the graft. Another media circuit ensures the graft is fully submerged. This bioreactor setup can be contained within a regular culture incubator so that the cell environment can be tightly controlled.

Chemically modification of scaffold surfaces can also be used to influence cell adhesion. For example, cross-linking or addition of functional groups can be used to tailor the surface properties according to tissue requirements (Tallawi et al., 2015).

Table 1.2: Summary of popular methods for signal cue incorporation. Vascular endothelial growth factor (VEGF), basic fibroblast growth factor (bFGF), arginine-glycine-aspartate (RGD) peptide, carboxyl group (COOH).

Signals	Examples
Biological	Immobilisation of biomolecules such as growth factors (e.g., VEGF, bFGF). Provision of specific cell media (e.g., cell differentiation medium) Coating with ECM proteins (e.g., fibronectin, collagen). Incorporation of peptide sequences (e.g., RGD)
Biomechanical	Scaffold properties (e.g., porosity, topography, stiffness) Simulation of physiological forces (e.g., shear stress, cyclic strain)
Chemical	Addition of functional groups (e.g., COOH) Cross-linking

1.3.3. Cells

For engineered tissue to perform functionally, it is essential that a cellular component is incorporated as they promote development of neo-tissue and improve long-term graft patency (Kurobe et al., 2012). As previously mentioned, this may be performed in situ by functionalising the scaffold with biomolecules that encourage homing or migration of cells into the scaffold; however, in many applications in vitro cell seeding is preferred.

Broadly speaking, cells used for tissue engineering and regenerative medicine can be classed as autologous or allogeneic. Autologous cells are isolated from a patient's own tissue whilst allogeneic cells come from a donor of the same species. Autologous cells are arguably the gold standard as they possess improved biocompatibility and reduce risk of rejection or thrombosis; however, they are not always available (Mirensky et al., 2008).

The precise choice of cell source is a contentious decision in tissue engineering, which is dependent on the specific application. For neonatal vascular tissue engineering, we can identify certain properties that would be desirable for the cell source as outlined in **Table 1.3**.

Table 1.3: Ideal properties for cells used for neonatal vascular tissue engineering in CHD correction.

Property	Description
Availability	Cell source should be readily available, ideally without the need for an invasive procedure to harvest tissue. For use in infant recipients', cells should be attainable in sufficient numbers shortly after birth.
Safety	Cells should not elicit a response from the host immune system, which is a major cause for implant rejection (Domev et al., 2014). Additionally, ideally cells should be resistant to calcification, which is a high risk in paediatric patients (Avolio, Caputo, et al., 2015).
Purity	For clinical translation, the cell product must be carefully characterised and assessed for purity to ensure harmful cells do not enter the body.
Plasticity	The capacity to differentiate into vascular lineages is important in the development of functional vascular tissue; however, lineage committed progenitors may be preferred to pluripotent cells due to safety concerns (Avolio, Caputo, et al., 2015; Bajpai et al., 2012).
Pro-angiogenic	Promotion of angiogenesis is crucial for vascularisation and long-term survival of engineered tissue. The majority of tissue thicker than 1mm will become necrotic before perfusion of host-derived micro vessels can occur (Chang et al., 2017; K. Lee et al., 2009).
Integration	Cells should integrate into the scaffold, producing and degrading the extracellular matrix to allow growth of tissue (Howard et al., 2008).

In the following section, I have summarised common cell types employed for vascular tissue engineering.

Endothelial cells (ECs): ECs are one of the preferred cell types for vascular tissue engineering due to their natural role in coverage of the intima layer and realization of ant-thrombotic activity and vasoactive function through the production of nitric oxide. Applications often use them for luminal seeding of grafts or scaffolds to provide a non-thrombogenic surface (Geenen et al., 2015). Autologous ECs are easily isolated and purified from many tissues; however, they

lack the plasticity to form other components of the tissue and therefore many approaches use them in combination with other cell types (Ju et al., 2017).

Vascular smooth muscle cells (VSMCs): VSMC are a vascular specific mature cell type that make up a large proportion of the arterial wall tunica media and are therefore an obvious choice for vascular tissue applications. They are responsible for elastin synthesis, which is a key protein for tissue functionality and cell-cell signalling, but often absent in engineered grafts (Patel et al., 2006). Although isolation is relatively simple, VSMCs adopt a synthetic phenotype under in vitro culture, which play a different role in vascular maintenance. The synthetic phenotype is characterised by a higher migration and proliferation rate as well as greater synthesis of ECM proteins and a downregulation of contractile proteins (Rensen et al., 2007). Consequently, to harness the elastic contractile abilities of these cells for vascular tissue engineering, they must be differentiated to a mature contractile phenotype before use, or alternatively stem cell-derived VSMCs are used (Bacakova, Travnickova, Filova, Matejka, et al., 2018).

Induced pluripotent stem cells (iPSCs): iPSCs can be obtained from reprogramming somatic cells. As these cells are derived from adult cells, they are readily available and once reprogrammed they can differentiate into cells of all three germ layers. Due to their pluripotency, iPSCs can be used to generate cells of the vascular lineage such as ECs and VSMCs, and form multi-component layered vascular grafts (Ayoubi et al., 2017; Gui et al., 2016; Nakayama et al., 2015; Yoder, 2015). Furthermore, stem cells produce higher yields of ECM components than adult cells (Song et al., 2018). Despite possessing many desirable properties for vascular tissue engineering, safety concerns regarding possible tumorigenesis have limited iPSC use for clinical applications (Mayshar et al., 2010; Okano et al., 2013).

Mesenchymal stem cells (MSCs): MSCs are currently one of the optimal options. These are a population of heterogenous adult stem cells that can be isolated from a variety of tissues, such as bone marrow and Wharton's Jelly (WJ) (Avolio, Caputo, et al., 2015; Ghafarzadeh et al., 2016; Howard et al., 2008). These are an attractive cell type due to their availability, differentiation potential, and immunoregulatory role (Dimarino et al., 2013). Indeed, bone marrow MSCs have been used both directly and to generate VSMCs for production of vascular grafts (Bajpai et al., 2012). Although MSCs have been extensively studied, limitations with

this cell type have impeded progress. For example, the heterogeneity of the cells and non-selective culture may diminish any therapeutic effect. In fact, evidence suggests there may be advantages of using more purified progenitor populations (Cathery et al., 2018; Gomez-salazar et al., 2020).

In summary, each of these cell types possess beneficial properties for vascular tissue engineering; however, all have limitations that may hinder their success. Further investigation of suitable cell sources should be a priority for future vascular tissue engineering applications.

1.3.4. Vascular Tissue Engineering for CHD Applications: Successes and Challenges

As introduced at the start of this subsection, tissue engineering has the potential to address the limitations of corrective CHD surgery. Specifically, the lack of graft growth potential in RVOT reconstruction in malformations such as ToF present a significant challenge, which currently results in frequent reoperation. By incorporating different aspects of tissue engineering, researchers have already begun to realise this potential. For example, Syedain et al. developed an acellular graft with demonstrated growth potential for use in RVOT reconstruction (Syedain et al., 2016). The grafts, fabricated from decellularized fibroblast ECM and fibrin gel, were implanted into 8-week-old lambs. At week 50, grafts were explanted to evaluate remodelling and growth. Analysis demonstrated in situ cellularisation by ECs and mature smooth muscle cells, along with a substantial increase in collagen and elastin content. Furthermore, lambs demonstrated normal growth, with graft diameter and volume increasing by 56% and 216%, respectively. These results are particularly exciting as very few studies have managed to address the issue of matching somatic growth.

More recently, a variety of studies from the Caputo group have explored the possibility of using different cell types to functionalise CorMatrix grafts with some promising results (Albertario et al., 2019; Ghorbel et al., 2019; Iacobazzi et al., 2020). Albertario et al initially seeded CorMatrix grafts with thymus MSCs from piglets and, after 2 weeks in vitro conditioning, implanted them into the RVOT of 20 – 25kg female piglets. 4.5 month follow up demonstrated improved myocardial strain and endothelialisation; however, many other properties such as

diameter growth were no different to the unseeded control. Similarly, Iacobazzi et al demonstrated the feasibility of using Wharton's Jelly-mesenchymal stem cells (WJ-MSCs) to create improved grafts for CHD correction (Iacobazzi et al., 2020). The authors seeded WJ-MSCs onto a CorMatrix scaffold, and after a period of 10 days conditioning in vitro, the graft was implanted in 3 – 4-week-old piglets. A 6 month follow up demonstrated presence of an organised smooth muscle cell and luminal endothelialisation in MSC seeded CorMatrix conduits. Furthermore, there was no sign of thrombosis or adverse remodelling. Although these results are encouraging, the authors noted a full-scale study should be performed to evaluate if the MSC-engineered graft was functionally superior to acellular CorMatrix. Indeed, in vitro studies preimplantation did not demonstrate any significant differences in mechanical properties or ECM remodelling. Ghorbel et al. arguably demonstrated the most exciting results of this sequence of studies. Here, the authors explored the possibility of using human umbilical cord MSC-derived VSMCs to functionalise acellular CorMatrix grafts. Following a similar model to the other studies, the left pulmonary artery of 12 – 15 kg piglets was reconstructed using the engineered conduit. A 6-month follow up revealed cellularised grafts possessed a homogenous endothelium and thick multi-layered muscular media, which was not present in the acellular control. Furthermore, a significant increase in circumference was observed in the cellular graft, which suggested growth potential.

Despite studies demonstrating initial success in developing improved graft technology that can address the unmet needs of congenital heart surgery, there still remains a lack of clinically applicable tissue engineering products (Boyd et al., 2019). Zilla et al suggest this may be due to the limited applicability of cardiovascular animal models (Zilla et al., 2020). Namely, rapid trans-anastomic endothelialisation of small acellular grafts occurs in animal models but is limited in humans. The average graft in the study of Syedain et al was only 17 mm (Syedain et al., 2016). This size graft is usually endothelialised within weeks in animal models, ensuring adverse effects such as thrombosis do not have time to develop; however, this process can take months in humans (Zilla et al., 2020). This indicates a need for functionalisation of grafts to speed up this process in humans. Additionally, vascularisation remains a key issue (Mastrullo et al., 2020; Song et al., 2018). In large blood vessels, such as the pulmonary artery, an adventitial layer containing microvasculature exist called the vasa vasorum (Jo et al., 2014). This layer provides a blood supply to the mural cells, ensuring nutrients are delivered and waste products removed. Engineered grafts lack this layer, which hinders the complexity and size of

the tissue produced as well as long-term survival (Mastrullo et al., 2020). Indeed, Albertario et al. acknowledged that angiogenesis may further improve the functionality of their engineered grafts (Albertario et al., 2019). It is clear that for tissue engineering to realise its potential and translate to clinical success, there are still many challenges to overcome. It is possible that functionalising grafts with more suitable cells may address some of these limitations (Mastrullo et al., 2020).

1.4. Pericytes

Pericytes are a multifunctional cell type with exciting potential for tissue engineering and regenerative medicine applications. These cells play a commanding role in maintaining homeostasis through their involvement in many physiologic processes, including modulation of immune response, vascular development, regulation of blood flow, stabilization of vessels, and contribution to the endothelial barrier integrity (Alexander Birbrair et al., 2015; Stark et al., 2013; Van Dijk et al., 2015). Consequently, utilization of these cells for vascular tissue engineering applications may provide a solution to the current challenges. Here we summarize what a pericyte is and the role they play in processes that are of particular importance for tissue engineering and regenerative medicine.

1.4.1. Definition and Identification

Pericytes were initially defined by their anatomical location, encircling the endothelium of microvascular capillaries, terminal arterioles, and post-capillary venules (Van Dijk et al., 2015). They can be found within most tissues of the body; however, their morphology, biology and density vary between organs depending on the stringency of the endothelial barrier properties. For example, the pericyte to EC ratio can be as great as 1:100 within the skeletal muscle through to 1:3 and 1:1 in the central nervous system (CNS) and retina, respectively, regions where vessel integrity and trans-endothelial movement is tightly regulated (Shepro, 1993).

Phenotypically, pericytes express a range of antigenic markers that help with their identification. No single antigen can be regarded as being pericyte-specific, meaning their identification is based on a combination of markers. Commonly, these include neural/glial

antigen 2 (NG2) proteoglycan, platelet-derived growth factor receptor-β (PDGFRβ) and CD146 **(Table 1.4)**, together with mesenchymal markers, such as CD90 and CD105, but absence of CD56, a surface antigen expressed in neurons, glia and skeletal muscle, and hematopoietic and endothelial markers, such as CD45 and CD31, respectively. It is worth keeping in mind, however, that due to the heterogeneity of these cells and lack of an agreed phenotype, different research groups have reported the presence of pericytes within the same tissue but with conflicting antigenic profiles (Avolio, Rodriguez-Arabaolaza, et al., 2015; W. C. W. Chen et al., 2015).

More recently, cells with pericyte-like properties have also been described within the wall of larger vessels, thereby challenging the original concept of pericytes localizing only to the microvasculature. For example, we were the first to describe such cells present around the adventitial vasa vasorum of the human saphenous vein (Campagnolo et al., 2010). These cells are CD34 positive but CD31, CD146 and CD45 negative. At the same time, they also co-express typical pericyte markers including NG2, PDGFRβ, CD105 and CD90. Corselli et al. have also demonstrated the presence of $CD34^{+}/CD146^{-}/CD31^{-}$ cells around larger blood vessels of multiple organs that co-express pericyte markers in culture following exposure to vascular growth factors (Mirko Corselli et al., 2012).

Due to the absence of a unique marker, tracking pericyte lineage has traditionally proven difficult. So far, studies have suggested pericytes develop from either the ectoderm or mesoderm, depending on their anatomical location. More specifically, through use of neural crest fate mapping models, it has been shown that pericytes in the central nervous system, thymus, retina and choroid have developed from differentiated neural crest-derived cells (Foster et al., 2008; Trost et al., 2013). On the other hand, as summarised by Armulik et al, pericytes found in coelomic organs, such as the lungs, liver or coronary vessels, have been identified as mesothelium derived (Armulik et al., 2011). Here it has been suggested that mesothelial cells undergo an epithelial-to-mesenchymal transition, followed by a migration to a specific organ and differentiation into pericytes (Armulik et al., 2011). To further add to the complexity of these cells, recent publications have suggested that pericytes from the same tissue can have a heterogenous origin (Dias Moura Prazeres et al., 2017; Yamazaki et al., 2017). For example, Chen et al demonstrated coronary pericytes also arise from endocardial cells undergoing endothelial-to-mesenchymal transition, and some retinal pericytes have been

shown to be bone-marrow derived in addition to some originating in the neural crest (Pfister et al., 2013). It is clear there is still a lack of understanding regarding pericyte ontogeny and development. More work to identify the origin of a type of pericyte could help identify their regenerative potential for particular pathologies. For example, ensuring pericytes used for treatment are derived from the same germ layer as the transplant site could improve beneficial effects. Indeed, pericytes have different functions depending on the source within the body. For example, although CNS pericytes share similar properties to peripheral vasculature pericytes with regards to their role in angiogenesis, vessel integrity and haemodynamic regulation, there are some features unique to this population (Beazley-Long et al., 2018). Firstly, CNS pericytes have been shown to differentiate into a microglia-like phenotype in a model of stroke, which is thought might drive neuroinflammation in some chronic pain states (Özen et al., 2014). Furthermore, CNS pericytes contribute towards leukocyte transendothelial migration into the CNS by increasing blood flow and releasing factors that promote leukocyte chemoattraction, which contribute to CNS neuronal sensitisation (Beazley-Long et al., 2018). This indicates a role of this pericyte source in generation of pain. Additionally, CNS pericytes of neuroectodermal origin have a distinctive ability to form neuronal phenotypes, which has not been seen in other pericytes sources (Winkler et al., 2011). This neuronal fate capacity may contribute to their function in modulation of the blood brain barrier and blood spinal cord barrier, where pericyte coverage is more dense than many other vessel barriers (Abbott, 2000).

Table 1.4: Antigenic markers commonly used to identify pericytes from different organs and anatomical locations.

Marker	Function	Expression	Possible Explanation for Expression	Reference
NG2 (Neural/glial antigen 2)	Membrane proteoglycan that mediates cell-cell and cell-extracellular matrix interactions.	Positive in pericytes of arterioles and capillaries as well as vasa vasorum, however, negative in venule pericytes.	NG2 contributes to transmembrane signalling and has been linked to promotion of cell proliferation and motility. It is therefore not surprising that this is expressed in pericytes, a highly mobile and proliferative cell type. NG2 has also been suggested to play a role vascular network homeostasis, with its absence in venous vessels contributing to regulation of arterial/venous anastomoses.	(Crisan et al., 2008, 2009; Murfee et al., 2005; Ozerdem et al., 2001; Stallcup, 2017)
PDGFRβ (platelet-derived growth factor receptor-beta)	Tyrosine-protein kinase receptor that mediates the differentiation of pericyte progenitor cells.	Ubiquitous marker of micro vessel and adventitial pericytes	During angiogenesis, vessel stabilisation is achieved via pericyte recruitment. This is achieved via PDGF-β signalling and therefore it is essential for pericytes to express the receptor for this, PDGFR-β.	(Armulik et al., 2011; Crisan et al., 2009; Geevarghese et al., 2014; A. P. Hall, 2006)
CD146 (melanoma cell adhesion molecule or MCAM)	Membrane glycoprotein involved in heterophilic cell-cell interactions.	Marker of brain, bone marrow, myocardial and skeletal muscle pericytes. Negative in adventitial pericytes.	CD146 has been shown to regulate PDGFRβ pericyte endothelial signalling in the blood-brain barrier development. CD146 has also been suggested as a marker for multipotency which explains its presence in pericytes. The absence of this marker in adventitial pericytes has not been explored.	(Avolio, Rodriguez-Arabaolaza, et al., 2015; Campagnolo et al., 2010; ÇELEBİ SALTIK et al., 2017; J. Chen et al., 2017; Crisan et al., 2008, 2009; Russell et al., 2010; Vono et al., 2016)
CD13 (aminopeptidase N)	aminopeptidase N is a membrane type II metalloprotease. It is implicated in cell migration, cell survival and angiogenesis.	Marker of cerebral pericytes associated with the blood—brain barrier	It is thought that pericytic aminopeptidase N is involved in metabolism of neurotransmitter in the blood brain barrier and is therefore restricted to cerebral pericytes.	(Armulik et al., 2011; Kunz et al., 1994; Ramsauer et al., 1998)

αSMA (alpha-smooth muscle actin)	Highly conserved contractile protein involved in cell motility, structure, integrity, and intercellular signalling.	Pericytes express αSMA at a concentration of one tenth smooth muscle cells but six-fold higher than endothelial cells. They can increase their expression in response to stress or vascular remodelling.	αSMA is a crucial contractile protein involved in vasoconstriction. Pericytes control blood flow in capillaries via an active response which requires expression of contractile proteins. This expression is most likely lower than smooth muscle cells as pressure in capillaries is lower than the arterial system which require greater contraction.	(X. Cai et al., 2009; Crisan et al., 2009; Stephan Nees et al., 2013; Verbeek et al., 1994)
Nestin	Intermediate filament of the cytoskeleton involved in the remodelling of the cell.	Markers of a subpopulation of pericytes in brain, bone marrow, liver and skeletal muscle that shows multipotential regenerative ability.	Nestin was originally described as a neural progenitor marker, however, studies have suggested a link between nestin expression and neovascularization providing a possible explanation for pericytic expression.	(Crisan et al., 2008; Kunisaki et al., 2013; Nakagomi et al., 2015; Suzuki et al., 2010; L. Xie et al., 2015)
ALP (alkaline phosphatase)	Enzyme found in the blood that plays an integral role in metabolism in the liver.	In vivo marker expressed across different pericyte subsets, with notable expression in skeletal pericytes.	The physiological function of ALP remains obscure with little description in the literature. Pericyte expression and locality to blood vessels could indicate a role in the release of ALP into the bloodstream.	(Farup et al., 2015; Sharma et al., 2014; Vono et al., 2016)
CD34	Transmembrane phosphoglycoprotein thought to play a role in cytoadhesion, and regulation of differentiation and proliferation	In the absence of CD31, a marker for endothelial cells which also express CD34, expression of this antigen acts as a marker for a subpopulation of adventitial pericytes.	The function of CD34 as a surface antigen is still unknown, however, it is linked to stem cell and progenitor activity, and pronounced differentiation capacity, which may account for expression in certain pericytes.	(Avolio, Rodriguez-Arabaolaza, et al., 2015; Campagnolo et al., 2010; Sidney et al., 2014)

1.4.2. Role in Angiogenesis

The stimulation of angiogenesis, e.g. the formation of new vessels from the pre-existing vasculature, is an essential yet challenging requirement for tissue engineering (Jung et al., 2013; Novosel et al., 2011). It is essential that a cell population utilised for tissue engineering can actively engage with the angiogenic process in order to stimulate the outgrowth of mature and functional neo-vessels that allow a tissue engineered graft to integrate into the host tissue. Pericytes address this requirement by playing an active role during both the vessel sprouting and stabilization phases of angiogenesis.

Neovascular formation is initiated by the activation of quiescent vessels in response to angiogenic signals, such as VEGF, angiopoietin-2 (ANGPT-2) or chemokines. ANGPT-2, which is almost exclusively expressed by ECs, promotes detachment and migration of pericytes from the endothelial layer. This action is carried out via the inhibition of Tie2 receptors. Historically, ANGPT-2 was thought to be an autocrine modulator of the ANGPT/Tie signalling pathway. However, recent studies have demonstrated Tie2 receptor expression on pericytes as well as ECs (Teichert et al., 2017). The identification of these Tie2 receptors highlights the importance of pericytes for angiogenesis and vessel stabilization. Pericyte expression of angiopoietin-1 (ANGPT-1), in the absence of ANGPT-2, activates both pericyte and EC Tie2 receptors, triggering downstream pathways that contribute to vascular maturation. However, in the presence of ANGPT-2, the Tie2 receptors are inhibited, promoting cell migration and new angiogenic activities. This is also evidenced in the recent study by Augustin and co-workers, who demonstrated pronounced activation of angiogenesis following the silencing of pericyte Tie2 (Teichert et al., 2017).

To aid detachment of pericytes and EC migration, both cell types secrete MMPs which degrade the basement membrane (Carmeliet et al., 2011). After detachment, pericytes change their quiescent phenotype, shorten their processes, increase in volume and begin to proliferate (Ribatti et al., 2011). Meanwhile, ECs loosen their junctions, which in combination with the action of VEGF, increases the permeability of the endothelial layer and allows passage of plasma proteins which lay down ECM (Carmeliet et al., 2011). ECs migrate outward into the new ECM in response to angiogenic factors. They are led by a single EC with high migration and low proliferation rates, known as a ‘tip cell’, which migrates towards a VEGF gradient

(Gerhardt et al., 2003). This VEGF signalling is spatially restricted via pericyte expression of VEGF receptor 1 (Eilken et al., 2017). Neighbouring ECs, called 'stalk cells', fall in behind the tip cell and form the lumen as the growing sprout extends into the avascular area (Carmeliet et al., 2011). Eventually the sprouting branch fuses with a neighbouring branch to form a primitive vessel. In order to stabilize these primitive vessels, pericytes are recruited via signals such as platelet derived growth factor β and B (Geevarghese et al., 2014; A. P. Hall, 2006). Both the newly recruited pericytes and ECs facilitate the maturation process via secretion of paracrine factors, such as transforming growth factor-beta (TGF-β) and ANGPT-1, which promote pericyte re-attachment and endothelial barrier formation, while at the same time suppressing EC proliferation and migration (Allt et al., 2001; Armulik et al., 2011). An illustration of this role pericytes play in angiogenesis can be found in figure 1.10 (Laredo et al., 2019).

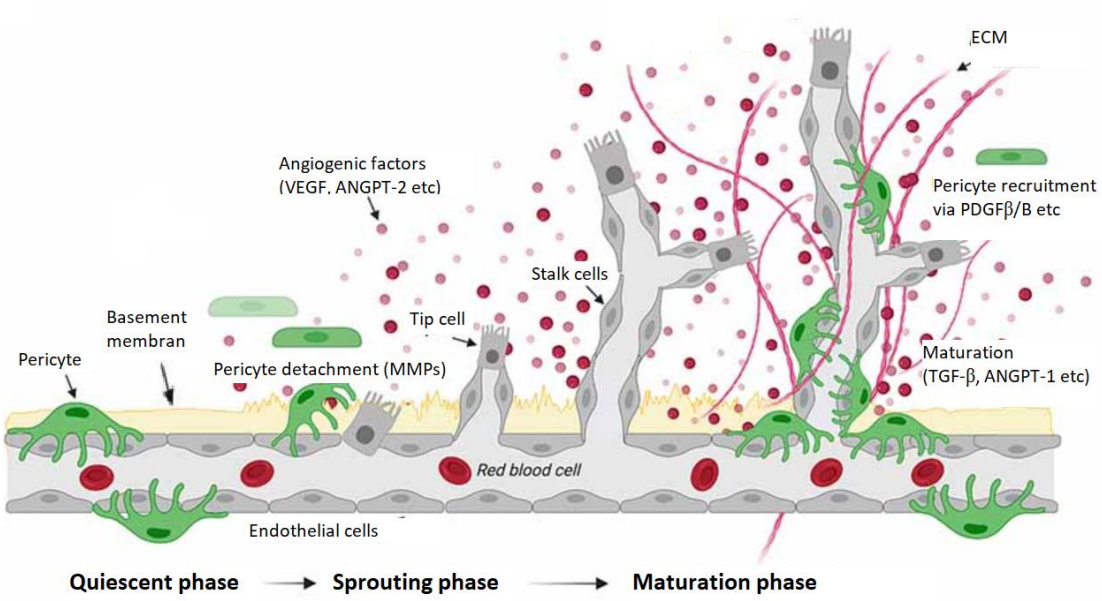

Figure 1.10: Pericytes in angiogenesis. An illustration of the role of pericytes through the different phases of angiogenesis. Angiopoietin-1 (ANGPT-1), angiopoietin-2 (ANGPT-2), matrix metallaproteinase (MMP), platelet derived growth factor β/B (PDGFβ/B), transforming growth factor- β (TGF- β), vascular endothelial growth factor (VEGF), extracellular matrix (ECM). Figure adapted from Laredo et al., 2019.

1.4.3. Differentiation Potential

Pericytes are a multipotent cell type that share part of their origin with MSCs (Mirko Corselli et al., 2013). Pericytes that reside within an established microvasculature are predominantly quiescent, however, they can trans-differentiate into typical cells of the mesenchymal lineage, such as VSMCs, adipocytes, chondrocytes, osteocytes, myocytes, and neural cells (A Birbrair et al., 2013; Alexander Birbrair et al., 2017; Nwadozi et al., 2020). Although studies have identified this multipotent nature of pericytes, it is thought that this capacity may be organ specific and that multipotency is linked to an absence of T-Box transcription factor 18 (Yamazaki et al., 2018; Yianni et al., 2018). Additionally, moderately little is known about the molecular pathways that dictate trans-differentiation in vivo. In some cases, the metabolic state may contribute towards determining pericyte fate. For example, evidence suggests that complete osteogenic differentiation of pericytes is reliant on oxidative phosphorylation and/or oxidant stress (Nwadozi et al., 2020). Pericyte differentiation may also be triggered by tissue injury or disease, and may contribute to regenerative mechanisms (Alexander Birbrair et al., 2015). For example, several studies show the ability of pericytes to differentiate into immune cells, such as dendritic cells and macrophage-like cells, which play an important role in mediating inflammation under pathological conditions (Balabanov et al., 1996; Krautler et al., 2012). It is also known that pericytes demonstrate a strong activated response to ischemia/hypoxia. Following an ischemic stroke, cerebral pericytes may differentiate into neural cells, vascular cells, and microglia, producing all the components of the neurovascular unit (Sakuma et al., 2016). Specifically in relation to vascular tissue engineering, previous data from our group has demonstrated the ability of pericytes to differentiate towards the VSMC lineage in vitro (Avolio, Rodriguez-Arabaolaza, et al., 2015; Campagnolo et al., 2010). In vivo, following sprout formation during angiogenesis, pericytes either return to their quiescent state or trans-differentiate into smooth muscle cells, contributing to capillary arterialisation (Volz et al., 2015). This is driven by transcriptional regulator myocardin in addition to TGF- β - Smad/Notch signalling, that may be triggered by changes in interaction with the basement membrane laminin (Nwadozi et al., 2020). This indicates pericytes possess the capacity to form functional vascular tissue with ability to contract and dilate, which is of specific interest to this project.

1.4.4. Regulation of Blood Flow

Similar to VSMCs, pericytes express contractile-related proteins such as alpha smooth muscle actin (α-SMA), myosin, tropomyosin and vimentin (Bandopadhyay et al., 2001). It is thought that because of these contractile proteins, together with their location around capillaries, pericytes are able to control blood flow in the microvasculature. In the retina, cerebellum and cerebral cortex, pericytes have been shown to modify capillary diameter in reaction to depolarization, neurotransmitter action or neuronal activity (Attwell et al., 2016). This was shown to be an active response as capillary contraction was observed before arteriole contraction (Hall et al., 2014). This ability to contract and control blood vessel tone further outlines the potential pericytes hold for vascular tissue engineering.

1.4.5. Immunomodulation

The ability of pericytes to regulate the immune response is an important property for a regenerative cell type as it opens up the possibility of allogenic cell delivery. The major reason for transplant rejection is the response of the adaptive immune system to alloantigens through activation of T cells (Domev et al., 2014). Activation of T cells is regulated via three signals, antigen presentation via cell surface major histocompatibility complex (MHC) class I or II stimulatory molecules, costimulation with costimulatory molecules and secretion of cytokines (Domev et al., 2014). With regards to these T cell activation pathways pericytes from various sources have been reported to be poorly immunogenic (Domev et al., 2014; Maier et al., 2011). Pericytes do not basally express MHC class II molecules, such as HLA-DR, nor costimulatory molecules CD80/CD86 (Maier et al., 2011). Instead pericytes were found to mediate the formation of suppressive allogeneic CD4+CD25highFoxP3+CD1272 Tregs, regulatory T cells that maintain immunologic self-tolerance, in a TGF-β-dependent and PD-L1-dependent manner (Domev et al., 2014). In addition, even after induction of class I and II MHC molecules, pericytes were unable to stimulate allogeneic CD4 T cell proliferation or cytokine release, and in fact rendered the T cells unresponsive to ECs of the same donor (Maier et al., 2011).

This T cell inhibition has also been identified in retinal pericytes using T cell proliferation assays (Tu et al., 2011). Here it was demonstrated that retinal pericytes were able to

significantly inhibit active T cell proliferation and inflammatory cytokine production. This inhibition was activated through both cell-cell contact and release of factors such as PD-L1 and IL-10. In addition to this the retinal pericytes were able to reduce inflammation induced apoptosis in neighbouring ECs (Tu et al., 2011).

Together these studies indicate that pericytes play an active role in the immune response, which may be harnessed in vascular tissue engineering applications to reduce graft rejection caused by the adaptive immune system. Further detail of this behaviour is summarised in an excellent review by Navarror et al.; however, this area of research is extensive and thus a detailed review of the field was considered outside of the scope of the project aim (Navarro et al., 2016)

1.4.6. Isolation of Pericyte Populations for Clinical Applications

Pericytes have been isolated from several human tissues (Campagnolo et al., 2010; Dellavalle et al., 2007; Maier et al., 2010; S. Nees et al., 2012; Paul et al., 2012; Sarugaser et al., 2005; Shi et al., n.d.; Zannettino et al., 2008); however, not all of these methods or cell populations are suitable for use in clinical applications. For clinical viability it is important that there is a standardized isolation protocol in place that is minimally invasive for the patient and results in a well-characterized and highly pure cell population. Once isolation has been accomplished, pericyte populations are cultured and expanded in vitro until clinically viable numbers have been generated. The process of culturing differs between groups, with many varieties of growth medium and surface coatings used to provide a suitable environment for the pericyte populations (Gokcinar-Yagci et al., 2015). Microscopy, flow cytometry and immunocytochemistry (ICC) can all be used to achieve a stringent phenotypic characterization of the cell population (Avolio, Rodriguez-Arabaolaza, et al., 2015; Campagnolo et al., 2010; M Corselli et al., 2013; Crisan et al., 2008, 2009, 2012; Gokcinar-Yagci et al., 2015). Unfortunately, due to the absence of a unique pericyte marker, this alone is not sufficient to distinguish pericytes from similar cells, such as VMSCs. It is therefore crucial to perform a functional characterization of the cells to supplement the antigenic screening as angiogenic assays can identify pericytes from other mesenchymal cells, such as fibroblasts or bone marrow-derived MSCs, by their enhanced ability to stabilize endothelial networks (Blocki et al., 2013).

1.4.7. Pericytes in Vascular Tissue Engineering

As indicated in the previous section, the unique angiogenic, differentiation and immunomodulation properties of pericytes make them attractive cell source for tissue engineering applications. Indeed, pericytes have already demonstrated exciting results in vascular tissue engineering studies. Carrabba et al. developed a composite PCL-gelatin scaffold functionalised with adventitial pericytes for stimulation of arteriogenesis in peripheral ischemia (Carrabba et al., 2016). 3 weeks after implantation in a mouse limb ischemia model, the cellularised grafts produced an increase in limb blood flow recovery and perivascular arteriogenesis in comparison to control conditions or acellular grafts, highlighting the regenerative effect of pericytes. Similarly, others have demonstrated the efficacy of skeletal muscle pericyte engineered vascular grafts (He et al., 2010). The authors implanted pericyte-seeded bi-layered elastomeric tubular scaffolds into the abdominal aorta of rats. After 8 weeks, analysis of grafts revealed extensive remodelling, including elastin and collagen synthesis and cells expressing typical VSMC markers. Furthermore, patency of grafts was 100% compared to only 38% in unseeded grafts.

Studies from our group have also demonstrated the value of pericytes for neonatal tissue engineering application. Specifically, pericytes with considerable regenerative properties have been successfully isolated and expanded from human cardiac tissue (Avolio, Rodriguez-Arabaolaza, et al., 2015). In vitro studies using these cells have demonstrated their capacity to engraft and penetrate clinical grade CorMatrix patches after static and dynamic cell seeding and conditioning in a bioreactor. Furthermore, in vivo implantation of cardiac pericyte seeded CorMatrix conduits into the left pulmonary artery of 4-week-old piglets was performed in a follow on study (Alvino et al., 2020). Four months after implantation, grafts were analysed. No signs of calcification were detected, and blood flow was measured in the normal range. Moreover, smooth muscle cell and EC infiltration was noted along with the appearance of organised vessel structures in the adventitia that resembled the vasa vasorum. Together, these studies demonstrate the possible benefits of using pericytes for neonatal vascular tissue engineering, A possible caveat to this approach, is the invasive nature of cardiac pericyte isolation. As the authors noted, isolation is performed during initial palliative surgical intervention for CHD correction; however, as we have explained earlier, initial primary correction is now preferred due to the reduction in reoperation rate and other risks associated

with surgery. This leads us to ask, are there more suitable pericyte sources for use in neonatal tissue engineering?

1.4.8. Umbilical Cord: An Ideal Source of Pericytes?

The umbilical cord provides a pathway for blood transport between the foetus and placenta. The full-term cord is on average 50 – 60 cm long and composed of an umbilical vein, which carries oxygen rich blood (mean pO2 of 29.3 mm Hg) from the placenta to the foetal heart, and two umbilical arteries, which carry oxygen depleted blood (mean pO2 of 18.3 mm Hg) back to placenta (Sjöstedt et al., 1960; Spurway et al., 2012). These vessels are embedded within Wharton's Jelly, which is surrounded by an epithelial layer, also known as the amnion (**Figure 1.11;** (Stefańska et al., 2020)). Remnants of the allantois may also be present.

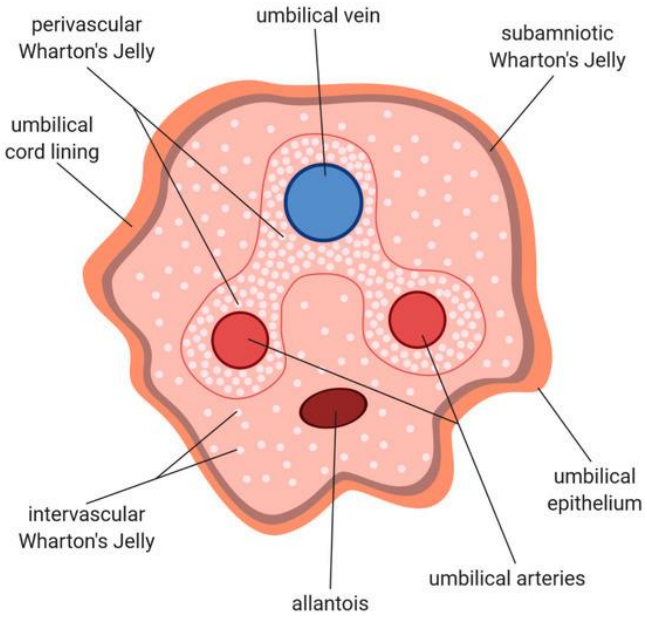

Figure 1.11: Umbilical cord structure. Figure source: Stefańska et al., 2020.

The umbilical cord is discarded at birth and therefore represents an excellent source of autologous cells that can be obtained in a non-invasive manner. The tissue is also abundant in stem cells and progenitor cells that could be used for cardiovascular regenerative medicine (Crisan et al., 2012; Weiss et al., 2006). Indeed, many studies have explored the regenerative

potential of umbilical cord blood MSCs or MSCs isolated from the WJ region of the cord (Abbaszadeh et al., 2020; Jaing, 2014; Kalaszczynska et al., 2015). Alternatively, researchers have identified and isolated a unique population of perivascular cells with exciting possibilities for tissue regeneration applications, including skeletal regeneration and lung repair (Forbes et al., 2020; Montemurro et al., 2011; Sarugaser et al., 2009; Tsang et al., 2013). Furthermore, Crisan et al. demonstrated the presence of a pericyte layer within the umbilical artery (Crisan et al., 2012).

Together, these studies indicate that umbilical cord tissue contains pericytes that could offer similar regenerative potential to cardiac pericytes. These cells may be preferable to cardiac pericytes for use in neonatal tissue engineering in CHD correction due to the non-invasive way they can be harvested. Moreover, prenatal diagnosis of CHD allows preparation for extraction of cells at birth, and subsequent expansion to develop engineered grafts in time for primary repair of ToF, which should be performed at age 3 – 12 months (Van Arsdell et al., 2000).

1.5. Rationale for Thesis

CHD is the most prevalent congenital abnormality, affecting approximately 1% of new-borns globally, with incidence rate seemingly increasing over the last 50 years (Liu et al., 2019). Although prognosis has significantly improved, CHD remains one of the primary causes of perinatal mortality, accounting for over 250,000 deaths in 2017 (Zimmerman et al., 2020). Complex malformations such as ToF often require immediate surgical correction using a prosthetic graft. Unfortunately, current grafts have limitations and need to be substituted through repeated interventions due to pathologic remodelling and failure (Avolio, Caputo, et al., 2015; Erikssen et al., 2015).

In recent years, engineering of prosthetic grafts with regenerative cells, such as MSCs, has emerged as a potential solution (Bajpai et al., 2012; Mantakaki et al., 2018). However, MSCs represent a heterogeneous population characterized by wide diversity across different tissue sources. Evidence from our group and others have highlighted the potential advantage of using more homogeneous perivascular mesenchymal populations, such as microvascular and adventitial pericytes, for applications of vascular regenerative medicine (Cathery et al., 2018; Gomez-salazar et al., 2020). Moreover, we demonstrated the feasibility of reconstructing the

pulmonary artery of piglets using grafts engineered with pericytes immunosorted from cardiac tissue (Alvino et al., 2020). Cardiac pericytes attract ECs and produce ECM proteins, which may help to alleviate the limitations of the acellular technology. Nonetheless, the use of heart-derived cells is only compatible with a two-stage intervention – an invasive harvesting followed by implantation – with risks superior to an immediate correction approach (Arenz et al., 2013; Gerrah et al., 2015; Pigula et al., 1999). An alternative cell population from an easily accessible tissue would therefore offer obvious advantages over cardiac pericytes.

1.5.1. Aims and Objectives

In this present study, we aimed to explore the feasibility of isolating antigenically pure pericytes from the umbilical cord to generate autologous pericyte-engineered grafts for correction of ToF. We hypothesized that umbilical cord pericytes (UCPs) could mimic the promising results we have seen with cardiac pericytes; however, with the advantage that UCPs can be acquired immediately after birth without the use of invasive surgery. By seeding UCPs onto CorMatrix, a clinically approved scaffold with potential for rapid commercialization, and conditioning in a bioreactor we could create a functional vascular graft that could overcome current limitations. The native regenerative properties of pericytes may facilitate integration and remodelling of the CorMatrix conduit over time, resulting in a graft that will match the somatic growth and provide a definitive treatment of the congenital defect.

The following experimental objectives were adopted to test the above theory:

1. Develop an efficient protocol for isolation and expansion of UCPs from the umbilical cord.
2. Characterise the angiogenic and vascular differentiation capabilities of UCPs to confirm suitability for vascular tissue engineering.
3. Explore the ability of UCPs to support non-pathological remodelling of the extracellular environment.
4. Demonstrate that UCPs can engraft into acellular CorMatrix scaffolds, promoting ECM remodelling and improving graft mechanical properties.

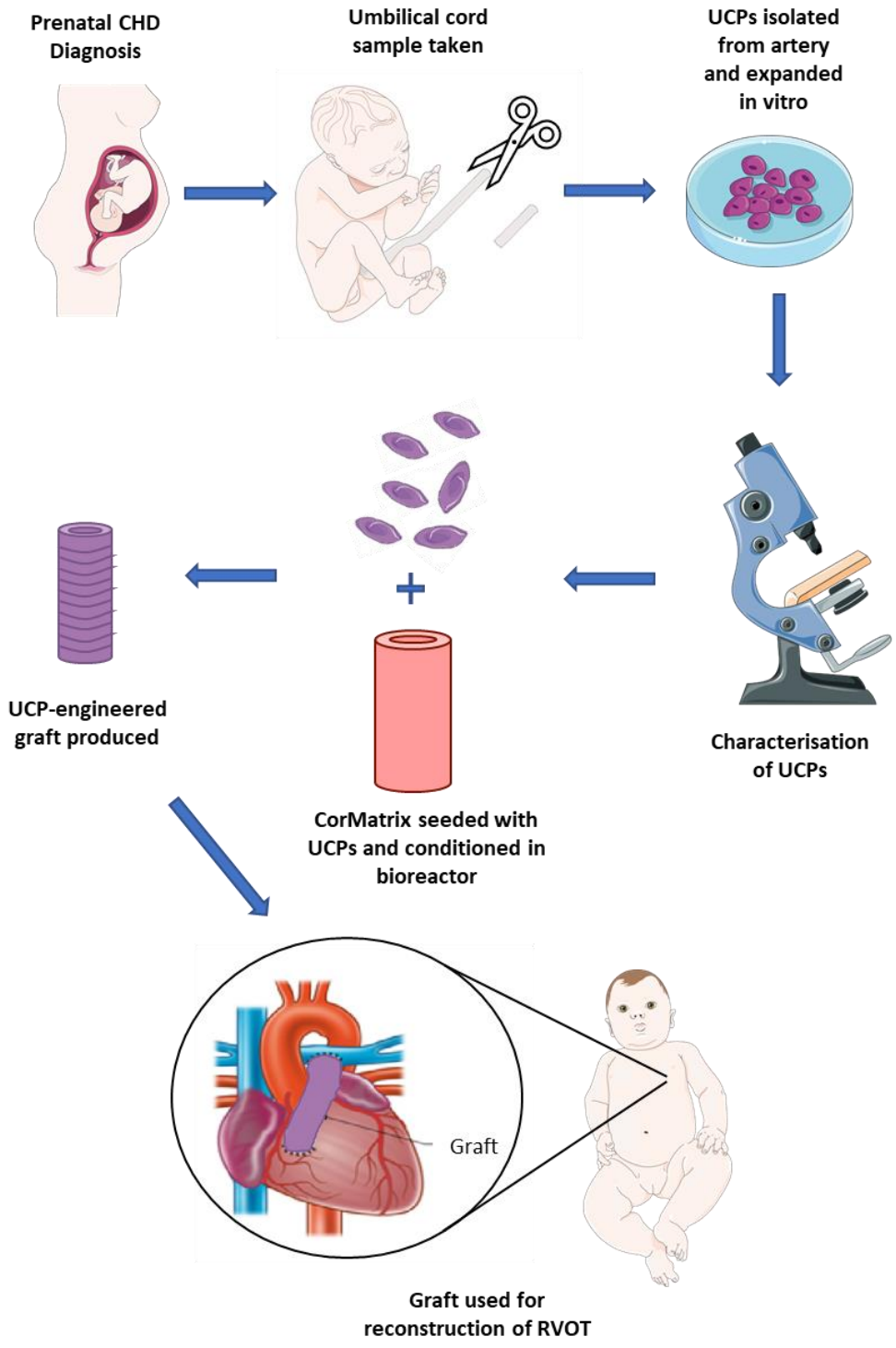

Figure 1.12: Flow diagram of project aim. Congenital heart disease (CHD), umbilical cord pericytes (UCP), right ventricular outflow tract (RVOT). Figure adapted from smart.servier.com

2. Methods and Materials

2.1. Ethics

Full-term human umbilical cord samples were obtained with informed consent from St. Michael's Hospital, Bristol, UK. Their use throughout the project was approved by the Southwest Research Ethics Committee (license 11/HO107/4) and conformed to the principles outlined in the Declaration of Helsinki.

2.2. Cell Culture

Unless otherwise specified, cells were cultured in endothelial cell basal medium-2 (EBM-2; PromoCell) supplemented with endothelial cell growth medium-2 supplement mix (PromoCell), comprising of final concentrations of 2% foetal bovine serum (FBS), 5 ng/ml recombinant human epidermal growth factor (EGF), 10 ng/ml recombinant human bFGF, 20 ng/ml insulin-like growth factor (R3 IGF-1), 0.5 ng/ml recombinant human VEGF 165, 1 ug/ml ascorbic acid, 22.5 ug/ml heparin and 0.2 ug/ml hydrocortisone. For brevity, this medium is referred to as endothelial cell growth medium-2 (EGM-2) throughout this thesis. Unless specified, all media was pre-warmed to 37 °C before use and replenished every 2-4 days. Additionally, all media contains phenol red for indication of pH.

All cell culture practices were performed under a class II microbiology safety cabinet using sterile protocol. Unless otherwise specified, all cells were cultured in a standard incubator and maintained at 37ºC/5% CO_2. Culture flasks and plates were obtained from Greiner Bio One.

Note that some of the purchased cell lines were expanded in different culture media than primary pericytes, as per manufacturer guidelines. The different culture media have different levels of serum and different combinations of growth factors, which affects the cell phenotype. To reduce the effect of culture media on comparative experiments, where possible a single type of media was used for all cells; however, the effect of culture media on cell behaviour cannot be eliminated entirely.

2.2.1. Umbilical Cord Pericyte (UCP) and Placental Pericyte (PLP) Culture and Subculture

Foetal pericyte cell lines were initially isolated from the umbilical arteries and placenta tissue using the methods developed and detailed in section 3.3. After reaching confluence, cells were washed once with Dulbecco's Phosphate-Buffered Saline (DPBS; Thermo Fisher Scientific) and incubated with trypsin-ethylenediaminetetraacetic (EDTA) (0.05% (w/v) trypsin, 0.02% (w/v) EDTA) at 37ºC/5% CO_2 for 2 – 4 minutes, with gentle agitation every 2 minutes. Trypsin

is a proteolytic enzyme which cleaves peptide chains in the focal adhesions that anchor cells to the culture dish. EDTA is a calcium chelator which assists the cell detachment process by weakening cell-cell and cell-matrix interactions. Once all cells were disassociated, EGM-2 was added to the trypsin-EDTA-cell suspension at a ratio of 2:1 to deactivate the trypsin. The suspension was then centrifuged at 300g for 5 – 10 minutes at room temperature (RT), the supernatant was removed, and the cell pellet resuspended in EGM-2. Cells were split 1:3 and cultured in EGM-2, on tissue culture plastic precoated with 0.01% bovine gelatin and 10ug/ml fibronectin in DPBS. Gelatin and fibronectin were added to improve cell adhesion as cells seeded on uncoated plastic was observed to detach and spontaneously form spheroid-like structures. Cells were used for experiments between passage 3 and passage 7.

2.2.2. Human Umbilical Vein Endothelial Cell (HUVEC) Culture and Subculture

Pooled HUVECs were purchased from Lonza. HUVECs were cultured and split using a similar protocol to UCPs and PLPs. The only exception to this was that culture surfaces were coated with 0.5% bovine gelatin before cells were seeded. Cells were used for experiments between passage 4 and passage 6.

2.2.3. Normal Human Dermal Fibroblast (NHDF) Culture and Subculture

Adult NHDFs were purchased from Lonza. Cells were cultured in fibroblast growth medium-2 (Lonza), comprised of fibroblast basal medium supplemented with FGM™-2 Fibroblast SingleQuots™ Kit (human bFGF, Gentamicin-Amphotericin (GA-1000), 2% FBS and insulin). Passaging of cells followed the same protocol as UCPs and PLPs. Cells were cultured on uncoated surfaces and used for experiments between passage 3 and 7.

2.2.4. Human Pulmonary Artery Smooth Muscle Cell (HPASMC) Culture and Subculture

HPASMC were purchased from PromoCell. Cells were cultured in smooth muscle basal medium 2 supplemented with smooth muscle cell growth medium 2 supplement mix (PromoCell), comprising of final concentration of 5% FBS, 0.5ng/ml EGF, 2ng/ml bFGF and 5ug/ml recombinant human insulin. Cell passaging followed the same protocol as UCPs and PLPs. Cells were cultured on uncoated surfaces and used for experiments between passage 3 and 7.

2.2.5. Mesenchymal Stem Cell (MSC) Culture and Subculture

Umbilical cord matrix/WJ human MSCs were purchased from PromoCell and expanded in mesenchymal stem cell growth medium 2 (PromoCell) for generation of frozen stocks. MSCs were cultured on uncoated surfaces and passaged using the same protocol as UCPs and PLPs. Cells were used for experiments between passage 3 and passage 7.

2.2.6. Human Embryonic Kidney 293T cell (HEK293T) Culture and Subculture

HEK293Ts were cultured in Dulbecco's modified eagle medium (DMEM; Thermo Fisher Scientific; [+] 4.5g/L D-Glucose, L-Glutamine [+] Pyruvate) supplemented with 10% (v/v) FBS. To passage, HEK293Ts were washed very gently in DPBS and incubated with trypsin-EDTA for 1 min. After 1 min, medium was added to neutralise the trypsin and cells were centrifuged at 300g for 5 minutes at RT. HEK293Ts were split 1:6 and cultured on uncoated surfaces. Cells were used for experiments between passage 10 and passage 25.

2.2.7. Cryopreservation and Resuscitation

Confluent cell monolayers were detached from culture plastic as previously described in 2.2.1-2.2.6. After centrifugation, cell pellets were resuspended in freezing medium. For HEK293T cells, freezing medium comprised of 50% (v/v) DMEM, 40% (v/v) FBS and 10% (v/v) dimethyl sulphoxide (DMSO; Sigma Aldrich); a cryoprotectant that stops intracellular and extracellular ice crystals forming during the freezing process. For all other cell types, freezing medium comprised of 10% (v/v) DMSO in FBS. The cell suspension was transferred to a cryovial and placed in a CoolCell freezing container at -80^{o}C. The freezing container ensures the cells are frozen at a steady rate of -1^{o}C/minute, which further reduces the chance of ice crystals forming. After 24 hours, cells were transferred into liquid nitrogen for long-term storage.

To thaw cells, vials were transferred to a 37^{o}C water bath and rapidly warmed. Cells were then cultured as previously described, and the medium was replenished after 24 hours to remove the remaining DMSO.

2.2.8. Cell Counting

After detaching cells and resuspending them in 1ml of medium, cells were counted using a Neubauer haemocytometer. Briefly, 10µl of cell suspension was mixed 1:1 with 0.4% (w/v) trypan blue solution; a blue dye which only permeates dead cells. 10µl of this solution was then inserted into a Neubauer haemocytometer and unstained live cells counted in the four large

corner squares, each measuring 1mm^2. The number of cells was calculated using the following formula:

$$Concentration\left(\frac{cells}{ml}\right) = \frac{Cell\ count\ \times\ 10{,}000\ \times\ dilution\ factor}{number\ of\ squares\ counted}$$

Where number of squares counted = 4, and the dilution factor =2, this becomes:

$$Concentration\left(\frac{cells}{ml}\right) = Cell\ count\ \times\ 5000$$

2.3. Histology

Foetal tissue was analysed in order to understand the structure of the umbilical cord and placenta tissue and identify pericytes location within the tissue. Additionally, pericyte-seeded CorMatrix vascular grafts were histologically analysed for cellular presence and extracellular protein deposition. The following protocols were utilised for complete characterisation of grafts and tissue.

2.3.1. Preparation of Samples

Samples were initially washed in phosphate-buffered saline (PBS) and then either fixed in 4% paraformaldehyde (PFA) for 24 hours at 4^{o}C or immediately snap frozen in optimal cutting temperature compound (OCT; VWR International) and stored at -80^{o}C. After fixation, samples were either embedded in paraffin or transferred to 30% (w/v) sucrose in PBS. The sucrose solution acts as a cryoprotectant, dehydrating the tissue so that ice crystals do not form during freezing. After 24 hours, once samples had been dehydrated, they were frozen in OCT and stored at -80^{o}C for further analysis.

Frozen tissue slides were prepared by cutting 8µm sections using a CryoStar NX50 cryostat (Thermo Fisher Scientific), set to -20^{o}C, and mounted onto Superfrost Plus slides (Thermo Fisher Scientific) before storing at -80^{0}C. Paraffin embedded tissue slides were prepared by cutting 5um section using a Shandon Finesse 325 microtome (Thermo Fisher Scientific) and mounting on Superfrost Plus slides. Slides were stored at RT.

2.3.2. Haematoxylin and Eosin (H&E) and Verhoeff's Van Geison (EVG)

H&E staining was used to visualise tissue structure and cell distribution. Haematoxylin stains cell nuclei blue and eosin stains the cell cytoplasm and ECM pink.

EVG was used for the analysis of elastin deposition in pericyte-seeded CorMatrix (CorMatrix Cardiovascular) vascular grafts. This technique uses an iron-haematoxylin stain which is specific for elastic fibres and a counter stain for collagen. The elastin is stained black whilst collagen and cell cytoplasm are stained red and yellow, respectively.

Slides were stained using a Shandon Varistan 24-4 slide stainer (Thermo Fisher Scientific).

2.3.3. Mallory's Trichrome Stain

Mallory's trichrome staining was used to visualise the collagen content of grafts. Collagen is stained blue, nuclei bright red and muscle orange to red. Slides were washed in distilled water (ddH_2O) and then incubated for 1 hour in 0.1% Azocarmine G solution at 60°C. Following incubation, slides were left to cool for 10 minutes and washed in ddH_2O before incubating in 5% Phosphotungstic Acid for 90 minutes at RT. Slides were then washed again in ddH_2O and incubated in Mallory solution for up to 2 hours. Finally, slides were washed again in ddH_2O before mounting coverslips using DPX mounting medium (Sigma-Aldrich).

2.3.4. Immunohistochemistry (IHC)

OCT embedded tissue sections were used for IHC. Slides were briefly thawed at RT. Snap frozen tissue sections were fixed in cold acetone at -20°C for 5 minutes and air dried for 20 minutes. Tissues that were already fixed in 4% PFA were not processed with acetone. Slides were hydrated in PBS for 10 minutes and permeabilised with 0.01% Triton-X100 (Sigma-Aldrich) in PBS for 10 minutes at RT. After washing with PBS (2 x 5 minutes), non-specific binding sites were blocked using 5% FBS in PBS for 30 minutes at RT. Primary antibodies (**Table 2.1**) were incubated overnight at 4°C, followed by either donkey anti-sheep alexa fluor 488, goat anti-mouse alexa fluor 568 or goat anti-rabbit alexa fluor 647 (1:200; all Life Technologies) for 60 minutes at RT in the dark. Sections were counterstained using DAPI and mounted using Fluoromount G (Thermo Fisher Scientific). Images were taken using a Zeiss Observer.Z1 microscope and processed using Zen Pro and ImageJ software packages.

Table 2.1: List of primary antibodies used for immunohistochemistry. αSMA = alpha smooth muscle actin, CD = cluster of differentiation, NG2 = neural/glial antigen.

Antibody	Dilution	Host Species	Supplier
αSMA	1:100	Mouse	DAKO (M0851)
CD31	1:100	Mouse	R&D systems (BBA7)
CD34	1:100	Sheep	R&D systems (AF7227)
CD146	1:50	Rabbit	Abcam (ab75769)
NG2	1:50	Rabbit	Millipore (AB-5320)
Vimentin	1:400	Rabbit	Abcam (ab92547)

2.4. Immunocytochemistry (ICC)

ICC was used for the initial characterisation of isolated cell lines, the evaluation of phenotypic change during vascular smooth muscle differentiation studies, and to detect cell derived ECM. The staining protocol was the same for all studies except for the choice of antibody (**Tables 2.2 – 2.4**).

Adherent cells and decellularised monolayers were washed with PBS (1x 3 minutes) and fixed with 4% (w/v) PFA for 10 - 15 minutes at 4°C. Fixed cells were washed with PBS (3x 3 minutes) and blocked for 30 – 60 minutes with blocking solution (either 5% FBS in PBS or 5% normal goat serum in PBS). This step reduces unspecific binding of antibodies to other proteins expressed by the cells. For detection of intracellular antigens, cells were permeabilised prior to blocking using 0.1% (v/v) Triton-X100 in PBS for 10 minutes at 4°. Cells were incubated with primary antibodies diluted in blocking solution overnight at 4°C on a see-saw plate rocker. Specific antibodies and dilutions can be found in **Tables 2.2 – 2.4**. After incubation, cells were washed with PBS (3x 3 minutes) and then incubated with secondary antibodies (1:200; goat anti-rabbit alexa fluor 488 or goat anti-mouse alexa-fluor 488 depending on primary host species; both Life Technologies) at RT in the dark, on a see-saw plate rocker. After 1 hour, cells were washed in PBS (3x 3 minutes) and counterstained with DAPI (1:1000). Finally, cells were washed once more in PBS and mounted with Fluoromount G to improve prolonged

storage of stained cells. Images were acquired using a Zeiss Observer.Z1 microscope and processed using Zen Pro and ImageJ software packages. Unstained and no primary controls were included for all studies. Cells were stored at 4^{o}C in the dark.

Table 2.2: List of primary antibodies used for initial phenotypic characterisation. CD = cluster of differentiation, GATA4 = GATA binding protein 4, NANOG = homeobox protein NANOG, NG2 = neural/glial antigen 2, OCT4 = octamer binding transcription factor 4, SOX2 = sex determining region Y-box 2, VECAD = vascular endothelial cadherin.

Antibody	Dilution	Permeabilise	Host Species	Supplier
CD31	1:50	No	Mouse	R&D systems (BBA7)
CD34	1:50	No	Mouse	DAKO (7165)
CD146	1:100	No	Rabbit	Abcam (ab75769)
GATA4	1:100	Yes	Rabbit	Abcam (ab61767)
NANOG	1:100	Yes	Rabbit	Abcam (ab80892)
NG2	1:50	No	Rabbit	Millipore (AB-5320)
OCT4	1:100	Yes	Rabbit	Abcam (ab18976)
SOX2	1:100	Yes	Rabbit	Millipore (AB5603)
VECAD	1:50	Yes	Mouse	Santa Cruz (SC-9989)
Vimentin	1:400	Yes	Rabbit	Abcam (ab92547)

Table 2.3: List of primary antibodies used for vascular smooth muscle differentiation studies. aSMA = alpha smooth muscle actin, MKI67 = marker of proliferation Ki-67, NMMyoIIB = non-muscle myosin IIB, SM-MHC = smooth muscle myosin heavy chain.

Antibody	Dilution	Permeabilization	Host Species	Supplier
aSMA	1:100	Yes	Mouse	DAKO (M0851)
Calponin	1:100	Yes	Rabbit	Abcam (ab46794)
Ki-67 (MKI67)	1:100	Yes	Mouse	DAKO (M7240)
NMMyoIIB	1:200	Yes	Rabbit	Abcam (ab204358)
SM-MHC	1:100	Yes	Rabbit	Abcam (ab53219)
Transgelin	1:50	Yes	Mouse	Santa Cruz (sc-271719)

Table 2.4: List of primary antibodies used for ECM studies.

Antibody	Dilution	Permeabilization	Host Species	Supplier
Collagen I	1:100	Yes	Rabbit	Chemicon (AB745)
Fibronectin	1:200	Yes	Rabbit	Abcam (ab299)
Laminin	1:100	Yes	Rabbit	Abcam (ab11575)

2.5. Flow Cytometry

The purity of isolated pericytes was evaluated by analysing the antigenic expression profiles of individual cell lines using flow cytometry. Cell lines were analysed as soon as sufficient cell numbers were obtained (passage 3/4). Suitable cell lines were expanded and used for further experimentation.

Confluent cells (>1 million cells) were washed once with DPBS and removed from flasks with trypsin/EDTA solution. Cells were centrifuged at 300g for 10 minutes before washing the cell pellet with 2ml DPBS and repeating the centrifuge step. The cell pellet was then resuspended in 400 – 800µl DPBS, depending on the number of staining and control tubes included (200,000 cells/tube). 100µl was transferred to tube 1 (unstained control) and tube 2 (live/dead control). The remaining solution was transferred to tube 3 (staining tubes). 100µl of fluorescence activated cell sorting (FACS) buffer (1% (w/v) bovine serum albumin (BSA; Sigma-Aldrich) plus 1mM EDTA in DPBS) was added to tube 1, which was then stored until analysis at 4^{o}C. 50µl from tube 2 was heated at 95^{o}C for 5 minutes to kill the cells before returning to them to the tube. Zombie NIR Fixable Dye (Biolegend) was added to tube 2 and 3 at a concentration of 1:100 and incubated for 20 minutes at RT in the dark. Zombie NIR Fixable Dye is only permeant to cells with compromised membranes and is therefore included to stain non-viable cells. Cells were washed with FACS buffer and centrifuged to obtain a pellet. Tube 2 was resuspended with 200 µl buffer and stored until analysis at 4^{o}C. Tube 3 was incubated with Human Fc Receptor Binding Inhibitor (eBioscience) at a dilution of 1:5 in FACS buffer and incubated for 20 minutes at RT. After 20 min, 50µl was transferred to each staining tube and 50µl of antibody mixture added to each tube (**Table 2.5**). After 30 minutes incubation in the dark at 4^{o}C, cells were washed with FACS buffer, centrifuged, and resuspended in 200µl buffer ready for analysis.

Unstained and live/dead control tubes allowed gating of positive cells and exclusion of non-viable cells. Fluorescence minus one (FMO) controls were included for fluorophores PE and PerCP in 3 cell lines. FMO controls allow detection of any signal spread into the channel of interest when using multiple fluorophores in a single staining tube. For example, if no PE signal was detected in the unstained control, however, a weak PE signal was detected in one of the staining tubes which included PE, FITC, PerCP, APC and PE-Cy7, this may be due to spread of another fluorophore being falsely identified as PE. To exclude this possibility, an FMO control is established with all fluorophores bar the one of interest, PE, included. Any increase

in signal with PE included is measured against this control. FMOs were only included for PE and PerCP as the increase in signal intensity for positively stained cells was small for these fluorophores and some overlap was observed. For full fluorophore spectrum and Novocyte excitation channels see appendix A. HUVEC were analysed as a positive control for endothelial markers. Analysis was completed using a Novocyte 3000 Flow Cytometer System (ACE Bioscience) and FlowJo software package. Compensation beads (BD) were used to determine voltage and gating parameters for each fluorophore. The compensation matrix was applied to each sample during analysis.

Table 2.5: List of antibodies used for flow cytometry. PDGF-B = platelet derived growth factor receptor beta. Normal staining panels consisted of CD31/NG2/CD105/CD45/CD73 or CD34/PDGFR-B/CD44/CD146/CD90.

Antibody	Fluorophore	Dilution	Supplier
CD31	FITC	1:10	BD (555445)
CD34	FITC	1:20	Miltenyi (130-081-001)
CD44	APC	1:500	eBioscience (17-0441-32)
CD45	PerCP-Cy5.5	2:25	Miltenyi (130-094-975)
CD73	PE-Cy7	3:100	BioLegend (344010)
CD90	PE-Cy7	3:100	BioLegend (328124)
CD105	APC	1:25	Life Tech (MHCD10505)
CD146	PerCP-Cy5.5	1:10	R&D Systems (FAB932C)
NG2	PE	1:20	BD (562415)
PDGFR-B	PE	3:100	BioLegend (323606)
Zombie NIR Fixable Dye	APC-Cy7	1:100	BioLegend (423105)

2.6. Doubling Time and Viability

To evaluate the expansion capacity and condition of isolated cell lines, an assessment of doubling time and viability was completed.

Cells were seeded in duplicate in a 6-well plate at a density of 30,000 cell per well (~3000 cells/cm^2) on day 0. On day 4, 5, 6 and 7, cells were detached and counted as previously described in method 2.2.8 using trypan blue staining of non-viable cells. Cells were all cultured in their respective expansion media listed in section 2.2.

For calculation of doubling time, a growth curve was generated, plotting number of live cells against time in days. The doubling time was then determined using the following formula, where N_o and N_t represent the number of live cells at the beginning and end of the log phase of cell growth respectively, and t represents time in hours:

$$growth\ rate = \frac{\ln\left(\frac{N_t}{N_o}\right)}{t}$$

$$doubling\ time = \frac{\ln(2)}{growth\ rate}$$

Viability was calculated at each time point using the following formula:

$$Viability\ (\%) = \frac{number\ of\ live\ cells}{number\ of\ total\ cells}\ x\ 100$$

2.7. Secretome Characterisation by Enzyme-Linked Immunosorbent Assay (ELISA)

Conditioned medium (CM) was collected from cells for analysis as follows: Cells were seeded at a density of 200,000 per T25 and cultured in full EGM-2 until roughly 80% confluence. Medium was then removed, and cells were washed with DPBS. 2.5ml of conditioning medium (EGM-2 with FBS and VEGF excluded from the supplement kit) was added to each T25 flask before incubating for 48 hours.

Cells were conditioned in both hypoxia (2% O_2) and normoxia (20% O_2). After 48 hours, medium was removed and centrifuged at 500g for 10 minutes at RT. The supernatant was collected and stored at -80ºC until analysis. Cells were counted as in method 2.2.8 and the number recorded for normalisation of data.

Anti-human ELISA kits (R&D Systems) were used to measure the levels of ANGPT-1 (DY923), ANGPT-2 (DY623), VEGF-A (DY293B), stromal derived factor 1 (SDF-1; DY350), hepatocyte growth factor (HGF; DY294) and monocyte chemoattractant protein-1 (MCP-1; DY279) in CM. Briefly, high binding 96-well plates (greiner bio-one) were incubated with kit specific capture antibody overnight. Plates were washed with wash buffer (0.05% Tween 20 in PBS) and blocked with kit reagent diluent (1% BSA in PBS) for 1 hour. Plates were then incubated for 2 hours with CM, control medium or the standard. After 2 hours, plates were washed with wash buffer and incubated for 2 hours with kit specific detection antibody. The wash step was repeated before incubating plates with kit Streptavidin-horseradish peroxidase (HRP). Finally, plates were washed and incubated with kit colour substrate reagent for up to 20 minutes before stopping the reaction with kit stop solution and measuring the optical density on a Dynex Opsys MR microplate reader set to 450nm. For step-by-step protocol details and dilutions, see manufacturer's instructions and certificate of analysis. Quantities were normalised by number of cells and hours conditioned.

2.8. Angiogenesis

Cells were assessed for their ability to promote angiogenesis using the following in vitro assays. The medium collected in method 2.7 was used for analysis of CM, and a control medium of EGM-2 with FBS and VEGF excluded from the supplement kit was included.

2.8.1. Matrigel Tube Formation Assay

A 96-well plate was coated with 40µl of Matrigel (BD Biosciences). To evaluate the angiogenic properties of CM, 10,000 HUVECs were seeded onto the Matrigel coated wells and then incubated with either EGM-2 (positive control), CM or control medium. To directly assess the angiogenic effect of cells, isolated pericytes were seeded alone (10,000/well) or in co-culture with HUVECs (2,500 isolated pericytes, 10,000 HUVECs), in EGM-2. After 6 hours incubation, tube formation was imaged under brightfield at 50x.

2.8.2. Fibroblast-Endothelial Co-culture Angiogenesis Assay

A fibroblast-EC co-culture assay was utilized as an alternative method to evaluate the angiogenic capacity of cells. The assay was adapted from a previously published method (Hetheridge et al., 2011; Richards et al., 2016).

For analysis of CM, NHDFs were seeded in a 96-well plate (4,000 cells/well) and cultured over 5 days until a confluent monolayer had formed. HUVECs were then seeded (4,000 cells/well)

in either CM, control medium or EGM-2 (positive control). A 96-well plate was used to limit the volume of CM used. After 6 days incubation, replenishing the medium every 2 days, co-cultures were washed with PBS (1 x 3 minutes) and fixed with 4% PFA for 10 minutes at 4ºC.

The angiogenic effect of cells in co-culture with ECs was also assessed. Similar to above, NHDFs were seeded in a 24-well plate (16,000 cells/well) and cultured over 5 days until a confluent monolayer had formed. In parallel, cells of interest were expanded and labelled with DsRED via lentiviral transduction, as described in method 2.9. HUVECs (16,000 cells/well) and cells of interest (4,000 cells/well) were then added to the wells and incubated in EBM-2 supplemented with 10% FBS. HUVECs were seeded alone in EBM-2 (10% FBS) as a control. The FBS content of the medium was optimised so that a low level of endothelial network formation was observed in the control condition. After 6 days incubation, refreshing the medium every 2 days, co-cultures were washed with PBS (1 x 3 minutes) and fixed with 4% PFA for 10 minutes at 4ºC.

Following fixation, wells were washed again with PBS (3 x 3 minutes) before blocking with 5% FBS in PBS and incubating overnight at 4ºC with anti-CD31 antibody (1:200, R&D Systems) in blocking buffer. After incubation, wells were washed with PBS (3 x 3 minutes) and incubated for 1 hour at RT with anti-mouse alexa fluor 488 (1:200; Life Technologies). Images were acquired at 200x or 25x using a Zeiss Axio Observer.Z1 microscope and analysed with ImageJ. Results were normalised by control conditions to account for any inherent differences in HUVEC cell lines ability to form endothelial networks.

2.9. Lentiviral Cell Labelling

For certain assays, cells were modified to express a green fluorescent protein (GFP) or DsRED sequence, which enabled specific tracking of cells during an experiment. Constructs were prepared using the pLVX plasmid shown in **Figure 2.1**, containing either a GFP or DsRED sequence under the control of a CMV promotor.

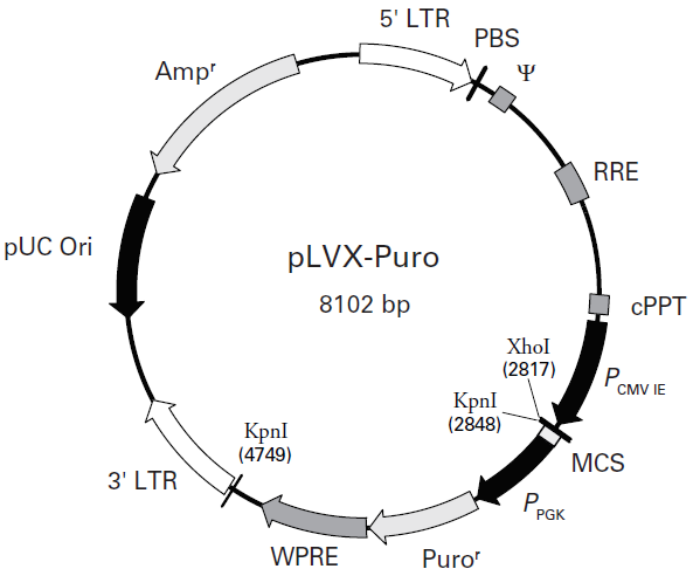

Figure 2.1: Lentiviral expression vector map. pLVX-Puro vector contains a multiple cloning site (MCS) for expression of protein of interest, driven by a CMV promoter. Puro^r provides puromycin resistance for selection of stable transductants and Amp^r provides *E.coli* ampicillin resistance for bacterial selection. All elements necessary for production of replication-incompetent lentivirus are included. For further information see appendix B.

2.9.1. Plasmid Transformation

To replicate constructs, high-efficiency chemically competent Stbl2 *E. coli* were transformed with the pLVX plasmid. 20µl of Stbl2 *E. coli* were mixed with 10µl of the plasmid and incubated on ice for 15-30 minutes. After incubation, Stbl2 *E. coli* were heat shocked at 42°C for 45 seconds to allow the plasmid to enter the bacteria and returned to the ice for 2 minutes. 200µl of LB broth was added to the bacteria, which were then placed in a shaking incubator at 35°C and 180rpm for up to 1 hour. This allowed the bacteria sufficient time to express the

ampicillin resistance gene included in the plasmid. Bacteria were then cultured overnight at 35ºC on agar plates supplemented with 100ng/ml ampicillin. Only transformed bacteria with the ampicillin resistance gene formed colonies, which cultured overnight in 200ml of LB broth supplemented with 100ng/ml ampicillin in a shaking incubator at 35ºC and 180rpm. Plasmids were purified using Qiagen Plasmid Maxi kit following manufacturer's instructions. Briefly, the bacterial culture was centrifuged (6000g, 15 minutes, 4ºC) and resuspended in 10ml of kit P1 Buffer. Following this, the suspension was mixed with kit P2 buffer (10ml, 5 minutes, RT) and kit P3 buffer (10ml, 20 minutes, on ice) sequentially. The suspension was then centrifuged (20,000g, 30 minutes, 4ºC) and the supernatant added to a QIAGEN-tip equilibrated with 10ml of kit QBT Buffer. After emptying by gravity flow, the QIAGEN-tip was washed (2 x 30ml kit QC Buffer) and DNA eluted in 15ml of kit QF Buffer. DNA was precipitated by adding 10.5ml of isopropanol, centrifuging (15000g, 30 minutes, 4ºC) and discarding the supernatant. The DNA pellet was then washed with 5ml of 70% ethanol, centrifuged (15000g, 10 minutes, 4ºC), and supernatant discarded before redissolving the DNA in TE Buffer.

2.9.2. Transfection and Production of Lentivirus

HEK293T were used as host cells to produce the lentiviral particles. Cells were seeded in a 6cm petri dish and cultured until 70% confluence before transfecting. 7ug pLVX-Puro with GFP or DsRED insert, 0.93ug VSV-G expressing envelope plasmid and 1.86ug psPAX.2 lentiviral packaging vector were diluted in 700µl optimem (Thermo Fisher Scientific) supplemented with 10µl PLUS™ reagent. 20µl Lipofectamine™ LTX reagent (Thermo Fisher Scientific) was diluted in 700µl optimum, combined with diluted plasmids, and incubated at RT for 5 minutes. HEK293T were then washed with optimem and incubated overnight with the lipofectamine-plasmid suspension. After 12-16 hours incubation, once fluorescence was observed as in **Figure 2.2**, medium was changed to EGM-2 and left for 48 hours before collecting the supernatant containing lentiviral particles. The lentiviral medium was then filtered through a 0.22um mesh and stored at -80°C.

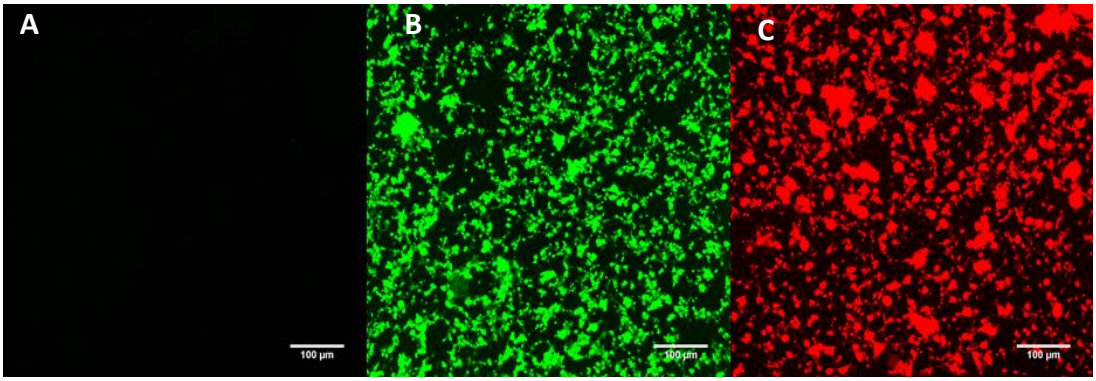

Figure 2.2: HEK293T Transfection Efficiency. A) Non transfected HEK293T. B) HEK293T transfected with pLVX-Puro containing GFP insert. C) HEK293T transfected with pLVX-Puro containing DsRED insert. Scale bar = 100um. Images were acquired using a Zeiss Axio Observer.Z1 fluorescence microscope.

2.9.3. Transduction

HUVEC, foetal cell lines and MSC were expanded to 60-70% confluency in EGM-2 before transducing with lentiviral medium supplemented with 10ug/ml polybrene, which enhances the lentiviral infection efficiency. Cells were incubated for 24 hours at 37°C/5% CO_2 before washing cells and exchanging the medium with fresh EGM-2. After 24-48 hours, cells began to express either GFP or DsRED depending on the insert used (**Figure 2.3**). Following this, cells were expanded and utilised for further experimentation.

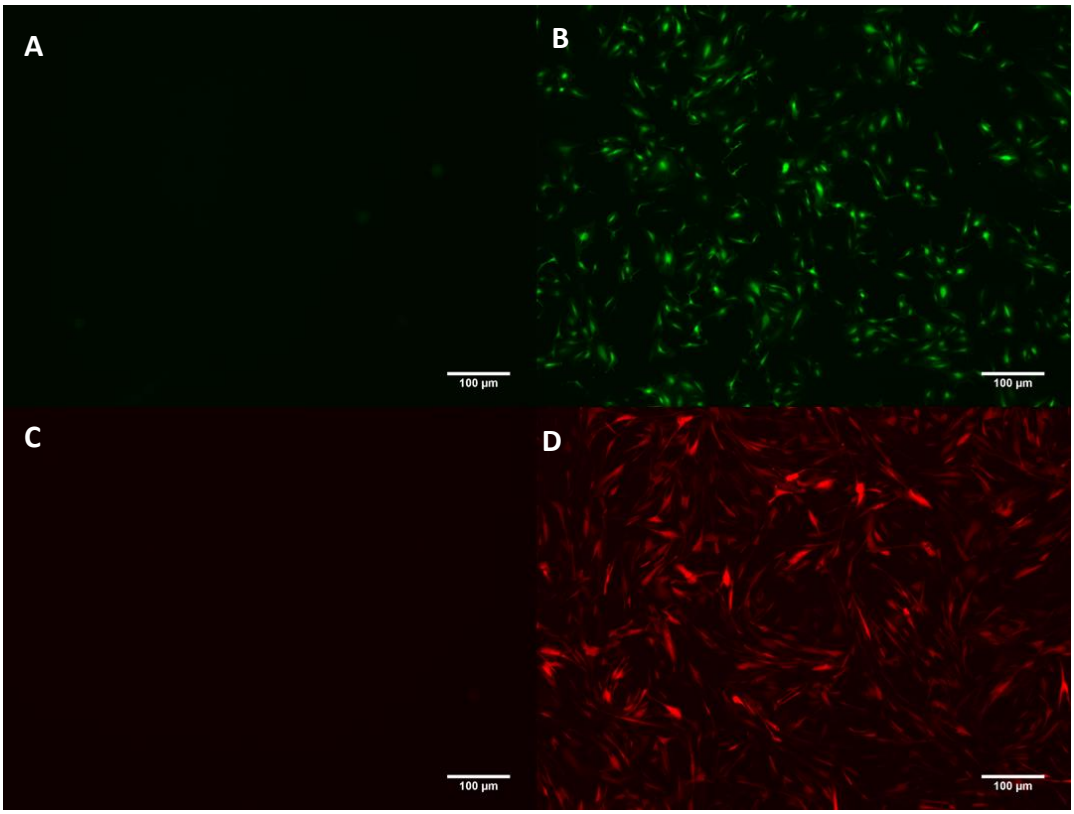

Figure 2.3: Example of Transduction Efficiency. A) Non-transduced HUVEC. B) HUVEC transduced with GFP lentiviral medium. C) Non-transduced UCP. Lower D) UCP transduced with DsRED lentiviral medium. Scale bar = 100um. Images were acquired using a Zeiss Axio Observer.Z1 fluorescence microscope.

2.10. Vascular Smooth Muscle Cell Differentiation

VSMC differentiation of foetal pericytes was achieved by exposing cells to inductive media. Media comprised of EGM-2 supplemented with 2ng/ml human TGF-β1 (Peprotech) with EGF and FGF excluded due to their attenuation of TGF-β (Peehl et al., 1998).TGF-β is a key regulator of smooth muscle cell phenotype previously used for differentiation studies (Tang et al., 2011).

Cells were seeded in EGM-2 in a 12 (40,000 cells/well), 24 (20,000 cells/well) and 96-well plate (4,000 cells/well) for protein, RNA, and ICC analysis, respectively. Once cells reached 70-80% confluence, medium was changed to differentiation medium and cells cultured for 15 days, refreshing the medium every 3 days. Following incubation, cells were harvested for protein, RNA and ICC analysis as detailed in methods 2.11-12 and method 2.4. Undifferentiated cells cultured in EGM-2 were used as a control.

2.11. Gene Analysis

Reverse transcription quantitative polymerase chain reaction (RT-qPCR) was used to evaluate changes in gene expression after VSMC differentiation (method 2.10) and calcification studies (method 2.19).

2.11.1. RNA Extraction and Purification

Total RNA was extracted from cells using a miRNeasy Mini Kit (Qiagen) according to manufacturer's instructions. Briefly, 700µl Qiazol Lysis Reagent was added to cell monolayers to disrupt and homogenise samples. Qiazol also inhibits RNase activity and facilitates the removal of cellular DNA and proteins. 140µl chloroform was vigorously mixed with the sample before centrifuging (15,000g, 15 minutes, 4^{o}C). This separates the sample into aqueous and organic phases. The aqueous phase, which contains the RNA, was collected whilst the DNA and protein remain in the interphase or organic phase. The aqueous phase was then mixed with 100% ethanol (1.5 x volume of aqueous phase) to help precipitation of RNA, before transferring to a RNeasy Mini column and centrifuging (8,000g, 15 seconds, RT). The RNA is bound by the column membrane whilst other contaminants are washed away through sequential wash and centrifugation steps (700µl RWT buffer, 2 x 500µl RPE buffer: 8000g, 15 – 120 seconds, RT). The bound RNA was then eluted by adding 30µl RNase-free water and centrifuging (8,000g, 1 minute, RT). Eluted RNA was analysed using a Nanodrop spectrophotometer ND-1000. Concentration of RNA (ng/µl) was determined by measuring

absorbance at 260nm. Proteins have a peak absorbance at 280nm and other contaminants such as phenol have a peak absorbance at 230nm. Calculation of these ratios were used to indicate purity of samples. All samples demonstrated a 260nm/280nm ratio of approximately 2.0, indicating pure RNA extraction (DNA ~1.8). RNA samples were stored at -80ºC until complementary DNA (cDNA) synthesis.

2.11.2. Complementary DNA Synthesis

cDNA was synthesised using a High-Capacity RNA-to-cDNA Kit (Life Technologies) according to the manufacturer's instructions. Briefly, for each RNA sample, 150ng RNA was added to a 0.2ml PCR tube and topped up to 4.5µl (9µl for low RNA concentrations) with RNase-free water. A master mix comprising of 0.5µl (1µl) per sample of 20x RT Enzyme Mix and 5µl (10µl) per sample of 2X RT Buffer mix was prepared. The enzyme mix contains reverse transcriptase MuLV and RNase inhibitors. The buffer contains dNTPs along with random octamers and oligo dT-16, which anneal to the sample RNA and provide a starting point for reverse transcriptase enzymes. 4.5µl (9µl) of the master mix was added to each sample to give a total reaction volume of 10µl (20ul). Samples were then incubated in a thermal cycler at 37ºC for 60 minutes, before stopping the reaction at 95ºC for 5 minutes and holding at 4ºC. Samples were diluted with nuclease-free water to a concentration of 5ng/µl cDNA and stored at -20ºC.

2.11.3. Quantitative Polymerase Chain Reaction (qPCR)

Quantitative PCR analysis was performed on a QuantStudio 5 Flex Real-Time PCR system (Applied Biosystems) using either probe-based (TaqMan™ primer-probes; Thermo Fisher; **Table 2.6**) or SYBR Green (see **Table 2.7** for primer details) technology. 5µl reactions were prepared in a MicroAmp Optical 384-well reaction plate (Life Technologies) as follows:

For TaqMan™ primer-probes, wells comprised of 2.5µl TaqMan™ Universal Master Mix II with UNG (Thermo Fisher Scientific), 0.25µl TaqMan™ primer-probe (20x), 1µl 5ng/µl cDNA sample and 1.25µl nuclease-free water. For SYBR green, wells comprised of 2.5µl Power SYBR Green PCR Mix (Thermo Fisher Scientific), 0.5µl primer mix (10x), 1µl 5ng/µl cDNA sample and 1µl nuclease-free water.

Plates were sealed with MicroAmp™ Optical Adhesive Film (Thermo Fisher Scientific) and centrifuged for 30 seconds using a Labnet mini plate spinner. The RT-qPCR protocol was set on the QuantStudio 5 Flex Real-Time PCR system as follows:

- UNG Incubation: 50ºC for 2 minutes.
- Polymerase Activation: 95ºC for 10 minutes.
- Amplification: 40 cycles
    - Denature: 95ºC for 15 seconds.
    - Anneal and extend: 60ºC for 1 minute.
- Melt Curve (SYBR Green only): 95ºC for 15 seconds, 60ºC for 1 minute, 95ºC for 15 seconds.

Reactions were run in triplicate. Analysis was performed using average C_T values and the fold change in gene expression between experimental (differentiated/stimulated cells) and control (undifferentiated/unstimulated) conditions calculated using the $2^{-\Delta\Delta Ct}$ Livak method (Livak et al., 2001). Results were normalized using internal control gene *UBC* or *GAPDH*.

Table 2.6: List of Taqman™ primer-probes used for RT-qPCR.

Target Gene	Probe ID
ACTA2 (aSMA)	HS00426835
CNN1 (Calponin)	HS00154543
MYH10 (NMMyoIIB)	HS00992055
MYH11 (SM-MHC)	HS00975786
TAGLN (Transgelin)	HS01038777
UBC (Ubiquitin C; Housekeeper)	HS00824723

Table 2.7: List of Primers used for SYBR Green RT-qPCR.

Target Gene	Qiagen Primer ID
GAPDH (Glyceraldehyde 3-phosphate dehydrogenase; Housekeeper)	QT00079247 (Hs_GAPDH_1_SG)
BMP2	QT00012544 (Hs_BMP2_1_SG)
RUNX2	QT00020517 (Hs_RUNX2_1_SG)
SOX9	QT00001498 (Hs_SOX9_1_SG)
SP7	QT00213514 (Hs_SP7_1_SG)
BGLAP	QT00232771 (Hs_BGLAP_1_SG)

2.12. Protein Analysis

Protein analysis was completed on differentiated and undifferentiated cells to confirm if changes in gene expression were translated to the protein level.

2.12.1. Protein Extraction and Quantification

Cell monolayers were washed twice with cold PBS and lysed using cold RIPA buffer (Life Technologies) supplemented with 1/100 (v/v) protease inhibitor cocktail (P8340 Sigma Aldrich), containing 4-benzenesulfonyl fluoride hydrochloride (AEBSF), Aprotinin, Bestatin, E-64, Leupeptin and Pepstatin A, and 1/50 (v/v) phosphatase inhibitor cocktail 2 (P5726 Sigma Aldrich), containing Sodium orthovanadate, Sodium molybdate, Sodium tartrate and Imidazole. Monolayers were disrupted using a cell scraper, collected in a 1.5ml Eppendorf tube and stored at -80ºC. After thawing samples, tubes were centrifuged at 15,000g, for 15 minutes at 4ºC. The supernatant was collected, and protein concentration quantified using Pierce™ BCA Protein Assay (Thermo Fisher). Briefly, 5µl of protein sample was denatured by heating to 100ºC for 5 minutes and then made up to 10µl with ddH_2O. Standards (0 – 2ug/µl) were prepared in 10µl ddH_2O with BSA. A master mix was prepared of 200µl reagent A and 4µl reagent B per sample. 190µl of master mix was added to each tube and incubated in a heat block at 37ºC for 30 minutes. The contents of each tube were transferred to a transparent 96-well plate and absorbance at 560nm measured using a Dynex Opsys MR microplate reader. Protein concentrations were calculated using the standard curve.

2.12.2. Western Blot

Western blotting is a technique used to identify specific proteins within complex samples. Denatured proteins are separated by size using sodium dodecyl sulfate-polyacrylamide gel electrophoresis (SDS-PAGE). SDS is an ionic detergent which helps denature and bind proteins, giving them a uniform negative charge. The negatively charged proteins migrate towards the positive anode during electrophoresis, with smaller proteins migrating at a faster rate. Once separated, the proteins are transferred to solid membrane via electrophoretic transfer. As before, the negatively charged proteins migrate out of the gel towards the membrane. Proteins of interest can now be identified in the membrane by probing with specific antibodies.

2.12.2.1. SDS-PAGE

1.5mm thick two layered gels (stacking followed by running) were prepared as set out in **Table 2.8**. The percentage of acrylamide is inversely proportional to gel pore size. A 10% running

gel was used as standard, however, for detection of large proteins 8% running gel was used. 10ug of protein (20ug for detection of poorly expressed proteins) was mixed with laemmli loading buffer (1X working concentration; **Table 2.9**) and heated to 100ºC for 5 minutes. The β-mercaeptoethanol and SDS in the loading buffer linearize the protein, whilst the glycerol and Bromophenol Blue R-250 weigh down and help visualise the separation. The protein samples were then loaded into wells in the stacking gel and immersed in 1X running buffer (**Table 2.9**). The gel was initially run for 20 minutes at 60V to help concentrate the sample protein into a single band. The lower pH and large pore size in the stacking gel also facilitate concentration of the sample protein. After 20 minutes, the voltage was changed to 120V and gel run for a further 60 – 90 minutes until the bands were sufficiently resolved. A pre-stained 10 – 250kDa PageRuler Plus protein ladder (Thermo Fisher Scientific) was run in parallel to allow identification of proteins based on molecular weight.

2.12.2.2. Protein Transfer and Detection

Following SDS-PAGE, proteins were transferred to a 0.22µm pore size polyvinylidene difluoride (PVDF) membranes (GE Healthcare). The PVDF membrane was hydrated and equilibrated through sequential washes with 100% Methanol (1 minute), dH_2O (5 minutes) and transfer buffer (10 minutes; **Table 2.9**). Proteins were transferred using wet transfer. The membrane was placed on top of the resolved gel, and then sandwiched between filter paper and sponges pre-soaked in cold transfer buffer (**Table 2.9**). This was then placed into a BioRad Mini Protean Tetra System tank, ensuring the membrane was between the gel and anode. The tank was then placed into a polystyrene box containing ice to ensure efficient heat dissipation, and current of 0.25A was applied for 60 – 75 minutes until complete transfer. Following transfer, membranes were blocked in 5% non-fat milk diluted in tris-buffered saline with 0.05% Tween-20 (TBST) wash buffer (**Table 2.9**) for 1 hour at RT on a see-saw plate rocker. Membranes were incubated with primary antibodies (**Table 2.10**) diluted in blocking buffer either overnight at 4ºC or for 1 hour at RT. Membranes were washed in TBST wash buffer (3 x 10 minutes) and incubated with either anti-mouse or anti-rabbit ECL-HRP-conjugated secondary antibodies (1:10,000 in blocking buffer; GE Healthcare) for 1 hour at RT. Membranes were washed (3 x 10 minutes) and incubated with Amersham™ ECL Reagent (GE Healthcare) for 5 minutes. A BioRadChemiDoc MP was used to image membranes, with exposure set between 1 and 90 seconds. If required, membranes were washed (1x 10 minutes) and stripped using Restore™ PLUS Western Blot Stripping Buffer (Thermo Fisher Scientific)

for 10 minutes. Following this, membranes were washed in TBST wash buffer (1x 10 minutes) and re-blocked before probing for additional proteins as described.

Protein bands were semi-quantified by densitometry using ImageJ software and normalised to β-Tubulin loading control.

Table 2.8: Polyacrylamide Gel Composition. Tris-HCL = tris hydrochloride, APS = ammonium persulfate, TEMED = tetramethylethylenediamine.

Gels	Reagent	Final Concentration
Running Gel 8%/10%	1.5M tris-HCL, pH8.8	375mM
	30% Acrylamide	8%/10%
	SDS	0.1%
	dH2O	-
	APS	0.1%
	TEMED	0.0008%
Stacking Gel	0.5M tris-HCL, pH6.8	125mM
	30% Acrylamide	4%
	SDS	0.1%
	dH2O	-
	APS	0.075%
	TEMED	0.001%

Table 2.9: Buffer Composition. Laemmli loading buffer should be diluted to 1X in sample. Running and transfer buffers must be diluted to 1X working solution in dH_2O before use. Cold 100% Methanol must be added to working concentration of transfer buffer before use (final concentration 20%).

Buffers	Reagent	Final Concentration
6X Laemmli Loading Buffer	0.75M tris-HCL, pH6.8	0.75M
	SDS	6%
	Glycerol	30%
	Bromophenol Blue R-250	0.018%
	β-mercaeptoethanol	6%
10X Running Buffer (pH8.3)	Tris Base	250mM
	Glycine	1.92M
	SDS	1%
	dH2O	-
10X Transfer Buffer (pH8.3)	Tris Base	250mM
	Glycine	1.92M
	dH2O	-
TBST Wash Buffer	Trizma (1M pH8)	20mM
	NaCl	150mM
	Tween-20	0.05%
	dH2O	-

Table 2.10: Primary antibodies for western blotting

Antibody	Dilution	Host Species	Supplier
aSMA	1:5000	Mouse	DAKO (M0851)
B-Tubulin	1:5000	Mouse	Cell Signalling Technology (2148S)
Calponin	1:5000	Rabbit	Abcam (ab46794)
NMMyoIIB	1:500	Rabbit	Abcam (ab204358)
SM-MHC	1:500	Rabbit	Abcam (ab53219)
Transgelin	1:500	Mouse	Santa Cruz (sc-271719)

2.13. Migration

For cells utilised for tissue engineering of a vascular graft, it is important that they promote rapid endothelialisation of the luminal side of the graft. Once a graft is transplanted into a patient, endothelialisation tends to occur through trans anastomotic ingrowth, the migration and proliferation of native ECs from either end of the graft (Sánchez et al., 2018). Consequently, a scratch-wound assay was chosen as the most suitable model to evaluate any potential pro-migratory effect from isolated pericytes.

HUVECs were seeded in EGM-2, on a 0.5% gelatin coated 96-well plate at a density of 5000 cells/well. Once HUVECs formed confluent monolayers, wells were scratched down the centre using a 10µl pipette tip and washed twice with DPBS to remove non-adherent cells. After washing, wells were treated with CM or control medium (see method 2.7). All medium was supplemented with 2mM hydroxyurea, which inhibits cell proliferation and ensures any closure of the gap, or 'wound', can be attributed to migration. Phase-contrast photos of the wells were taken immediately after treatment with medium using a Leica DMi1 inverted microscope and assigned time point 0. After 12 hours incubation, wells were imaged again. The gap area in pixels was measured at 0 hours and 12 hours using ImageJ, as demonstrated in **Figure 2.4**.

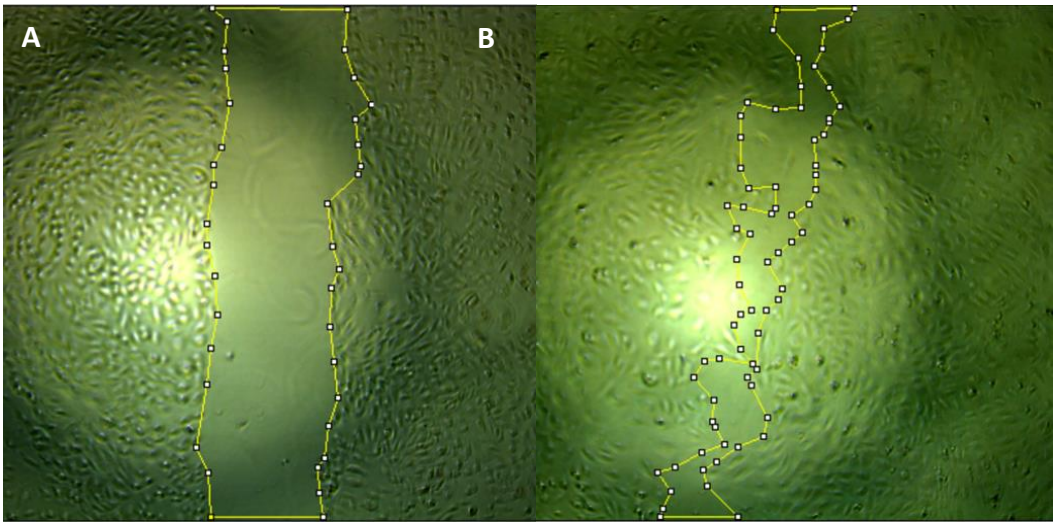

Figure 2.4: Example of scratch-wound migration assay quantification. Using ImageJ, the perimeter of the gap was drawn along the leading edge of HUVECs. The area bounded by the yellow perimeter was then measured. A) EGM-2 positive control at 0 hours. B) EGM-2 positive control at 12 hours.

Percentage gap closure was calculated using the following formula:

$$Gap\ Closure\ (\%) = 100\ x\ \frac{Area_{t=0} - Area_{t=12}}{Area_{t=0}}$$

Results were expressed as a fold change in gap closure versus the baseline level. The effect of MSC CM was analysed for comparison.

2.14. Contraction Assay

The ability of cells to contract and form functional vascular tissue was assessed by seeding undifferentiated and differentiated cells in a collagen gel contraction assay. This is a simple assay where cells are seeded into collagen gels in a well-plate. The cells and gels are fed with culture media in the same way as normal cell culture whilst the cells and gel equilibrate. Contraction in undifferentiated and differentiated cells is then induced using a vasoactivator or inhibited using an excitation uncoupling agent to understand if the cells can actively contract in response to a stimulus. If the cells can contract, they will shrink the gel after it is released from the well. This contraction can be quantified and compared between different cells and conditions by measuring the change in gel after stimulation. A detailed methodology of this is set out below. Differentiated cells were acquired using the differentiation protocol established in method 2.10. The collagen gel was prepared using rat tail collagen 1 (3mg/ml), PBS (10X), 1N NaOH, EGM-2 or cell suspension, and the following formulae:

$$Volume\ of\ collagen\ required\ (V_1) = \frac{Final\ concentration\ of\ collagen\ gel \times\ Total\ gel\ volume\ (V_t)}{Initial\ concentration\ of\ collagen}$$

$$Volume\ of\ PBS(10\times)\ required\ (V_2) = \frac{V_t}{10}$$

$$Volume\ of\ 1N\ NaOH\ required\ (V_3) = V_1 \times 0.025$$

$$Volume\ of\ EGM2\ or\ cell\ suspension\ required\ (V_4) = V_t - (V_1 + V_2 + V_3)$$

Gels were prepared in 24 well plates with a final volume and concentration of 500µl/well and 2mg/ml respectively, with 200,000 cells seeded per well. All reagents were kept on ice whilst preparing the gels. PBS (10X) was initially mixed with 1N NaOH and either EGM-2 or cell

suspension before carefully adding the collagen solution (volumes were calculated according to formulae above). Gels were left to polymerise for 1 hour at 37ºC/5% CO_2 before the addition of 500µl EGM-2 and incubation for 24 hours for cells to equilibrate and stress to develop in the gels. After 24 hours, medium was changed to 500µl of either fresh EGM-2 (control), EGM-2 supplemented with vasoactive agent 0.1uM Endothelin-1 (activated state) or EGM-2 supplemented with 0.1uM Endothelin-1 and excitation uncoupling agent 10mM 2, 3-Butanedione Monoxime (BDM; inhibited state). Gels were left for a further 1 hour before gently releasing the outside of the gels from the plastic wells using a sterile 10 µl pipette tip. The gels were then left for an additional 24 hours to allow the cells to contract. Following this, a photo of the contracted gels was taken as shown in **Figure 2.5**. Contraction was quantified using ImageJ by measuring the area of the contracted gel and comparing this to the original area of the gel before contraction, which was equivalent to the well area. Data was further normalised by cell number to account for any variations. This change in area gives an indication of the relative cell contraction. It was expected that pericytes that have undergone differentiation into VSMCs would contract more, shrinking the collagen gel more than undifferentiated pericytes, which would confirm a functional change in the cells in addition to phenotypical changes in smooth muscle associated protein expression.

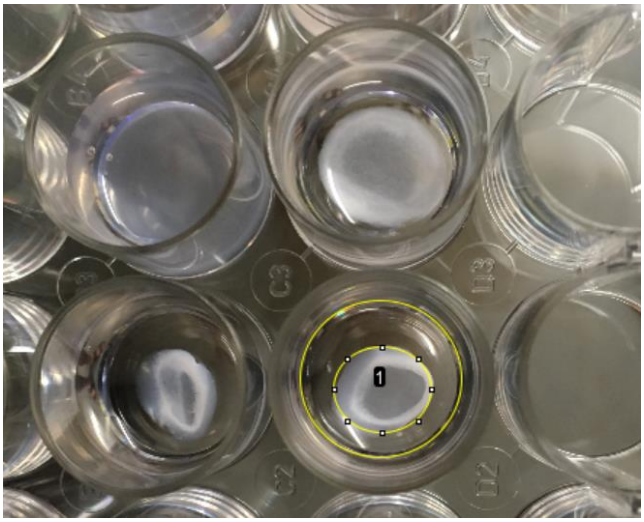

Figure 2.5: Example image of collagen gel contraction assay quantification. ImageJ was used to quantify the area of the contracted gel and total well. These values were then used to calculate contraction. Images of gels were acquired using a regular camera.

2.15. Decellularisation of ECM

Confluent cell monolayers were decellularised to assess the production of ECM. Cells were seeded at a density of 12,500 cells/well in a 96 well plate and cultured for 3 days to allow enough time to form confluent monolayers and produce extracellular proteins. A protocol for decellularization was adapted from Pattabhi et al. (Pattabhi et al., 2015). After 3 days, monolayers were washed twice with cold PBS and then incubated with cold PBS-1mM EDTA for 24 hours at 4ºC. After 24 hours, plates were gently shaken to detach cells and washed three times with cold PBS-1mM EDTA. This process was then repeated until all cells had been removed. Decellularised matrices were fixed along with cell monolayer controls and analysed by ICC for collagen, fibronectin and laminin as detailed in method 2.4.

2.16. Quantification of Extracellular Proteins

To further evaluate cellular production of ECM, the elastin and collagen content of confluent cell monolayers was quantified using the Biocolor Fastin™ Elastin assay and Sircol™ soluble and insoluble collagen assays, as described below. Cells were seeded in 2ml of EGM-2 at a density of 200,000 cells/well in a 6 well plate. At 3 and 5 days after seeding, monolayers and medium were processed for elastin and collagen. For day 5 time point, 2ml of EGM-2 was added to wells on day 3 to ensure cells received adequate nutrients.

Elastin:

For processing of elastin, culture medium was removed, and monolayers were washed twice with PBS before incubating with 500ul/well trypsin-EDTA (0.05% (w/v) trypsin, 0.02% (w/v) EDTA) at 37ºC/5% CO2 for 10 minutes. Plates were mechanically agitated to dislodge monolayers and the suspension was transferred to a 1.5ml Eppendorf for immediate analysis or frozen at -80ºC. The cell suspension was centrifuged at 3000rpm for 10 minutes at RT, and cell pellet retained in 300µl of supernatant. Cell bound elastin was then converted to soluble α-elastin by adding 100µl 1M oxalic acid (0.25M final concentration) and incubating at 100ºC for 1 hour. 250µl of the soluble α-elastin solution was mixed with an equal volume of elastin precipitating reagent, vortexed and incubated for 15 minutes at RT. Tubes were then centrifuged at 10,000g for 10 minutes at RT to remove supernatant, and mixed with 1ml of dye reagent before placing in mechanical shaker for 90 minutes at RT. After incubation with dye reagent, tubes were centrifuged again at 10,000g for 10 minutes at RT, supernatant removed, and 250µl of dye dissociation reagent added and mixed by vortex. 200µl of sample or kit-

supplied reference standard was transferred to a standard white 96 well and read using a GloMax Discover Microplate Reader at the closest wavelength to 513nm.

Collagen:

To evaluate collagen production, CM was filtered through a 0.22um filter and collected. Cell monolayers were washed twice with PBS and incubated with 1ml/well of 0.1mg/ml pepsin in 0.5M acetic acid, overnight on a rocking shaker at 4ºC, which facilitated the release of bound collagen. Monolayers were broken up using a cell scraper, collected into a 1.5ml Eppendorf and centrifuged at 15,000g. Supernatant was collected for soluble collagen analysis and the cell pellet retained for quantification. Samples were either processed immediately or stored at -80ºC for future analysis.

For processing of soluble collagen, 100µl of acid neutralising reagent was added to the supernatant, followed by the addition of 200µl of cold isolation/concentration reagent. For CM, only isolation/concentration medium was added. Samples were incubated in an ice-water tank at 4ºC overnight.

For processing of insoluble collagen, 300µl of fragmentation medium was added to the retained cell pellets before incubating for 2-3 hours at 65ºC.

After insoluble and soluble collagen processing, all samples were centrifuged at 15,000g for 10 minutes at 4ºC. Supernatant was removed, and soluble and insoluble collagen samples were resuspended in 100µl of 0.5M acetic acid and 100µl of deionized water, respectively. 1ml of Sircol™ dye reagent was added to each sample and incubated for 30 minutes at RT, mixing every 5 minutes using a vortex. Samples were centrifuged at 15,000g for 10 min at RT, supernatant was removed and 750µl of ice-cold acid-salt wash gently added above pellets. This centrifugation step was completed once more and 250µl of alkali reagent added to the pellet, mixing by vortex to release collagen bound dye. 200µl of sample or kit-supplied reference standards was transferred to a standard white 96 well and read using a GloMax Discover Microplate Reader at 550-570nm.

2.17. Detection of Matrix-Metalloproteinases (MMPs)

To assess the ability of cells to degrade the ECM, cell lysates and CM were screened for the presence of MMPs. 500,000 cells were seeded in a T25 culture flask and cultured until cells

were confluent. Once cells reached confluence, medium was replaced with 3ml of fresh EGM-2 and conditioned for a further 48 hours. Medium was then collected and centrifuged to remove floating cells before storing at -80ºC. Cell monolayer were washed once with PBS and 200µl of 2X Cell Lysis Buffer (abcam), diluted 1:1 with dH_2O and supplemented with 1/100 (v/v) protease inhibitors (Sigma), was added to each T75 flask and cell monolayers removed using a cell scraper. The cell lysate was centrifuged at 15,000g for 15 minutes at RT, and the supernatant collected. Protein concentration was quantified as in method 2.12 and the sample was frozen at -80ºC until analysis.

CM and cell lysates were analysed using a dot blot approach Human MMP Antibody Array Membrane-ab134004 (abcam) according to manufacturer's instructions. Briefly, membranes were blocked in 1X Blocking Buffer (abcam) for 30 minutes at RT. Following blocking, membranes were incubated with 1ml CM or 250µg cell lysate diluted in 1ml of 1X Blocking Buffer for 2 hours at RT or overnight at 4ºC. For CM control, a membrane was incubated with unconditioned EGM-2. Membranes were washed (3 x 5 minutes Wash Buffer I, 2 x 5 minutes Wash Buffer II) and incubated with 1X Biotin-Conjugated Anti-Cytokines for 2 hours at RT or overnight at 4ºC. The wash step was repeated, and membranes incubated with 1X HRP-Conjugated Streptavidin for 2 hours at RT or overnight at 4ºC. The wash step was then completed a final time and membranes incubated with 500µl of detection buffer mixture (1:1 Detection Buffer C and Detection Buffer D). Membranes were imaged within 5 minutes of incubation with detection buffer mixture using a BioRad ChemiDoc MP. Images were semi quantified by densitometry using ImageJ and normalised to the membrane positive control, which is consistently expressed between membranes. Results were normalised to either total protein or total CM volume per T25 culture flask as appropriate.

2.18. Collagenase Activity

Collagenase activity was assessed using a fluorometric Collagenase (Collagen Degradation/Zymography) Assay Kit-ab234624, according to manufacturer's instructions. 500,000 cells were seeded in a T25 culture flask and cultured until cells were confluent. Medium was then replaced with 3ml of fresh EGM-2 and conditioned for a further 48 hours. Medium was collected and centrifuged to remove floating cells before storing at -80ºC. Cell monolayers were washed once with PBS, and 100µl of kit supplied Cell Lysis Buffer added

before scraping and collecting the cell lysate. The lysate was then centrifuged at 16,000g for 10 minutes at 4ºC. The supernatant was collected, and total protein quantified as before. Cell lysate was stored at -80ºC until analysis. For analysis of intracellular collagenase activity, 190µg of cell lysate was diluted in 50µl of kit supplied collagenase buffer and added to a 96-well plate. For analysis of extracellular collagenase activity, 50µl of undiluted CM was added to the 96-well plate. 50µl of collagenase substrate solution (2µl collagenase substrate in 50µl collagenase buffer) was added to each well and fluorescence measured on kinetic mode at 520nm for 1 hour at 37ºC using a GloMax Discover Microplate Reader. A positive control was included on the same plate.

For analysis of data, a standard curve was produced using an array of FITC standard dilutions (0 – 500pmol/well) measured using a GloMax Discover Microplate Reader at endpoint mode. The following equation was used to calculate activity:

$$Sample\ Collagenase\ Activity\ \left(\boldsymbol{X}, \frac{U}{ml}\right) = \frac{\boldsymbol{B}\ \times 1000}{\boldsymbol{A}\ \times \boldsymbol{C}}\ \times Dilution\ Factor$$

$$Sample\ Collagenase\ Activity\ \left(\frac{U}{mg}\right) = \frac{\boldsymbol{X}}{\boldsymbol{P}}$$

B = sample collagenase activity as calculated (RFU/min), **A** = gradient of the FITC standard curve (ΔRFU/pmol), **C** = µl of sample used in assay, **P** = protein concentration in lysate (mg/ml).

Total intracellular and extracellular collagenase activity was calculated by scaling measurements according to total protein and total CM volume per T25 culture flask.

2.19. Calcification

The ability of isolated pericytes to resist calcification was tested by exposing cells to a high phosphate medium. Cells were cultured in EGM-2 until 80-90% confluency before changing the medium to DMEM high glucose (Gibco) supplemented with 4% FBS and 2.6 mM high phosphate buffer (Na_2HPO_4/NaH_2PO_4, pH 7.4). Medium was refreshed every 2 days up to a maximum time point of 5 days, as determined by alizarin red staining. DMEM high glucose supplemented with 4% FBS was used as a control medium.

After 5 days, cell monolayers were either analysed for calcium content or processed for RNA extraction and subsequent analysis of osteochondrogenic gene expression (method 2.11).

Alizarin red S, which binds calcium to form an orange/red pigment, was used to visualise calcium deposits in the cell monolayers (96-well plate). Cells were then imaged using a Leica DMi1 inverted microscope. Bound alizarin red s was quantified by dissolving in 50µl 10 % acetic acid per well of a 96 well plate and measuring the optical density on a Dynex Opsys MR microplate reader set to 405nm. Further analysis of calcium deposition was completed using a colorimetric calcium assay kit (abcam ab102505). Briefly, cell monolayers (12-well plate) were washed once with DPBS before adding 300µl of 0.6N hydrochloric acid (HCL) per well and incubating for 16 hours at 4ºC. The calcium in the monolayer dissolves in the acid. 25µl of calcium standard or HCL samples were added to a 96-well plate and mixed with 30µl assay buffer plus 45µl chromogenic reagent. After 10 min incubation, the calcium ions in the sample or standard form a chromogenic complex with o-cresolphthalein, which can be measured using a Dynex Opsys MR microplate reader set to 575nm. Total protein content of the monolayers was quantified by adding 50µl lysis buffer (0.1NaOH, 0.1% SDS, 1:100 protease inhibitor, 1:50 phosphatase inhibitor) and processed as in method 2.12. Results were normalised by total protein content and total volume of sample.

2.20. Tissue Engineering Studies

The following methods were established for optimisation of cell seeding onto CorMatrix (CorMatrix Cardiovascular) scaffolds, and the subsequent conditioning and analysis. Histological analysis techniques can be found in method 2.3.

2.20.1. Seeding Optimisation

Before producing the vascular graft, the pericyte seeding conditions were optimised for the CorMatrix scaffold.

2.20.1.1. Seeding Density

Sections of CorMatrix were cut to the size of either a 48 well or 96 well plate. Sections were then placed in wells, ensuring the smooth side of the CorMatrix was face-down, and sterile crowns were then placed on top to ensure the sections were fixed at the bottom of the wells. EGM-2 was added and the CorMatrix sections were left to condition for 24 hours at 37ºC. After

24 hours, the medium was removed and pericytes were seeded at 10,000, 20,000 or 30,000 cells/cm2. Crowns were reinserted and the seeded CorMatrix sections were conditioned for 5 days, with half the medium replaced after 3 days. In parallel, cells were seeded on culture plastic at the corresponding densities to evaluate the effect of the scaffold on cell behaviour. After 5 days, all samples and CM were collected for analysis and determination of optimum seeding density.

2.20.1.2. Scaffold Coating

Once the optimum seeding density was determined by assessing cell viability, proliferation and density, scaffold coating conditions were explored to evaluate if coating of the CorMatrix scaffold could improve cell adhesion and establish a more uniform cell distribution. As with optimisation of seeding density, CorMatrix sections were cut to size and conditioned for 24 hours at 37ºC. After 24 hours, CorMatrix scaffolds were treated with either fresh EGM-2, 0.01% bovine gelatin and 10mg/ml fibronectin in DPBS, or FBS for 2 hours at 37ºC. After 2 hours, coating solutions were removed, and cells were seeded and conditioned as before. After 5 days, the cell seeded scaffolds and CM were collected for analysis.

2.20.2. Production of Pericyte-Seeded CorMatrix Grafts

Cellularised CorMatrix grafts were prepared through a process of static and dynamic conditioning. 40mm x 30mm sections of CorMatrix were first cut and positioned in sterile crowns (**Figure 2.6A**). The crowns ensured the scaffold remained submerged in medium in a horizontal orientation. The unseeded CorMatrix patch was then primed for 24 hours in EGM-2 at 37ºC/5% CO_2. After 24 hours, the medium was removed and pericytes were seeded under optimised conditions. The seeded scaffolds were then conditioned for 5 days in a static environment at 37ºC/5% CO_2. After 5 days, grafts were either harvested for analysis or transferred to dynamic conditioning. Harvested grafts were processed as follows:

- Grafts were trimmed to a 30mm x 20mm seeded section.
- Four 20mm x 5mm sections were cut for mechanical analysis.
- Two 5mm x 5mm sections were cut for viability, proliferation, and density analysis.
- One 10mm x 5mm section was fixed and embedded in paraffin.
- One 10mm x 5mm section was fixed and embedded in OCT
- One 10mm x 5mm section was snap frozen in OCT
- CM was collected and stored at -80ºC

Before dynamic conditioning, the statically conditioned pericyte-seeded CorMatrix grafts were stitched into a conduit shape with the pericytes facing the external abluminal side of the conduit. The conduits were left submerged in medium whilst the bioreactor system was set up. The bioreactor system consisted of a Masterflex L/S digital 07528-20 peristaltic pump, silicone tubing (3.175mm internal diameter (ID), 6.35mm outer diameter (ODI)), pump cassette tubing (PharMed BPT tubing, 2-stop, 2.79 mm ID), a multi chamber stand for sample set up, and up to six 3DCulture Pro bioreactor chambers (**Figures 2.6B & C**). The flow rate of the pump is determined by RPM and the diameter of the cassette tubing. Dynamic conditioning is used by tissue engineers to promote differentiation and maturation of engineered grafts. The flow rates used often vary quite considerably between research groups, from 1mL/min up to 250mL/min (Baba et al., 2021; X. Ma et al., 2017; Tschoeke et al., 2008). The flow rate needs to be sufficient to stimulate the cells and graft, without causing it to burst or degrade. In this case the pump was set to 90RPM, which equates to 24ml/minute for the given cassette tubing. This was optimised in previous studies according to how the cells and graft responded to the flow (Alvino et al., 2020).

Components were sterilised before use with disinfectant and autoclaved (121^{o}C for 30 minutes). The conduit was then positioned into the bioreactor chamber and filled with EGM-2 before conditioning for a further 7 days. After 7 days, the conduits were processed as above.

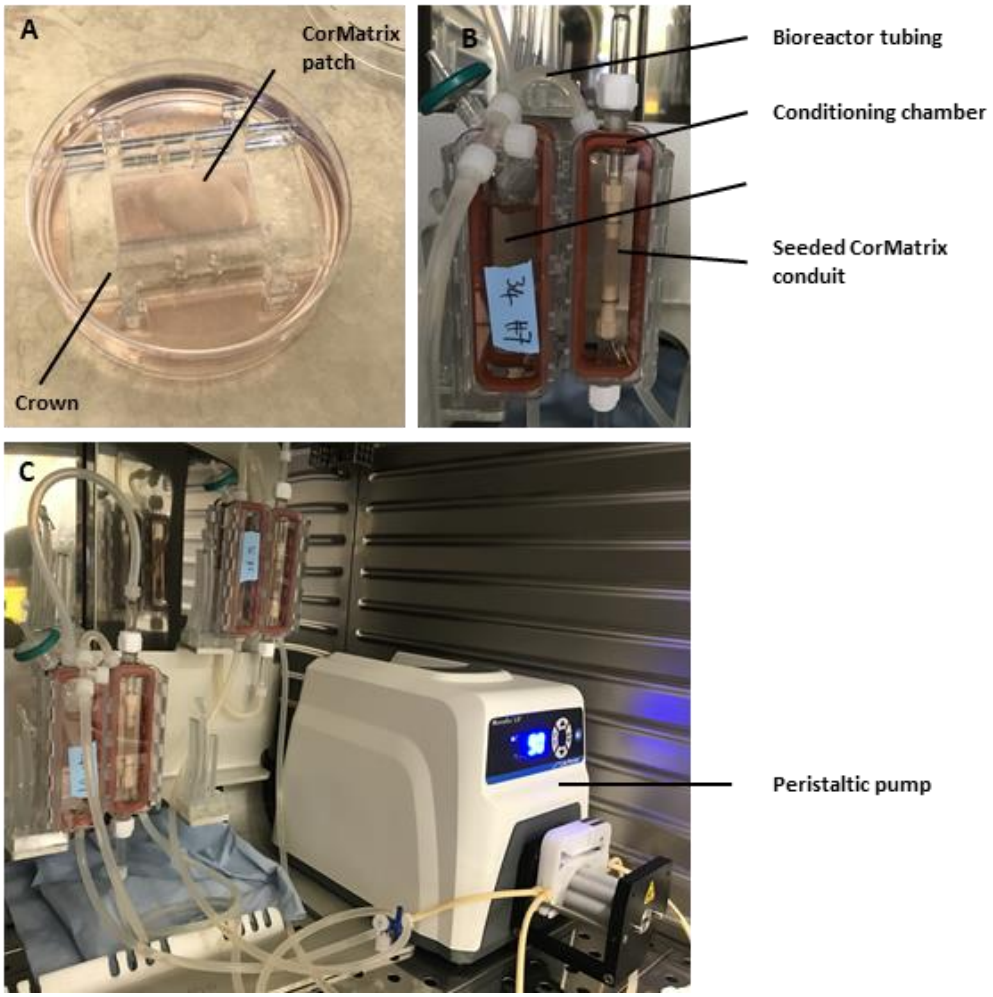

Figure 2.6: Bioreactor system set up. A) CorMatrix graft positioned in crown for static conditioning. B) Close up of 3DCulture Pro bioreactor housing the pericyte seeded CorMatrix conduit. The bioreactor is comprised of a conditioning chamber for graft attachment, a reservoir chamber for media storage and tubes connected to a pump to facilitate flow. C) Bioreactor system comprising of Masterflex L/S digital 07528-20 peristaltic pump, tubing and 3DCulture Pro bioreactor chamber, which each contain a separate conduit. The peristaltic pump drives the media around the system.

2.20.3. Analysis of Proliferation, Density and Viability/Cytotoxicity

Optimisation experiments and subsequent grafts were analysed for cell proliferation, density and viability/cytotoxicity using the following techniques.

2.20.2.1. Cell Proliferation and Density

To calculate cell proliferation, scaffolds and cells were stained using the proliferation marker Ki67, purchased from DAKO, and DAPI. For the full method see method 2.4. Images were quantified by counting the number of Ki67 positive and DAPI positive cells in each field of view. Density of cell seeding was calculated by counting the DAPI positive cells and scaling the results according to the image field.

2.20.2.2. Cell Viability/Cytotoxicity

A LIVE/DEAD™ Viability/Cytoxicity Kit was purchased from Thermo Fisher Scientific. This kit utilises Calcein AM and Ethidium homodimer-1. Calcein AM is a non-fluorescent cell-permeant dye which is converted to green-fluorescent calcein only in live cells. Ethidium homodimer-1 can only enter cells with damaged membranes, generating a red fluorescence after binding to nucleic acid. After conditioning, cells and scaffolds were washed with EBM-2, and incubated for 30 minutes at 37ºC in EBM-2 supplemented with 2µM Calcein AM and 4µM Ethidium homodimer-1. For the last 10 minutes Hoechst was added to each (1:1000 Thermo Fisher Scientific). For a dead staining control, some cells were treated with 0.1% (w/v) saponin in DPBS for 10 minutes before staining. Cells were imaged immediately after the incubation using a Zeiss Observer.Z1 microscope and processed using Zen Pro and ImageJ software packages. Where possible, images were quantified by counting the Calcein AM positive and ethidium homodimer-1 positive cells and calculating the percentage of viable cells using the following equation:

$$Viability\ (\%) = \frac{number\ of\ calcein\ positive\ cells}{number\ of\ total\ cells}\ x\ 100$$

There are alternative methods that can be used to assess cell viability and cytotoxicity, such as intracellular ATP and glutathione levels (Chapple et al., 2016), or lactate dehydrogenase (LDH) levels in conditioned media. LDH release was initially measured. LDH is a cytosolic enzyme which is released into cell culture medium when the plasma membrane of a cell is damaged (Kumar et al., 2018). As such, it can be used as a further indicator of cell cytotoxicity.

Using an LDH-Glo™ Cytotoxicity Assay (Promega), CM was measured as per manufacturer's instructions. The principle of the assay is described in **Figure 2.7**.

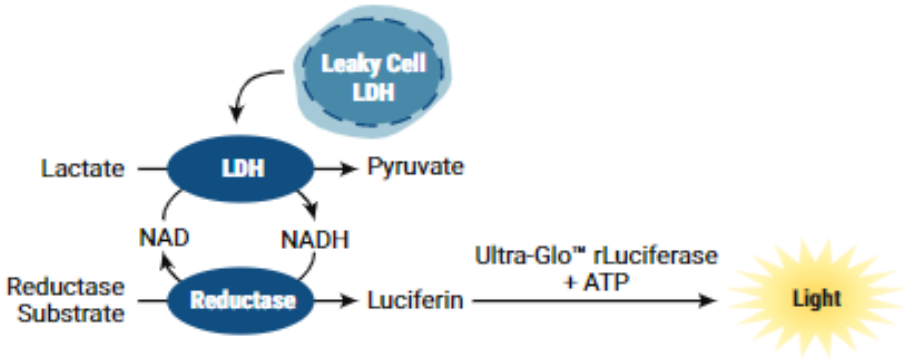

Figure 2.7: LDH-Glo™ Cytotoxicity Assay Principle. Lactate Dehydrogenase (LDH) release from damaged cell membranes catalyses the oxidation of lactate with concomitant reduction of nicotinamide adenine dinucleotide (NAD+) to NADH. Reductases use the NADH and reductase substrate to produce luciferin, which is converted to a bioluminescent signal by Ultra-Glo™ Luciferase. The luminescent signal generated is proportional to the amount of LDH present. Figure and legend source: https://www.promega.co.uk/products/cell-health-assays/cell-viability-and-cytotoxicity-assays/ldh-glo-cytotoxicity-assay/?catNum=J2380

Briefly, immediately after seeding optimisation experiments 8µl of CM was added to 92µl of LDH buffer (200mM Tris-HCL (pH7.3), 10% Glycerol, 1% BSA) and stored at -80C before analysis. The buffer increases the stability of LDH when freezing. Before analysis, samples were thawed and diluted 1:8 in LDH buffer to give a final dilution of 1:100. 50µl of diluted sample was added to single wells of a 96-well plate in duplicate. LDH detection reagent was prepared by thawing LDH detection enzyme mix and reductase substrate (both included in assay kit). 50µl of LDH detection enzyme mix and 0.25µl reductase substrate per sample were combined by inverting 5 times. 50µl of the LDH detection reagent was added per well in a 96-well plate and luminescence recorded after 60 minutes. A GloMax Discover Microplate Reader was used to quantify luminescence. Results were normalised by the number of cells and expressed as a fold change vs control. Purified LDH from rabbit muscle (included in assay kit) and neat LDH buffer were used as positive and negative controls.

2.20.4. Collagen Presence in Graft Conditioned Medium

The presence of collagen in medium collected after the static and dynamic conditioning of grafts was assessed using a human Pro-Collagen I alpha 1 ELISA kit (R&D Systems) as per manufacturer's instructions. Results were normalised by conditioning time. For a more detailed description of the ELISA process see methods 2.7.

2.20.5. Mechanical Analysis

Mechanical properties of static and dynamic conditioned grafts were analysed using an Instron 3343 device (Illinois Tool Works Inc). As previously mentioned, four sections of 20mm x 5mm were harvested from the grafts. For dynamic conditioned grafts, these sections were cut so that the longest end was perpendicular to the flow direction, as shown in **Figure 2.8A**. The sections were then clamped and stretched lengthwise using the tensile machine, set at 10mm/min. Tests were carried out at 37^{o}C in PBS to better represent in vivo conditions (**Figure 2.8B**). This method of mechanical analysis has been previously established to test the circumferential mechanical properties of tissue engineered grafts (Alvino et al., 2020). It was chosen instead of stretching the construct axially, as the analysis aimed to evaluate how the graft responds and expands to circumferential stress, as is the case under physiological blood pressure. Ideally, the burst pressure would have been assessed; however, this kind of system was not available. If the amount of material was not limiting, axial analysis would have also been completed on the intact construct; however, due to the cost of the scaffold and need for tissue sections for other methods of analysis such as histology, this was not possible. The exact area and length of each section was measured using Vernier callipers, and a stress-strain curve plotted in order to calculate the young's modulus, ultimate tensile strength, and rupture strain (**Figure 2.8C**). The Young's Modulus was calculated from the gradient of the elastic section of the curve and allowed us to estimate the stiffness/elasticity of the graft. Ultimate tensile strength was estimated from the peak tensile stress, which is the maximum tensile stress a material can withstand without breaking. Rupture strain was taken as the maximum elongation before breaking. This value could be used to estimate the maximum expansion or compliance of the conduit.

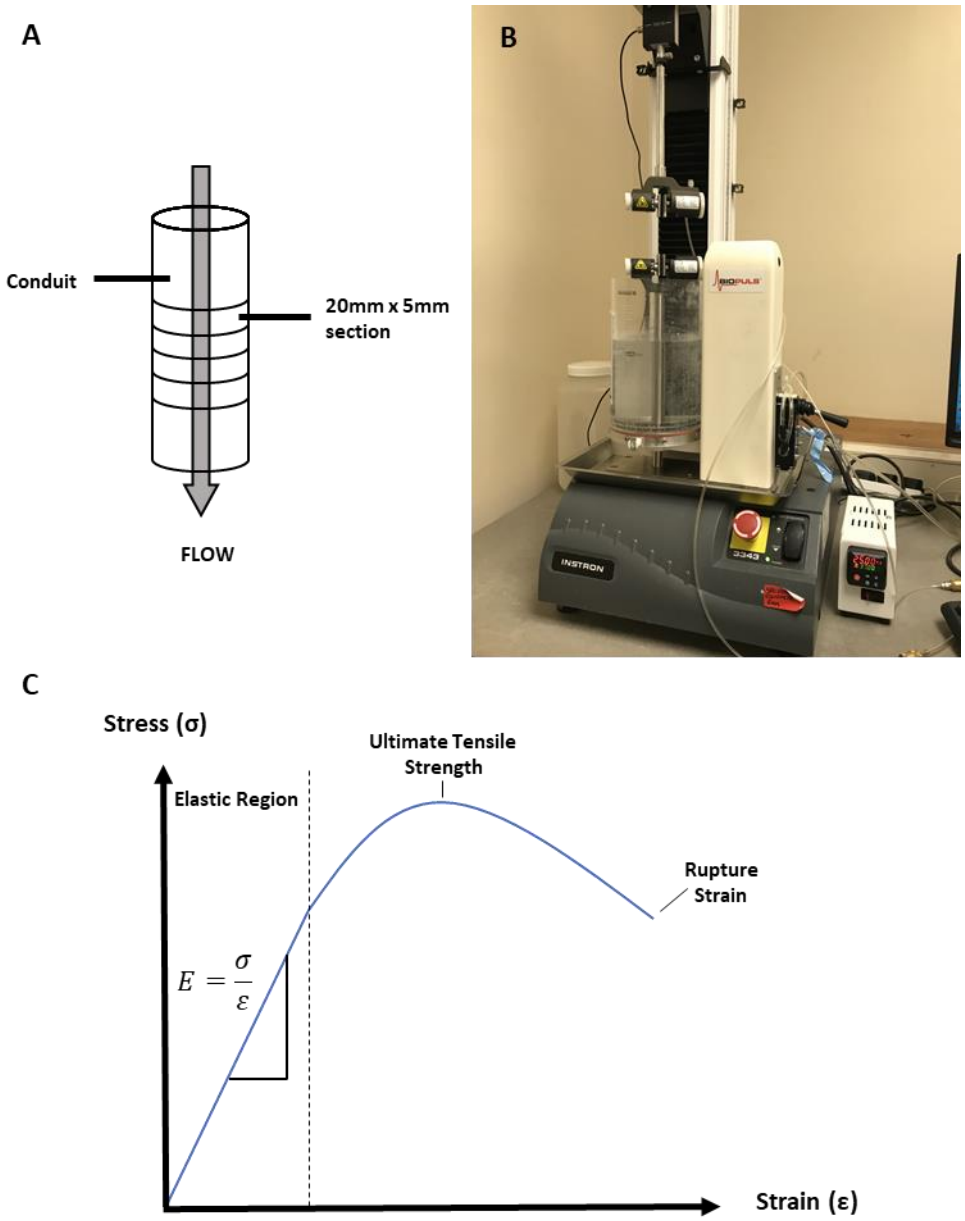

Figure 2.8: Mechanical Analysis. (A) Sections taken for mechanical analysis are perpendicular to flow direction. (B) Instron 3343 setup. (C) Representative stress-strain curve for calculation of mechanical behaviour of scaffold. E = Young's Modulus, σ = stress and ε = strain.

2.21. Statistical Analysis

All statistical analysis was performed using GraphPad Prism 6 software and Microsoft Excel. Where experiments only consisted of two groups, a student's t-test was used to analyse the data. For analysis of more than two groups, a one- or two-way analysis of variance (ANOVA) was applied depending on the number of independent variables, followed by student's t-tests, Dunnett's, Sidak's or Tukey's post-hoc analysis. All data are presented as mean ± the standard error of the mean (SEM), and $p<0.05$ was used as the cut-off value for statistical significance. Unless otherwise stated, for isolated pericytes n numbers in figures represent the number of different donors pericyte cell lines. For purchased commercial cell lines, such as HUVEC and MSCs, n numbers represent separate experiments using different vials of the same bulk cell population.

3. Isolation of Umbilical Cord and Placenta Pericyte Cell Lines

3.1. Introduction

A myriad of techniques have been developed for the dissociation of specific cell populations from human tissue, which can be categorised into three methodologies: adherence, density and antibody binding (Tomlinson et al., 2013). These are typically assessed based on purity (the proportion of target cells to non-target cells isolated) and recovery (the number of target cells obtained compared to the number of initially available target cells) (Hu et al., 2016).

Adherence selection is a simple and low cost method used to culture cells such as MSCs; however, it is not suitable for applications where purity is essential, such as in clinical use, due to the requirement of a consistent, sterile cell population produced under good manufacturing practice conditions (Gomez-salazar et al., 2020; Tomlinson et al., 2013). Density-based methods generally utilise centrifugation to separate cells based on their density. They are useful for eliminating large populations of unwanted cells; however, alone they lack the accuracy to distinguish between cell types of similar densities.

In contrast with these techniques, antibody binding-based methods can offer a high degree of specificity which makes them the gold standard for selection of homogenous cell populations. Antibody based sorting can be largely broken down into two distinct techniques: FACS and magnetic activated cell sorting (MACS). FACS is a specialised form of flow cytometry that involves labelling cells with a fluorophore-conjugated antibody and subsequently sorting the cells based on their fluorescent signal. MACS relies on labelling cells with specific antibodies conjugated to magnetic beads. Application of an external magnet is then used to retrieve the labelled cells. Whilst FACS offers high specificity and an ability to sort cells by multiple parameters, utilisation of this technique requires expensive equipment and a high degree of skill. Furthermore, for clinical use, extensive redesign of the equipment is required to ensure parts of the instrument in contact with cells can be easily replaced to reduce the chance of cross-contamination (Ährlund-Richter et al., 2009). In contrast, MACS offers a much simpler and cost-effective alternative which can still deliver a high level of specificity and throughput, and is therefore typically the adopted choice for clinical applications (Hu et al., 2016; Tomlinson et al., 2013).

To achieve efficient immunosorting of cells, careful consideration must also be paid to the choice of antibody used for labelling. Whilst certain cells express unique antigens, pericytes lack a ubiquitous specific marker, meaning there is no standardised protocol for isolation (Dias

Moura Prazeres et al., 2017; Yamazaki et al., 2018). For isolation of pericytes from the umbilical cord, CD146 may present a good option as it has been successfully utilised to isolate perivascular cells from the cord (Gökçinar-Yagci et al., 2016; Tsang et al., 2013). Similarly, NG2 is a viable option, it having been identified as a specific marker of perivascular cells in the umbilical artery (Crisan et al., 2012). Another potential alternative is the selection of CD31-/CD34+ cells based on a methodology previously established by our research group (Avolio, Rodriguez-Arabaolaza, et al., 2015; Campagnolo et al., 2010). These selection antibodies have been used to extract adventitial pericytes from saphenous vein, and therefore may be adapted for isolation of a similar pericyte population in the umbilical vessels. In fact, unpublished pilot data demonstrated initial feasibility of this approach in the cord tissue.

In the following chapter, the possibility of sorting pericytes from cord and placenta tissue using immunomagnetic sorting was explored. The initial feasibility of different isolation methodologies for clinical applications was confirmed through an evaluation of cell purity, viability, and growth potential.

3.2. Objectives

The following objectives were established in order to facilitate the establishment of pericyte cell lines for future studies:

- Develop methodology for efficient isolation of pericyte cell lines from human umbilical artery or placenta tissue.
- Confirm isolated cell lines possess a pure pericyte-like phenotype.
- Confirm isolated cell lines possess sufficient expansion capacity and maintain viability in vitro.
- Generate frozen cell stocks for future studies

3.3. Pericyte Isolation Protocols

Umbilical cord and placenta were donated from St. Michaels Hospital, Bristol. Umbilical cord sections of ~10cm in length were cut from the placental end of the cord using a scalpel. A scalpel was used to remove a piece of tissue from the foetal side of the placenta rich in chorionic villi. Umbilical cord or placenta tissue was then washed thoroughly in DPBS to remove any blood. The amniotic epithelial layer was removed and discarded. Using a sterile scalpel and forceps, umbilical vein and arteries were carefully separated from the surrounding WJ in order to remove WJ-MSCs and washed again in DPBS. At this stage, different isolation methods were explored as detailed below. Samples were processed within 48 hours of birth.

3.3.1. Umbilical Cord Adventitial Pericyte Isolation using Enzymatic Digestion and CD31-/CD34+ Selection

The initial isolation of pericytes from human umbilical cord samples was attempted by adapting a protocol previously established by our research group. This protocol provided for isolation of a subset of pericytes present in the vasa vasorum of large blood vessels (termed adventitial progenitor cells) and later utilised to isolate a similar population in cardiac tissue (Avolio, Rodriguez-Arabaolaza, et al., 2015; Campagnolo et al., 2010).

Umbilical cord arteries were manually minced using sterile scissors and a scalpel until nearly homogenous. The homogenate was centrifuged, and the supernatant was removed. Tissue was weighed so that each 15ml falcon tube contained a maximum of 1g (total<5g). 13.5ml of DMEM (Thermo Fisher Scientific) and 250ul of 5mg/ml Liberase II TM Research Grade (Sigma-Aldrich) were added to each 15ml falcon to obtain an enzymatic solution with a concentration of 0.45WU/ml. The solution was then incubated at 37^{o}C with constant agitation using a rotator for up to 2 hours or until tissue was fully digested. The enzymatic digestion was stopped by adding DMEM supplemented with 10% FBS up to a final volume of 40ml. The solution was then passed sequentially through 70µm, 40µm and 30µm cell strainers to ensure a single cell suspension. Cells were centrifuged and resuspended in 0.5% BSA + 2mM EDTA pH8 (Ambion) in DPBS. Cells were depleted of ECs using anti-CD31 conjugated beads (Miltenyi Biotech) and purified using anti-CD34 conjugated beads (Miltenyi Biotech) according to manufacturer's instructions. CD31-/CD34+ UCPs (CD34 UCPs) were then cultured as set out in methods 2.2.

3.3.2. Umbilical Cord Pericyte Isolation using Explant Outgrowth and CD31-/NG2+ Selection

An isolation protocol utilising explant outgrowth rather than enzymatic digestion was employed to provide an alternative, and possibly more effective, option for isolating a pure population of pericytes from the umbilical cord. NG2 (a marker associated with pericytes) was used to sort cell populations rather than CD34 or CD146 (Cathery et al., 2018). An outline of the method is illustrated in **Figure 3.1**.

Sections (1-3mm^2) of umbilical artery were placed in a flask using a Pasteur pipette, leaving 10mm between each tissue section. A drop of FBS was added to each explant piece to aid attachment, and flasks were incubated for 30 minutes at 37ºC and 5% CO_2. Following this, EGM-2 was slowly added to the flask, taking care not to detach explants. After 7-10 days in culture, colonies of cells were observed migrating out from the explants. The explant tissue was removed using sterile forceps, and the migrated cells were harvested. This heterogenous cell population was then purified using immunomagnetic selection. Briefly, cells were incubated with anti-CD31 microbeads in column buffer, comprising of 0.5% (w/v) BSA and 2mM pH8 EDTA (Ambion), according to manufacturer's instructions. The suspension was filtered through a magnetic column, keeping the CD31– cell population, and the selection process was repeated using anti-AN2/NG2 beads (Miltenyi Biotech), retaining the CD31–/NG2+ pericyte population. The acquired CD31-/NG2+ UCPs (NG2 UCPs) were then cultured as detailed in chapter 2.

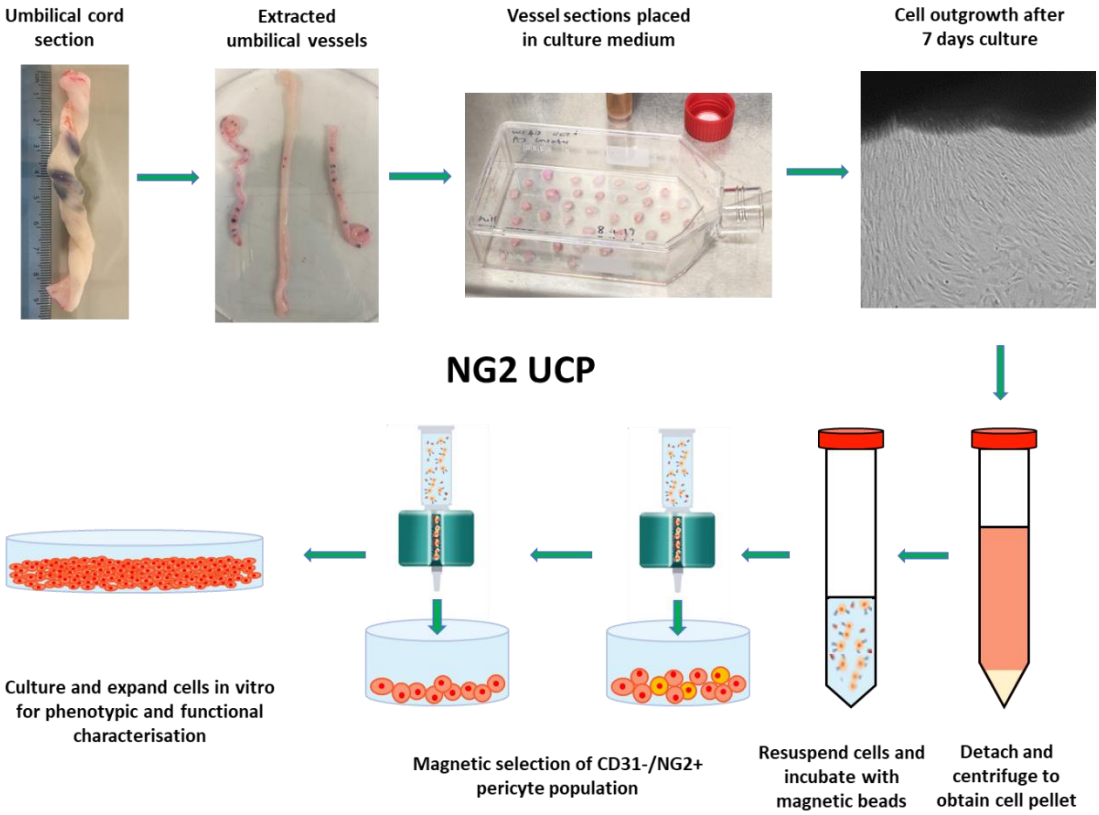

Figure 3.1: Overview of protocol for isolation of $NG2^{+}/CD31^{-}$ umbilical cord pericytes (NG2 UCPs). Umbilical vessels were extracted from the cord and the Wharton's Jelly removed. 1-3mm^2 sections of umbilical artery were placed in a flask and cultured in EGM-2. After 7-10 days, the tissue sections were removed, and migrated cells were collected. The cells were sorted to obtain a $NG2^{+}/CD31^{-}$ UCP population using immunomagnetic selection. The purified cell population was cultured in endothelial growth medium 2 (EGM-2) and expanded for further experimentation.

3.3.3. Umbilical Cord Pericyte Isolation using Enzymatic Digestion and CD31-/CD146+ Selection

CD146 is widely regarded as a marker for pericytes, and has been previously employed for isolation of perivascular cells from umbilical cord (Gökçinar-Yagci et al., 2016; Tsang et al., 2013). An adaption of this method was used as an alternative isolation strategy, which is illustrated in **Figure 3.2**.

Briefly, the ends of the umbilical arteries were sutured using surgical thread to reduce digestion of lumen and subsequent release of ECs. Arteries were immersed in 2ml of 1mg/ml collagenase type 1 (Life Technologies) in DPBS and incubated overnight at 37°C and 5% CO_2. The enzymatic reaction was stopped by diluting with DPBS (1:10). The solution was passed sequentially through 70um, 40um and 30um cell strainers to ensure a single cell suspension. Cells were then resuspended in 0.5% BSA + 2mM EDTA pH8 in DPBS, depleted of ECs using anti-CD31 conjugated beads and purified using anti-CD146 conjugated beads (both Miltenyi Biotech) according to manufacturer's instructions. CD31-/CD146+ UCPs (CD146 UCPs) were seeded in EGM-2 and cultured as set out in methods 2.2.

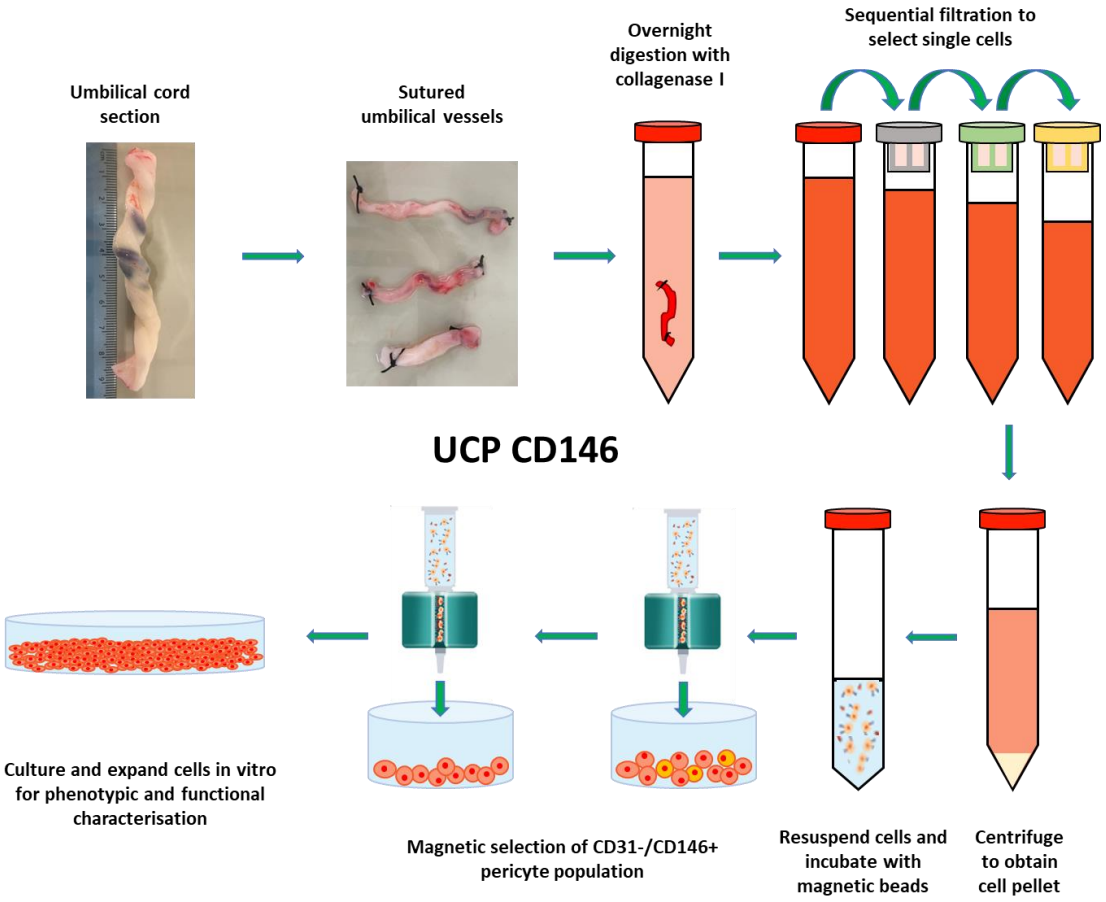

Figure 3.2: Overview of protocol for isolation of CD146+/CD31- umbilical cord pericytes (CD146 UCPs). Umbilical vessels were extracted from the cord and the Wharton's Jelly removed. Ends of arteries were sutured and then placed in 1mg/ml collagenase type 1 and digested overnight. Enzymatic reaction was stopped by diluting in DPBS and a single cell suspension was obtained by passing digest through sequential filters (30um – 70um). The cells were sorted to obtain an $CD146^{+}/CD31^{-}$ UCP population using immunomagnetic selection. The purified cell population was cultured in endothelial growth medium 2 (EGM-2) and expanded for further experimentation.

3.3.4. Placenta Adventitial Pericyte Isolation using Enzymatic Digestion and CD31-/CD34+

The original CD31-/CD34+ isolation protocol was used to investigate whether this subset of pericytes could be found in the placental tissue. The protocol is outlined in **Figure 3.3** and follows the same process as section 3.3.1, except it utilises placenta instead of umbilical cord. 2g of placental tissue was used per isolation and CD31-/CD34+ PLPs (CD34 PLPs) were cultured as set out in methods 2.2.

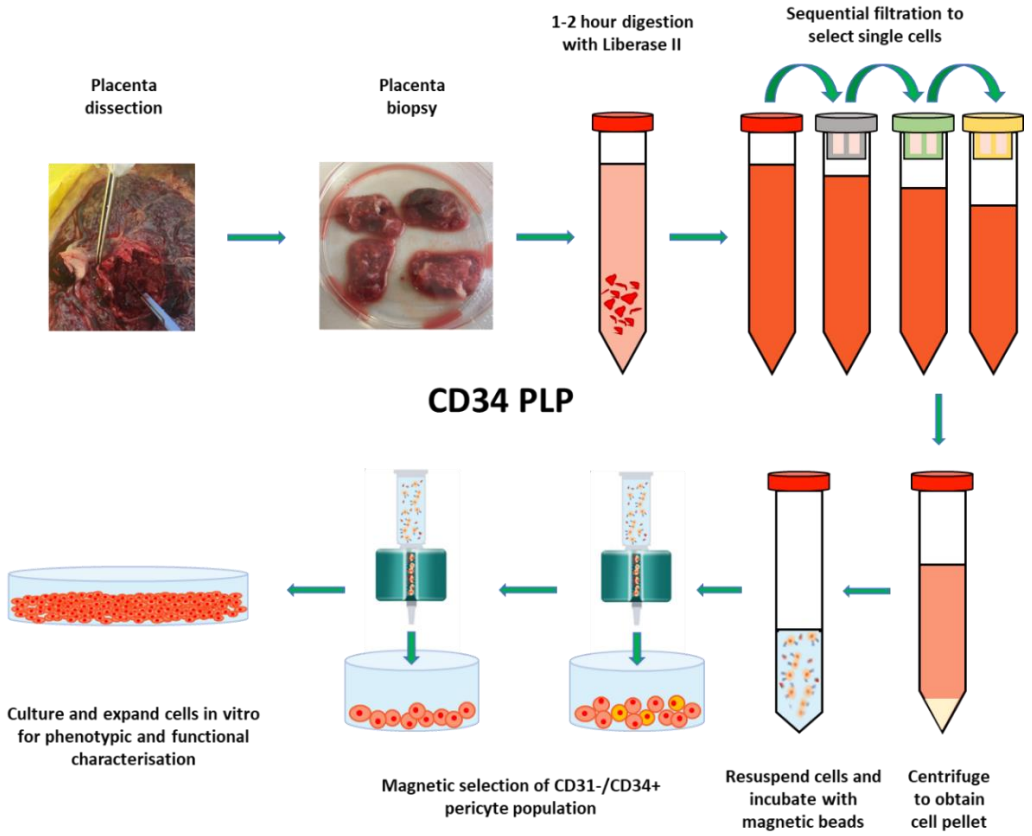

Figure 3.3: Overview of protocol for isolation of $CD34^{+}/CD31^{-}$ placenta pericytes (CD34 PLPs). Placenta biopsy was removed from foetal side of placenta. Placenta was homogenised and digested in Liberase II for up to 2 hours. Digestion was stopped by adding Dulbecco's Modified Eagle Medium (DMEM) supplemented with 10% foetal bovine serum (FBS), and a single cell suspension was obtained by passing digest through sequential filters (30um – 70um). The cells were sorted to obtain a $CD34^{+}/CD31^{-}$ PLP population using immunomagnetic selection. The purified cell population was cultured in endothelial growth medium 2 (EGM-2) and expanded for further experimentation.

3.4. Results

3.4.1. Feasibility of Isolation Protocols

In the initial phase of the project, the aim was to determine if pericytes could be separated from umbilical cord using an immunomagnetic beads sorting protocol previously established for extraction of CD31-/CD34+ pericytes from saphenous vein and cardiac tissue. Using this method, a total of 11 umbilical cord isolations were attempted, however only 1 viable CD34 UCP cell line was successfully expanded, resulting in an isolation efficiency of just 9.1% (**Figure 3.4**). To improve the prospects of pericyte isolation, alternative methods were explored as detailed in section 3.2. A total of 9 isolations were completed using a novel isolation strategy which incorporated explant outgrowth, followed by purification of CD31-/NG2+ cells. From the 9 attempts, 8 viable NG2 UCP cell lines were produced, resulting in a highly efficient methodology (88.9%). In parallel, pericyte isolation from the umbilical cord was also attempted by adapting a previously established method for isolating perivascular cells based on the classical pericytes associated marker CD146. Isolation efficiency of CD146 UCPs using this method was slightly lower than NG2 UCPs at 77.8%.

Although isolation of CD34+ pericytes from umbilical cord was not successful, it was hypothesised that it might be possible to isolate this population from an alternative tissue source. After 12 months, placental tissue was acquired in addition to the umbilical cord samples in order to test the feasibility of this isolation. From 7 isolation attempts, 5 viable CD34 PLP cell lines were successfully expanded, resulting in a 71.4% efficiency.

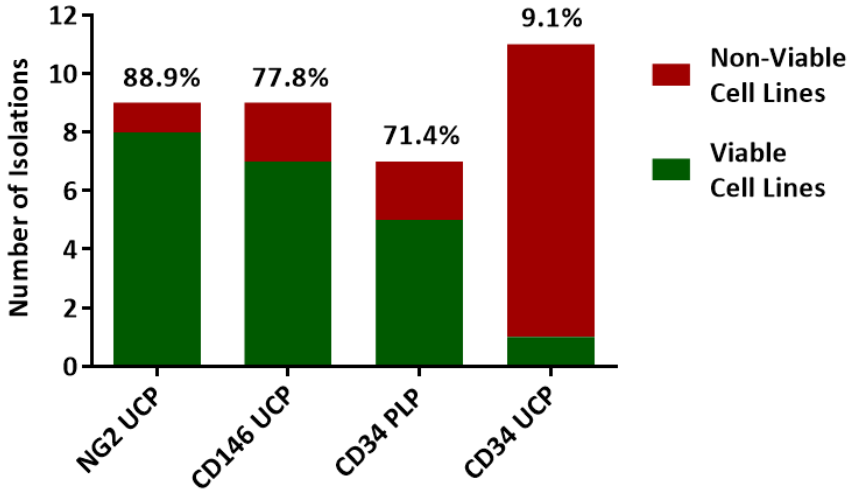

Figure 3.4: Efficiency of different isolation methodologies. Number of successful (green) and unsuccessful (red) cell isolations from umbilical cord and placenta. The percentage above each column indicates the efficiency of the isolation protocol.

3.4.2. In situ Localisation of Umbilical Cord and Placenta Pericytes

The presence and location of pericytes was confirmed through histological analysis of umbilical cord and placenta as set out in methods 2.3. The structure of the umbilical cord artery can be seen in **Figure 3.5**. A distinct tunica intima (TI) is illustrated by the lumen surrounded by ECs highlighted by the blue nuclei stain (**Figure 3.5B**). The tunica media (TM) and tunica adventitia (TA) layers have been roughly marked on **Figures 3.5B and D**. The dark stain in the tunica media of **Figure 3.5D** illustrates the presence of elastic fibres in this smooth muscle cell rich layer. The outer TA is mainly composed of collagen fibres, as demonstrated by the red stain. No vasa vasorum can be seen in the histological analysis of the umbilical cord.

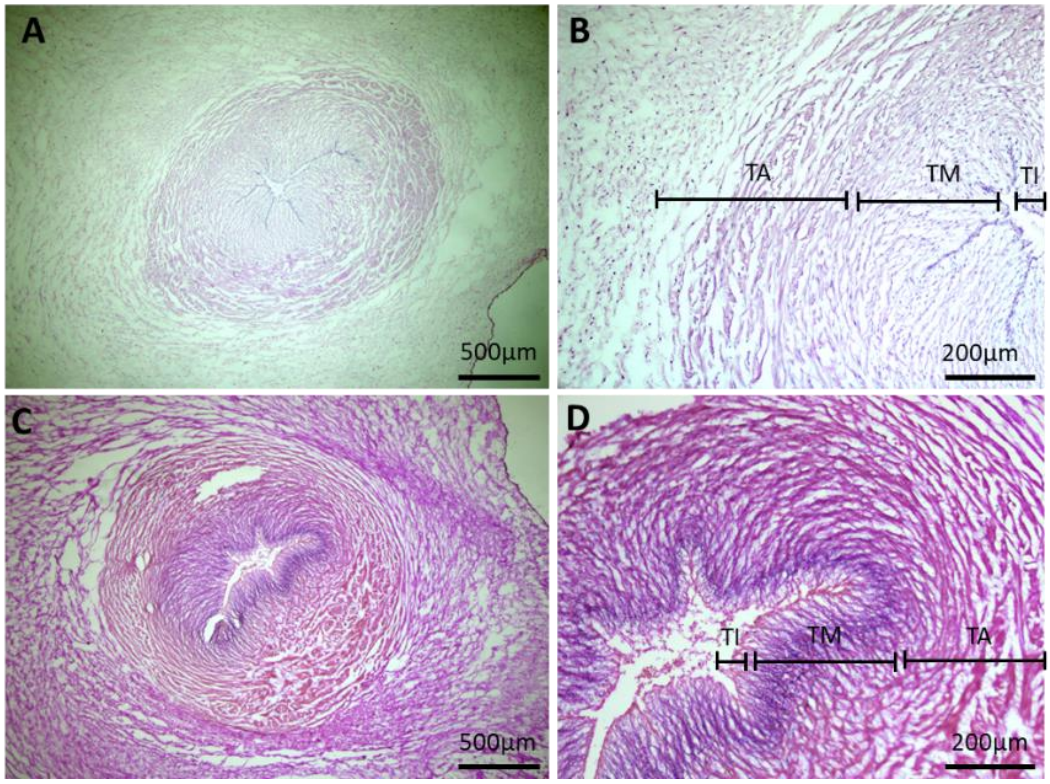

Figure 3.5: Histological analysis of umbilical cord artery. The figure demonstrates the structure of the umbilical artery which was used to obtain isolate umbilical cord pericytes (UCPs). A-B) Haematoxylin and Eosin (H&E) staining of umbilical artery. C-D) Verhoeff's Van Geison (EVG) staining of umbilical artery. TI = tunica intima and lumen, TM = tunica media, TA = tunica adventitia. Scale bar = 500µm (A and C), scale bar = 200µm (B and D). This figure is a representative image of n = 3 donor samples.

Sporadic staining of NG2+/CD31-/CD34- cells can be seen in the perivascular layer of the artery confirming the presence of NG2 UCPs in the tissue **(Figure 3.6)**. The endothelial layer is highlighted by the CD31+/CD34+ expression around the lumen. No CD34 UCPs were detected in the tissue. Analysis of CD146 expression revealed a band of CD146+/CD31-/CD34- cells in the inner section of the perivascular layer (**Figure 3.7**). These cells appeared more localised than NG2 UCPs, which demonstrated a more scattered distribution.

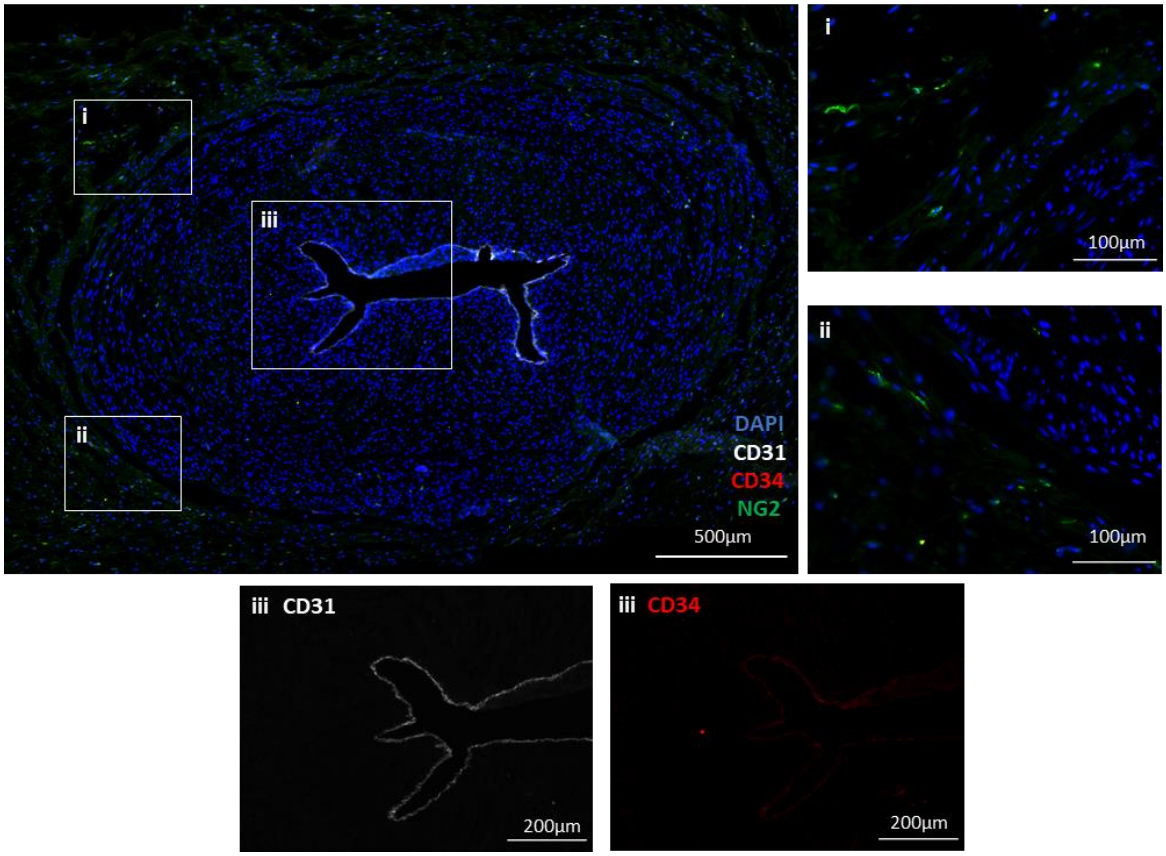

Figure 3.6: In situ localisation of NG2 UCPs. Immunohistochemical analysis of umbilical artery showing sporadic staining of NG2 positive pericytes negative for CD31 and CD34 in the perivascular layer. Scale bar = 500µm. Inserts in (i) and (ii) show close up images of NG2+ umbilical cord pericytes (NG2 UCPs). Scale bar = 100µm. Insert (iii) demonstrates CD31 and CD34 staining is restricted to the endothelial layer. Scale bar = 200µm. DAPI = blue, CD31 = white, CD34 = red and NG2 = green. This figure is a representative image of n = 3 donor samples.

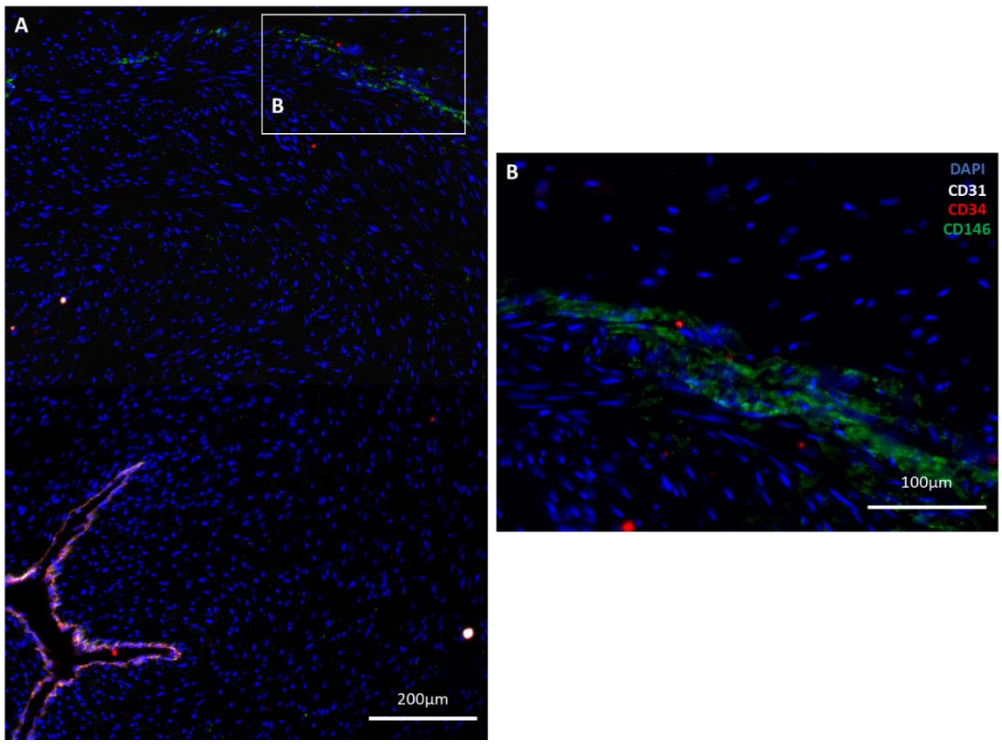

Figure 3.7: In situ localisation of CD146 UCPs. (A) Immunohistochemical analysis of umbilical artery showing sporadic staining of CD146 positive pericytes negative for CD31 and CD34 in the perivascular layer. Scale bar = 200µm (B) Inserts demonstrating close up image of CD146+ umbilical cord pericytes (CD146 UCPs). Scale bar = 100µm. DAPI = blue, CD31 = white, CD34 = red and CD146 = green. This figure is a representative image of n = 3 donor samples.

The structure of the placenta tissue was difficult to highlight due to the compaction of villous trees during the processing of placenta tissue. This resulted in dense overlapping of cells in places, as highlighted by the blue nuclei stain, and a mottled pattern of tissue and cells in the histology slides (**Figure 3.8**). The EVG stain demonstrates a lack of elastin fibres, with the collagen highlighted in pink and cell cytoplasm stained yellow. No discernible placental structures were visible from the histological analysis.

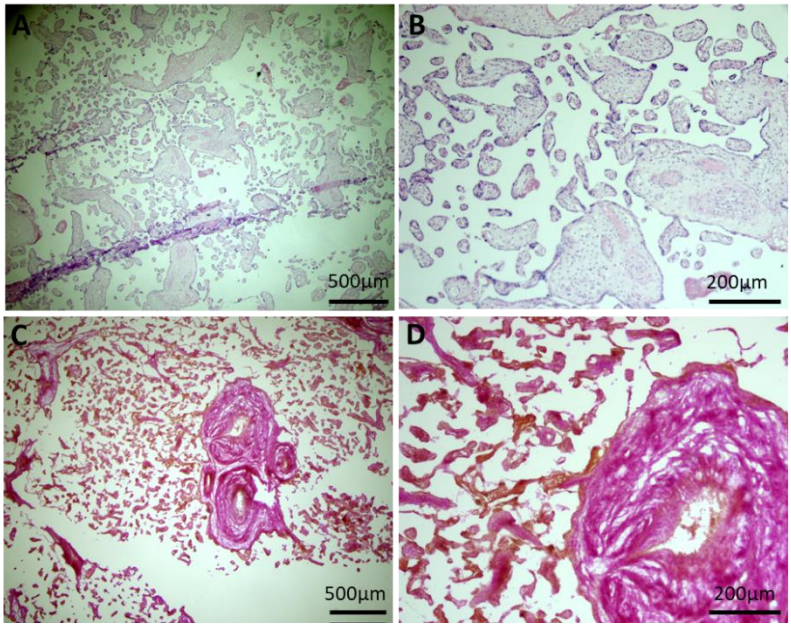

Figure 3.8: Histological analysis of placenta. Figure demonstrates the structure of the placenta which was used to obtain isolate placenta pericytes. (A-B) Haematoxylin and Eosin (H&E) staining. (C-D) Verhoef's Van Geison (EVG). Scale bar = 500µm (A and C), scale bar = 200µm (B and D). This figure is a representative image of n = 3 donor samples.

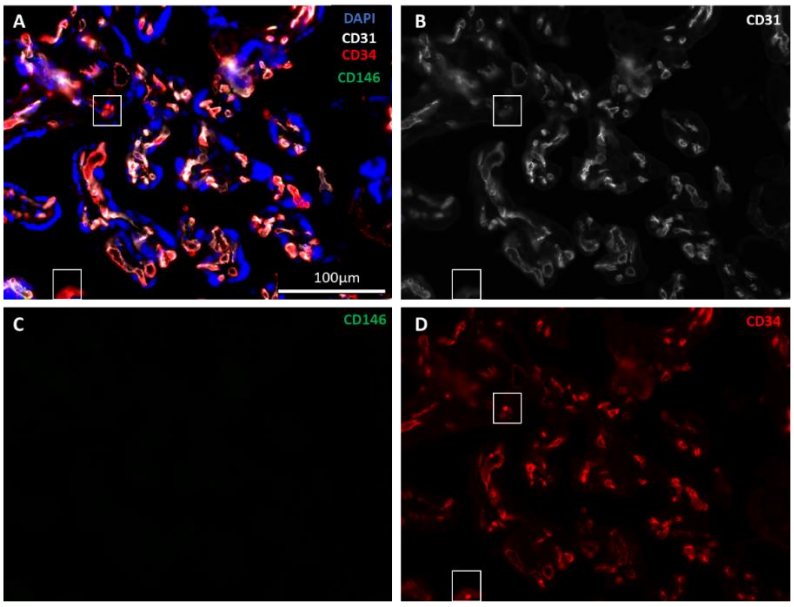

Figure 3.9: In situ localisation of CD34 PLPs. (A) Composite immunohistochemical image of placenta tissue highlighting CD34+/CD31-/CD146- placenta pericytes (CD34 PLPs) in white boxes. (B) CD31 expression in placenta tissue. (C) CD146 expression in placenta tissue. (D) CD34 expression in placenta tissue. DAPI = blue, CD31 = white, CD34 = red, CD146 = green. Scale bar = 100µm. This figure is a representative image of n = 3 donor samples.

The dense layering of cells in tissue sections made it difficult to locate individual CD34+/31- cells in the placenta. As demonstrated by the nuclei staining in **Figure 3.9**, there is an abundance of overlapping cells. Despite this, individual CD31-/CD34+ cells can be identified as highlighted by the white boxes in **Figures 3.9A, B and D**. CD146 expression was not detected.

3.4.3. Confirmation of Pericyte Phenotype

Isolated cells were systematically characterised to confirm that the cells demonstrated a pure pericyte-like phenotype.

Phase contrast microscopy was used to acquire images of cell morphology under in vitro culture conditions (**Figure 3.10**). Similar to pericytes previously isolated by our research group (Campagnolo et al., 2010), cells did not grow well on uncoated culture plastic, forming spheroids, as illustrated in figure 3.10A. Considering this, a solution of 0.01% bovine gelatin

and 10ug/ml fibronectin in DPBS was used to precoat culture plastic before seeding cells. NG2 UCPs (**Figure 3.10B & C**) and CD146 UCPs (**Figure 3.10D & E**) demonstrated a typical pericyte spindle shaped morphology, which was particularly evident at low confluence. Although CD34 PLPs demonstrated a similar spindle shape, the cells appeared considerably smaller than both NG2 UCPs and CD146 UCPs, as illustrated in **Figure 3.10F & G**.

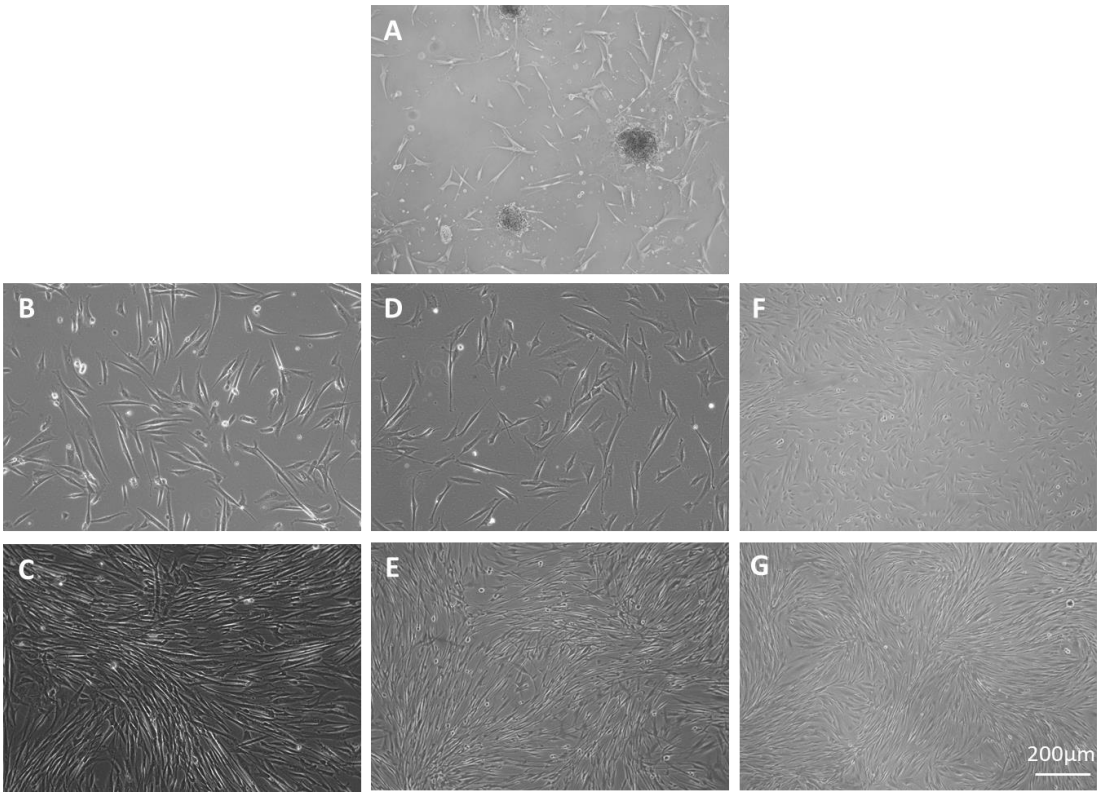

Figure 3.10: Morphology of isolated cells in culture. (A) Spheroid formation in cell cultured on uncoated plastic. Representative image of n = 3. (B & C) NG2 UCP morphology at low and high confluence in culture. Representative image of n = 8. (D & E) CD146 UCP morphology at low and high confluence in culture. Representative image of n = 7. (F & G) CD34 PLP morphology at low and high confluence in culture. Representative image of n = 5. Scale bar = 200µm for all images.

To confirm that our isolated cells represented a pericyte phenotype, an immunocytochemical analysis (method 2.4) was completed for an array of antigenic markers. The absence of endothelial markers CD31, CD34 and VE-Cadherin (VECAD) expression demonstrated there was no contamination of ECs in any of the isolated cell types (**Figure 3.11**). Despite CD34

PLP isolation based on their expression of CD34, there was no expression observed once expanded in culture.

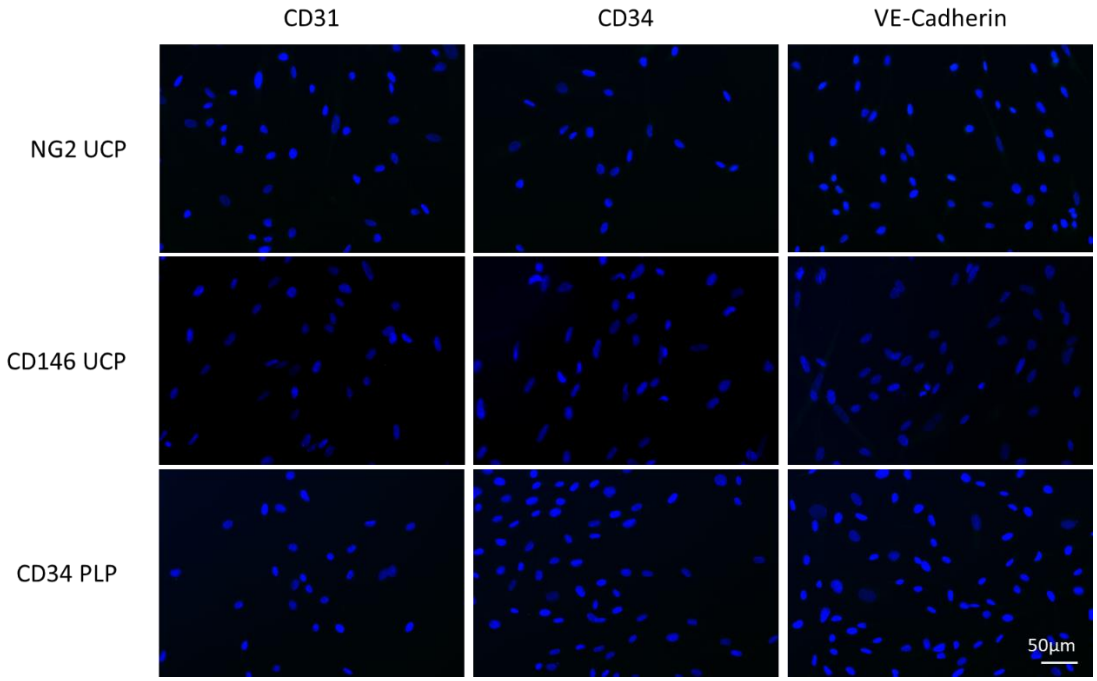

Figure 3.11: Immunofluorescent analysis of isolated pericyte populations for expression of endothelial markers CD31, CD34 and VE-Cadherin. Top three panels show representative images for NG2 UCPs expression profile (n = 8). Middle three panels show representative images for CD146 UCPs expression profile (n = 7). Bottom three panels show representative images for CD34 PLPs expression profile (n = 5). Nuclei were stained using DAPI. Vascular endothelial cadherin (VE-Cadherin). Scale bar = 50µm for all images.

All pericyte populations expressed NG2 and Vimentin, however, CD34 PLPs did not express CD146 (**Figure 3.12**). This was consistent with previous results for CD31-/CD34+ pericyte populations.

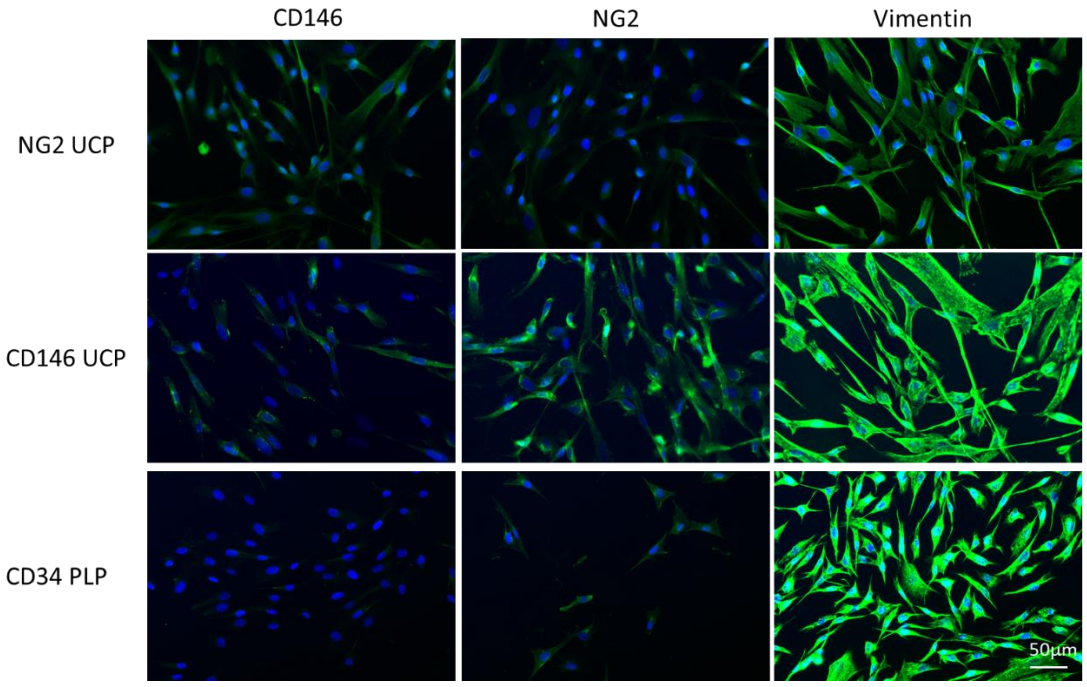

Figure 3.12: Immunofluorescent analysis of isolated pericyte populations for expression of pericyte markers CD146, NG2 and Vimentin. Top three panels show representative images for NG2 UCPs expression profile (n = 8). Middle three panels show representative images for CD146 UCPs expression profile (n = 7). Bottom three panels show representative images for CD34 PLPs expression profile (n = 5). Nuclei were stained using DAPI. Scale bar = 50µm for all images.

In addition to characterisation of endothelial and pericyte markers, cells were also analysed to assess their stemness potential by immunostaining for GATA-binding protein 4 (GATA4), homeobox protein NANOG, octamer-binding transcription factor 4 (OCT4) and sex determining region Y-box 2 (SOX2). NANOG, OCT4 and SOX2 are all essential transcription factors for driving pluripotent-specific expression of numerous genes and maintaining a pluripotent self-renewing stem cell phenotype, whilst GATA4 is implicated in cardiac differentiation (Armiñán et al., 2008; Chambers et al., 2003; Rizzino, 2009; Rodda et al., 2005). As demonstrated in **Figure 3.13**, all cell populations expressed stemness-associated markers. Expression was concentrated in the nucleus; however, some transcription factors were detected in the cytoplasm. Interestingly, in cells where cytoplasmic expression was detected, a drop in nuclear expression was observed. This is illustrated in the representative image for NG2 UCP GATA4 and SOX2 expression (**Figure 3.13**).

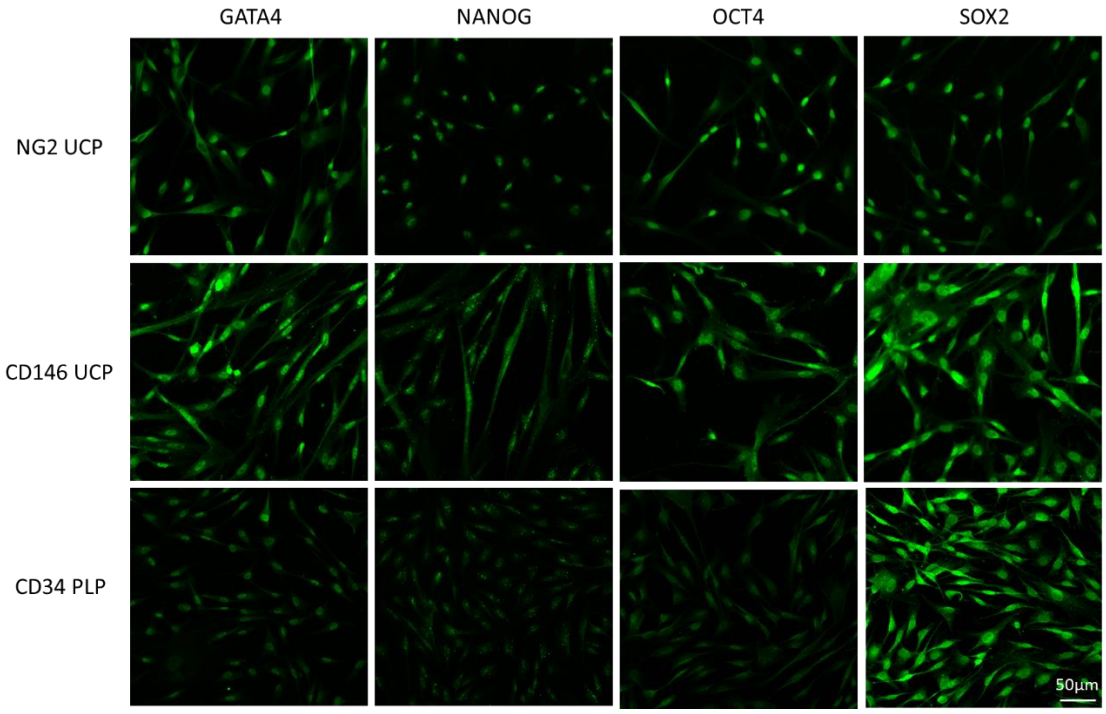

Figure 3.13: Immunofluorescent analysis of isolated pericyte populations for expression of stemness markers GATA4, NANOG, OCT4 and SOX2. Top three panels show representative images for NG2 UCPs expression profile (n = 8). Middle three panels show representative images for CD146 UCPs expression profile (n = 7). Bottom three panels show representative images for CD34 PLPs expression profile (n = 5). Cardiac transcriptional factor GATA-binding protein 4 (GATA4), transcription factor NANOG, octamer-binding transcription factor 4 (OCT4), and sex-determining region Y-box 2 (SOX2). Scale bar = 50µm for all images.

In addition to qualitative analysis by immunocytochemical staining, cell surface marker expression was analysed using flow cytometry (method 2.5) to assess the purity of isolated cell populations. Forward scatter indicates relative size of the cell whilst side scatter indicates the cell granularity. These values were plotted to exclude any debris and identify if the cell population is heterogenous or represents a single population. As demonstrated in **Figure 3.14A**, there was only one cell type identified along with some debris. Plotting forward scatter-area versus forward scatter-height (**Figure 3.14B**) ensured only single cells were analysed, excluding doublets which would skew fluorescence measurements. A zombie live/dead dye was used to ensure only live cells were analysed. To set this gate, half the cells in the analysis tube were killed and stained as set out in the methods, and the stained cells were excluded from

analysis (**Figure 3.14C**). **Figures 3.14D-M** represent a typical expression profile for NG2 UCPs. There is heavy overlap between stained cells and the negative control for endothelial and haematopoietic markers (**Figures 3.14D-F**), which demonstrates the majority of cells did not express these proteins. In contrast, there is a distinct increase in fluorescent signal for mesenchymal and pericyte associated markers, as demonstrated by the position of the blue histograms in **Figures 3.14G-M**.

The flow cytometric data collected for all cell lines is summarised in **Figure 3.15A**. This data demonstrates that less than 5% of cells in isolated pericyte cell lines expressed endothelial markers CD31 and CD34, as well as haematopoietic marker CD45. This was also observed in MSCs, which were included as a comparative control. Greater than 95% of analysed cells in NG2 UCP, CD146 UCP and MSC populations displayed mesenchymal markers CD105, CD73, CD90 and CD44. CD34 PLPs demonstrated a similarly homogenous expression of CD105 and CD90 (>95%); however, they also demonstrated variable expression of CD73 and CD44 as indicated by the large error bars and significantly lower average number of positive cells. In fact, in two CD34 PLP donor populations less than 50% of cells expressed these markers, which may suggest this isolation protocol does not result in a consistent cell product. 60-80% of pericytes expressed NG2 and PDGFR-β with no significant differences between NG2 UCPs, CD146 UCPs and CD34 PLPs. Interestingly, significantly less MSCs expressed NG2 (<20%) and PDGFR-β (<50%), which may indicate a difference in phenotype between pericytes and MSCs. This difference in expression was not due to the effect of culture media as MSCs that were cultured in EGM-2 demonstrated no difference in marker expression to those that were cultured in MSC medium (**Figure 3.15B**). As expected, CD146 was expressed more in CD146 UCPs than other cell types; however, this expression was only seen in around 50% of isolated cells. Once again, there was relatively little difference in expression levels between NG2 UCPs and CD146 UCPs, indicating that the isolation protocols could be selecting overlapping cell populations; however, significantly less CD34 PLPs and MSCs expressed CD146.

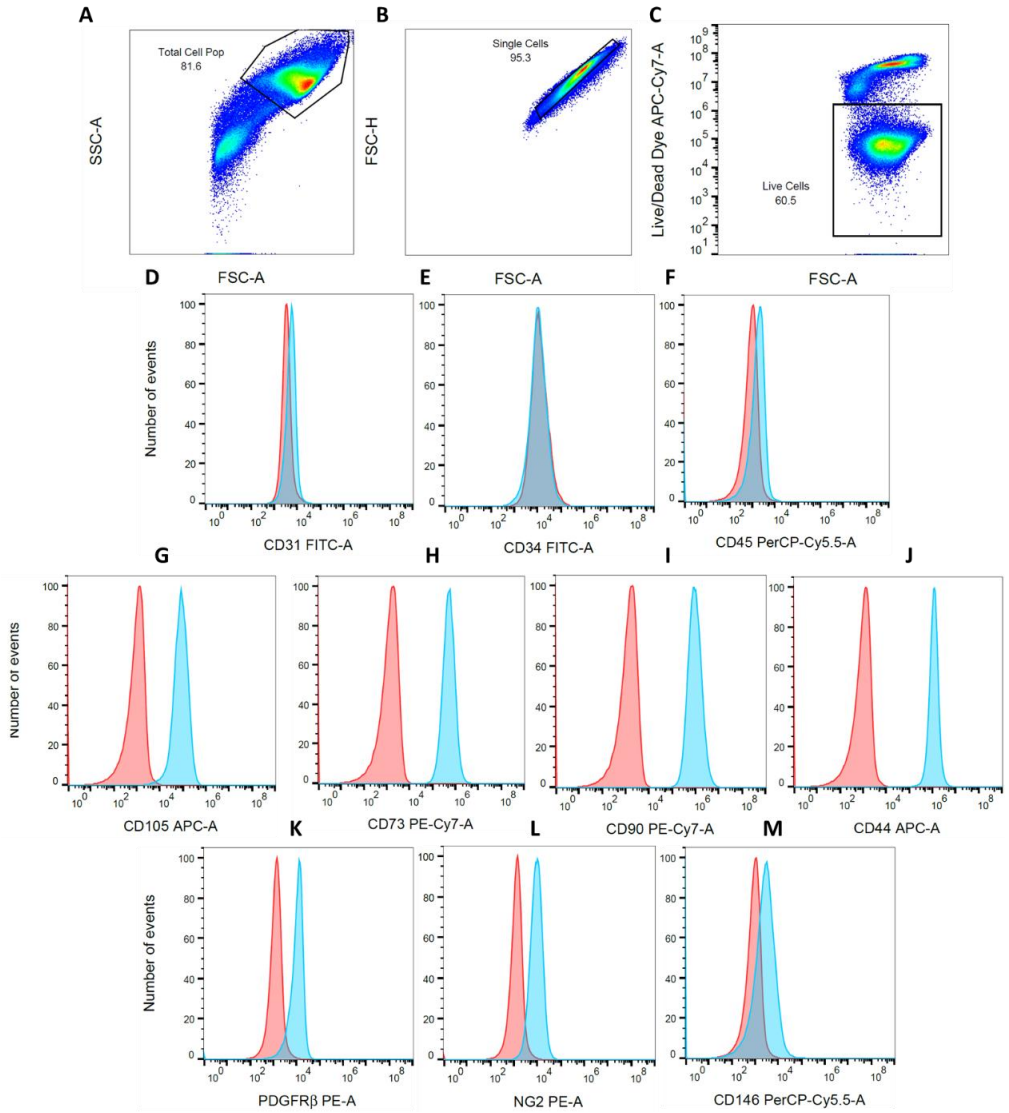

Figure 3.14: Gating strategy and representative histogram for NG2 UCPs surface marker expression analysed by flow cytometry. (A-C) Gating strategy used to analyse only live single cells in the population. SSC-A = side scatter area, FSC-A = forward scatter area, FSC-H = forward scatter height. Note that cells in panel C were deliberately killed to set the gate and is not representative of viability in a normal cell line. (D-F) Representative histograms for endothelial markers CD31 and CD34, and haematopoietic marker CD45. (G-J) Representative histograms for mesenchymal markers CD105, CD73, CD90 and CD44. (K-M) Representative histograms for pericyte associated markers platelet-derived growth factor receptor beta (PDGFR-β), NG2 and CD146. Negative control staining profiles are demonstrated by the red histograms and specific antibody staining profiles are demonstrated by the blue histograms.

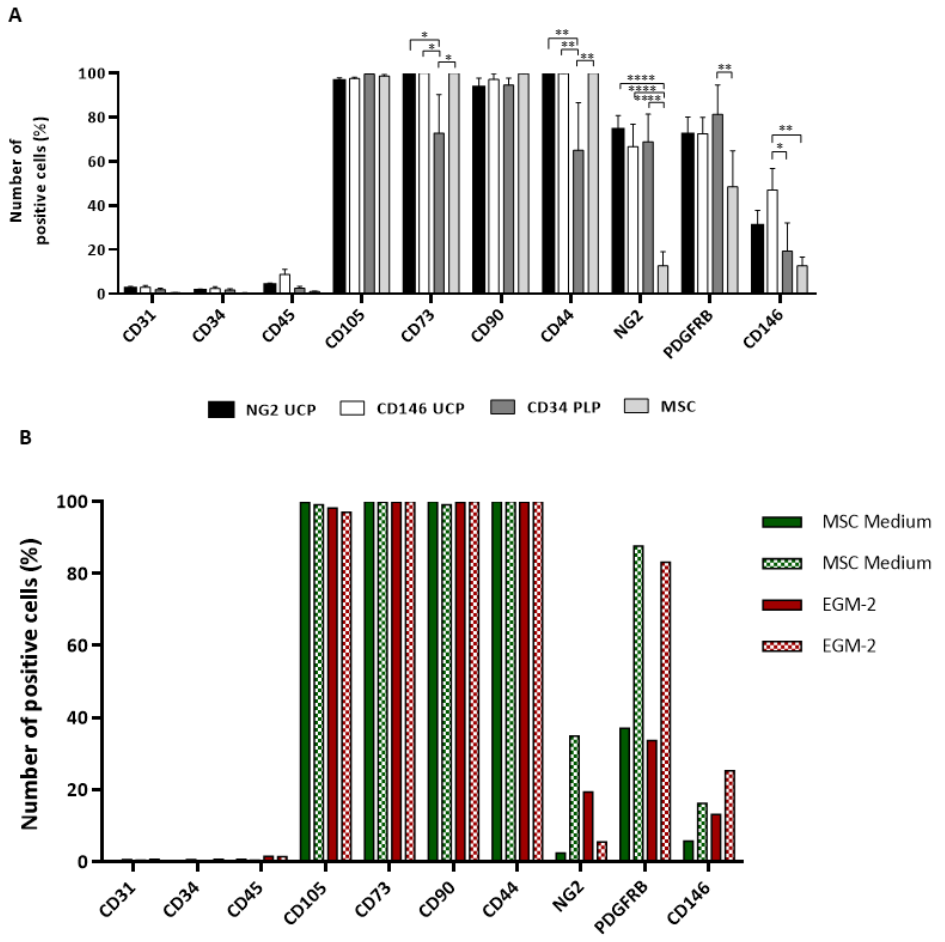

Figure 3.15: Summary of expression profile obtained using flow cytometry. (A) Comparison of expression profiles for isolated cell lines. Data represents means (± S.E.M). NG2 UCP $n = 7$, CD146 UCP $n = 7$, CD34 PLP $n = 5$, MSC $n = 5$; * $p<0.05$ ** $p<0.01$ *** $p<0.001$ **** $p<0.0001$ as determined by two-way ANOVA followed by Tukey's post-hoc test. MSCs were included for comparative control. (B) Expression profile of MSCs after culturing for 7 days in either MSC medium or endothelial growth medium-2 (EGM-2). Each column represents an individual experiment. Platelet-derived growth factor receptor beta (PDGFR-β).

3.4.4. Evaluation of Expansion Capacity and Viability

To further understand the feasibility of using isolated pericytes for clinical applications, we needed to ensure the cells could be expanded sufficiently in culture whilst maintaining a high level of viability throughout in vitro expansion. A growth curve was produced by seeding cells and counting viable cells on consecutive days (method 2.6), as illustrated in **Figure 3.16A**.

NG2 UCPs, CD146 UCPs and MSCs demonstrated a similar growth profile, proliferating from an initial seeding of 30,000 cells to a maximum of around 500,000 cells after 7 days. CD34 PLPs demonstrated slightly different behaviour, reaching a maximum viable cell number of 750,000 cells after 6 days, which then dropped on day 7. This reduction in viable cells may be due to the cells becoming overconfluent when expanding beyond 750,000 cells per well, resulting in cell apoptosis. Doubling time was calculated from the log phase of growth (between the 4-day and 7-day time points) for each individual donor cell line (**Figure 3.16B**). There were no significant differences in cell doubling time, with all isolated cell types taking between 50 and 80 hours to double in number. In addition to doubling time, viability was calculated from the number of viable and non-viable cells. As demonstrated in **Figure 3.16C**, more than 85% of cells remained viable throughout culture expansion for all umbilical cord and placenta pericytes. The only exception to this was the viability of CD34 PLPs after 7 days of culture, which was significantly lower than other cell types at just over 75%. This correlated with the drop in cell numbers observed on day 7 of the growth curve in **Figure 3.16A**.

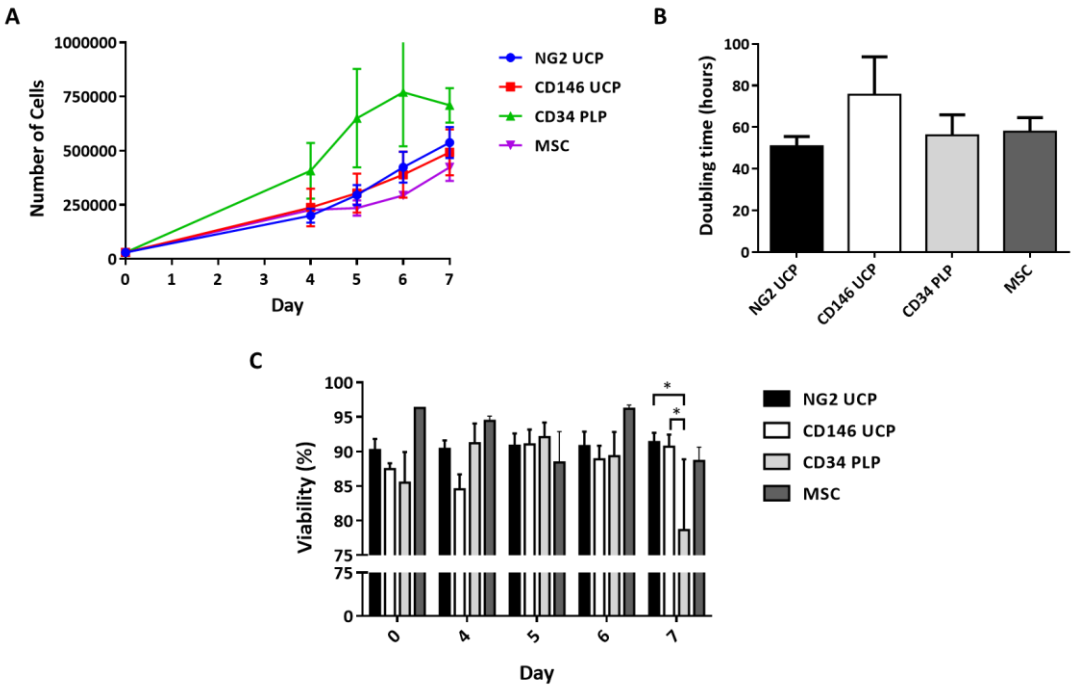

Figure 3.16: Expansion capacity and viability of cells in culture. (A) Cell growth curve. Data represents means (± S.E.M). NG2 UCP *n* = 6, CD146 UCP *n* = 5, CD34 PLP *n* = 4, MSC *n* = 3. (B) Cell doubling time in culture, calculated from cell growth curve. Data represents means (± S.E.M). NG2 UCP *n* = 6, CD146 UCP *n* = 5, CD34 PLP *n* = 4, MSC *n* = 3. (C) Viability analysis of cells in culture. Data represents means (± S.E.M). NG2 UCP *n* = 6, CD146 UCP *n* = 5, CD34 PLP *n* = 4, MSC *n* = 3; * $p<0.05$ as determined by two-way ANOVA followed by Tukey's post-hoc test. MSCs were included for comparative control.

3.5. Discussion

For translational research, it is essential to consider the clinical requirements for cell therapy and tissue engineering applications. One of the key challenges for clinical translation is reducing the variability of cell-based products (Ährlund-Richter et al., 2009; Silverman et al., 2019). As the process of cell selection has been identified as one of the main sources of variation, it is essential to optimise the isolation of protocol to reduce heterogeneity of the cell product.

Initially, isolation of CD31-/CD34+ adventitial pericytes from the umbilical cord was attempted based on a methodology previously established by our research group (Avolio, Rodriguez-Arabaolaza, et al., 2015; Campagnolo et al., 2010). CD34 expression in the absence of CD31 is pericyte-specific in the vessel wall, and therefore was identified as an ideal selection marker. Additionally, pericytes isolated using this marker have demonstrated improved progenitor activity and enhanced regenerative potential (Alvino et al., 2018; R. Katare et al., 2011; R. G. Katare et al., 2013; Sidney et al., 2014). Despite pilot data suggesting that CD31-/CD34+ adventitial pericytes could be isolated from the umbilical cord, after 11 isolation attempts using up to 5g of umbilical cord tissue, only 1 donor cell line could be expanded beyond passage 2. This isolation efficiency was extremely low in comparison to saphenous vein and cardiac pericytes previously isolated using this method, which indicated that this was not a feasible approach for isolation of pericytes from umbilical cord tissue (Avolio, Rodriguez-Arabaolaza, et al., 2015; Campagnolo et al., 2010). Histological analysis of the umbilical cord vessels demonstrated an absence of a vasa vasorum, confirming observations from previous studies (Sexton et al., 1996; Williams et al., 1996). Previously, CD31-/CD34+ pericytes had either been isolated from capillaries and arterioles in the heart or the vasa vasorum of the saphenous vein, and therefore the absence of this layer in the umbilical vessels may explain the lack of successful isolations. Indeed, Schugar et al. previously demonstrated that CD34 expression may be restricted to the endothelial layer in the umbilical vessels (Schugar et al., 2009). Accordingly, *in situ* IHC confirmed the absence of $CD31^{-}/CD34^{+}$ pericyte-like cells in umbilical vessels. This suggests that both the single successful isolation and pilot data were most likely a result of non-specific cell capture, which has been identified as a potential flaw of MACS (Hu et al., 2016).

Due to the lack of success isolating pericytes from umbilical cord based on the CD31-/CD34+ methodology, alternative protocols were explored. To improve chances of successful isolation

and ensure further time was not taken up by this initial project goal, different methodologies were explored in parallel. As detailed in section 3.2, two methods were employed to isolate pericytes from the umbilical cord. Firstly, a novel protocol was developed based on explant outgrowth followed by immunomagnetic selection of NG2+/CD31- cells. NG2 presented an optimal selection marker due to its association with pericytes and expression in the umbilical arteries (Crisan et al., 2012). Explant outgrowth was employed due to the potential advantages over a traditional enzymatic isolation of cells. In fact, incorporation of explant pieces in cell isolation has been reported to increase cell yield by providing additional growth factors and supportive extracellular structures, as well as reducing costs and omitting the proteolytic stress linked with enzymatic digestion (Hendijani, 2017; Yoon et al., 2013). In line with these studies, this new methodology resulted in the highest efficiency of isolation as well as a greater initial cell yield due to the outgrowth of cells before purification. Surprisingly, immunohistochemical analysis only identified sporadic staining of NG2 positive cells within the perivascular region of the umbilical artery, whereas Crisan et al. identified a distinct NG2 positive pericyte layer within the umbilical artery (Crisan et al., 2012). This result may be due to different methods of tissue processing. Nevertheless, the study by Crisan et al. indicates that NG2 is a suitable selection marker for UCPs.

In parallel, an alternative isolation protocol utilising a collagenase digestion and purification of CD31-/CD146+ cells was explored. CD146 has been widely used for purification of pericytes including perivascular cells surrounding the umbilical vessels, and therefore presented a reliable alternative (Cathery et al., 2018). In situ analysis identified a band of CD31-/CD146+ cells mainly localised in the peripheral vascular wall that mirrored previous studies (Baksh et al., 2007; Montemurro et al., 2011). Interestingly, Schugar et al demonstrated more widespread CD146 staining throughout the vascular wall, further highlighting the impact tissue processing can have on expression (Schugar et al., 2009). Nonetheless, data demonstrated CD146 can be used to isolate pericytes from the cord with an isolation efficiency that was comparable to the NG2 UCP protocol.

Although the initial aim of the study was to establish a protocol for isolation of pericytes from the umbilical cord, due to the lack of success encountered early on, alternative foetal tissue sources were explored. It was hypothesised that placenta tissue, home to a dense microvascular network, could contain the initial CD31-/CD34+ pericyte population that was explored. This hypothesis was confirmed through successful isolation of 5 donor cell lines and in situ

identification of cells within the placenta tissue, thereby demonstrating the feasibility of this protocol for placenta pericyte isolation.

Rather than limit the focus at this stage to exploring one of the three successful isolation methods, we decided to explore and compare the three different populations in order to establish which cells posed the greatest regenerative potential and applicability for vascular tissue engineering. All isolated cell populations demonstrated the typical spindle-like morphology that pericytes display in vitro; however, CD34 PLPs presented a smaller and less elongated shape which is more reminiscent of early endothelial progenitor cells (EPCs) (Hur et al., 2004). In fact, CD34+/CD31- expression can be used to distinguish early EPCs, and therefore may result in isolation of a heterogenous cell population comprising of adventitial pericytes and early EPCs (Chopra et al., 2018; Hur et al., 2004). Antigenic characterisation was used to confirm the specificity of the isolation protocol and demonstrate that isolated cells displayed a typical pericyte-like expression profile. An absence of endothelial associated surface markers CD31, CD34 and VECAD indicated no non-specific capture of ECs within the isolation process. Interestingly, CD34 PLPs did not express CD34 in vitro. This lack of expression was anticipated due to the down regulation of CD34 expression in culture, which has previously been observed in CD31-/CD34+ pericyte populations (Avolio, Rodriguez-Arabaolaza, et al., 2015; Campagnolo et al., 2010). CD146, NG2 and Vimentin are antigenic markers associated with pericytes and were therefore analysed to further confirm that isolated cells phenotypically resembled pericytes. Expression of all three proteins were seen in NG2 UCPs and CD146 UCPs; however, CD34 PLPs did not express CD146, which is typical of adventitial pericytes (Campagnolo et al., 2010).

To understand if the isolated foetal pericytes maintained a certain level of stemness, which may indicate a capacity to differentiate into other vascular lineages, the expression of pluripotency markers was assessed. NANOG, OCT4 and SOX2 were screened due to their pivotal role in coordination of the regulatory network responsible for self-renewal and pluripotency, whilst GATA4 drives cardiac differentiation (Wang et al., 2012). Although previous studies had demonstrated that full-term umbilical cord perivascular MSCs lacked expression of key pluripotency markers, namely OCT4, isolated cells expressed all markers indicating that foetal pericytes maintain a multipotent state different to that of MSCs (Hong et al., 2013). Indeed, isolated cells demonstrated similar stemness profiles to human umbilical cord perivascular cells (HUCPVs) and cardiac pericytes, which exhibit unique potential for skeletal and cardiac

tissue regeneration (Avolio, Rodriguez-Arabaolaza, et al., 2015; Tsang et al., 2013; Yannarelli et al., 2013).

Despite the increased specificity of antibody-based isolation methods, there is still a risk of heterogeneity among cell populations. For clinical translation, flow cytometry has become a powerful tool to confirm the consistency of phenotype among bulk cell populations (Amos et al., 2011; Eaker et al., 2013). Using this technique, it was demonstrated that NG2 and CD146 selection protocols gave rise to similar cell populations with a consistent phenotype. This data also validated the immunocytochemical analysis, confirming a high purity cell population. The only exception to this was CD146 expression, which was detected in all cells by ICC but expressed by less than 50% of cells according to flow cytometric analysis. This drop in expression was also observed in HUCPVs isolated using CD146 selection and may be due to down regulation of CD146 in cultured cells (Gökçinar-Yagci et al., 2016; Jin et al., 2016). NG2 and PDGFR-β were also expressed by only 70% of cells, which is likely due to a reduction in expression of the markers after prolonged culture rather than contamination, as colour density plots only identified one cell population. In contrast, CD34 PLPs demonstrated a high degree of variability between cell lines, which indicates that the protocol did not isolate a consistent cell population. A commercial cell line of WJ-MSCs were included as a comparative control due to their use in tissue engineering and cell therapy applications, and similarities with pericytes (Bajpai et al., 2012; Mantakaki et al., 2018; Saeedi et al., 2019). In fact, there is evidence to suggest that pericytes simply represent the in vivo counterpart of MSCs (de Souza et al., 2016; Gomez-salazar et al., 2020). Considering this, it was important to identify any differences that would highlight the unique identity of pericytes as a more refined subset of mesenchymal cells. As demonstrated, there are considerably less MSCs expressing pericyte-associated markers NG2 and PDGFR-β, indicating a distinct phenotypic difference.

Generation of frozen cell stocks and subsequent successful thawing and culturing of cells demonstrated they were robust to cryopreservation, which is essential for prolonged storage and use in clinical applications (Ährlund-Richter et al., 2009; Silverman et al., 2019). Furthermore, all cell types could be rapidly expanded in culture to more than 10 million cells in under 6 weeks, as evidenced by the short cell doubling time. As feasibility studies demonstrated, this is more than adequate for the development of a tissue engineered vascular graft (Alvino et al., 2020). No evident differences in expansion capacity were detected between the different cell types; however, there was variability between individual cell populations

which was attributed to the biological variation between donors. Viability of cells also remained above 90% in all cell types except CD34 PLPs. A high viability is important for clinical applications due to the role apoptotic cells play in vascular calcification and therefore the drop in viability seen in CD34 PLPs after 7 days was concerning (Proudfoot et al., 2001). The increase in non-viable cells corelated with a dip in cell number and appearance of floating cells. Rather than forming a confluent monolayer, the cells became overconfluent and began detaching from the culture surface. This suggests that the mechanisms involved in contact inhibition may be dysfunctional in CD34 PLPs, which is implicated in tumour formation (Pavel et al., 2018). Consequently, this cell type may not be suitable for clinical use.

In summary, all 3 protocols were successfully used to isolate and expand pericyte-like cells from umbilical cord and placenta tissue. NG2 UCPs and CD146 UCPs appear the safest options going forwards due to their greater isolation efficiency, more consistent phenotype, and reliable expansion capacity; however, these differences are only marginal. Further functional characterisation of cells is required to better distinguish differences between cell types and conclude which is the optimal pericyte population for generation of a tissue engineered vascular graft.

4. Identifying the Optimal Pericyte Population for Vascular Tissue Engineering

4.1. Introduction

The arterial wall is a complex structure that is hard to mimic through tissue engineering. The tunica intima forms the luminal part of the vessel and is comprised of an endothelium, basement membrane, and in larger arteries, an internal elastic lamina. Surrounding this layer is the tunica media which contains up to 60 concentric layers of VSMCs; the most populous cell type in arteries (Bacakova, Travnickova, Filova, Matějka, et al., 2018). The outer tunica adventitia, which mainly consists of fibroblasts and pericytes, anchors the blood vessel to the surrounding tissue and supplies blood to the vessel wall through the vasa vasorum. In order to replicate the physiological function of the arterial wall, tissue engineered vascular grafts should ideally incorporate these layers.

Indeed, one of the primary challenges for vascular tissue engineering is the development of a tunica media-like layer to confer the graft with contractile properties. In a healthy native blood vessel, VSMCs are responsible for the regulation of vascular tone through vasoconstriction and vasodilation. Consequently, some studies have incorporated these cells in an attempt to enhance the contractile function of engineered grafts (Neff et al., 2011). Whilst functional improvements utilising VSMC directly have been reported, generally differentiated pluripotent cells or differentiated VSMCs are preferred (Bajpai et al., 2012; Y. Wang et al., 2014). Although under normal physiological conditions VSMCs exist in a quiescent contractile state, under pathologic stress these cells undergo a phenotypic transition to a proliferative synthetic non-contractile state, which contribute to atherosclerotic plaque formation and vascular stenosis (Bacakova, Travnickova, Filova, Matějka, et al., 2018). This synthetic form is usually adopted by VSMCs during in vitro culture expansion. To negate this, many studies utilise stem cells with VSMC differentiation potential to improve graft contractile properties (Bacakova, Travnickova, Filova, Matejka, et al., 2018). It is therefore desirable that cells used for vascular tissue engineering demonstrate a distinct ability to differentiate towards a VSMC fate.

To further improve graft technology and better mimic in vivo vessels, generation of a competent vascular system within the engineered tissue is required. Currently, vascularisation remains a limiting factor in the size and complexity of tissue engineered constructs (Mastrullo et al., 2020). In fact, engineered tissues thicker than 1mm are prone to becoming necrotic before perfusion by host-derived micro vessels (Chang et al., 2017). Whilst natural large vessels often comprise of a vasa vasorum to supply nutrients to the cells, engineered grafts are usually avascular, which compromises their long-term survival. In order to stimulate angiogenesis and

development of a vascular network, researchers have utilized a variety of strategies, ranging from direct 3D bioprinting of vascular-like networks to progressive release of growth factors such as VEGF and angiopoietins (Brudno et al., 2013; Jia et al., 2016; Zhang et al., 2013). Alternatively, vascularisation can be achieved by harnessing the properties of proangiogenic cells. By seeding scaffolds with a combination of proangiogenic cells, engineers can mimic the biological angiogenic process through natural cell signalling pathways (Mastrullo et al., 2020). In particular, perivascular cells have shown an ability to promote network formation in avascular scaffolds due to their native role within the vascular niche (Sathy et al., 2015; N. Wang et al., 2017). By evaluating the in vitro angiogenic properties of different cell types, it is possible to uncover favourable cell sources for tissue engineering.

4.2. Objectives

In the following chapter the functional properties of umbilical cord and placenta pericytes were investigated to determine which population would be optimal for vascular tissue engineering, and therefore conclude what pericyte population would be used for future studies. The following experimental objectives were set:

- Quantify the ability of isolated pericytes to differentiate into VSMCs.
- Characterise the secretome of isolated pericyte cell lines.
- Quantify the angiogenic capacity of pericytes through application of a tube formation assay.
- Conclude which pericyte population is optimal and compare the functional properties to WJ-MSCs.

4.3. Results

4.3.1. VSMC Differentiation Capacity

In order to evaluate whether umbilical cord and placenta pericyte populations could form functional smooth muscle-like tissue, cells were exposed to medium containing TGF-β to stimulate differentiation into VSMCs (method 2.10). Differentiated and undifferentiated cells were assessed for expression of an array of antigenic markers, which are used to indicate the phase of VSMC phenotype, ranging from synthetic to a mature contractile phenotype.

To initially check if the cells had successfully differentiated towards a VSMC phenotype, gene expression of smooth muscle associated markers were analysed using qPCR (method 2.11). *ACTA2* and *CNN1* were upregulated considerably, with all cells demonstrating a 10-20-fold increase in *ACTA2* and >50-fold increase in *CNN1* (**Figure 4.1A-B**). Only a modest 2-3-fold upregulation of *TAGLN* and 2-4-fold increase in *MYH10* was observed; however, *MYH11*, which is usually only expressed by mature VSMC, was upregulated 5-fold in NG2 UCPs and CD146 UCPs (**Figure 4.1C-E**). Although CD34 PLP *MYH11* expression increased, there was considerable variation between donor cell lines which further suggests a heterogeneity of this population. In general, all differentiated umbilical cord and placenta pericyte populations increased their expression of VSMC; however, due to variations in upregulation between donor cell lines, many of these changes did not reach statistical significance. There were no discernible differences between the different cell populations.

In addition to quantifying the upregulation of VSMC marker mRNA levels, the mRNA levels of differentiated pericytes were compared to differentiated HPASMCs. Since the overriding project goal was the generation of a vascular graft to reconstruct the pulmonary artery at the RVOT, HPASMCs were chosen for comparison. As **Figure 4.2** illustrates, differentiated umbilical cord and placenta pericytes expressed similar levels of *ACTA2*, *TAGLN* and *MYH11*; however, expression of *CNN1* and *MYH10* was significantly lower. Nevertheless, mRNA levels were still comparable to HPASMCs, suggesting that differentiation at the genetic level was successful.

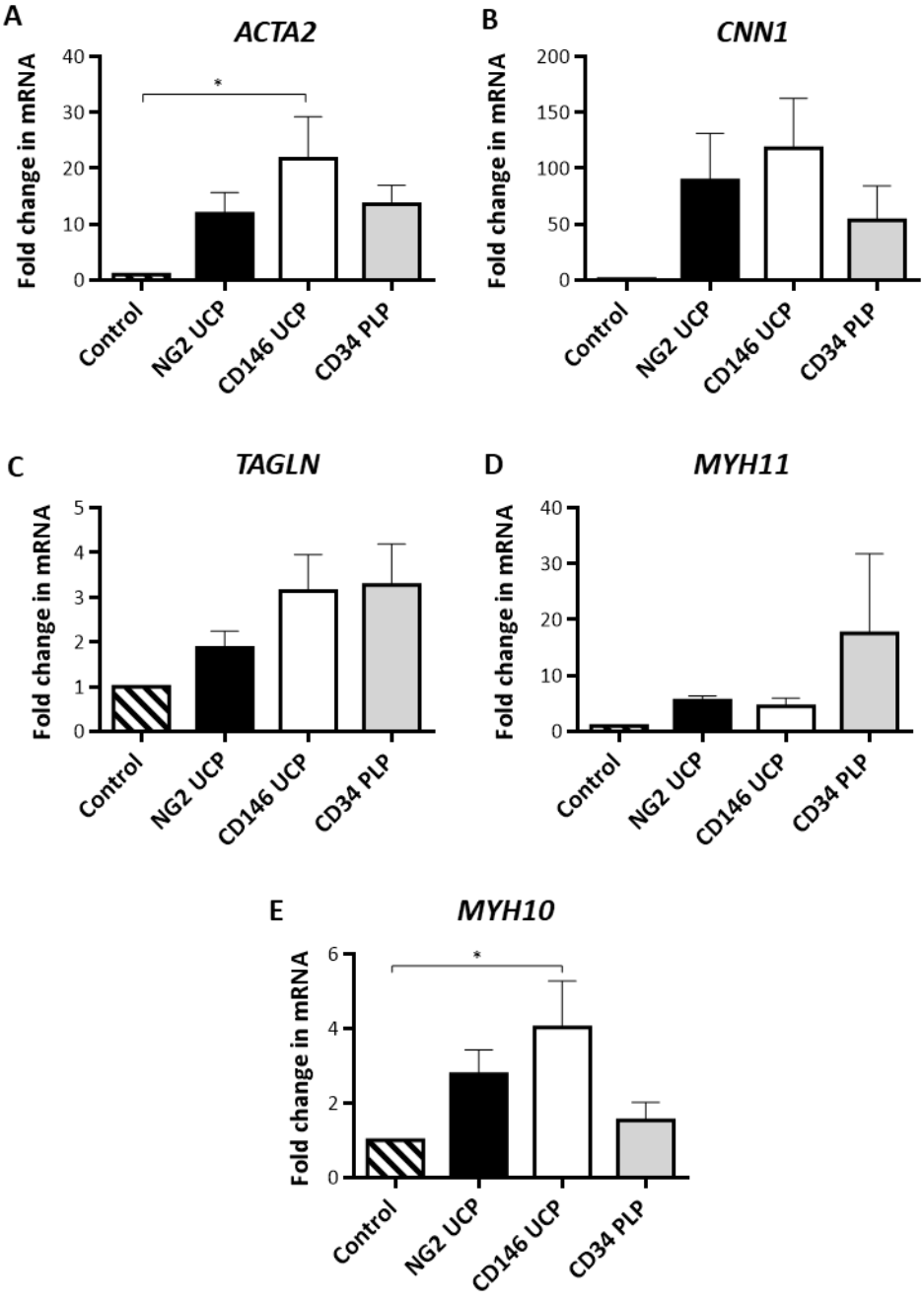

Figure 4.1: Fold change in mRNA levels of VSMC markers after differentiation vs undifferentiated (control). (A) ACTA2 = alpha smooth muscle actin (αSMA). (B) CNN1 = Calponin. (C) TAGLN = Transgelin. (D) MYH11 = smooth muscle myosin heavy chain (SM-MHC). (E) MYH10 = non muscle myosin IIB (NMMyoIIB). Data represents means (± S.E.M). NG2 UCP n = 5, CD146 UCP n = 6, CD34 PLP n = 4. * $p<0.05$ as determined by one-way ANOVA followed by Tukey's post-hoc test.

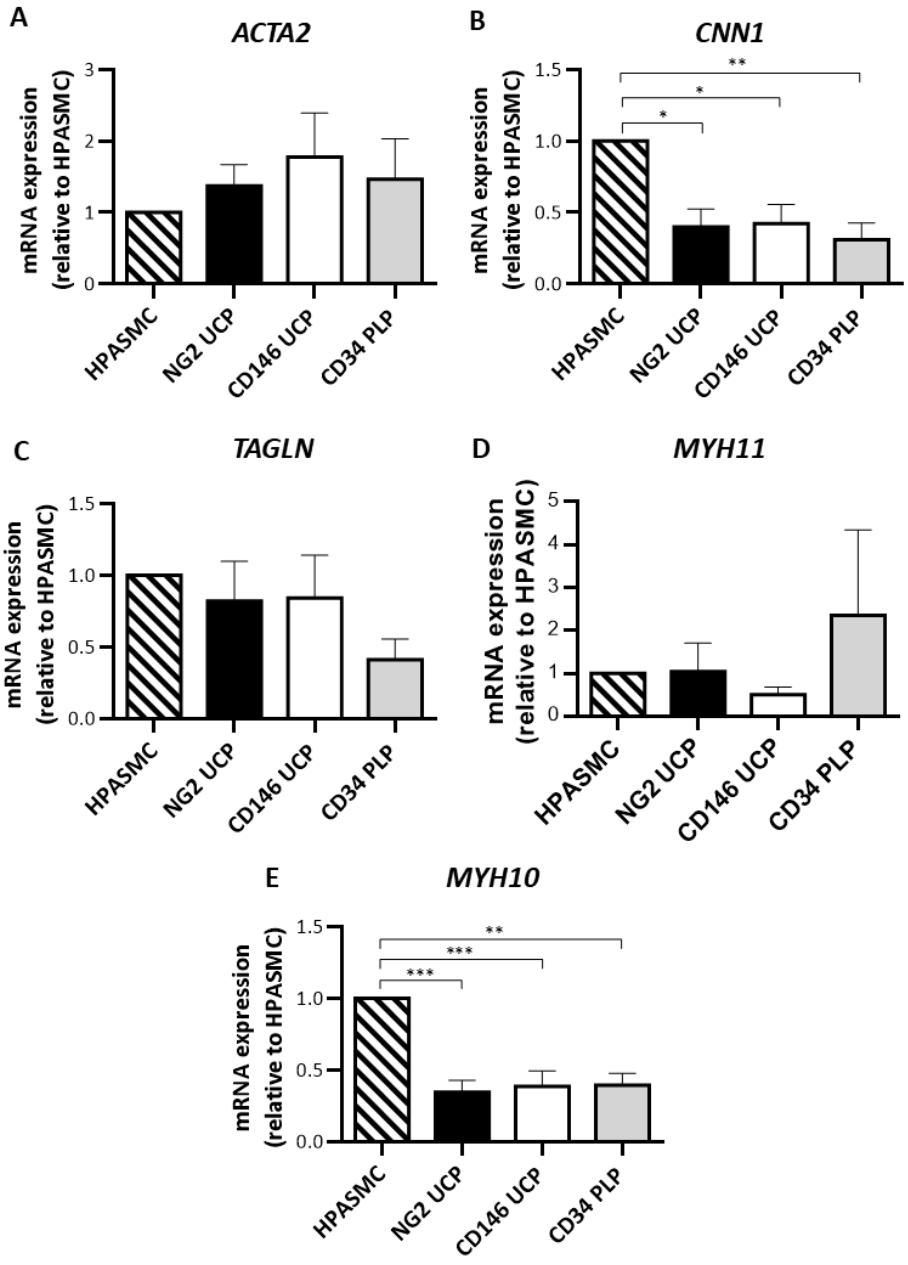

Figure 4.2: mRNA levels of VSMC markers in differentiated pericytes relative to differentiated human pulmonary artery smooth muscle cells (HPASMC). (A) *ACTA2* = alpha smooth muscle actin (αSMA). (B) *CNN1* = Calponin. (C) *TAGLN* = Transgelin. (D) *MYH11* = smooth muscle myosin heavy chain (SM-MHC). (E) *MYH10* = non muscle myosin IIB (NMMyoIIB). Data represents means (± S.E.M). NG2 UCP n = 5, CD146 UCP n = 6, CD34 PLP n = 4, HPASMC n = 4. * $p<0.05$, ** $p<0.01$, *** $p<0.001$ as determined by one-way ANOVA followed by Tukey's post-hoc test.

To confirm that the changes in gene expression were translated, protein levels were analysed by western blot (method 2.12). Similar to mRNA analysis, protein levels of all VSMC associated markers were upregulated; however, the degree of upregulation varied between the different cell types (**Figure 4.7**). αSMA was increased 5-10-fold, with CD34 PLPs demonstrating the largest increase (**Figure 4.7A**). NG2 UCPs demonstrated the most significant increase in Calponin (20-fold), whilst CD146 UCPs and CD34 PLPs increased by 10-fold (**Figure 4.7B**). In contrast to the modest increase in mRNA levels, transgelin was increased significantly in NG2 UCPs and CD34 PLPs (**Figure 4.7C**). Importantly, all cell lines demonstrated a small but significant upregulation in smooth muscle myosin heavy chain (SM-MHC), which suggests differentiation towards a specific VSMC phenotype rather than a myofibroblastic phenotype. Furthermore, NG2 UCP also showed a 4-fold increase in NMMyoIIB (**Figure 4.7D & E**). These results did not mirror the mRNA analysis, which suggested that CD146 UCPs displayed the most significant change in phenotype. In fact, at the protein level NG2 UCPs and CD34 PLPs showed the greatest change in expression. **Figure 4.4** demonstrates representative images for the upregulation observed in protein expression. β-tubulin was used as a loading control and 10μg protein loaded for detection of all VSMC markers except for SM-MHC (20μg).

To validate the western blot analysis and detect fibre distribution, cells were analysed by ICC before and after differentiation. From **Figure 4.5** and **Figure 4.6**, we see that before differentiation cells are negative for αSMA and calponin; however, after 15 days there was clear acquisition of positive fibres. This effect is similarly observed in HPASMC. In contrast, there was only a subtle upregulation of transgelin and NMMyoIIB at the fibre level (**Figure 4.7 & 4.8**). Careful examination of **Figure 4.7** demonstrates a distinct presence of transgelin in a few NG2 UCPs and CD146 UCPs. NMMyoIIB was more widely expressed by all differentiated cell types; however, expression was not as strong as αSMA or calponin (**Figure 4.8**). No observable expression of SM-MHC was detected by ICC in either the umbilical cord and placenta pericytes, or the HPASMC control cell line (**Figure 4.9**). These results differed slightly from the protein quantification obtained using western blot analysis (**Figure 4.2 & 4.3).** Specifically, the immunocytochemical staining of transgelin (**Figure 4.7**) was faint compared to the western blot images. This was likely due to the different ways the cells were processed before analysis. For example, the fixation for ICC analysis may have masked the epitope, affecting the image quality. Alternatively, the western blot analysis may be more

sensitive than the method used for ICC, and therefore may have picked up low levels of protein expression that weren't obvious at the fibre level. Nonetheless, it still appears that a change in phenotype towards VSMCs was observed.

Detection of Ki67 (a marker for proliferation) was used to determine if cells had changed from a proliferative state to a more mature form (Scholzen et al., 2000). Representative images in **Figure 4.10** show a visible reduction in Ki67 expression between the differentiated and control cells.

Together this data suggests that all umbilical cord and placenta pericyte populations have some capacity to differentiate towards a VSMC phenotype in line with the HPASMC control. Although CD146 UCPs demonstrated more significant changes at the gene level, NG2 UCPs and CD34 PLPs displayed a more considerable upregulation in VSMC at the protein level.

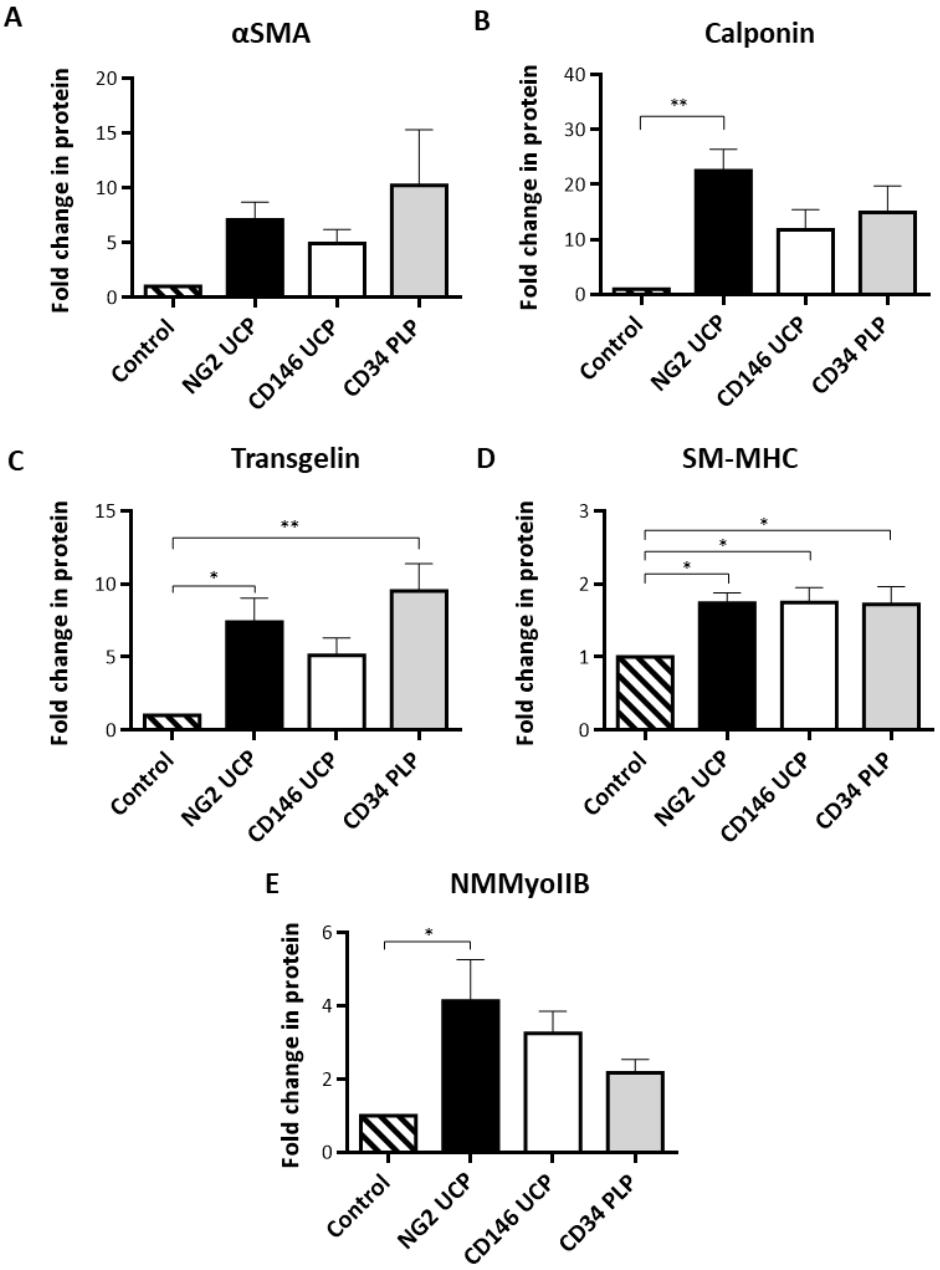

Figure 4.3: Fold change in protein levels of VSMC markers after differentiation vs undifferentiated (control). (A) Alpha smooth muscle actin (αSMA). (B) Calponin. (C) Transgelin. (D) Smooth muscle myosin heavy chain (SM-MHC). (E) Non muscle myosin IIB (NMMyoIIB). Data represents means (± S.E.M). NG2 UCP n = 6, CD146 UCP n = 6, CD34 PLP n = 5. * $p<0.05$, ** $p<0.01$ as determined by one-way ANOVA followed by Tukey's post-hoc test.

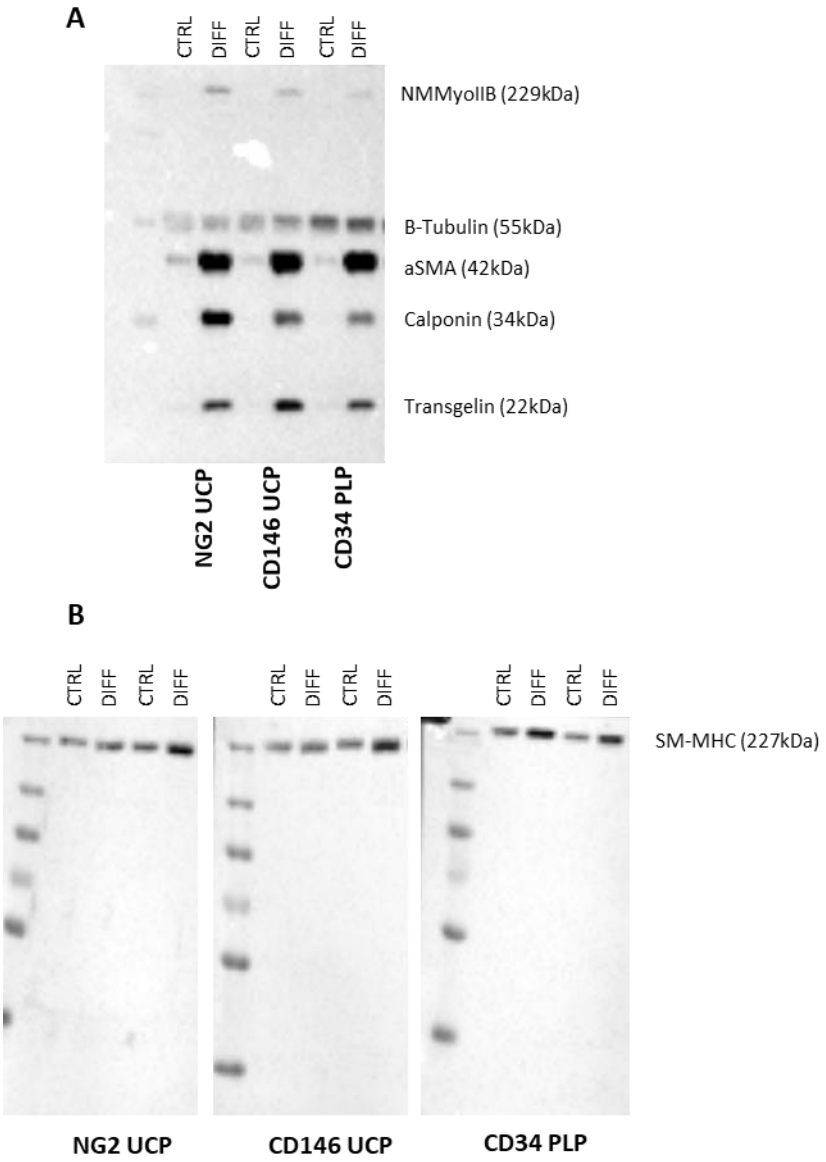

Figure 4.4: Representative western blot images used for quantification of protein upregulation. (A) Representative membrane for alpha smooth muscle actin (αSMA), calponin, transgelin. and non-muscle myosin IIB (NMMyoIIB) expression. (B) representative membranes of smooth muscle myosin heavy chain (SM-MHC) expression. CTRL = control/undifferentiated cells, DIFF = differentiated cells. Western blot analysis was completed with 6 different donor cell lines for NG2 UCP and CD146 UCP, and 5 different donor cell lines for CD34 PLPs.

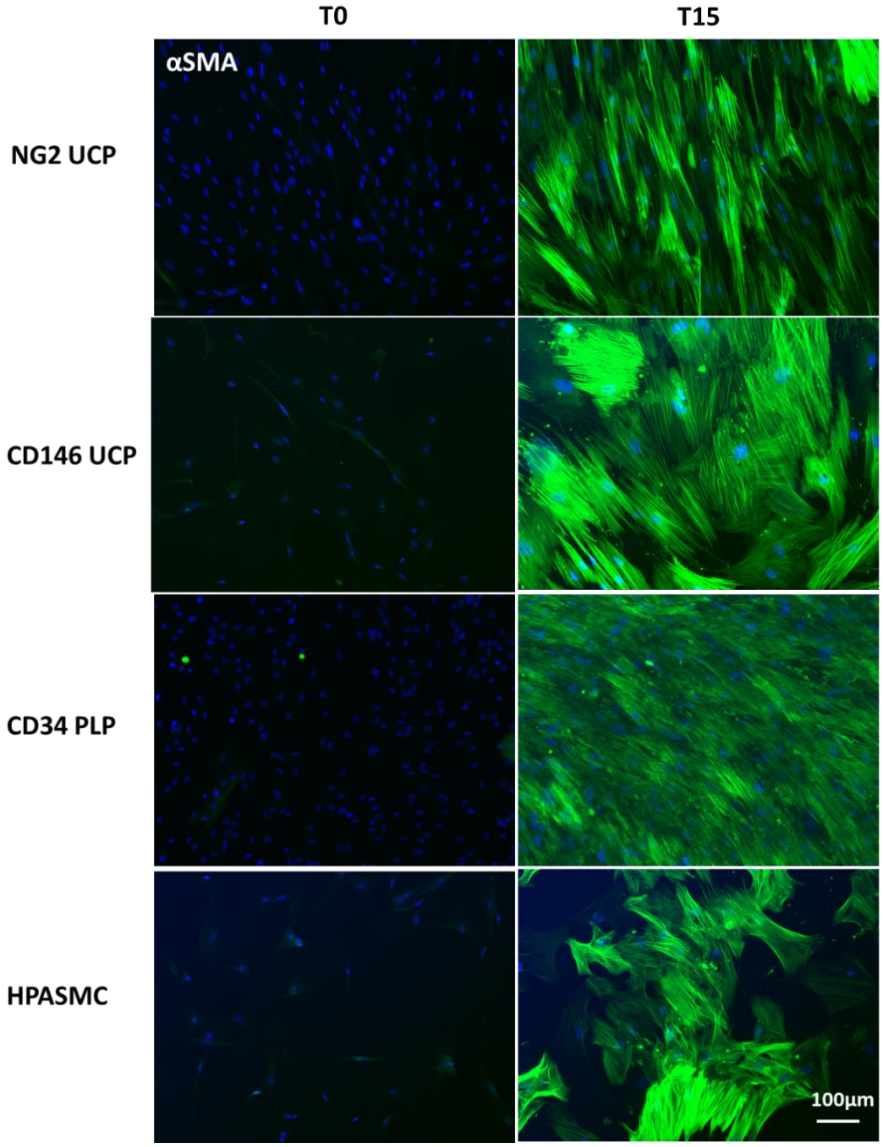

Figure 4.5: Representative immunocytochemical staining of alpha smooth muscle actin (αSMA) expression at day 0 (undifferentiated) and day 15 (differentiated). Scale bar 100µm.

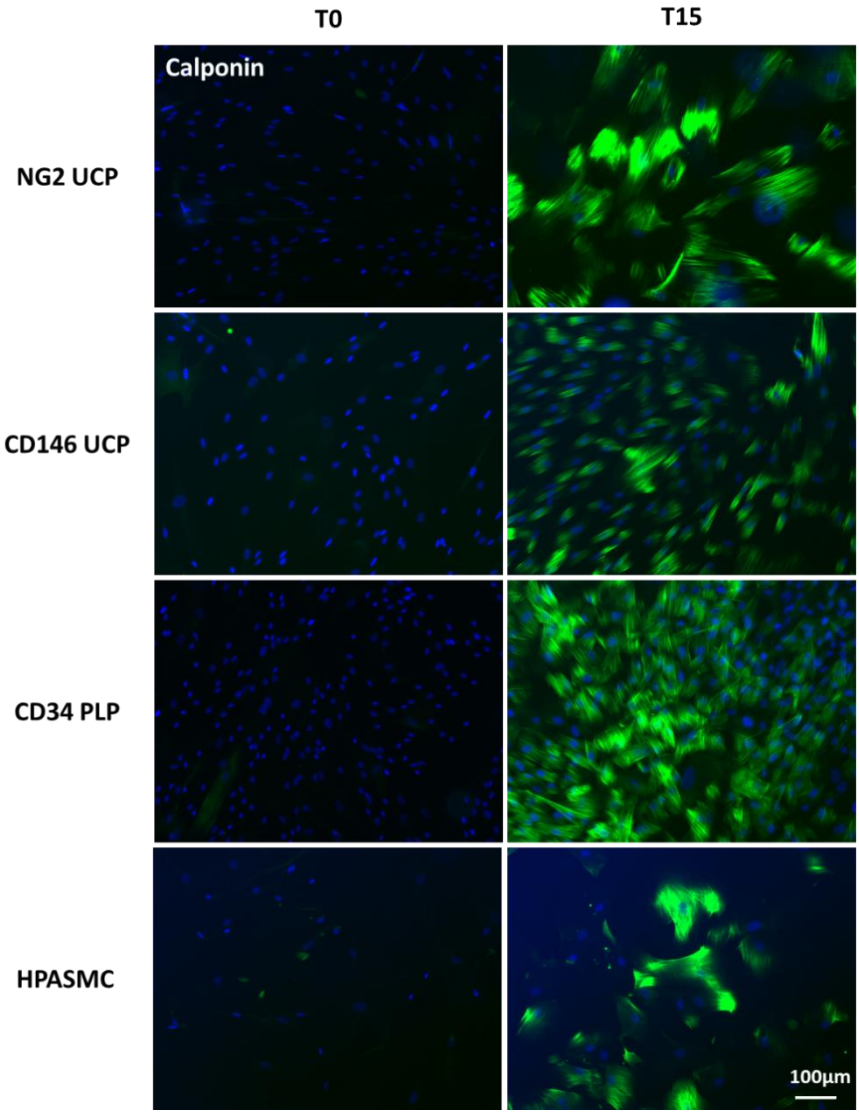

Figure 4.6: Representative immunocytochemical staining of calponin expression at day 0 (undifferentiated) and day 15 (differentiated). Scale bar 100µm.

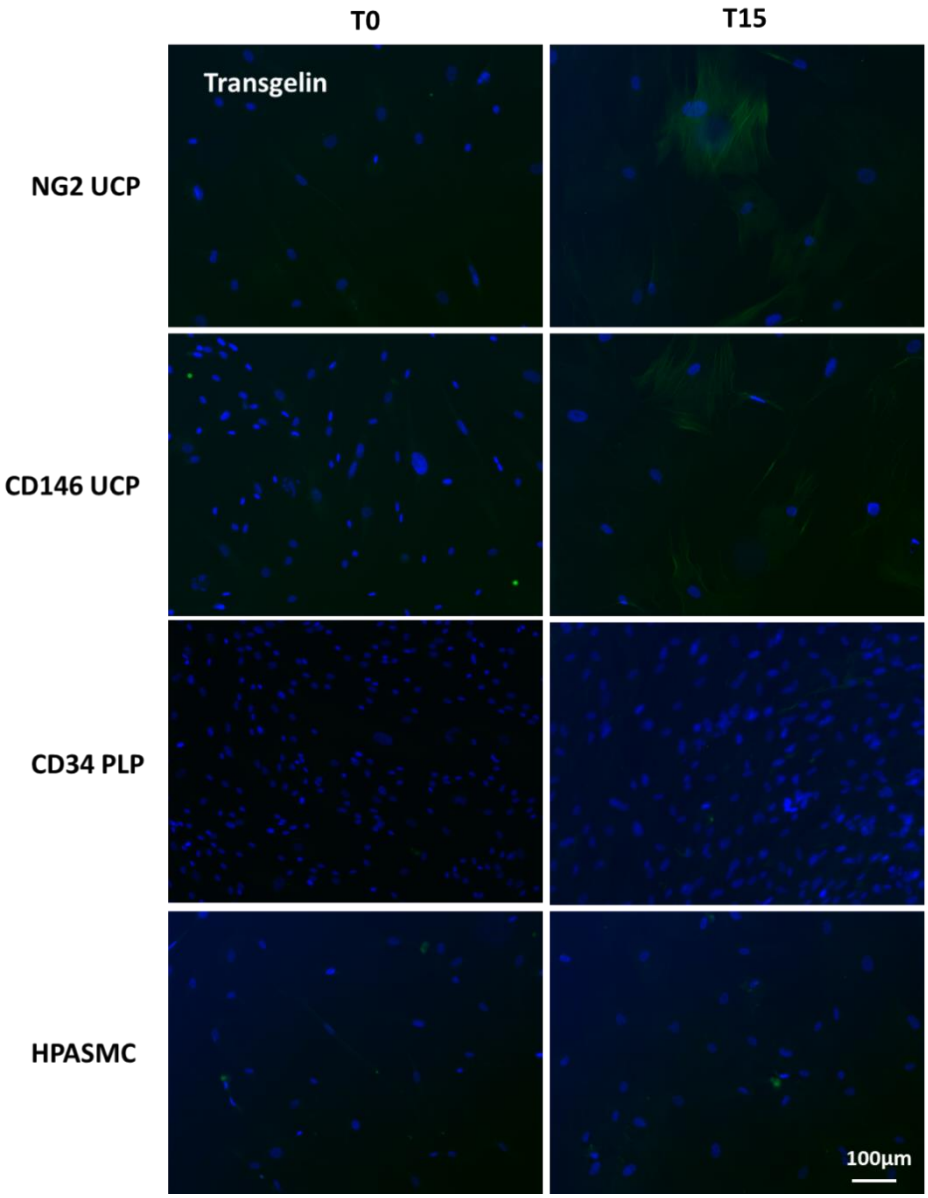

Figure 4.7: Representative immunocytochemical staining of transgelin expression at day 0 (undifferentiated) and day 15 (differentiated). Scale bar 100µm.

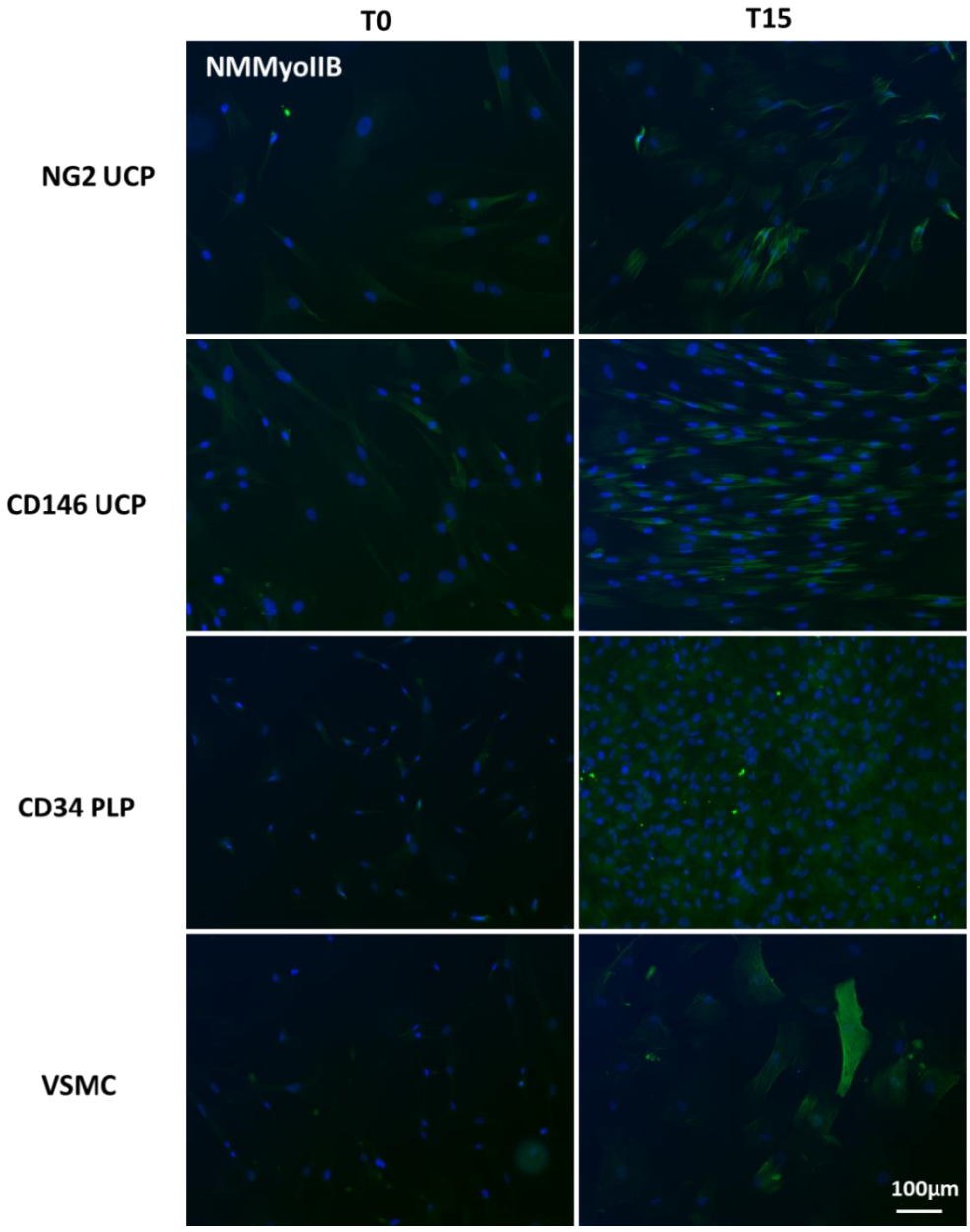

Figure 4.8: Representative immunocytochemical staining of non-muscle myosin IIB (NMMyoIIB) expression at day 0 (undifferentiated) and day 15 (differentiated). Scale bar 100µm.

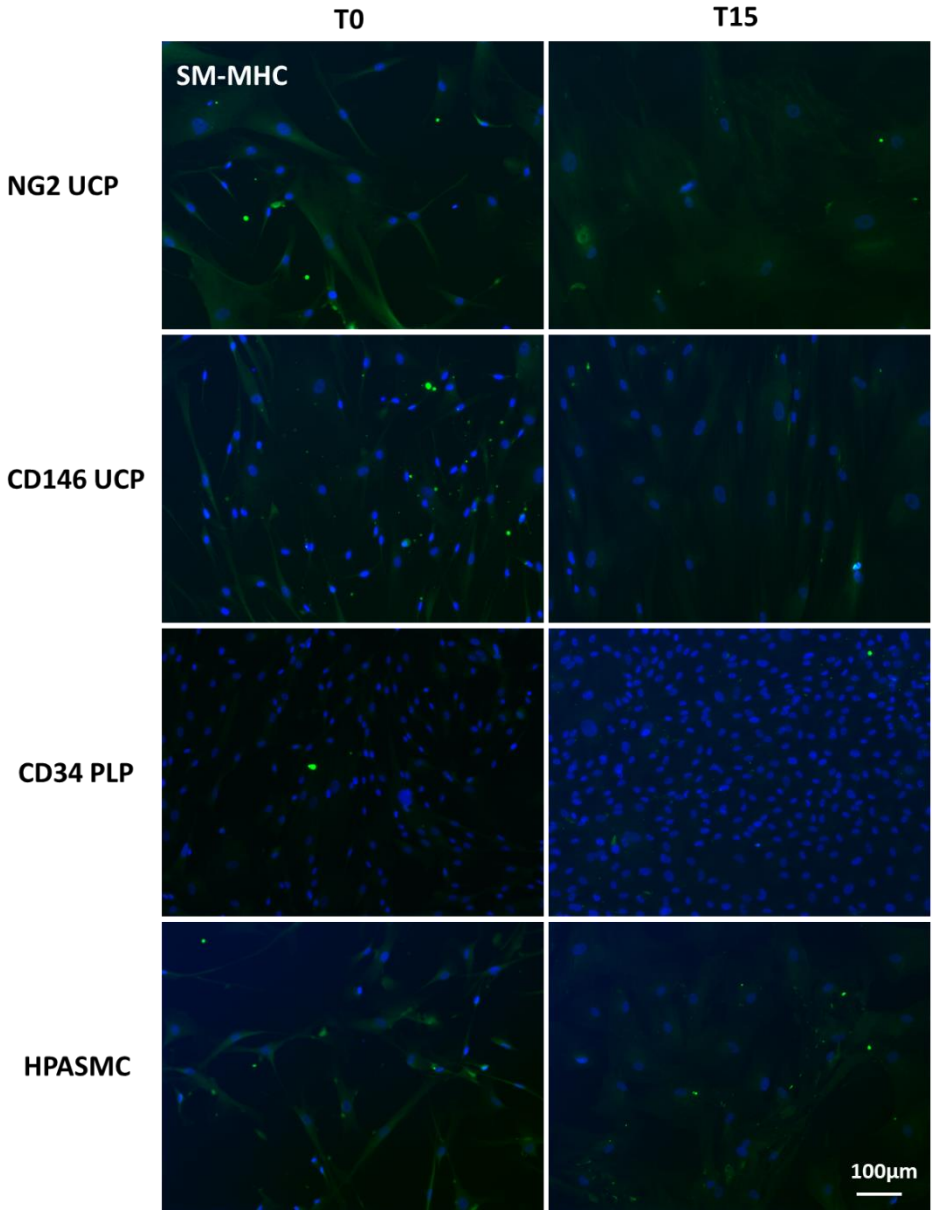

Figure 4.9: Representative immunocytochemical staining of smooth muscle myosin heavy chain (SM-MHC) expression at day 0 (undifferentiated) and day 15 (differentiated). Scale bar 100µm.

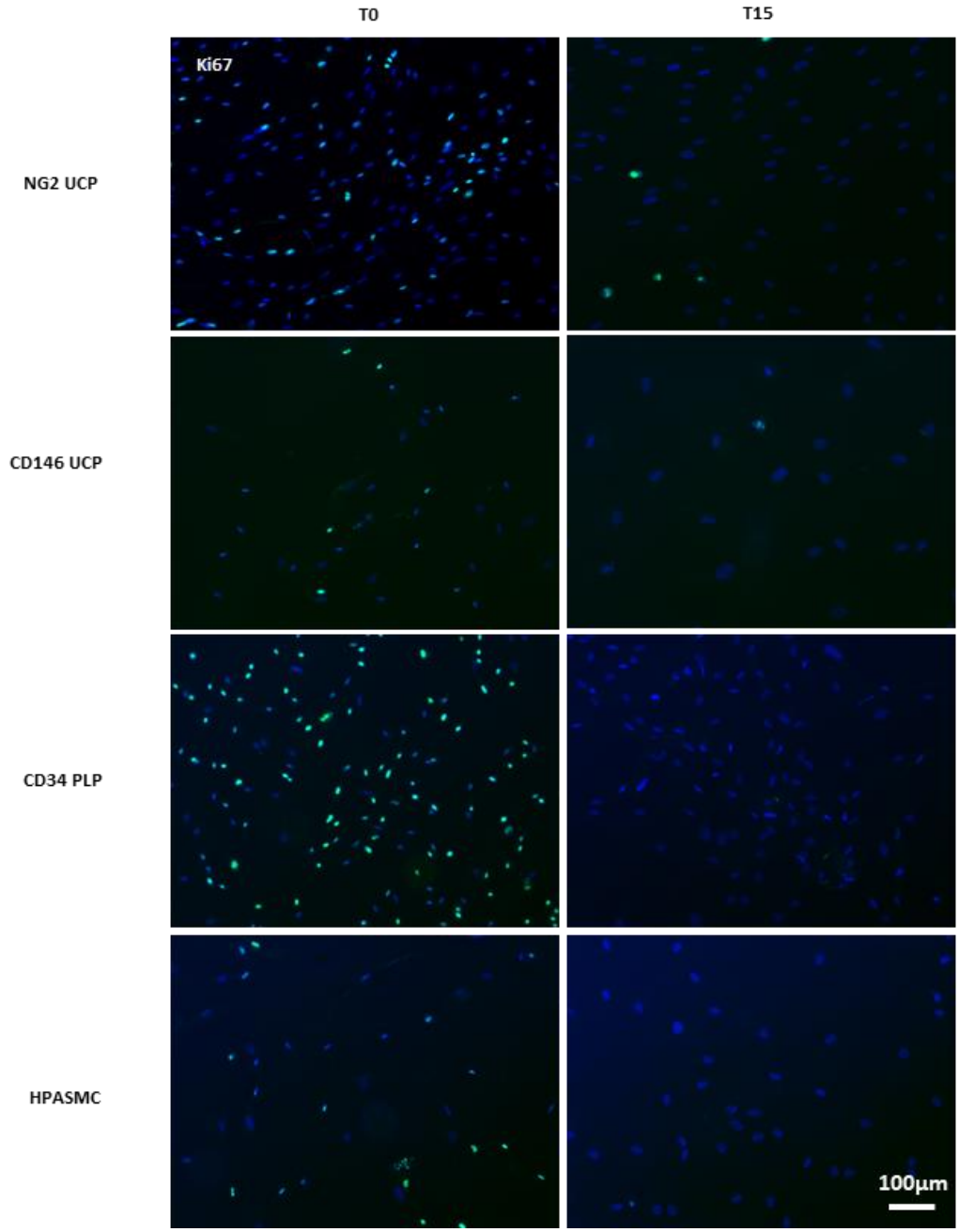

Figure 4.10: Representative immunocytochemical staining of proliferation marker Ki67 expression at day 0 (undifferentiated) and day 15 (differentiated). Scale bar 100µm.

4.3.2. Characterisation of Secretome

To provide a further layer of cell characterisation and investigate the potential regenerative properties of the different populations of umbilical cord and placenta pericytes, cell secretions were screened for an array of factors involved in angiogenesis and arteriogenesis. As detailed in the methods 2.7, cells were conditioned for 48 hours in serum/VEGF free EGM-2 so that secreted growth factors could be effectively quantified. CM was collected from cells exposed to hypoxia (2% O_2) as well as normoxia (20% O_2) so that we could understand how the cells may respond to a low oxygen environment.

The three populations of pericytes demonstrated similar secretion of ANGPT-1 in both normoxic and hypoxic conditions (**Figure 4.11A**). Under normoxia, pericytes secreted >400pg/hr/million cells; however, in hypoxic conditions this was significantly reduced by 100-200pg/hr/million cells (two-way ANOVA, $p = 0.0457$). ANGPT-1 secretion was significantly higher in pericytes than HUVEC CM, which did not secrete measurable amounts. This was expected due to the association between pericytes and ANGPT-1.

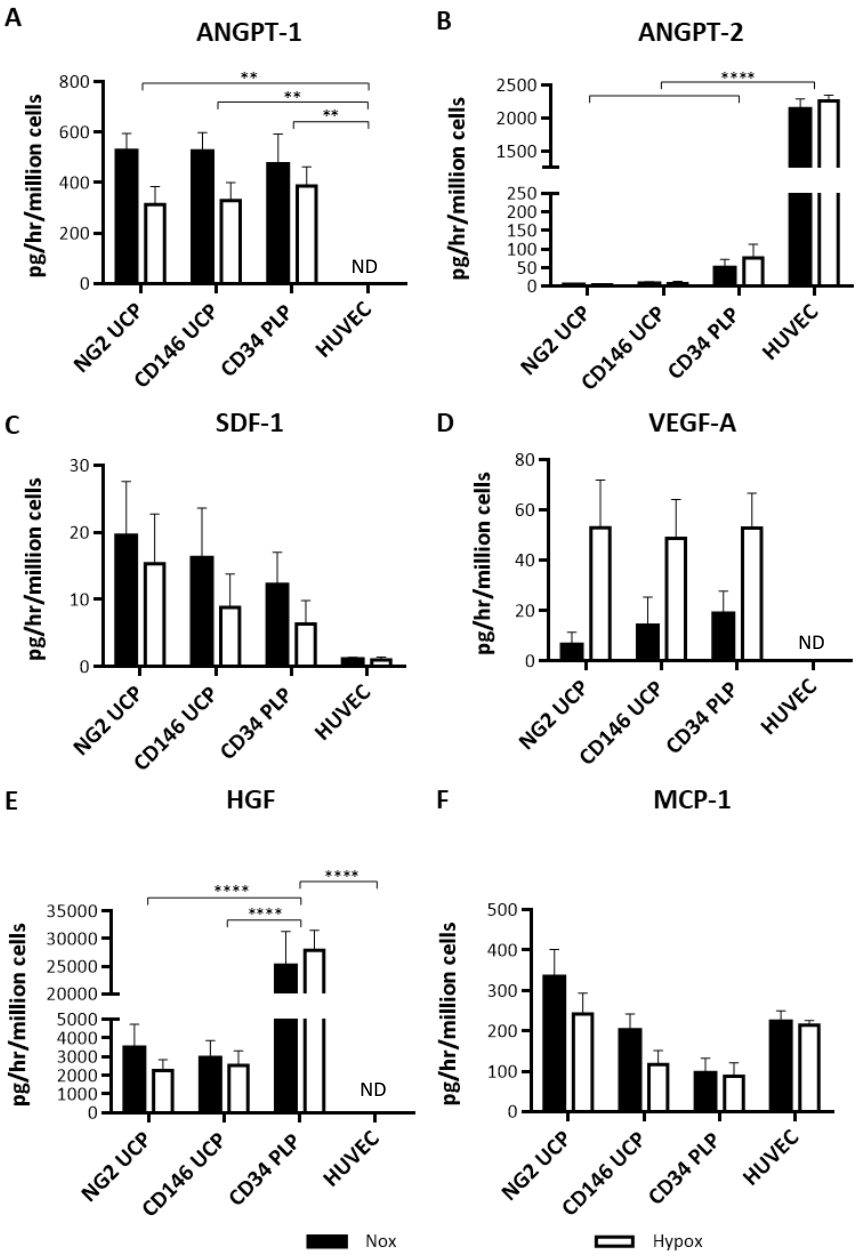

Figure 4.11: Characterisation of Pericyte Secretome. (A) Angiopoietin-1 (ANGPT-1). (B) Angiopoietin-2 (ANGPT-2). (C) Stromal derived factor-1 (SDF-1). D) Vascular endothelial growth factor-A (VEGF-A). (E) Hepatocyte growth factor (HGF). (F) Monocyte chemoattractant protein-1 (MCP-1). ND = not detectable. Data represents means (± S.E.M). NG2 UCP n = 6, CD146 UCP n = 6, CD34 PLP n = 5, where each n represents a different donor line. HUVEC n = 3 experiments. ** p<0.01, **** p<0.0001 as determined by two-way ANOVA followed by Tukey's post-hoc test. Normoxia (Nox), Hypoxia (Hypox).

ANGPT-2 was not secreted in NG2 UCP or CD146 UCP (**Figure 4.11B**); however, measurable quantities were detected in CD34 PLP (Nox: 48.9 ± 23.6 pg/hr/million cells, Hypox: 76.1 ± 37.0 pg/hr/million cells). This was surprising as ANGPT-2 is primarily produced by ECs and not generally associated with pericytes. In line with this, HUVEC CM contained significantly more ANGPT-2 (Nox: 2133 ± 156.1 pg/hr/million cells, Hypox: 2260 ± 88.1 pg/hr/million cells). No significant differences were detected between hypoxic and normoxic CM.

SDF-1 was secreted in small amounts by all pericyte populations; however, there was a large degree of variability as demonstrated by the error bars (**Figure 4.11C**). No significant differences were detected between the different cell types. HUVEC CM only contained trace amounts of SDF-1.

As **Figure 4.11D** demonstrates, all pericyte populations produced moderate amounts of VEGF-A (mean 5-20pg/hr/million cells), which increased considerably in hypoxic CM (mean ~50pg/hr/million cells). In general, hypoxic conditioning had a significant impact on the VEGF-A production (two-way ANOVA, $p = 0.0055$). As expected, HUVEC did not produce any VEGF-A.

HGF was secreted in large amounts by all pericyte populations (**Figure 4.11E**); however, CD34 PLPs produced significantly greater amounts (Nox: 25056.8 ± 6222.2 pg/hr/million cells, Hypox: 27869.9 ± 3654.2 pg/hr/million cells) than either NG2 UCPs (Nox: 3460.2 ± 1277.6 pg/hr/million cells, Hypox: 2262.9 ± 566.5 pg/hr/million cells) and CD146 UCPs (Nox: 2909.2 ± 945.6 pg/hr/million cells, Hypox: 2523.6 ± 787.7 pg/hr/million cells), highlighting another distinct difference between this population and other pericytes. Hypoxic conditioning caused no observable change in HGF secretion from the normoxic CM. HUVEC did not secrete any HGF.

MCP-1 was secreted in considerable amounts by all cell types (**Figure 4.11F**). NG2 UCPs secreted the greatest amounts of MCP-1; however, the difference was not statistically significant. The data suggests that hypoxia reduces MCP-1 production; however, this effect was only moderate.

Overall, NG2 UCPs and CD146 UCPs demonstrate very similar secretion profiles. In normoxia, they both produce large amounts of ANGPT-1, HGF and MCP-1, and small amounts of VEGF-A and SDF-1. After hypoxic stimulus, ANGPT-1 secretion is reduced by almost half

and VEGF-A production is increased. CD34 PLPs demonstrate similar behaviour; however, they produce ten times more HGF along with substantial amounts of ANGPT-2.

4.3.3. Angiogenic Activity

Following the screening of angiogenic and arteriogenic factors, the ability of cells to enhance endothelial capillary-like networks was assessed. A 2D Matrigel assay was initially utilised for this purpose; however, limitations were encountered (method 2.8). As shown in **Figure 4.12**, HUVECs seeded in unconditioned control medium produced almost as much endothelial network formation as the EGM-2 positive control. This indicated that the assay may already be saturated with the effect of growth factors inherent to the Matrigel substrate and meant that quantification of any subtle pro-angiogenic effect of pericytes or conditioned media was undetectable. Rather than repeat the assay with reduced growth factor Matrigel, we decided to explore alternative in vitro angiogenic assays that more closely mimic the extra-cellular in vivo environment of vascular tissue. As an alternative method to assess angiogenic potential, a NHDF and HUVEC co-culture was utilised (method 2.8).

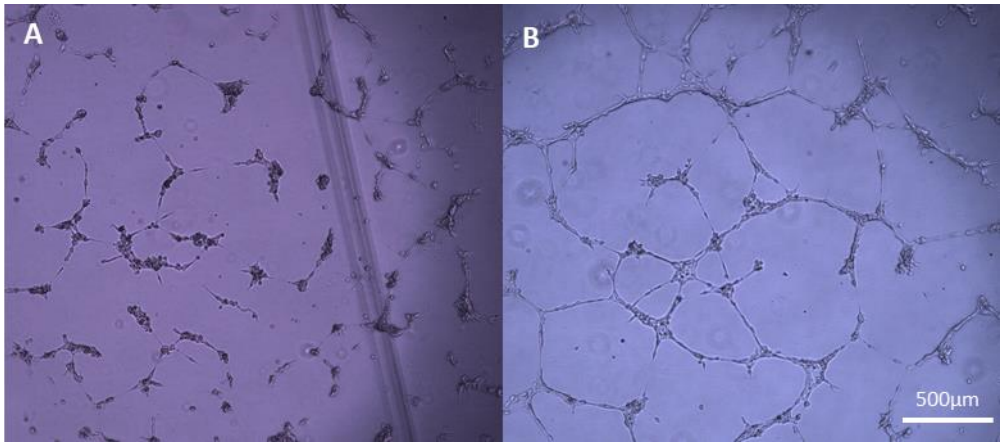

Figure 4.12: Matrigel Tube Formation Assay Example. (A) Unconditioned control medium. (B) EGM-2 Positive Control. Scale bar = 500µm.

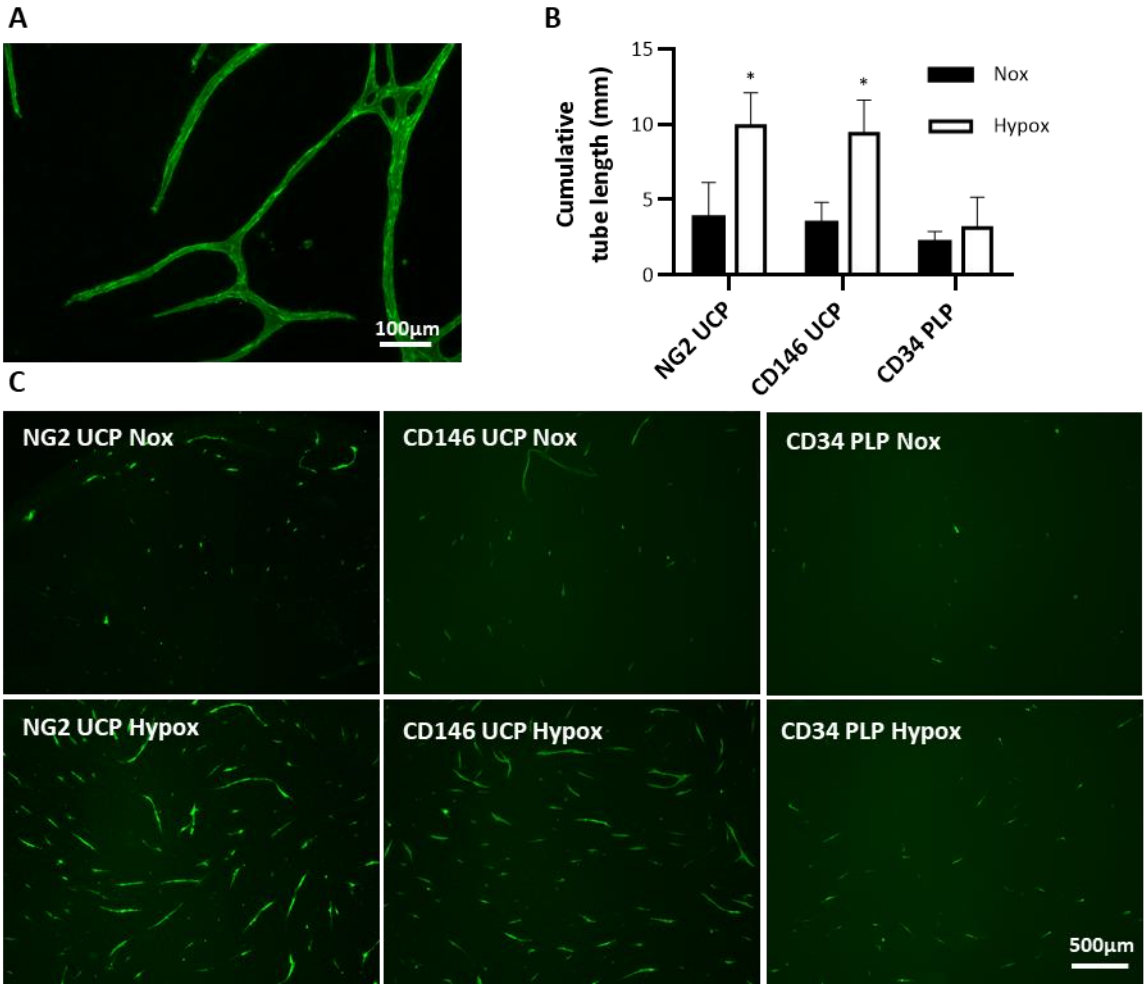

Figure 4.13: Angiogenic effect of cell conditioned medium (CM). (A) 200x magnification showing a closer view of the complexity of the endothelial network formation. (B) Cumulative tube network using normoxic and hypoxic CM. Note that basal medium control resulted in no network formation. For clarity, control has been omitted, however, a significant increase from control is represented directly above column. Data represents means (± S.E.M). NG2 UCP n = 6, CD146 UCP n = 6, CD34 PLP n = 5, Control Medium n = 4. * $p<0.05$ as determined by two-way ANOVA followed by Tukey's post-hoc test. (C) Representative images for endothelial tube formation induced by CM collected under normoxia (Nox) and hypoxia (Hypox). Scale bar = 500µm.

The assay was initially utilised for analysis of CM. 6 days after addition of pericyte CM, endothelial tube-like networks were observed using fluorescent microscopy (**Figure 4.13**).

These networks demonstrated a much more complex structure than the previously applied Matrigel assay, including lumen formation and distinguishable tip cells with projecting filopodia seen at the end of network branches (**Figure 4.13A**). Incubation of co-cultures with normoxic CM resulted in only a small increase (NG2 UCP: 3.8 ± 2.4 mm; CD146 UCP: 3.4 ± 1.4 mm; CD34 PLP: 2.1 ± 0.8 mm) in cumulative tube formation (**Figure 4.13B-C**); however, incubation with hypoxic CM caused a significant change in tube formation (two-way ANOVA, $p = 0.0192$). Specifically, CM from NG2 UCP and CD146 UCP resulted in a significant increase in tube formation in comparison to control medium (NG2 UCP: 9.9 ± 2.2 mm; CD146 UCP: 9.4 ± 2.2 mm). In contrast, no considerable increase in tube formation was observed with incubation of CD34 PLP hypoxic CM (3.1 ± 2.0 mm).

Following analysis of CM, the direct angiogenic influence of umbilical cord and placenta pericytes on ECs was investigated by incorporating them in the HUVEC and NHDF co-culture. As detailed in method 2.8, NHDF were cultured to provide a feeder layer before seeding HUVEC and pericytes prelabelled with DsRED (method 2.9). After 6 days, a complex network had formed, as demonstrated in **Figure 4.14A**. As the network formation was more complex than the network produced by CM alone, more data could be extracted from the assay to give a more detailed description of the angiogenic influence of umbilical cord and placenta pericytes. In accordance with results from CM analysis, both NG2 UCPs and CD146 UCPs produced a significant increase in tube length; however, no increase was observed from CD34 PLPs (**Figure 4.14B**). Although all pericyte populations induced a slight increase in number of branches, only NG2 UCPs produced a statistically significant change (**Figure 4.14C**). Average branch thickness was significantly increased by all pericyte populations, with NG2 UCPs again inducing the largest increase (**Figure 4.14D**). Finally, the average distance between pericytes and the endothelial branch was measured to give an indication of the association between ECs and pericytes. No significant differences were detected between the cell types.

Together, this data suggests that NG2 UCPs and CD146 UCPs hold greater angiogenic potential than CD34 PLPs. In general, NG2 UCPs induced the more complex endothelial capillary-like network formation.

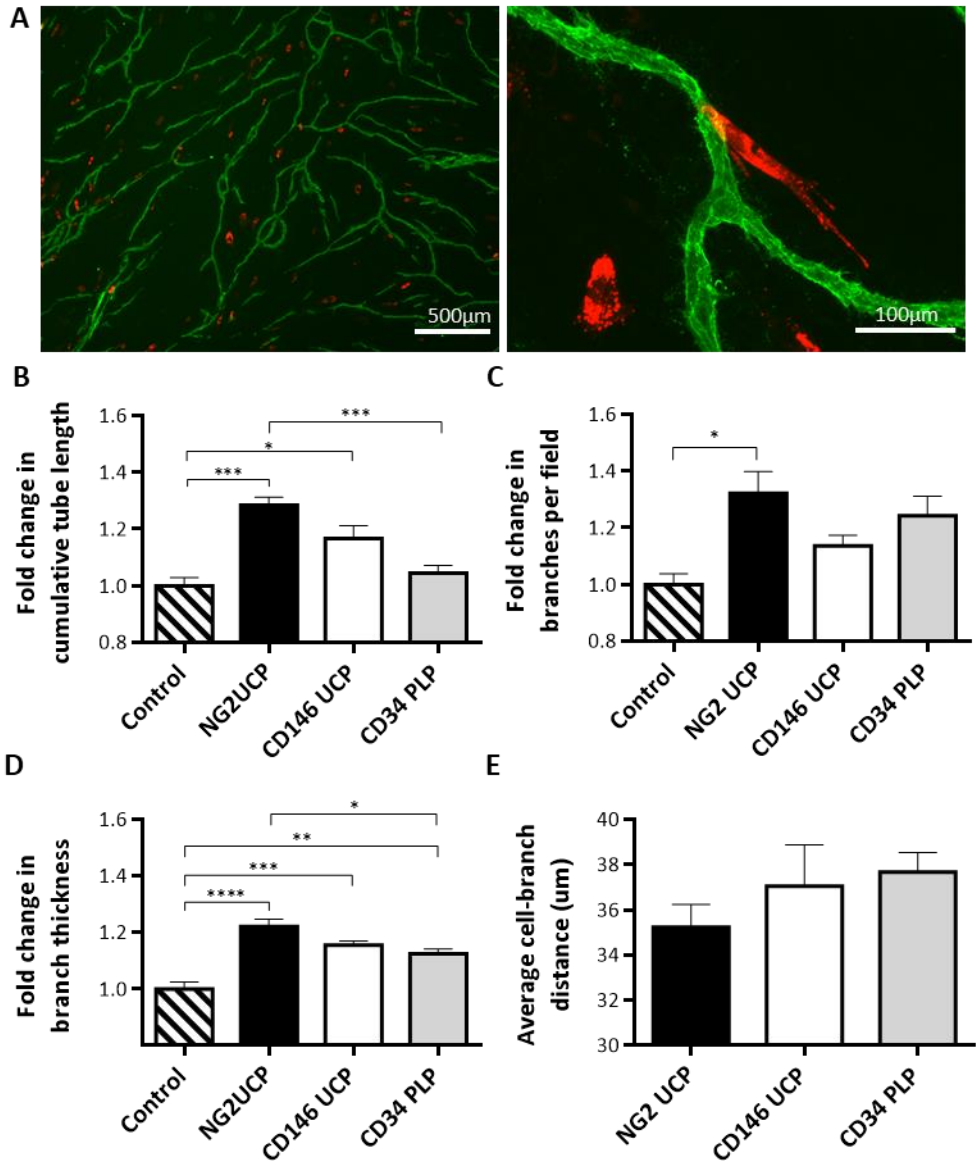

Figure 4.14: Direct angiogenic effect of pericytes in co-culture. (A) Example image of network formation (green) with the addition of pericytes (red). Left panel: scale bar 500µm, Right panel: scale bar 100µm. (B) Fold change in cumulative tube length induced by pericytes. (C) Fold change in branches per field induced by pericytes. (D) Fold change in branch thickness induced by pericytes. (E) Average distance between and nearest network branch. Data represents means (± S.E.M). NG2 UCP n = 6, CD146 UCP n = 6, CD34 PLP n = 5, where each n represents a different donor line. HUVEC only control n = 4, where each n represents a different experiment. * $p<0.05$, ** $p<0.01$, *** $p<0.001$, **** $p<0.0001$ as determined by one-way ANOVA followed by Tukey's post-hoc test.

4.3.4. Comparative Analysis of NG2 UCPs and MSCs

After review of the data from chapter 3 and 4, NG2 UCPs were selected as the most suitable of the three pericyte populations for vascular tissue engineering. These cells were taken forward for further analysis and eventual vascular graft production. For perspective, the differentiation and angiogenic properties of NG2 UCPs were compared to WJ-MSCs.

Comparison of gene regulation after VSMC differentiation demonstrated that MSCs exhibited a much greater increase in *ACTA2* and *TAGLN* after differentiation (**Figure 4.15**). In line with this, mRNA levels of *ACTA2* in differentiated MSCs were >3 times the level of differentiated NG2 UCPs or HPASMCs, whilst all other VSMC markers demonstrated no significant differences from NG2 UCPs (**Figure 4.16**). Interestingly, changes in gene expression did not equate with changes in protein expression. Despite MSCs demonstrating a much greater upregulation of *ACTA2* and *TAGLN*, there were no differences in αSMA and transgelin expression between MSCs or NG2 UCPs. Indeed, the only observable difference between the two cell types was a significantly higher upregulation of calponin in NG2 UCPs (**Figure 4.17**).

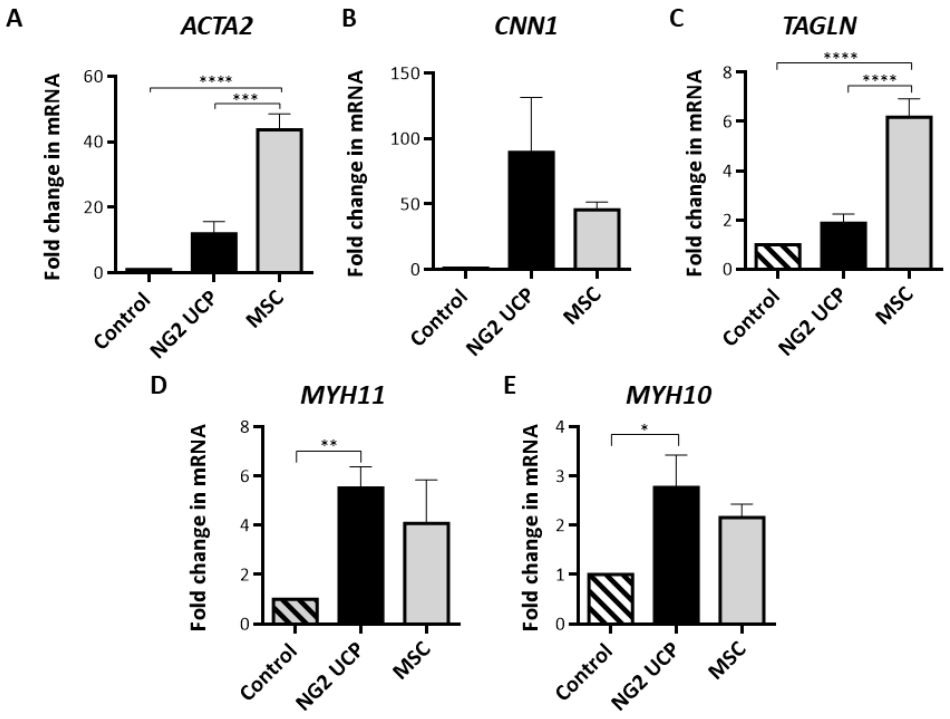

Figure 4.15: Comparison of NG2 UCPs and MSCs VSMC differentiation potential. Fold change in mRNA levels of VSMC markers after differentiation vs undifferentiated (control). (A) ACTA2 = alpha smooth muscle actin (αSMA). (B) CNN1 = Calponin. (C) TAGLN = Transgelin. (D) MYH11 = smooth muscle myosin heavy chain (SM-MHC). (E) MYH10 = non muscle myosin IIB (NMMyoIIB). Data represents means (± S.E.M). NG2 UCPs and MSCs, n = 5 and 3, respectively; * $p<0.05$ ** $p<0.01$ *** $p<0.001$ **** $p<0.0001$ as determined by one-way ANOVA followed by Tukey's post-hoc test.

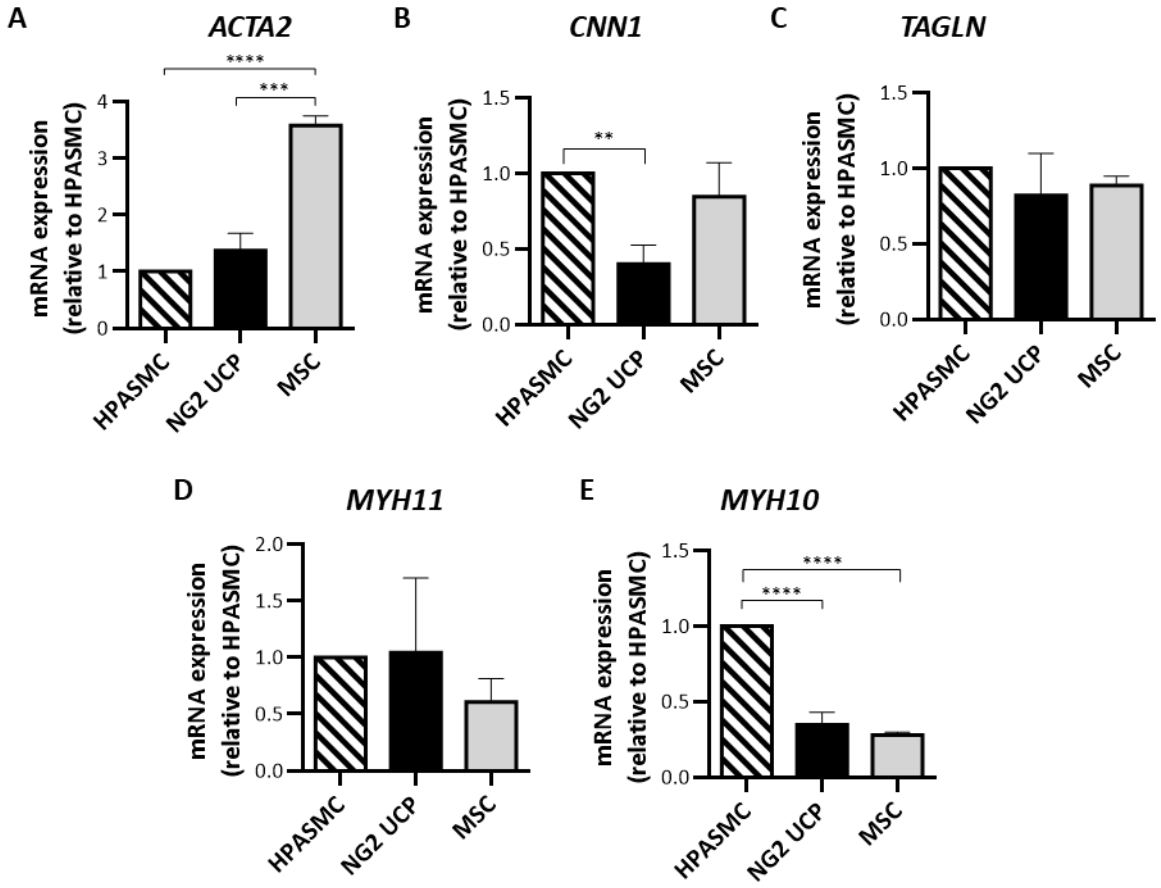

Figure 4.16: mRNA levels of VSMC markers in differentiated NG2 UCPs and MSCs relative to differentiated human pulmonary artery smooth muscle cells (HPASMC). (A) *ACTA2* = alpha smooth muscle actin (αSMA). (B) *CNN1* = Calponin. (C) *TAGLN* = Transgelin. (D) *MYH11* = smooth muscle myosin heavy chain (SM-MHC). (E) *MYH10* = non muscle myosin IIB (NMMyoIIB). Data represents means (± S.E.M). NG2 UCPs and MSCs, n = 5 and 3, respectively; ** $p<0.01$ *** $p<0.001$ **** $p<0.0001$ as determined by one-way ANOVA followed by Tukey's post-hoc test.

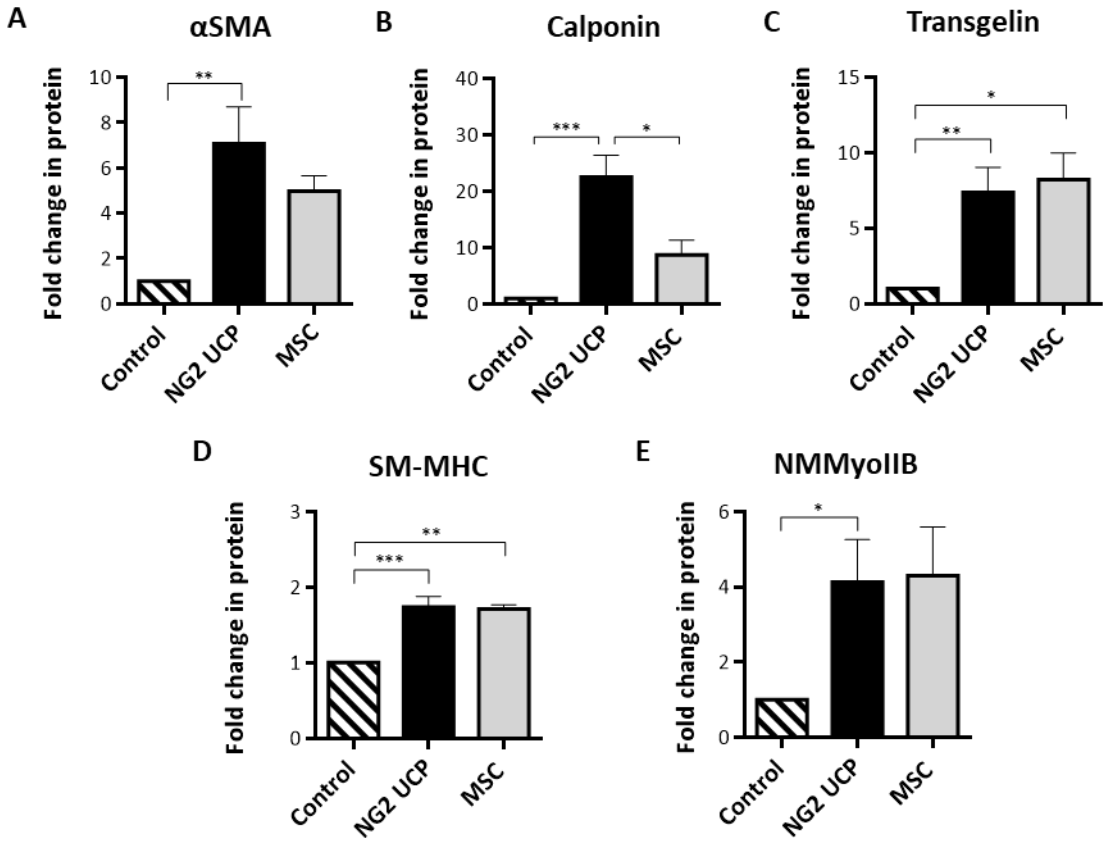

Figure 4.17: Comparison of NG2 UCPs and MSCs VSMC differentiation potential. Fold change in protein levels of VSMC markers after differentiation vs undifferentiated (control). (A) Alpha smooth muscle actin (αSMA). (B) Calponin. (C) Transgelin. (D) Smooth muscle myosin heavy chain (SM-MHC). (E) Non muscle myosin IIB (NMMyoIIB). Data represents means (± S.E.M). NG2 UCPs and MSCs, n = 5 and 3, respectively; * $p<0.05$ ** $p<0.01$ *** $p<0.001$ as determined by one-way ANOVA followed by Tukey's post-hoc test.

To identify if the change in antigenic phenotype corresponded to a functional readout, the contractile capacity of NG2 UCPs was assessed. As detailed in the method 2.14, differentiated and undifferentiated NG2 UCPs were seeded onto collagen gel. Cells were then stimulated before measuring the change in surface area of the collagen gel. After stimulation with endothelin-1, NG2 UCPs demonstrated active contraction, which was more evident after differentiation (58.9 ± 7.9 % vs 47.7 ± 5.8 % in the undifferentiated state). This effect was inhibited by BDM, an excitation-uncoupling agent (two-way ANOVA, p = 0.0053) (**Figure 4.18**). This data indicated that NG2 UCPs possess native contractile properties, as classically seen in pericytes, which are increased after acquisition of VSMC antigens during forced differentiation. This assay was only completed on NG2 UCPs to validate functional contraction in the chosen candidate due to the high material cost and cell requirement.

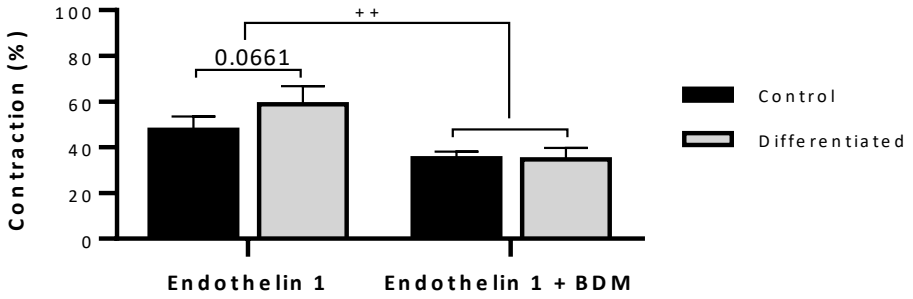

Figure 4.18: Gel contraction in differentiated and undifferentiated NG2 UCPs after activation with endothelin-1 in the presence or absence of BDM. 0.1μM endothelin-1 and 10mM 2, 3-Butanedione Monoxime (BDM) were used. Data represent means (± S.E.M) of n = 5 biological replicates. ++ $p<0.01$.

NG2 UCPs demonstrated a distinctly unique secretion profile to that of MSCs. Like NG2 UCPs, MSCs produce considerable amounts of ANGPT-1, HGF and MCP-1 under normoxic conditions; however, the quantities of these factors differed greatly (**Figure 4.19**). Whilst MSCs secreted significantly more ANGPT-1 (two-way ANOVA, p = 0.0035), NG2 UCPs produced significantly more HGF (two-way ANOVA, p = 0.0427) and MCP-1 (two-way ANOVA, p = 0.0026). NG2 UCPs also produced low levels of potent angiogenic factor VEGF-A, which was not detected in MSC secretions. Negligible amounts of ANGPT-2 and low levels

of SDF-1 were produced by both cell types. Under hypoxic conditioning, cells demonstrated a considerable change in their secretome. Both cell types demonstrated a similar reduction in ANGPT-1 and MCP-1 secretion. Interestingly, VEGF-A secretion was significantly increased in NG2 UCPs by ~40 pg/hr/million cells (Nox: 6.3 ± 5.1 pg/hr/million cells, Hypox: 53.0 ± 18.9 pg/hr/million cells).

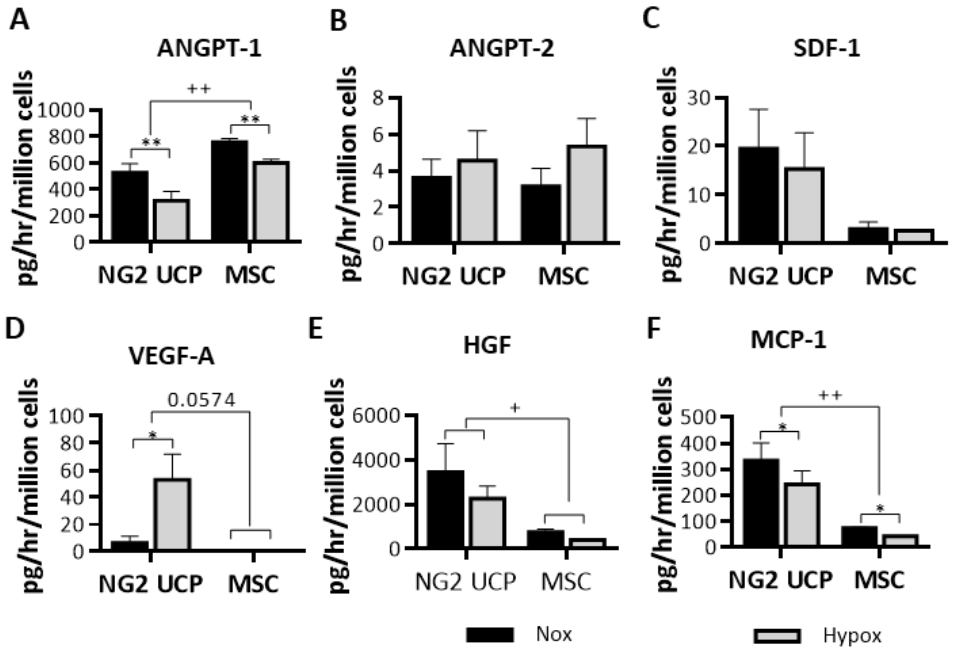

Figure 4.19: Comparison of NG2 UCPs and MSCs Secretome. Analysis of cell-secreted factors in cell-conditioned media, normalized for the volume of the collected supernatant, time of incubation and cell number. (A) Angiopoietin-1 (ANGPT-1). (B) Angiopoietin-2 (ANGPT-2). (C) Stromal derived factor-1 (SDF-1). (D) Vascular endothelial growth factor-A (VEGF-A). (E) Hepatocyte growth factor (HGF). (F) Monocyte chemoattractant protein-1 (MCP-1). Data represents means (± S.E.M). NG2 UCP n = 6, MSC n = 3; */+ $p<0.05$ **/++ $p<0.01$. * represents differences between hypoxia and normoxia, + represents differences between cell types as determined by two-way ANOVA followed by Student's t-test.

Comparison of the angiogenic activity of each cell line demonstrated distinct advantages of NG2 UCPs over MSCs (**Figure 4.20**). CM from NG2 UCPs induced significantly greater endothelial capillary-like network formation than MSC CM (two-way ANOVA, p = 0.0021) (**Figure 4.20A & B**). Similarly, the direct angiogenic influence of NG2 UCPs was superior to MSCs. Inclusion of NG2 UCP resulted in a significant increase in endothelial tube network length in comparison to the influence of MSCs, which resulted in no increase in network over the HUVEC-only control (**Figure 4.20D**). Both cell types induced a significant increase in the number and thickness of branches, although there were no significant differences between the two (**Figure 4.20E & F**). Finally, NG2 UCPs demonstrated a greater association with ECs as evidenced by their average distance to network branch, which was shorter than that of MSCs (**Figure 4.20G**). To confirm the angiogenic effect was not due to increased proliferation of NG2 UCPs, the number of cells per field of view was counted (**Figure 4.20H**). No significant differences were detected. Together, these data indicate that NG2 UCPs possess a multifactorial angiogenic potential, superior to that of MSCs.

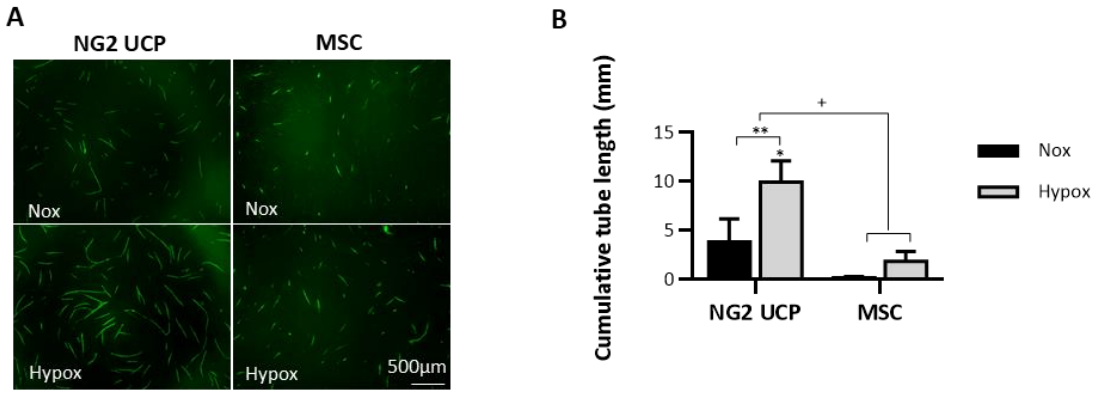

Figure 4.20: Comparison of NG2 UCPs and MSCs Angiogenic Potential. (A) Representative images of endothelial tube network formation after incubation with normoxic or hypoxic CM. Scale bar =500µm (B) Cumulative tube network using normoxic and hypoxic CM. Note that basal medium control resulted in no network formation. For clarity, control has been omitted, however, a significant increase from control is represented directly above NG2 UCP hypoxia column. Data represent means (± S.E.M). MSCs and NG2 UCPs, n = 3 and 6, respectively. */+p<0.05 **/++p<0.01. * represents differences between hypoxia and normoxia, + represents differences between cell types as determined by two-way ANOVA followed by Student's t-test.

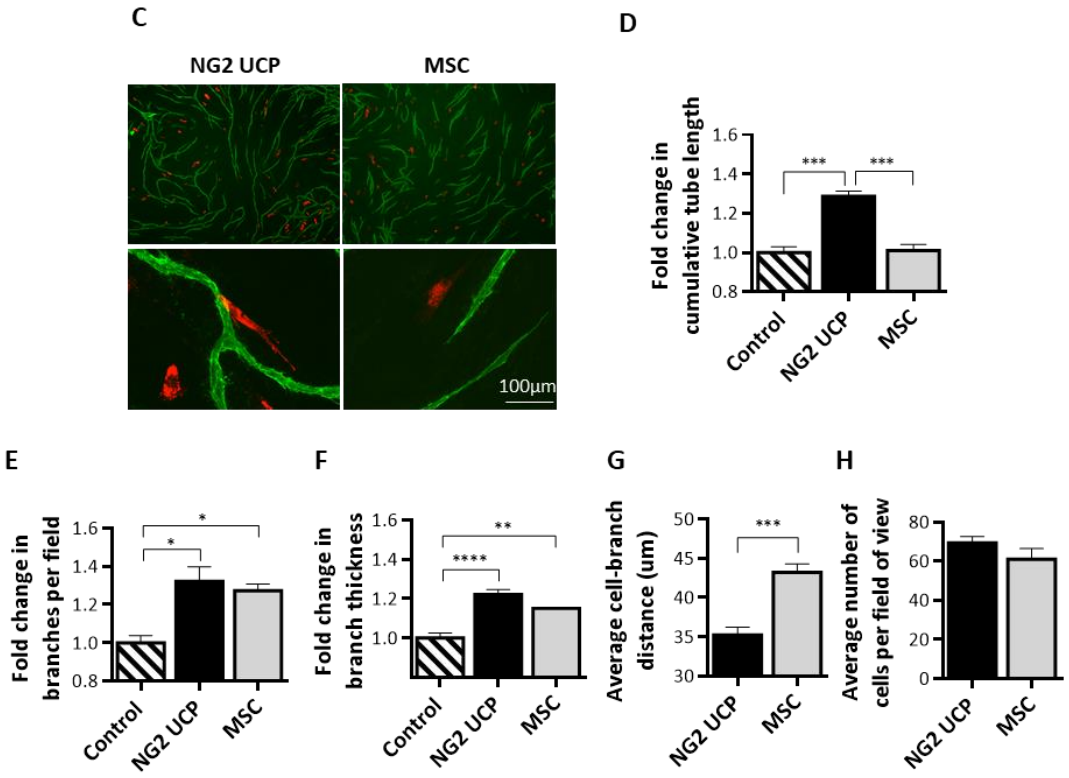

Figure 4.20: Comparison of NG2 UCPs and MSCs Angiogenic Potential (continued). (C) Representative images of endothelial tube network formation with the inclusion of red labelled NG2 UCPs or MSCs in the endothelial cell-fibroblast co-culture. Scale bars = 500µm, 100µm. (D) Fold change in cumulative tube length vs. endothelial cell-fibroblast only control. (E) Fold change in branches per field vs. endothelial cell-fibroblast only control. (F) Fold change in branch thickness vs. endothelial cell-fibroblast only control. (G) Average distance of cell to branch. (H) Average number of cells per field of view. For D - H, data represent means (± S.E.M) MSCs and NG2 UCP, n = 4 and 6, respectively. *$p<0.05$, **$p<0.01$, ***$p<0.001$, and ****$p<0.0001$. as determined by one-way followed by Tukey's post-hoc test, or by Student's t-test.

4.4. Discussion

The choice of cell source for vascular tissue engineering is contentious, yet it is pivotal to the success of vascular graft technology (Bajpai et al., 2012). Whilst significant emphasis is placed on where a cell source originates, less focus is placed on the functional capacity of the cell in question. Perhaps the key to successful clinical translation of cell therapy and tissue engineering-based research is to examine cell candidates based on preidentified functional requirements. For vascular tissue engineering, the objective is to confer engineered grafts with the properties of a native vessel. Despite the complexity of tissue, we can identify some key requirements which can help to achieve this. Chief among these is the ability to form contractile tissue and support the development of a blood supply. As previously described, pericytes standout as a suitable candidate due to their role in vascular stability and regulation of blood flow (Cathery et al., 2018). By examining the ability of our umbilical cord and placenta pericytes to carry out these functions, we can add a further layer of cell characterisation whilst simultaneously identifying which of our cell sources possess the greatest potential for vascular tissue engineering.

The VSMC phenotype varies along a spectrum, from the proliferative synthetic form often implicated in pathological processes, to the mature contractile form which plays a crucial role in normal vascular function (Bacakova, Travnickova, Filova, Matějka, et al., 2018; Rensen et al., 2007). To confirm that cells can adopt the contractile phenotype, rather than an unwanted synthetic or myofibroblastic phenotypic, expression of VSMC-associated markers αSMA, calponin, transgelin, SM-MHC and NMMyoIIB were evaluated. Expression of transgelin has been identified as a specific VSMC differentiation marker, whilst αSMA, Calponin and SM-MHC represent early, mid, and mature contractile markers of differentiated VSMC respectively (Bacakova, Travnickova, Filova, Matějka, et al., 2018; Hilenski et al., 2012; Rensen et al., 2007; Tawfik et al., 2014). Similarly, NMMyoIIB is associated with actin crosslinking and contractile properties (Vicente-Manzanares et al., 2009). All three pericyte populations demonstrated some capacity to differentiate towards a contractile VSMC phenotype, with evident upregulation of specific mid and early phase VSMC markers along with a significant reduction in proliferation. In particular, NG2 UCPs displayed the most consistent changes in VSMC-associated proteins. These cells demonstrated a significant upregulation of calponin, transgelin and NMMyoIIB via western blot analysis. This was confirmed by fibre visualisation, although the expression levels were weaker in trangelin,

possibly due to fixation methods or sensitivity of the assay. Despite a modest upregulation of SM-MHC which further verified a contractile phenotype, acquisition of a mature phenotype, as previously seen in cardiac pericytes, was not clearly demonstrated (Avolio, Rodriguez-Arabaolaza, et al., 2015). Notwithstanding, it is often difficult to achieve a mature phenotype in culture, as is evidenced by the lack of SM-MHC expression in differentiated HPASMCs. Indeed, in a review of human iPSC-derived VSMCs by Ayoubi et al., only eight of twenty-three studies demonstrated expression of mature contractile markers at both gene and protein levels (Ayoubi et al., 2017). It is likely that a mechanical stimulus, such as cyclical strain, may be required to maintain a fully functional mature phenotype, as has been suggested in MSC-derived VSMCs (Dan et al., 2015; Qiu et al., 2014). Nevertheless, the partial differentiation achieved in umbilical cord and placenta pericytes does indicate that they may exhibit contractile properties to functionalise an acellular graft.

By analysing secreted growth factors in both normoxic and hypoxic conditions, we aimed to understand the cells angiogenic potential and how this may change in response to a reduced oxygen environment such as an avascular tissue engineered construct (Malda et al., 2004; Suvarnapathaki et al., 2019). A cell that can adapt to this environment effectively may be favourable for tissue engineering. All pericyte populations demonstrated considerable secretion of angiogenic and arteriogenic factors, indicating endothelium supporting properties. In particular, under normoxia, a secretome indicative of a role in vascular stability was observed, as evidenced by large quantities of ANGPT-1 and MCP-1. ANGPT-1 is a perivascular-associated factor that is essential for vessel stability, which is achieved through reinforcing interactions between smooth muscle cells and ECs (Gowdak et al., 2018). Similarly, MCP-1 is involved in vessel maturation through recruitment of monocytes, and has been shown to enhance arteriogenesis (Heil et al., 2006; van Royen et al., 2001). Interestingly, only small amounts of SDF-1 were secreted. This is a notable difference to previously characterised pericyte populations and further highlights the heterogeneity of pericytes in different tissues (Avolio, Rodriguez-Arabaolaza, et al., 2015; Spencer et al., 2019).

Under hypoxic stimulus, the secretome appears to switch to an angiogenic state, demonstrating a significant upregulation of VEGF-A whilst simultaneously downregulating ANGPT-1 (and to a lesser extent MCP-1). VEGF is one of the most important regulators of vessel formation, stimulating angiogenesis and increasing vessel permeability (Gowdak et al., 2018). It works synergistically with HGF, which was secreted in large amounts in both normoxia and hypoxia,

to promote endothelial proliferation and migration, thereby amplifying the angiogenic activity of either factor alone (Xin et al., 2001). This indicates a tight regulation of the angiogenic process, whereby the cells play a supportive role under a well oxygenated environment and only secrete pro-angiogenic factors upon sufficient stimulus. This balance is important in ensuring pathological angiogenesis does not occur. Indeed, this behaviour may be preferable to similar cell types used for tissue engineering, namely cardiac pericytes and adipose-derived MSCs, which produce large quantities of angiogenic factors under normoxic conditions (Avolio, Rodriguez-Arabaolaza, et al., 2015; Blasi et al., 2011).

Aside from the general response of cells to oxygen levels, there were also some notable differences in characteristics between CD34 PLPs and both cord pericyte populations. Whilst NG2 UCPs and CD146 UCPs did not secrete the ANGPT-2, CD34 PLPs secreted measurable quantities in both normoxia and hypoxia. ANGPT-2 is a mostly endothelial specific growth factor, so this was somewhat surprising (Anja et al., 2004). Furthermore, in the absence of angiogenic stimulation, ANGPT-2 results in vessel regression indicating that secretion under normoxia may not be optimal (Gowdak et al., 2018). Expression of this factor maybe explained by the source of isolation tissue. Indeed, placenta tissue is known to express high levels of ANGPT-2 due to active vascular remodelling (Akwii et al., 2019). Alternatively, this may be a hallmark of CD34+ pericytes as ANGPT-2 secretion was observed in cardiac pericytes (Avolio, Rodriguez-Arabaolaza, et al., 2015). In fact, CD34+ pericytes have been shown to secrete extremely high levels of HGF, which was also observed in CD34 PLPs but not in cord pericytes.

To confirm the angiogenic effect of the cell secretome, an in vitro tube formation assay was implemented. Initial experiments using a Matrigel based assay, previously established in our lab, were unsuccessful. Matrigel systems use ECM derived from tumour cells as substrate for ECs. The ECs form 2D networks after a few hours; however, these networks quickly begin to regress within 24 hours. There is little migration of the cells, and no lumen formation, limiting its applicability as a sprouting angiogenesis model. Moreover, Matrigel is capable of inducing network formation in non-endothelial cells, further questioning its validity as an angiogenesis model (Hetheridge et al., 2011). The potency of growth factors in Matrigel results in over-stimulation of endothelial cells and studies have evidenced tubular structures in non-endothelial cells such as primary human fibroblasts and gioblastoma cells (Staton et al., 2009). More recently, this phenomenon has also been observed when culturing cardiac pericytes and

saphenous vein pericytes on Matrigel matrices in the absence of endothelial cells (Avolio, Rodriguez-Arabaolaza, et al., 2015; Campagnolo et al., 2010). The fact that tubular structures can be induced in non-endothelial cells using a Matrigel matrix means that the mechanism of network formation must not be representative of in vitro angiogenesis. Matrigel may still be a simple yet efficient tool for the initial identification of potential pro angiogenic effects; however, in order to obtain conclusive evidence of a cell's ability to promote angiogenesis, a model more representable of the in vivo niche is required. The fibroblast-HUVEC co-culture system addresses some of the limitations of the Matrigel system. The fibroblasts produce a 3-dimensional matrix (containing collagen type I, fibronectin, tenascin- C, decorin and versican) that provides a closer approximation to the in vivo state (Richards et al., 2016). ECs form 3D networks with lumen formation and distinguishable tip cells which do not regress within 24 hours. Additionally, any promotion of endothelial network formation can be attributed to the experimental conditions as NHDFs are not pro-angiogenic (Blasi et al., 2011).

Using the fibroblast-EC coculture assay incubated with pericyte-CM, we were able to corroborate secretomic data. All pericyte populations induced endothelial tube formation via paracrine mechanisms; however, this effect was only modest with normoxic CM. As predicted by the analysis of cell secreted factors, the hypoxic CM produced a significant increase in endothelial network formation, which was superior to the angiogenic paracrine effect of cardiac pericytes (Avolio, Rodriguez-Arabaolaza, et al., 2015). This may be due to the high secretion of ANGPT-2 seen in cardiac pericytes, which in the absence of angiogenic stimulation results in vessel regression (Gowdak et al., 2018). This paracrine angiogenic induction appeared to mirror the pattern in VEGF-A secretion, indicating that this may be the primary contributing factor. This behaviour is beneficial for cells used in vascular tissue engineering where we desire an initial induction of angiogenesis in the poorly oxygenated graft environment. Once micro vessels develop and integrate with host vasculature acting like a primitive vasa vasorum, the angiogenetic properties of the cells should be sufficient to sustain the network, rather than promote uncontrolled growth. Interestingly, CD34 PLP hypoxic CM did not increase network formation. This was surprising considering that the only noticeable differences in the factors analysed were ANGPT-2 and greatly enhanced HGF secretion. As ECs produce large quantities of ANGPT-2, it is unlikely that the contribution of CD34 PLP-derived ANGPT-2 could cause such a significant effect. It therefore must be a result of an imbalance in angiogenic factors, either caused by the HGF or other unexplored factors.

The supportive properties of isolated pericytes were further examined by including them in direct culture with ECs. This validated the data from CM, demonstrating that NG2 UCPs and CD146 UCPs had a greater proangiogenic influence over CD34 PLPs. Specifically, NG2 UCPs were the most supportive cell type, as evidenced by the significant increase in tube length, branches and branch thickness, which may be indicative of a more complex and mature network.

In order to confirm which pericyte population was optimal for vascular tissue engineering (and therefore which population we would focus upon in the latter stages of the project), we needed to address all the data from isolation efficiency, growth and viability, phenotypic characteristics, vascular differentiation capacity and angiogenic potential. As concluded in chapter 3, NG2 UCPs and CD146 UCPs demonstrated greater isolation efficiency, a more consistent phenotype, and more reliable expansion capacity when compared to the CD34 PLPs. NG2 UCPs also demonstrated a more consistent change in phenotype in response to forced VSMC differentiation. With respect to angiogenic potential, NG2 UCPs and CD146 UCPs demonstrated similar supportive properties, and although NG2 UCPs demonstrated slight superiority, it was not-statistically significant. In contrast, CD34 PLPs did not have a major influence on endothelial tube formation. In general, NG2 UCPs and CD146 UCPs demonstrated similar properties throughout; however, the isolation of NG2 UCPs was slightly more efficient with a larger yield of cells, and the cells induced a marginally greater angiogenic response. It is worth mentioning that despite defining NG2 UCPs and CD146 UCPs as two distinct populations based on their method of isolation, it is most probable that they represent the same population of cord pericytes, but NG2 is simply a more specific selection marker. In any case, NG2 UCPs were chosen as the optimal cell source for use in all further experiments and graft production.

To identify if our chosen pericytes possessed any therapeutic benefits over more traditionally explored regenerative cell types, we compared the properties of NG2 UCPs to WJ-MSCs. These cells were chosen for comparison due to their similar anatomical location and popularity in tissue engineering and regenerative medicine applications (Abbaszadeh et al., 2020; Bajpai et al., 2012; Saeedi et al., 2019). As evidenced in the previous chapter, we already showed that there were subtle differences in phenotypic characteristics between the two cell types; however, further characterisation would provide more definitive proof that NG2 UCPs represented a unique subset of mesenchymal cell.

The differentiation capacity of both cell types was comparable, with neither population expressing characteristics of a mature VSMC phenotype. In fact, there is no conclusive data to suggest that WJ-MSCs can differentiate to a mature VSMC fate. Recently, Mallis et al. claimed that VSMC can be efficiently derived from WJ-MSCs for use in vascular tissue engineering; however, the evidence is ambiguous (Mallis et al., 2020). Despite showing expression of *MYH11* at the gene level, immunocytochemical staining of cells appeared non-specific for SM-MHC. Indeed, if the results are accurate, most WJ-MSC-derived VSMCs express SM-MHC in the absence of αSMA, which would be highly unusual.

The phenotypic changes observed in differentiated NG2 UCPs were validated by a functional contraction assay. Vasoactive contraction was seen in both differentiated and undifferentiated states, as predicted by the contractile properties of pericytes in vivo. However, the contractile response to endothelin-1 was increased in differentiated NG2 UCPs (C. N. Hall et al., 2014; Mcdonald et al., 1995). Endothelin-1 is a potent vasoconstrictor, predominantly produced by ECs, and is the most abundant isoform of the endothelins (Davenport et al., 2016). It binds with endothelin receptors, triggering downstream pathways that lead to vasoconstriction, which is mainly mediated through VSMC expression of endothelin receptor a (Wynne et al., 2009). These results indicate that NG2 UCPs express endothelin receptors, allowing them to mimic the role of VSMCs in contraction and confer contractility to acellular grafts.

The secretome of a cell can elucidate their efficacy for specific clinical applications and is now being implemented in cell free regenerative medicine strategies (Ferreira et al., 2018). Indeed, recently researchers from the University of Pavia have demonstrated how the osteoinductive secretome of MSCs can be used to functionalise synthetic scaffolds and promote bone regeneration. For vascular tissue engineering, a secretome that contains an abundance of vascular growth factors such as VEGF or ANGPT-1 is beneficial. These factors are essential for EC recruitment and vascularisation of tissue, which has already been highlighted as a major challenge. Considering this, a comparison of secretomic data between NG2 UCPs and MSCs was performed, which demonstrated more significant differences between the cell types. Interestingly, MSCs secreted more ANGPT-1 than NG2 UCPs, which was surprising given that ANGPT-1 is mainly produced by pericytes and plays an integral role in their communication with ECs during angiogenesis (Dimberg et al., 2014). Despite this, NG2 UCPs in general displayed superior release of angiogenic and arteriogenic factors, namely VEGF-A, HGF and MCP-1. This data is in line with previous studies that have demonstrated weak

secretion of VEGF-A in WJ-MSCs, which may be linked to the avascular niche in which they reside (Arutyunyan et al., 2016; Widowati et al., 2017). Despite development of capillaries in this tissue during ontogenesis, these regress before full term and therefore there is little requirement for secretion of angiogenic growth factors (Arutyunyan et al., 2016). Together, this suggests that WJ- MSCs may not be angiogenic, thereby highlighting a distinct advantage of NG2 UCPs.

To validate this hypothesis, the angiogenic properties of MSCs were assessed using the same tube formation assay as before. As expected, NG2 UCPs induced a much greater increase in endothelial tube formation via paracrine signalling, which was likely due to the VEGF-A activity. Similarly, the direct influence of NG2 UCPs was superior to MSCs, which did not influence cumulative network capacity. These results contradict previous studies, which claim that MSCs from the WJ are proangiogenic (Choi et al., 2013; Shen et al., 2015). One hypothesis is that due to the non-selective isolation process (Dominici et al., 2006), WJ-MSC populations contain a sub population of UCPs from the perivascular layer of the umbilical vessels, which provide angiogenic capabilities to the population as a whole. Indeed, studies of MSCs are conflicting in their reports of the various contribution of secreted factors, with some concluding angiogenic activity is a result of VEGF-A secretions, whilst others attribute this to MCP-1 or HGF activity (Amable et al., 2014; Arutyunyan et al., 2016; Edwards et al., 2014; Shen et al., 2015). Coincidently, these were the factors that were secreted in abundance by NG2 UCPs in comparison to MSCs. It is possible that the secretions detected in those studies may have been a result of perivascular cell contamination, and NG2 UCPs represent an enriched fraction of MSCs with enhanced angiogenic activity. Certainly, it would seem improbable that a cell source with such strong angiogenic properties would reside in an avascular structure. In any case, from the data of this study, NG2 UCPs demonstrate a unique secretome and superior angiogenic properties that highlight them as an optimal candidate for vascular tissue engineering.

5. Evaluating the Ability of Cells to Support Non-Pathological Remodelling of the Extracellular Environment

5.1. Introduction

Despite significant progress in vascular graft technology over the previous decades, failure rates can be as high as 50% after 10 years (Pashneh-Tala et al., 2015). In general, failures are most commonly associated with adverse remodelling of the graft, which leads to thrombosis, intimal hyperplasia, atherosclerosis and calcification (Bajpai et al., 2012; Kalfa et al., 2013; Shoji et al., 2018). In paediatric patients, there is also the added challenge of providing a graft which can match the somatic growth of the patient (Mirensky et al., 2008). The somatic overgrowth results in the need for reoperation to replace the redundant graft with a larger more suitable option (Avolio, Caputo, et al., 2015; Drews et al., 2017). To provide a long-lasting vascular graft capable of integrating with the host, the cells used to functionalise grafts need to address these limitations by facilitating non-pathological remodelling of the graft so that overtime the tissue resembles the natural structure.

Thrombosis is one of the most common reasons for graft failure, which usually occurs due to an absence of, or damage to, the endothelial layer (Pashneh-Tala et al., 2015). The formation of an endothelium is therefore a crucial consideration for vascular tissue engineering. This monolayer of ECs has a myriad of important roles in maintaining homeostasis of the vessels. As well as their involvement in regulation of blood flow, ECs form a selectively permeable barrier for exchange of macromolecules and fluids into the surrounding vessel wall and tissue (Yau et al., 2015). Under normal conditions this barrier acts as a non-thrombogenic surface via expression of antiplatelet and anticoagulant agents such as tissue factor pathway inhibitor and thrombomodulin (Yau et al., 2015). Additionally, the endothelium regulates the inflammatory response through expression of cytokines and cell adhesion molecules (Yau et al., 2015). To reduce the chance of thrombotic complications, endothelialisation of the graft must be achieved. Primarily, this is attained through in situ mechanisms rather than pre-seeding of grafts, with grafts functionalized with growth factors or specific cells that promote host EC migration and attachment (Sánchez et al., 2018). Specifically, pericytes represent an excellent cell source due to their role in maintaining the integrity of the endothelial barrier (Bergers et al., 2005). In fact, previous studies have shown saphenous vein pericytes promote endothelialisation of poly(ε-caprolactone) (PCL) scaffolds (Campagnolo et al., 2016). Using a similar approach, it is possible to evaluate the promigratory influence of NG2 UCPs on ECs in vitro. This will help develop an understanding of the cells ability to stimulate reendothelialization, which can better inform the cell choice for tissue engineering.

Along with thrombosis, ectopic calcification is a considerable complication for development of functional vascular grafts for repair of congenital defects (Kalfa et al., 2013; Mantakaki et al., 2018). Ectopic calcification is the biomineralization of soft tissues that occurs due to injury, disease or age (Giachelli, 1999). This process commonly occurs in the cardiovascular system where it correlates with major adverse pathological events such as atherosclerosis and stenosis. Calcification is triggered by a variety of stimuli, such as loss of inhibitors, apoptotic bodies, hyperphosphatemia, hypercalcemia and induction of osteochondrogenesis (Wu et al., 2013).

Rather than being a passive age-related disease, calcification is now considered an active process driven by cells. Disruption of the endothelial layer triggers reorganisation of the vascular matrix and subsequent infiltration by immune cells (Rutkovskiy et al., 2017). During this process the cells such as MSCs and VSMCs trans-differentiate into myofibroblasts or osteoblasts in response to paracrine signalling. Myofibroblasts contract the matrix, causing cell aggregation and apoptosis. These apoptotic cells become the sites for sedimentation of calcium salts. Meanwhile, osteoblast differentiation driven by runt-related transcription factor 2 (*RUNX2*) and bone morphogenic protein 2 (*BMP2*) results in secretion of bone-associated proteins such as osteocalcin, osteopontin and alkaline phosphatase. Finally, calcium crystals are laid in the matrix and organised into structure resembling lamellar bone (Jover et al., 2018; Rutkovskiy et al., 2017). Consequently, the tissue stiffens and becomes dysfunctional.

Whilst much more common in aging demographics, calcification has been linked with congenital malformations (Jover et al., 2018). Specifically, calcific pulmonary stenosis has been observed in patients with ToF (Roberts et al., 1968). This could indicate that cellularised grafts used to reconstruct the RVOT may be under greater risk of calcification stimuli caused by the in vivo environment. To understand this risk and confirm cells will not become a site for induction of ectopic calcification, it is useful to assess the cellular response to calcification stimuli, such as hyperphosphatemia, in vitro. Analysis of the subsequent calcium deposition and any changes in osteochondrogenic genes, such as *RUNX2*, *BMP2* or bone gamma-carboxyglutamic acid-containing protein/osteocalcin (*BGLAP*), can be used to detect any beneficial calcification resistance properties of the cells (Giachelli, 1999; Karwowski et al., 2012).

A specific obstacle to overcome in paediatric patient care is ensuring vascular grafts are able to match somatic growth. As previously alluded to, somatic overgrowth is one of the leading

causes of graft failure and reoperation in treatment of CHD in children. As the child grows, there is a mismatch between the diameter of the graft and the native vessel around the anastomosis. This mismatch, along with a discrepancy in vessel compliance, not only leads to somatic overgrowth but can also promote intimal hyperplasia, which leads to further complications and reduced graft lifespan (Pashneh-Tala et al., 2015). It has been proposed that functionalisation of acellular grafts with cells may overcome this limitation by facilitating physiological remodelling of the graft through modulation of the ECM (Avolio, Caputo, et al., 2015). The ECM is a tightly controlled dynamic structure that is essential for development and homeostasis. It is mainly composed of collagens, elastic fibres and glycosaminoglycans; however, the relative levels of components vary between tissues (Cox et al., 2011). For example, in arteries there is a greater amount of collagen and elastin than in veins (Xu et al., 2014). These ECM proteins are secreted by cells, such as smooth muscle cells in vascular tissue, and contribute to mechanical properties of the tissue, amongst other things. To balance the secretion of extracellular proteins, enzymes involved in the degradation of the ECM are produced. In particular, MMPs and their inhibitors, tissue inhibitors of MMPs (TIMPs), play an integral role in this process, with each variant possessing different affinities for specific ECM proteins (Lu et al., 2011). Under normal homeostatic conditions, a fine balance is struck between the production of ECM components and secretion of enzymes, which supports active remodelling of the tissue (Lu et al., 2011). In acellular grafts, the absence of cells means this dynamic process does not occur, and consequently the graft is not remodelled in line with native tissue. Whilst the diameter of native vessels increases over time, the artificial graft remains constant (Pashneh-Tala et al., 2015). By functionalising grafts with cells that produce ECM components and proteases, it may be possible to stimulate remodelling of the graft. Furthermore, characterisation of the type of proteins and enzymes produced by cells can be used to understand a cells compatibility with certain scaffold or suitability for engineering particular tissues. For example, arteries are mainly composed of elastin and collagen type I (Jacob et al., 2001). Consequently, a cell source which secretes an abundance of collagen and elastin, along with the appropriate MMPs, may be beneficial for creating a graft used for the reconstruction of arterial tissue.

5.2. Objectives

In the following chapter we explore the ability of NG2 UCPs to support remodelling of the ECM. Specifically, we focus on how they may facilitate endothelialisation, resistance to calcification, and the ability to produce and degrade the extracellular environment. In order to accomplish this the following experimental objectives were established:

- Analyse the ability of cell CM to influence EC migration.
- Assess response of cells to calcific high phosphate medium.
- Quantify cell-derived ECM proteins, MMPs, and collagenase activity.

5.3. Results

5.3.1. Promigratory Phenotype

Recruitment of ECs into a graft is crucial for reendothelialization and reduction of thrombotic complications, and therefore it was useful to understand if NG2 UCPs could influence this process through secretion of chemoattractant factors. To evaluate this pro-migratory effect, a scratch wound assay was utilised. Both cell types were cultured under the same conditions and the same media for collection of conditioned medium/supernatant. The media collected was then transferred to HUVEC monolayer scratch plates (see method 2.7 and 2.13 for full details). ECs incubated with NG2 UCP CM migrated four times farther than ECs incubated with either unconditioned medium or MSC CM (**Figure 5.1**). Again, this highlighted a further advantage of using NG2 UCPs over MSCs for vascular tissue engineering applications.

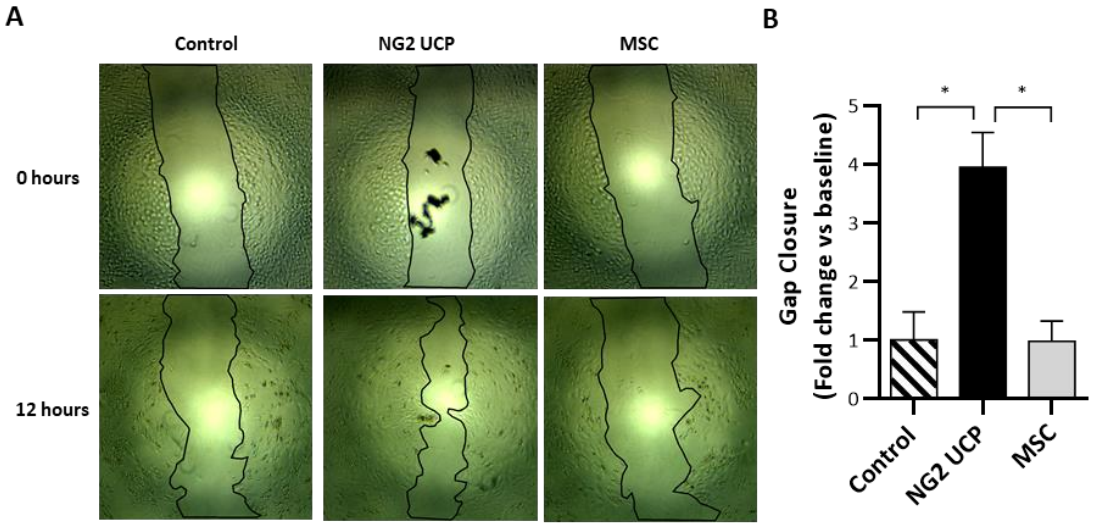

Figure 5.1: Promigratory effect of NG2 UCP and MSC conditioned medium on Endothelial Cells. A) Representative scratch-wound migration assay images at 0 and 12 h. B) Summary of fold change in migration vs. control. Data represent means (± S.E.M) of $n = 3$ biological replicates. *$p<0.05$ as determined by one-way ANOVA followed by Tukey's post-hoc test.

5.3.2. Resistance to Calcification

To investigate whether pericytes offered a resistance to calcification, the cells were exposed to a high phosphate (HP) medium for 5 days, before analysing calcium content and changes in gene expression (method 2.19). As before, MSCs were used for comparison.

Initial visual analysis via alizarin red s staining demonstrated a moderate accumulation of calcium deposits in HP exposed cells, as indicated by the red dye, which was not present in cells under normal culture conditions (**Figure 5.2A**). No differences were identified between the two cell types, however, a build-up of calcium was observed around the edges of the well, which was difficult to analyse. To solve this issue, bound alizarin red s was dissolved in acetic acid and then semi-quantified by measuring the absorbance and normalising by the control condition (bound alizarin red s found in cell monolayers incubated in control medium). This gives an indication of how easily cells calcify under inductive conditions. Using this method, it was determined that MSCs demonstrated a significant 1.27-fold increase in calcium

deposition, whereas NG2 UCPs only displayed a modest 1.1-fold change (**Figure 5.2B**). To confirm these results, the Ca^{2+} content of induced monolayers was quantified using a colorimetric o-cresolphthalein-based assay and normalised the result by total monolayer protein. Under normal culture conditions, there was no detectable Ca^{2+}; however, after exposure to HP, both MSCs and NG2 UCPs demonstrated a significant increase ($p = 0.0127$) in Ca^{2+} (251.6 ± 57.7 ng/μg total protein and 656.7 ± 74.7 ng/μg total protein, respectively) (**Figure 5.2C**). Despite both cell lines undergoing calcification, NG2 UCPs demonstrated some resistance compared with MSCs, with less than half of the Ca^{2+} deposits.

To further assess the effect of HP exposure, expression of major osteogenic markers *RUNX2*, *SOX9*, *BMP2*, *BGLAP* and *SP7/OSX* were studied. Interestingly, despite the accumulation of calcium deposits, which is indicative of calcification, no upregulation of osteogenic genes was observed in either MSCs or NG2 UCPs (**Figure 5.3**). Together, this suggested both cell types provided some resistance to calcification mechanisms, but NG2 UCPs performed marginally better than MSCs.

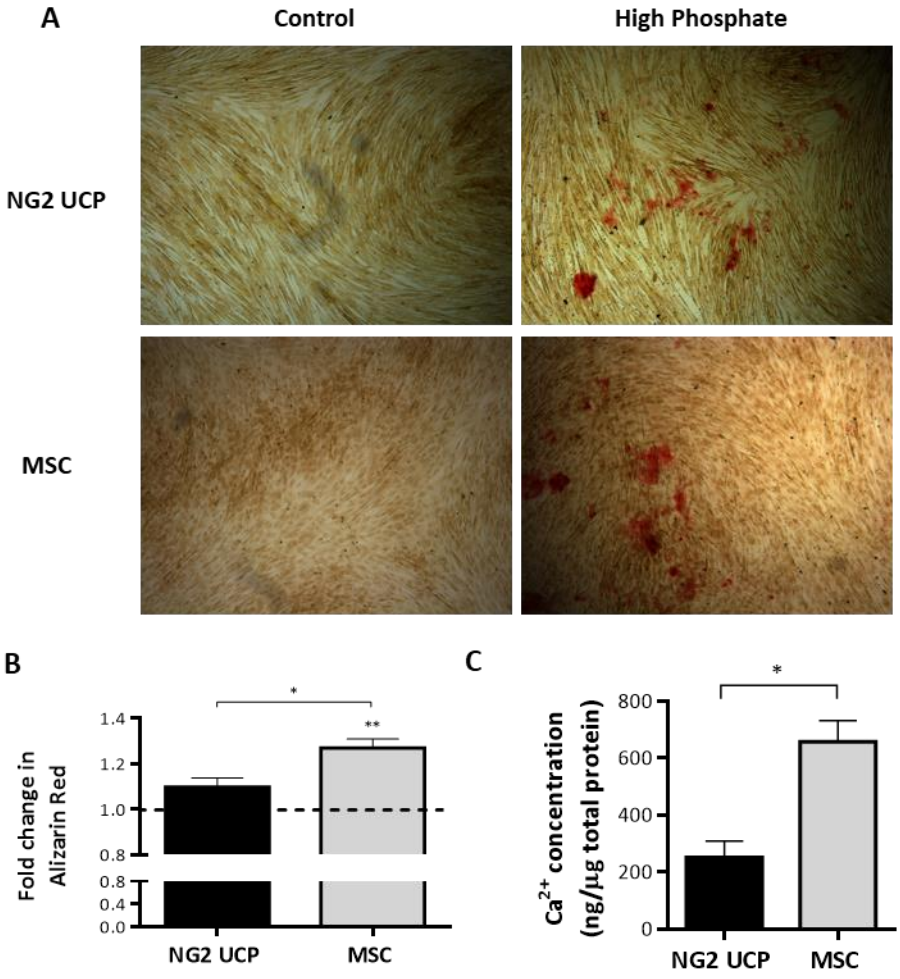

Figure 5.2: Calcification of NG2 UCPs and MSCs. (A) Alizarin red S staining of NG2 UCP and MSC monolayers after 5 days incubation with either high phosphate or control medium. (B) Fold change in bound alizarin red S after stimulation with high phosphate medium relative to control medium. Data represent means (± S.E.M). MSCs and NG2 UCPs, n = 3, which represents 3 control conditions and 3 high phosphate conditions. The dotted line represents no fold change (expression levels of cells cultured in the control media). * p<0.05 and ** p<0.01 as determined by one-way ANOVA followed by Tukey's post hoc test. ** directly over the column represents a significant change from the control condition. (C) Ca^{2+} concentration in NG2 UCP and MSC monolayers after 5 days incubation with either high phosphate or control medium. Data represent means (± S.E.M). MSCs and NG2 UCPs, n = 3. * p<0.05 as determined by student's t-test.

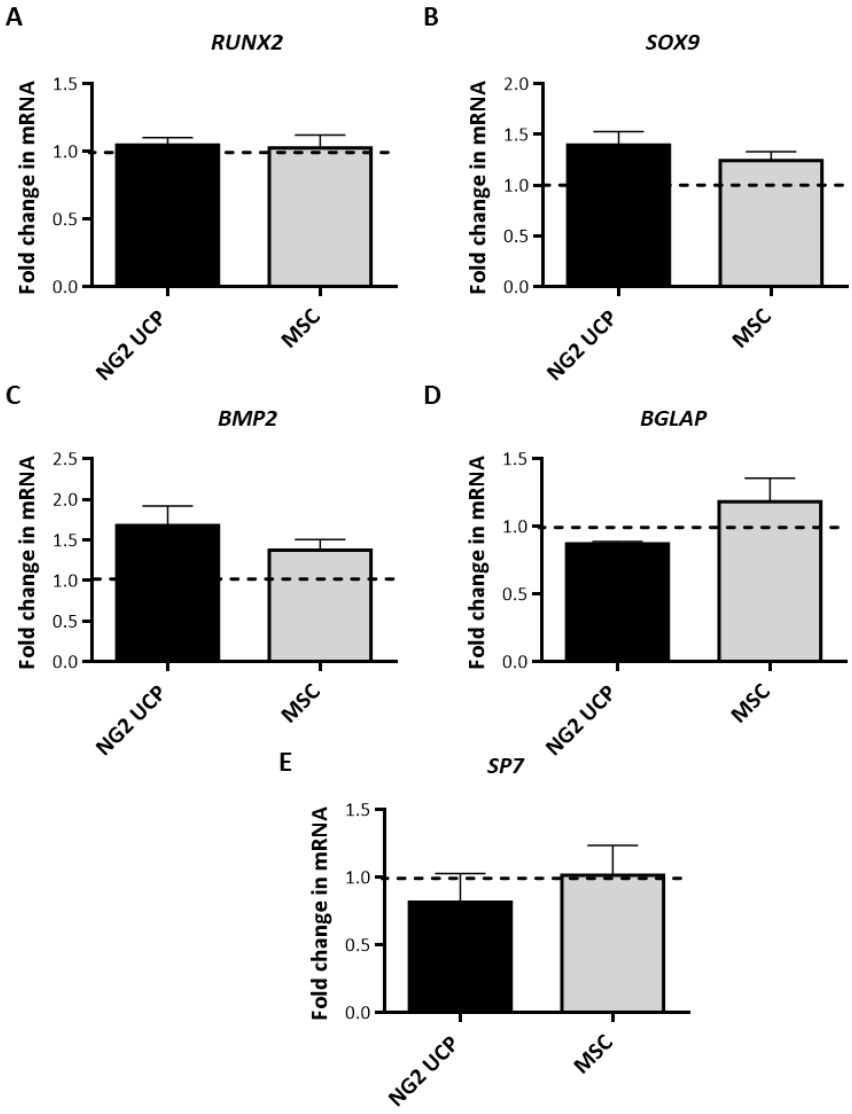

Figure 5.3: Fold change in mRNA expression levels of typical osteoblast markers following MSC or NG2 UCP 5 day exposure to high phosphate medium (relative to cells cultured for 5 days in control medium). A) *RUNX2* = runt-related transcription factor 2. B) *SOX9* = transcription factor SOX-9. C) *BMP2* = bone morphogenetic protein 2. D) *BGLAP* = bone gamma-carboxyglutamic acid-containing protein/osteocalcin. E) *SP7* = transcription factor SP7 or Osterix. Data represent means (± S.E.M). MSCs and NG2 UCPs, n = 3, which represents 3 control conditions and 3 high phosphate conditions. The dotted line represents no fold change (expression levels of cells cultured in the control media).

5.3.3. Ability to Remodel the Extracellular Environment

In order to understand whether NG2 UCPs could remodel the extracellular environment, production of ECM proteins and MMPs was investigated (methods 2.16 -2.18).

For evaluation of ECM proteins, cells were seeded at high confluence (20,000 cells/cm^2) and cultured for 3 or 5 days before quantifying the content of confluent monolayers. Time points less than 3 days did not allow the cells enough time to produce a substantial ECM, whilst monolayers left for longer than 5 days detached from the culture plastic. 2 time points were selected to identify if the matrix was actively modified over time. Results were contextualised by evaluating MSC ECM production in parallel.

Elastin was actively secreted into the ECM, as evidenced by a significant increase (two-way ANOVA, $p = 0.0067$) between day 3 and day 5 in both NG2 UCPs and MSC monolayers (1.87- and 1.71-fold increase respectively; **Figure 5.4A**). Interestingly, NG2 UCPs secreted significantly more elastin (day 3: $p = 0.004$, day 5 $p = 0.0055$), 61.5 ± 4.9ug and 115.2 ± 10.3 ug compared to just 20.7 ± 0.8 ug and 35.5 ± 0.4 ug in MSC monolayers. A similar pattern was observed regarding the soluble collagen quantified in monolayers and CM (**Figure 5.4B**). The collagen content increased over time, however, the initial superiority of NG2 UCPs vs MSCs (24.2 ± 1.3ug vs 13.1 ± 0.2ug at day 3) was lost after 5 days. Insoluble collagen content was similarly increased between time points ($p = 0.0391$); however, there were no significant differences detected between the two cell types (**Figure 5.4C**).

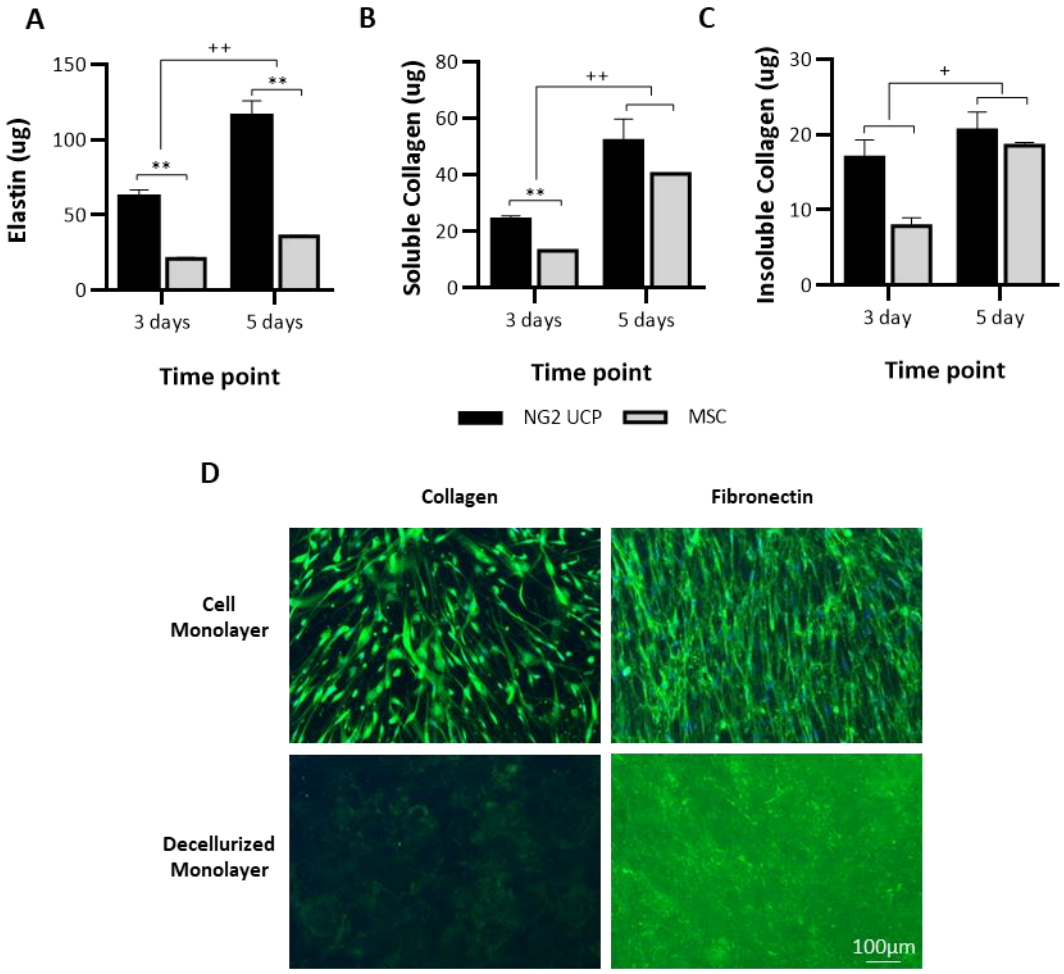

Figure 5.4: NG2 UCPs produce ECM proteins. A) Quantification of elastin in confluent cell monolayers. B) Quantification of pepsin acid-soluble collagen in confluent cell monolayers and CM. C) Quantification of insoluble collagen in confluent cell monolayers. D) Presence of extracellular proteins collagen and fibronectin in decellularized monolayers. Scale bar = 100 µm. Data represent means (± S.E.M). MSCs and NG2 UCPs, n = 2 and 6, respectively. */+p<0.05 and **/++p<0.01. * represents differences between cell types, + represents differences between time points, as determined by two-way ANOVA followed by Student's t-test.

Immunocytochemical staining was used to further examine the content of the ECM. Cellular expression of collagen and fibronectin was detected, along with presence in decellularized monolayers (**Figure 5.4D**). Although collagen and fibronectin deposits were detected, there

was no order to the deposited proteins. This was most likely due to the effect of the decellularization process as the fibronectin in cell monolayers appears in an organised form.

The presence of MMPs in NG2 UCPs was visualised using an array membrane. Localisation of MMPs was evaluated by measuring the presence in both cell lysates and CM. In general, TIMP levels were considerably greater than MMP levels, particularly TIMP-1 and TIMP-2, which displayed a mean pixel density at least 7 times greater than MMPs 2 - 13 (**Figure 5.5A**). The exception to this trend was MMP-1, which, along with TIMP-2, was significantly higher in CM (**Figure 5.5A - C**). For context, MMP levels were compared with MSCs. Due to the membrane cost, analysis of MSCs was only completed once. Although this meant no statistical differences could be evaluated, it highlighted the similarities in MMP and TIMP secretion between NG2 UCPs and MSCs, with both cell types favouring TIMP secretion (**Figures 5.5D & E**).

In line with the analysis of MMP presence in lysate and CM, the extracellular collagenase activity in CM was significantly higher ($p = 0.0004$) than intracellular activity assessed in the cell lysate (**Figure 5.5G**). In fact, extracellular activity accounted for 97% of the total active collagenases. Furthermore, the extracellular collagenase activity of NG2 UCPs was significantly higher than that of MSCs.

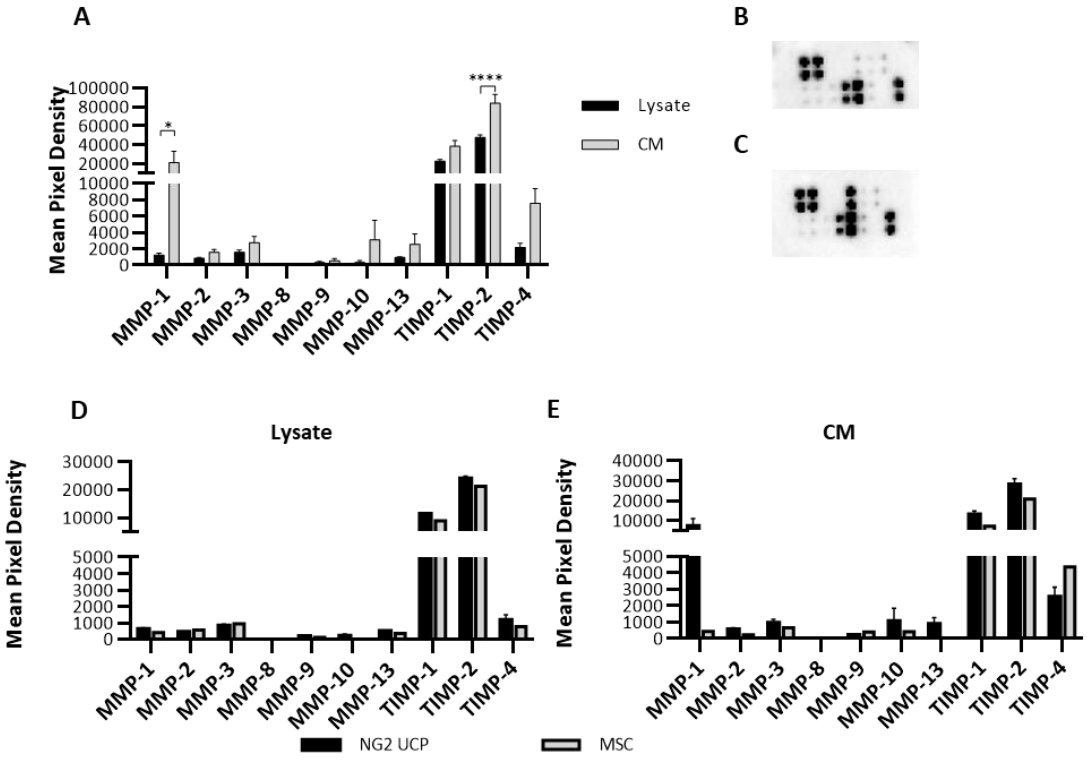

F

Pos	Pos	Neg	Neg	MMP-1	MMP-2	MMP-3	MMP-8
Pos	Pos	Neg	Neg	MMP-1	MMP-2	MMP-3	MMP-8
MMP-9	MMP-10	MMP-13	TIMP-1	TIMP-2	TIMP-4	Neg	Pos
MMP-9	MMP-10	MMP-13	TIMP-1	TIMP-2	TIMP-4	Neg	Pos

Figure 5.5: NG2 UCPs secrete active MMPs. (A) Relative MMP levels in NG2 UCP lysate and CM. Data represent means (± S.E.M), n = 4; *p<0.05 and ****p<0.0001 as determined by two-way ANOVA followed by Sidak's post hoc test. (B) Representative membrane for MMP presence in cell lysates. (C) Representative membrane for MMP presence in CM. (D) Comparison of lysate MMP levels in NG2 UCP and MSC. Data represent means (± S.E.M), n = 4 and 1, respectively. (E) Comparison of CM MMP levels in NG2 UCP and MSC. Data represent means (± S.E.M) n = 4 and 1, respectively. (F) Human MMP Antibody Array-Membrane map.

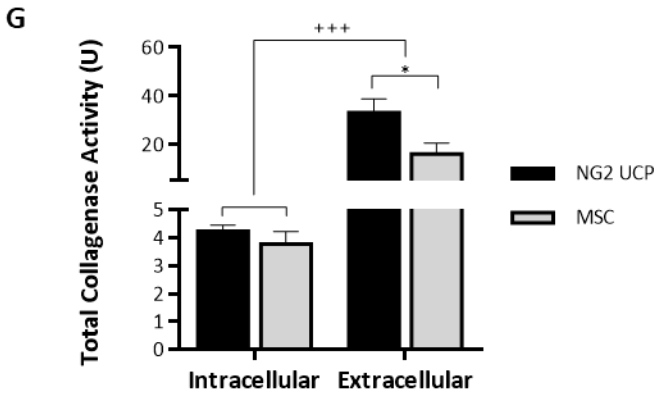

Figure 5.5: NG2 UCPs secrete active MMPs (continued). (G) Total intracellular (total protein) and extracellular (CM) collagenase activity in NG2 UCPs and MSCs per T25 culture flask. Data represent means (± S.E.M). MSCs and NG2 UCPs, n = 4 and 6, respectively. */+ $p<0.05$ and ***/+++ $p<0.001$. * represents differences between cell types, + represents differences between intracellular and extracellular activity as determined by two-way ANOVA followed by Sidak's post hoc test.

5.4. Discussion

The remodelling of a graft after implantation is crucial for its long-term patency. Vascular grafts often fail and require replacement after just a few years due to adverse remodelling, which results in complications such as thrombosis, intimal hyperplasia, calcification and atherosclerosis (Kalfa et al., 2013; Pashneh-Tala et al., 2015). Additionally, in paediatric patients, such as those undergoing surgery for CHD repair, grafts frequently fail due to somatic overgrowth (Drews et al., 2017). This results in multiple reinterventions, which places significant risk on the patient (Jacobs et al., 2014). Tissue engineering may address these failures by functionalising grafts with cells that support the remodelling of the extracellular environment. By characterising the influence of cells on the extracellular environment in vitro, we may be able to develop an understanding of their ability to promote favourable graft remodelling.

The development of thrombosis and intimal hyperplasia in vascular grafts is usually caused by an absence of a complete endothelium. Various strategies have been utilised to encourage endothelialisation of grafts and reduce associated complications. These methods are categorised as in vitro or in situ. The in vitro approach relies on seeding of grafts with ECs before implantation. Whilst providing more control over the endothelialisation process, cell retention after exposure to in vivo flow conditions is poor, with some studies reporting 95% cell loss after 24 hours (Sánchez et al., 2018). As a result, research often focuses on mobilisation of in situ mechanisms (**Figure 5.6**).

In animal models of transplanted vascular grafts, reendothelialization tends to occur through trans-anastomotic ingrowth. However, in humans this process is much slower and limited to less than 2 cm (Sánchez et al., 2018; Zilla et al., 2020). Consequently, this leads to incomplete endothelial layer formation and thrombotic complications. Implementation of a scratch wound migration model demonstrated that CM from NG2 UCPs enhanced EC migration, which may increase efficiency of trans-anastomotic ingrowth. This data suggests that NG2 UCPs can facilitate the development of a graft endothelial layer through paracrine signalling. This highlights a distinct advantage over other pericyte populations such as saphenous vein pericytes, which do no influence EC migration (Campagnolo et al., 2010). Furthermore, localized release of chemoattractant factors may also encourage engraftment of circulating cells (Fallout endothelialisation). Fallout endothelialisation happens in response to damage to the endothelium. Firstly, protein adsorption occurs on the exposed graft resulting in the

deposition of adhesion factors and prompting an inflammatory response. The inflammatory response triggers the release of chemokines and growth factors, such as VEGF, which recruit circulating EPCs and mediate their differentiation into mature ECs (Sánchez et al., 2018). Research groups have attempted to harness this mechanism to enhance endothelialisation of artificial grafts. For example, Smith et al. demonstrated that small intestinal submucosa conduits functionalised with immobilised VEGF and heparin captured circulating host monocytes. These cells reconstructed the endothelial layer and improved graft patency (Smith et al., 2019, 2020). Similarly, De Visscher et al showed coating of grafts with fibronectin and SDF-1α significantly increased endothelial coverage, which led to a significant reduction in intimal hyperplasia and adhesion of thrombotic material (De Visscher et al., 2012). Functionalisation of grafts with NG2 UCPs, which secrete both VEGF and SDF-1, could yield similar results. Additionally, the proangiogenic properties of NG2 UCPs may support transmural capillarisation, the process of capillary ingrowth from the perivascular tissue. This process has been described as the primary contributor to in situ endothelialisation (Pennel et al., 2018; Zilla et al., 2020). The induction in tube formation demonstrated in the previous chapter, indicates NG2 UCPs might support the sprouting of capillaries through the vessel wall to supply ECs for endothelium development. Overall, although in vitro data suggests NG2 UCPs can improve graft endothelialisation, the legitimacy of this conclusion cannot be substantiated without in vivo analysis.

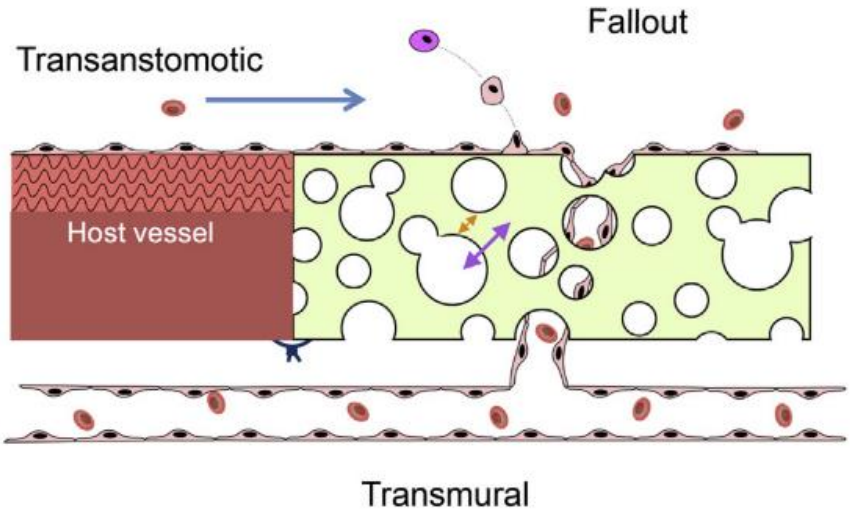

Figure 5.6: Schematic representation of the three forms of in situ endothelialisation. Figure source: Pennel et al., 2018.

Cardiovascular calcification is a common pathological condition that results in adverse remodelling of tissue, leading to stiffening of vascular tissue and stenosis of valves. In children, there is often an elevated risk due to the mobilisation of calcium during bone remodelling, which can accelerate the calcification process (Avolio, Caputo, et al., 2015). Specifically in patients with CHD, malformations put increased pressure on the cardiovascular system, which can initiate ectopic calcification (Jover et al., 2018; Kalfa et al., 2013; Roberts et al., 1968). Whilst there has been progress in the development of improved vascular grafts for reconstruction of cardiac defects, the effect of calcification on cells used for tissue engineering remains unknown. To elucidate this behaviour, NG2 UCPs were exposed to hyperphosphatemia and analysed the cells response. NG2 UCPs demonstrated an increased resistance to calcification in comparison to WJ- MSCs, as evidenced by the significantly smaller calcium deposits measured after exposure to the high phosphate environment. This data corroborated previous studies that have demonstrated the calcific resistance of pericytes (Jover et al., 2021). Here, researchers showed that saphenous vein pericytes demonstrated anti-calcific tendencies with low accumulation of calcium, even after 12 days exposure to high phosphate. In contrast, bone marrow (BM) MSCs produced large calcium deposits, similar to the behaviour of the WJ-MSCs that was examined. Whilst the calcific resistance of NG2 UCPs is

not as dramatic as saphenous vein pericytes, this evidence does suggest distinct benefits over MSCs. Indeed, previous evidence suggests MSCs facilitate vascular calcification (C. Xie et al., 2019).

It was hypothesised that MSCs may be more susceptible to calcification due to their propensity to differentiate into osteocytes under inductive conditions (Avolio, Caputo, et al., 2015). Undeniably, osteogenic differentiation capacity is a prerequisite for classification of MSCs (Dominici et al., 2006). To evaluate this theory, the expression of osteochondrogenic genes was analysed. Specifically, *BMP2*, *RUNX2*, *SP7*, *BGLAP* and *SOX9* were evaluated due to their role in calcification. During osteogenesis, BMP2 triggers the activation of osteogenic regulator RUNX2, which in turn activates expression of several osteogenic proteins such as SP7/Osterix. Osterix and RUNX2 also trigger BGLAP expression, a marker associated with differentiated osteoblasts. Together with SOX9, a chondrogenesis marker, these proteins contribute to mineralisation of the ECM and pathogenic calcification (Jover et al., 2018).

Neither NG2 UCPs or MSCs demonstrated a significant upregulation of any genes after exposure to hyperphosphatemia. This was surprising as osteogenic differentiation has been highlighted as the main way MSCs contribute to vascular calcification (C. Xie et al., 2019). Furthermore, WJ-MSCs have been proposed as a candidate for regenerative therapy in orthopaedic diseases due to their osteogenic potential (Ansari et al., 2018). In contrast, BM-MSCs significantly upregulate *BMP2*, *RUNX2*, *SOX9* and *SP7* in response to high phosphate (Jover et al., 2021). Perhaps WJ-MSCs possess a lower osteogenic potency than other MSC sources. Indeed, a recent study showed WJ-MSCs to be poorly osteogenic (Cabrera-pérez et al., 2019). Either way, both cell types demonstrated a similar resistance to osteogenesis, although this was inferior to saphenous vein pericytes which downregulated osteogenic gene expression and conferred anti-calcific properties via miR-132 (Jover et al., 2021). Despite this, overall NG2 UCPs displayed a greater resistance to calcification processes than MSCs, which may have beneficial implications for their use in repair of CHD.

The ECM of native arteries can dynamically remodel through a tightly regulated balance of matricellular protein production and MMP activity, whereas this dynamic phenomenon is lost in acellular grafts, resulting in lack of growth potential and susceptibility to degradation (Jacob et al., 2001). The main constituents of vascular ECM are collagens and elastin, which are present in different proportions according to the type and anatomical location of the tissue. In

fact, the arterial wall is made up of up to 50% elastin and 30% collagen (mainly collagen type I and III), which provides mechanical integrity and vessel elasticity (Kielty et al., 2007; Xu et al., 2014). Conversely, CorMatrix is made up of 90% collagen, predominantly collagen type I (Badylak et al., 2009; Mosala et al., 2016). These figures illustrate that remodelling of the acellular graft is not only required for growth potential, but also to restore vessel functionality. Indeed, a lack of elastin synthesis in tissue engineered vascular grafts has been highlighted as a major limitation to successful outcomes (Patel et al., 2006). Furthermore, elastin plays a pivotal role in cell signalling, regulating VSMC activity and phenotype. Noteworthy, we have shown that NG2 UCPs produce significant amounts of both collagen and elastin. Specifically, we saw a large discrepancy in elastin production between NG2 UCPs and MSCs, which highlights the unique behaviour of our isolated pericytes. Whether NG2 UCPs are able to produce these extracellular components in a graft environment remains to be seen, but in vitro data supports the idea that functionalization of acellular scaffold using NG2 UCPs may alter the mechanical properties of the graft through secretion of extracellular proteins. The high levels of NG2 UCP-derived elastin may also have important implications for promoting VSMC activity. Despite this, it should be noted that elastin in its secreted form does not automatically translate to a more elastic material. For increased elasticity, the formation of elastic fibres must occur. This is a complex process that first requires deposition of fibrillin-1 rich microfibrils, which is regulated by fibronectin assembly and acts as a template for secreted soluble tropoelastin (Kielty et al., 2007; Kinsey et al., 2008). Indeed, although NG2 UCP-derived fibronectin was observed in decellularized cell monolayers, a more detailed study of the NG2 UCP-derived ECM is needed to determine if they play a significant role in elastic fibre synthesis, a process which is mainly attributed to VSMCs (Patel et al., 2006).

Naturally, ECM production must be regulated to ensure there is minimal risk of pathological remodelling. MMP/TIMP activity plays a major role in the remodelling of the vascular wall during homeostasis and disease (Jacob et al., 2001). Although MMPs are present in uninjured blood vessels, there is a low turnover of collagen and elastic fibres due to an abundance of TIMPs which inhibit MMP activity. In injury or disease, the balance of MMPs and TIMPs is disrupted, resulting in excessive remodelling (Jacob et al., 2001). In accordance with this, MMP and TIMP presence and activity in isolated cells was analysed. Both intracellular and extracellular expression of MMP-1, MMP-2, MMP-3, MMP-9, MMP-10, and MMP-13 was detected. In general, extracellular MMP levels were higher, specifically collagenase MMP-1,

which was expected due to their major role in ECM homeostasis (Jobin et al., 2017). Interestingly, TIMP levels were much higher relative to MMP levels both internally and externally. Classically, increased TIMP levels have been associated with increased ECM accumulation or fibrosis (Arpino et al., 2015); however, more recent studies have begun to uncover a more complex role. Indeed, TIMP-1 has been implicated in restricting inflammation and fibrosis post injury, whilst TIMP-2 is required for activation of MMP-2 driven proteolysis (Arpino et al., 2015). Furthermore, a lack of TIMP-2 led to increased adverse remodelling in mice (Kandalam et al., 2011). As such, a heavy balance towards TIMP activity is not necessarily an indication that NG2 UCPs facilitate fibrosis. In fact, Lozito et al demonstrated that MSCs helped stabilise blood vessels through promotion of a similarly inhibitory proteolytic environment (Lozito et al., 2010).

Despite disproportionate levels of extracellular TIMPs, a moderate level of collagenase extracellular activity was observed, which was likely associated with the increased levels of extracellular MMP-1. This is an important result as MMP-1 acts on collagen type I, which is not only the predominant collagen in blood vessels but also in animal derived ECM such as CorMatrix (Mosala et al., 2016). Indeed, presence of MMP-1 has previously been used as a marker for graft remodelling (Albertario et al., 2019; Ghorbel et al., 2019). This activity therefore suggests that NG2 UCPs can contribute towards remodelling of the vascular wall and collagen based scaffolds (Oxford et al., 2019).

Together, the data presented in this chapter shows that NG2 UCPs promote endothelial migration, possess some resistance to calcification, and are capable of secreting and degrading ECM proteins. This might mean functionalisation of acellular grafts with NG2 UCPs may confer them with the ability to resist pathological processes such as calcification and thrombosis whilst also facilitating matrix remodelling and growth.

6. Fabrication of Umbilical Cord Pericyte-Engineered Vascular Grafts

6.1. Introduction

Current graft material for reconstruction of congenital heart defects such as ToF are obsolete due to pathologic remodelling and a lack of growth potential (Avolio, Caputo, et al., 2015; Erikssen et al., 2015). Tissue engineering may be a valuable tool for development of novel vascular grafts which may address these limitations. To realise this potential, careful consideration must be paid to the choice of scaffold and cellular component, along with the optimal growth conditions. NG2 UCPs present an excellent cellular option for neonatal vascular tissue engineering, as evidenced by their ease of isolation and in vitro expansion, together with their exciting regenerative properties; however, their efficacy for graft development has yet to be demonstrated. To accomplish this, the tissue engineering methodology must be established.

Firstly, a scaffold needs to be selected or designed based on the application needs. According to Thottappillil et al, for vascular tissue engineering, the scaffold should be biocompatible, demonstrating low thrombogenicity and immunogenicity (Thottappillil et al., 2015). The scaffold should also possess circumferential strength to withstand arterial pressure and surgical handling, whilst also demonstrating a degree of compliance as seen in native vascular tissue. Biodegradability should be balanced with ECM remodelling to ensure the mechanical integrity is not compromised (Thottappillil et al., 2015). Furthermore, for neonatal applications the scaffold should promote native tissue formation over time to facilitate natural tissue growth and reduce the need for replacement (Mosala et al., 2016).

Seeding methodology is another essential component for producing cellularised tissue engineered grafts. Although some approaches, such as 3D bioprinting, incorporate the cells within the scaffold, the majority utilise post scaffold fabrication seeding (Duan, 2017; Villalona et al., 2010). Traditionally, this had been accomplished using static cell seeding, which involves manual pipetting of cells directly onto the scaffold (Kurobe et al., 2012). This technique is the one of the simplest and widespread methods; however, low seeding efficiency and poor cell distribution have been reported in some studies, which is particularly evident for short seeding incubation times (Villalona et al., 2010). Other more complex seeding methodologies have been used to address these issues, namely, rotational seeding, which utilises rotation of the scaffold within a cell suspension to facilitate a more homogenous cell distribution. Despite improvement in efficiency and distribution, static seeding remains the most common method, possibly due to its simplicity and adaptability (Villalona et al., 2010). Another important aspect

of the seeding methodology is the number of cells used. Seeding density is dependent on several factors including the cells and scaffolds used, as well as the type of tissue to be engineered. Due to these considerations, it is hard to conclude an optimal density that fits all vascular tissue engineering applications and therefore this should be optimised experimentally.

Lastly, the environmental conditions must be optimised according to the tissue engineering application. For example, the provision of specific growth factors and biomechanical cues can influence the development of engineered tissue (A. Cai et al., 2018; Nakayama et al., 2014). Accordingly, bioreactors have been developed that better represent the physiological environment. These systems facilitate delivery of bioactive molecules and biomechanical cues, which has resulted in improved complexity of engineered tissues (Plunkett et al., 2011; Zhao et al., 2016). Indeed, for vascular tissue engineering, the application of dynamic flow and mechanical conditioning has enhanced ECM remodelling and mechanical properties of grafts, confirming the necessity of this step for in vitro vascular graft development (Flanagan et al., 2007; Seliktar et al., 2000).

In the following chapter, the concepts mentioned above have been utilised to develop a pericyte-engineered vascular graft suitable for use in neonatal tissue engineering.

6.2. Objectives

To assess the applicability of using NG2 UCPs to produce tissue engineered vascular grafts for neonatal tissue engineering, the following experimental objectives were established:

- Optimise the seeding conditions of NG2 UCPs onto acellular scaffold.
- Manufacture both planar and conduit shaped NG2 UCP-engineered grafts.
- Characterise the graft composition through histological analysis.
- Assess the mechanical performance of engineered grafts.
- Evaluate the feasibility of graft cryopreservation.

6.3. Results

6.3.1. Optimisation of Scaffold Seeding Density

Before creating the cellularised graft, the seeding conditions needed to be optimised for the CorMatrix scaffold, as the cell behaviour may differ in comparison to seeding on coated culture plastic. Initially, the seeding density required to create a confluent cell monolayer on top of the scaffold was investigated. Cells were seeded in 96-well plates at three levels of confluency and evaluated after 5 days static conditioning according to a variety of measures. Cells were cultured on coated plastic in parallel with scaffold experiments so that significant changes in cell behaviour and stress relative to normal in vitro culture conditions could be identified (Methods 2.20.1).

Density and proliferation were assessed by quantifying the total number of DAPI positive cells versus the number of Ki-67 positive cells (Methods 2.20.3). Results demonstrated that seeding cells at a 20,000/cm^2 significantly improved scaffold cell density in comparison to lower density seeding (19891 ± 2802 cells/cm^2 vs 8956 ± 931 cells/cm^2); however, seeding at a higher density did not significantly improve cell coverage further (23333 ± 3313 cells/cm^2 vs 19891 ± 2802 cells/cm^2; **Figure 6.1A & E**). Interestingly, cells grown on the scaffold did not reach the level of confluency that they did on coated culture plastic, with the confluency on average one-third of cell density on culture plastic (two-way ANOVA, p = 0.0005; **Figure 6.1B & E**). Despite a general trend that a higher density cell seeding resulted in lower numbers of proliferating cells, the differences were not statistically significant (**Figure 6.1C – E**).

Cell viability was evaluated qualitatively using a LIVE/DEAD^{TM} Viability/Cytoxicity Kit, which incorporated Calcein AM and ethidium homodimer-1 fluorescent dyes (Methods 2.20.3). Images demonstrated very few dead cells, which suggested the CorMatrix environment was not harmful to the cells (**Figure 6.2A**). In contrast to this, levels of CM LDH, a cytotoxicity indicator, were increased in scaffold seeded cells (>5-fold), indicating the cells may be more stressed on the CorMatrix scaffold (**figure 6.2B**). The fold change in LDH was less evident at higher seeding densities.

Overall, seeding at 10,000 cells/cm^2 demonstrated the lowest cell coverage and highest cell cytotoxicity. Seeding at 20,000 cells/cm^2 improved cell coverage and cytotoxicity; however, further increase in seeding density demonstrated relatively little difference in cell distribution

and behaviour. Consequently, a seeding density of 20,000 cell/cm^2 was chosen for subsequent experiments and generation of pericyte-engineered CorMatrix grafts.

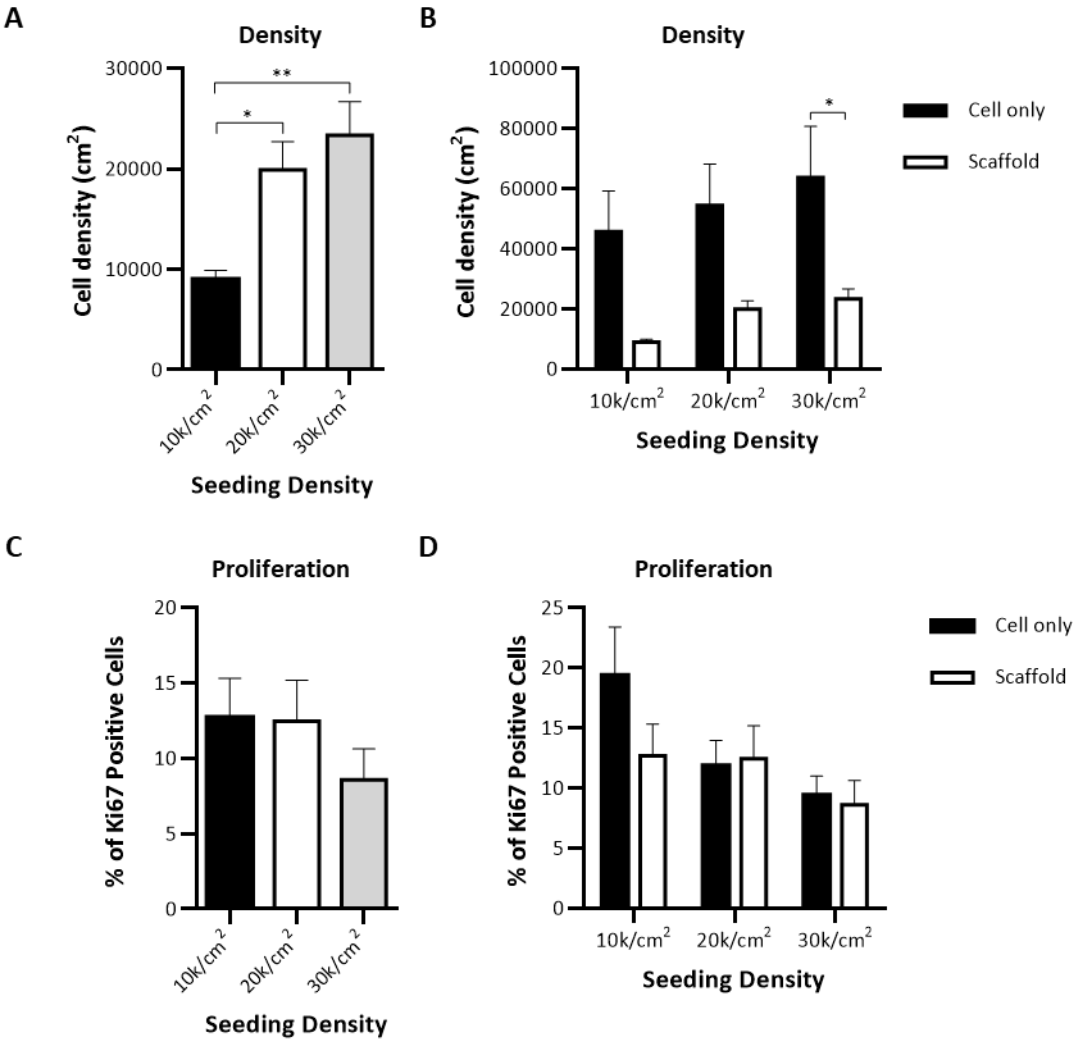

Figure 6.1: Analysis of cell density and proliferation. (A) Cell density after 5 days static conditioning (scaffold only). (B) Comparison of cell density after 5 days static conditioning on culture plastic or the CorMatrix scaffold. (C) Quantification of proliferative cells after 5 days static conditioning (scaffold only). (D) Comparison of cell proliferation after 5 days static conditioning on culture plastic or a CorMatrix scaffold. Data represents means (± S.E.M), n = 4. * $p<0.05$ and ** $p<0.01$ as determined by one-way ANOVA or two-way ANOVA followed by Sidak's or Tukey's post-hoc test.

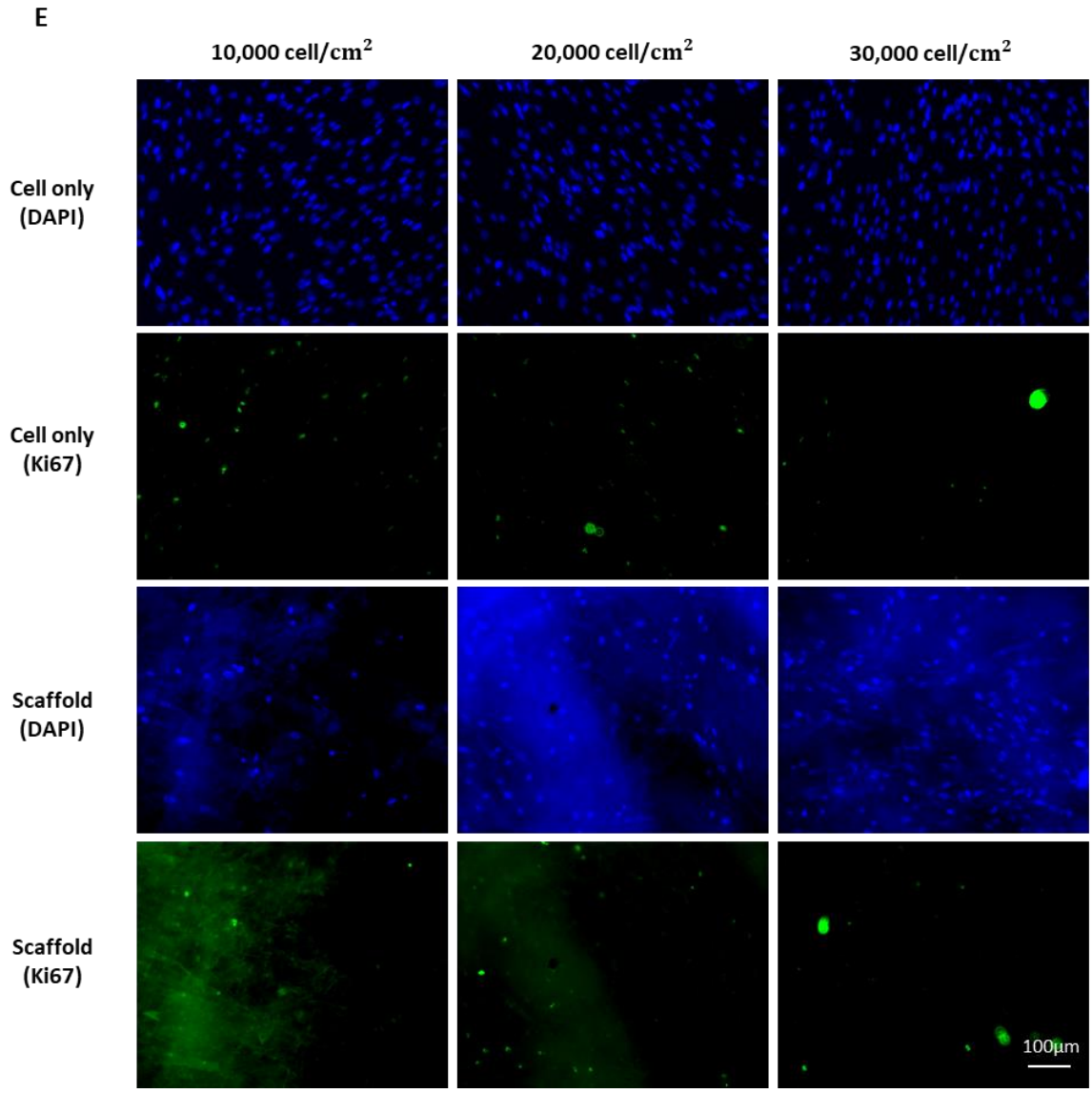

Figure 6.1: Analysis of cell density and proliferation (continued). (E) Representative images used to quantify cell density and proliferation after 5 days static conditioning on either culture plastic or the CorMatrix scaffold. DAPI (blue), Ki67 (green). Scale bar = 100µm.

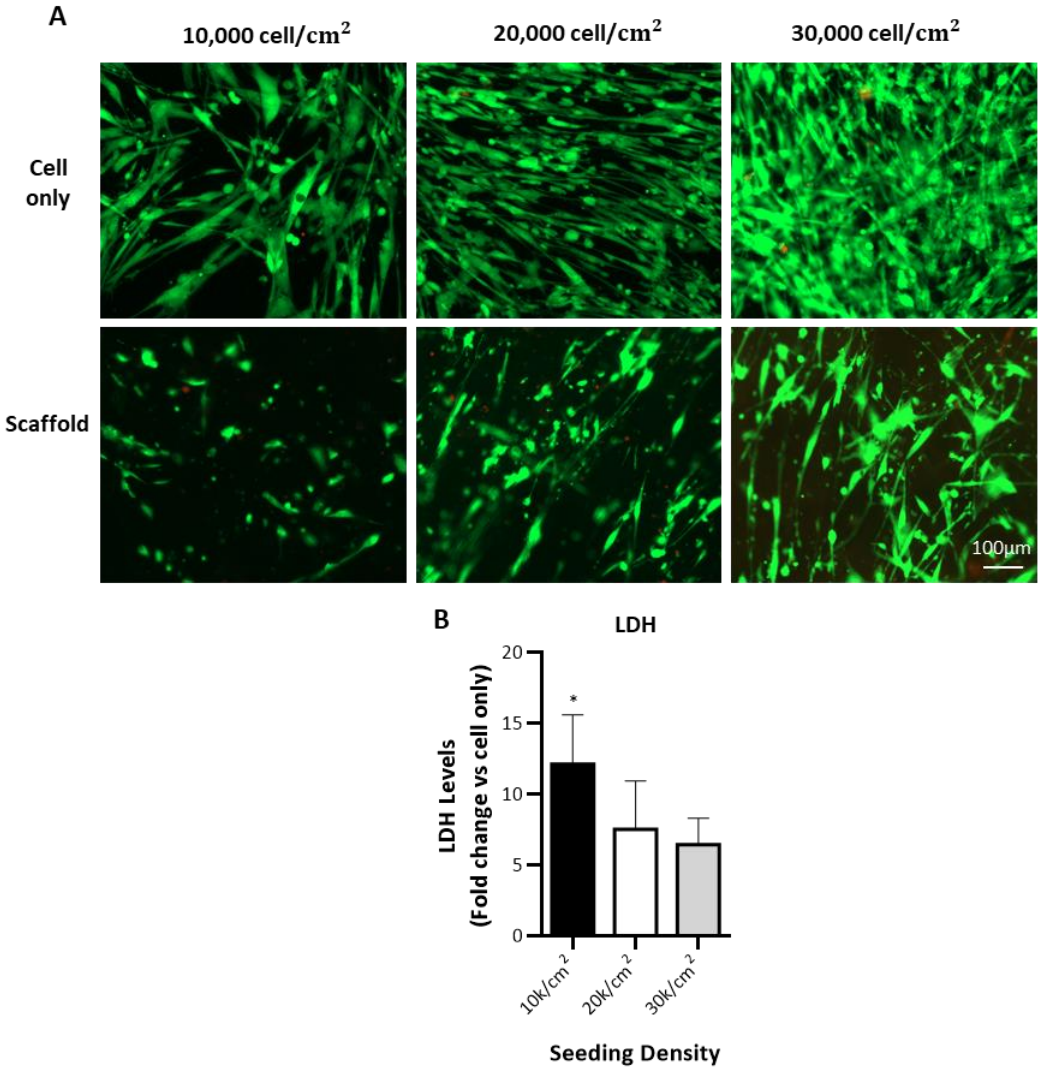

Figure 6.2: Analysis of cell cytotoxicity. (A) Cell viability after 5 days static conditioning on culture plastic (cell only) or a CorMatrix scaffold. Cytoplasmic green fluorescence = live (Calcein AM) cells, Nuclear red fluorescence = dead (ethidium homodimer-1) cells. Scale bar = 100µm. (B) Fold change in lactate dehydrogenase (LDH) levels in scaffold seeded cells vs culture plastic seeded cells (cell only). Data represents means (± S.E.M), n = 4. * $p<0.05$ as determined by one-way ANOVA followed by Tukey's post-hoc test.

6.3.2. Optimisation of Cell Attachment

Despite optimising the seeding density to facilitate the best cell coverage, the distribution of cells on the scaffold remained uneven. Areas of the CorMatrix were sparsely populated, as demonstrated in the representative image of NG2 UCPs seeded on uncoated CorMatrix (**Figure 6.3A).** To evaluate whether coating could improve cell distribution, cells were seeded on small sections of CorMatrix (96-well plate), which were coated with either FBS or fibronectin and gelatin (Methods 2.20.1). FBS significantly increased the cell density after 5 days static conditioning; however, this did not translate to an improvement in cell distribution (**Figure 6A &B**). Similarly, no differences in proliferation or viability were observed (**Figure 6C & D**). Coating with fibronectin and gelatin demonstrated no changes from uncoated CorMatrix. Overall, coating showed no improvement in the cell distribution, and therefore uncoated CorMatrix was used for generation of NG2 UCP seeded grafts.

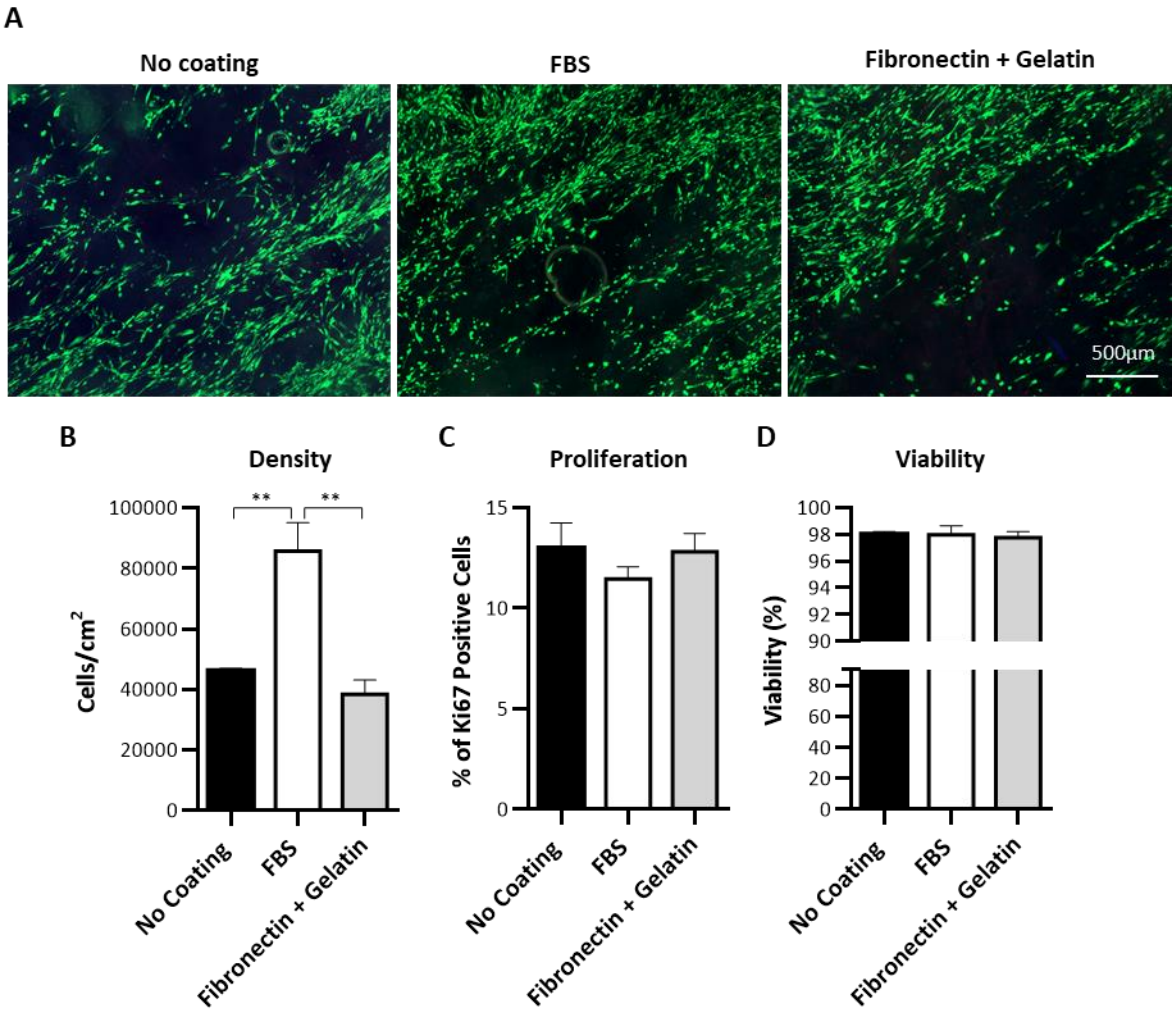

Figure 6.3: Analysis of scaffold coating. (A) Representative images of cell distribution under different scaffold coating conditions. Cytoplasmic green fluorescence = live (Calcein AM) cells, Nuclear red fluorescence = dead (ethidium homodimer-1) cells. Scale bar = 500µm. (B) Cell density after 5 days static conditioning under different scaffold coating conditions. (C) Cell proliferation after 5 days static conditioning under different scaffold coating conditions. (D) Cell viability after 5 days static conditioning under different scaffold coating conditions. Data represents means (± S.E.M), n = 3. ** $p<0.01$ as determined by one-way ANOVA followed by Tukey's post-hoc test.

6.3.3. Generation and Analysis of NG2 UCP Engineered Grafts

To assess the feasibility of using NG2 UCPs to create a biological graft, cells were seeded on an uncoated 40 x 30mm section of CorMatrix scaffold at a density of 20,000 cells/cm^2 (Methods 2.20.2). The graft was then left in static conditions for 5 days and either analysed immediately or shaped into a conduit and conditioned for a further 7 days in a bioreactor. The bioreactor provides biomechanical cues to facilitate tissue maturation by imitating the physiological environment. This is achieved using a peristaltic pump, which produces a pulsating fluid flow. Static culture was used before dynamic conditioning to ensure sufficient cell attachment and proliferation was achieved so that cells did not detach under flow.

Calcein AM-ethidium homodimer-1 viability staining demonstrated successful attachment of cells to the CorMatrix scaffold (**Figure 6.4A**). In fact, distribution appeared more uniform than in previous optimization experiments. After 7 days dynamic conditioning, the cells appeared more confluent and aligned in a uniform direction, perpendicular with the flow (**Figure 6.4B**). The dynamic conditioning was performed using a bioreactor that provided biomechanical cues, such as shear stress, using a media flow of 24mL/min to stimulate the graft and cell development. Further details of this process can be found in section 1.3.2 and section 2.20. The average cell density increased 2-fold after a 7-day dynamic conditioning, however, the variation between donor cell lines meant this change was not significant (**Figure 6.4C**). Similarly, there was a modest non-significant reduction in the number of Ki67 positive cells after dynamic conditioning (**Figure 6.4D**). Although cell viability remained >75% throughout static and dynamic, there was a significant reduction after dynamic conditioning ($p = 0.0293$; **Figure 6.4E**). Although the majority of the scaffold surface displayed uniform cell distribution, areas that had been gripped with forceps displayed sparse coverage (**Figure 6.4F**). The grafts had to be gripped using forceps to enable the stitching of planar scaffolds into conduits, and therefore this could not be negated.

Immunohistochemical analysis of the grafts demonstrated the development of a multi-cell layer on top of the CorMatrix, with cells retaining expression of the pericyte associated markers NG2 and vimentin (**Figure 6.5**). αSMA expression was evaluated to see if engrafted cells demonstrated changes in phenotype towards a more contractile state due to the scaffold environment and biomechanical signals provided by the bioreactor; however, no expression was observed. As expected, the control unseeded grafts had no cells nor NG2, Vimentin or αSMA expression.

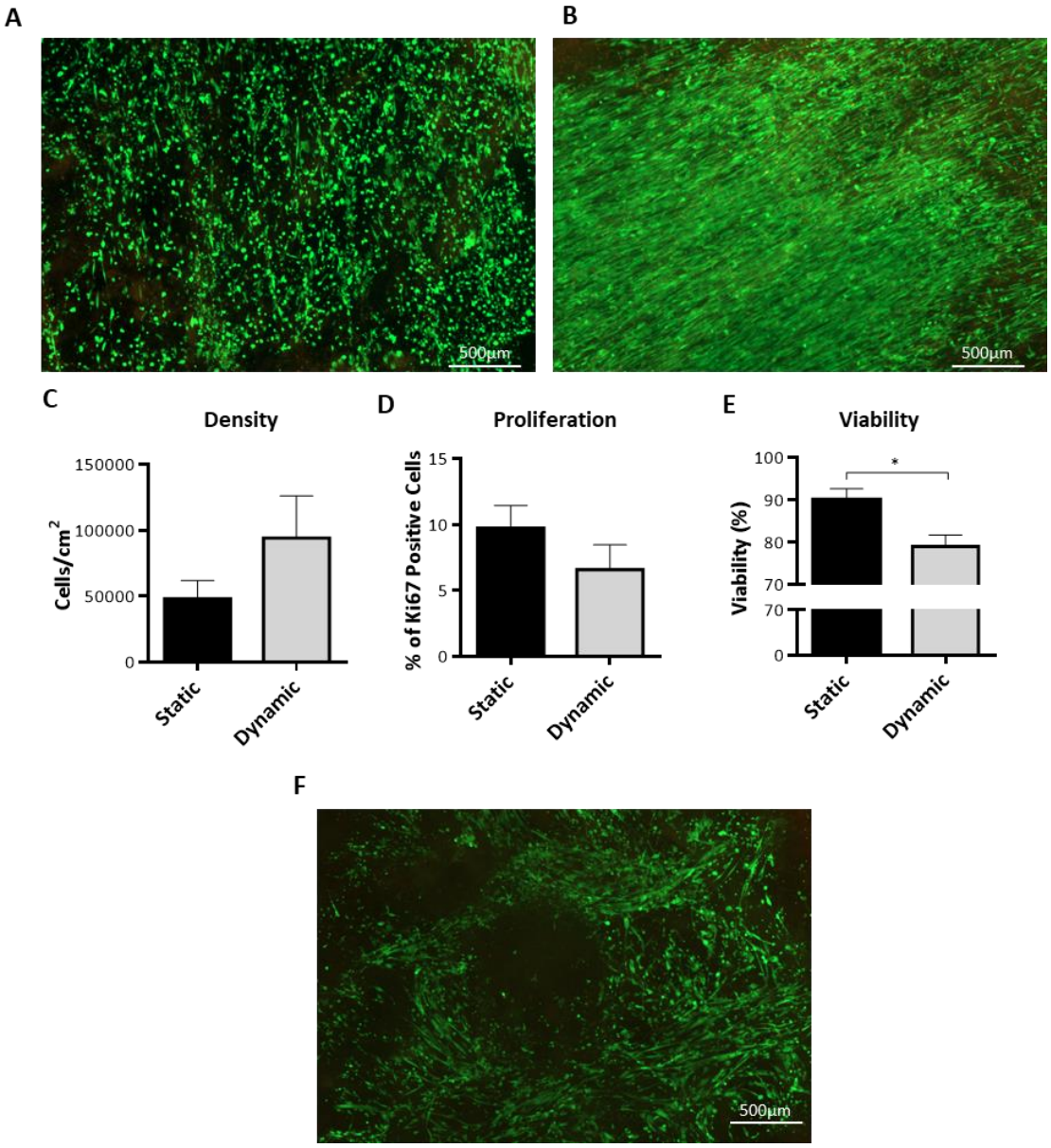

Figure 6.4: Analysis of cell engraftment on CorMatrix graft. (A-B) Representative images of cell distribution and viability after conditioning on CorMatrix scaffold. (A) static conditioning. (B) dynamic conditioning. Cytoplasmic green fluorescence = live (Calcein AM) cells, Nuclear red fluorescence = dead (ethidium homodimer-1) cells. (C) Cell density. (D) Cell proliferation. (E) Cell viability. (F) Image demonstrating areas of sparse cell coverage where the matrix was gripped. Static = 5 days static conditioning, dynamic = 5 days static plus 7 days dynamic conditioning. Data represent means (± S.E.M), n = 4. * $p<0.05$ as determined by Student's t-test. Scale bar = 500µm.

H&E staining further illustrated the development of a cellular layer in the UCP-seeded grafts, which appeared to mature and thicken after dynamic conditioning (**Figure 6.6**). Although no new elastin fibres were detected, collagen deposits were identified within the cellular layer after dynamic conditioning, as highlighted by the light blue stain. This corroborated previous data from chapter 5, demonstrating NG2 UCPs can remodel the ECM through secretion of extracellular proteins.

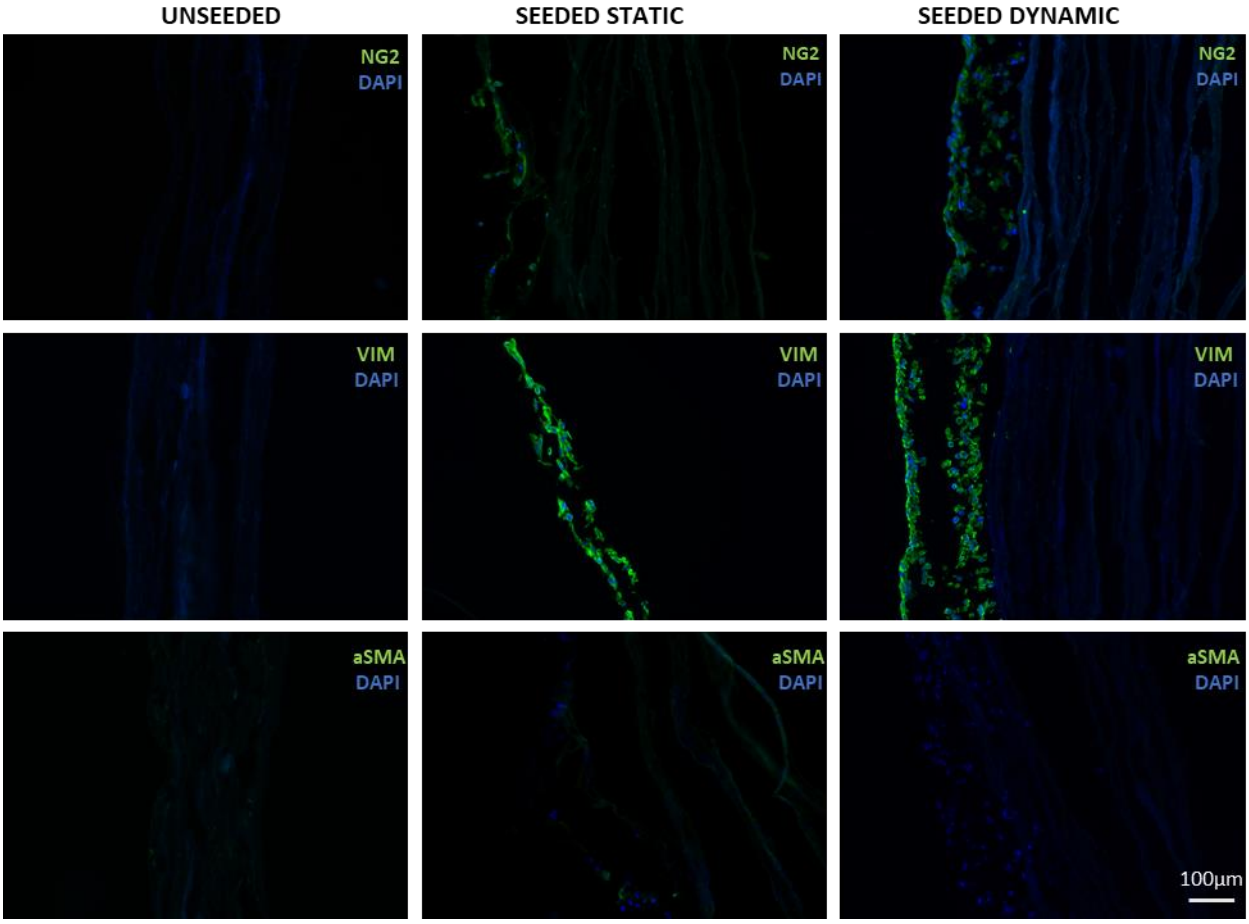

Figure 6.5: Representative immunohistochemical images demonstrating NG2 UCP presence in graft. DAPI = blue fluorescence. Neuron-glial antigen 2 (NG2), vimentin (VIM), alphas smooth muscle actin (αSMA) = green fluorescence. Scale bar = 100µm.

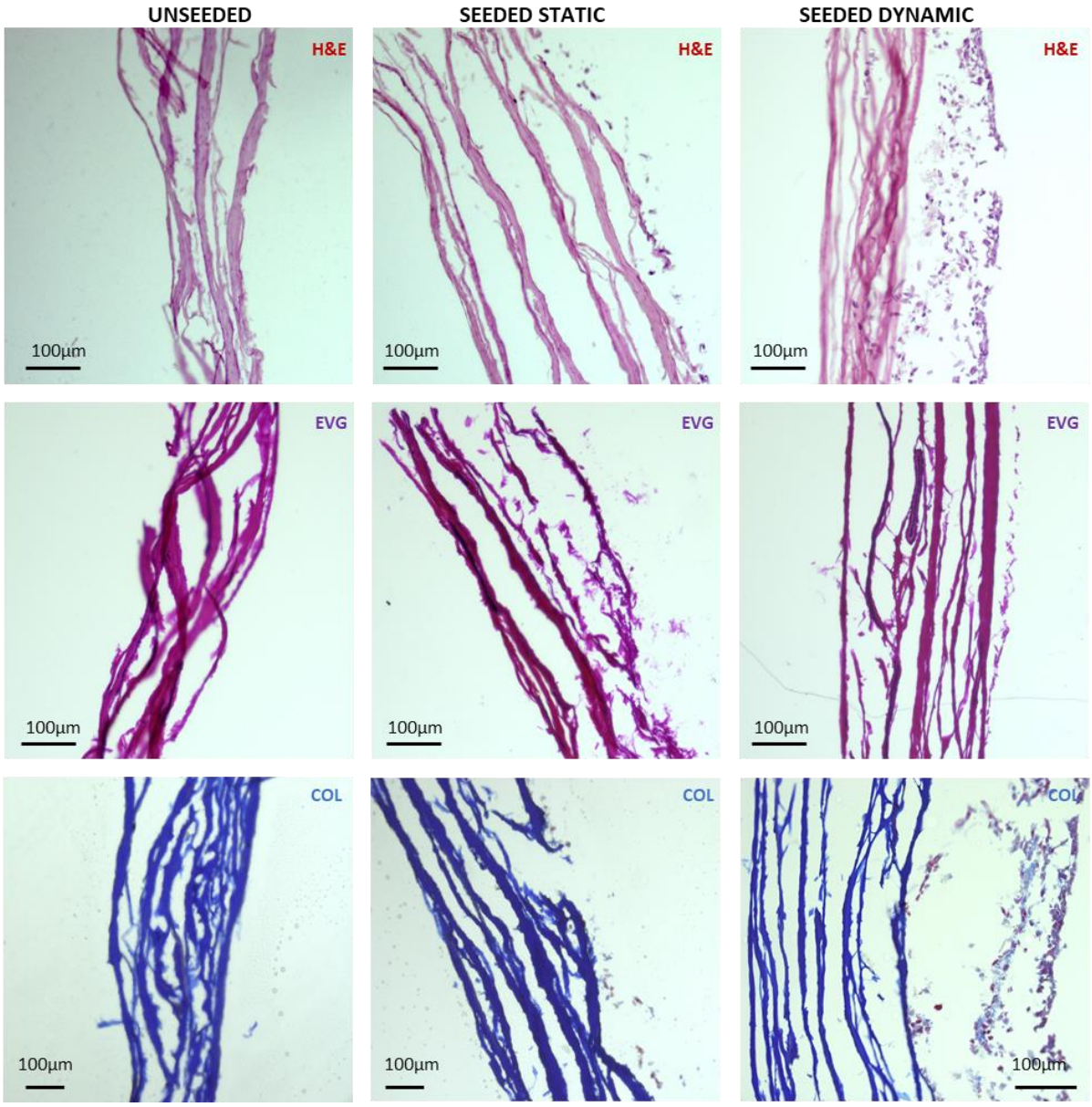

Figure 6.6: Representative images of haematoxylin and eosin staining (H&E), elastin van Gieson staining (EVG) and Mallory's trichrome collagen staining (COL) of NG2 UCP seeded CorMatrix grafts. Scale bar = 100µm.

An Instron tensile machine was used to investigate if NG2 UCPs could modify the mechanical properties of CorMatrix. Unseeded and seeded CorMatrix grafts were stretched until rupture, as detailed in Methods 2.20.5. The setup of the stretched graft is demonstrated in **Figure 6.7 A**. Additionally, both static conditioned planar scaffolds and dynamically conditioned conduits were analysed to validate the necessity of bioreactor conditioning process. For mechanical

analysis of conduits, circumferentially cut strips were stretched lengthwise. Under physiological conditions the pressure of pulsatile blood flow causes blood vessels to expand due to their compliance. Consequently, this method of analysis was performed to understand the circumferential mechanical properties and compliance of the graft, rather than stretching conduit lengthwise, which would not elucidate this information. Ideally a burst pressure test would be used to quantify the pressure required to rupture the engineered conduit; however, this equipment was not available in the lab.

Importantly, a significant reduction in the Young's Modulus of UCP-seeded grafts in comparison to the unseeded control was detected (two-way ANOVA, $p = 0.0008$) (**Figure 6.7B**). Young's Modulus is a measure of stiffness and a reduction in this value means the material has become more elastic. The difference in elasticity observed after static conditioning (static seeded 15.7 ± 1.5 MPa vs static unseeded 21.4 ± 2.2 MPa) was amplified by dynamic conditioning (dynamic seeded 11.5 ± 0.6 MPa vs dynamic unseeded 19.3 ± 1.4 MPa). Generally, dynamic conditioning appeared to reduce stiffness of both seeded and unseeded scaffolds, although this was not quite statistically significant (two-way ANOVA, $p = 0.0516$). The ultimate tensile strength was not affected by cell seeding or conditioning, which is an important result as it means the MMPs produced by the cells have not compromised the structural integrity of the graft (**Figure 6.7C**). In concurrence with elasticity measurements, there was a significant increase in rupture strain in seeded grafts (two-way ANOVA, $p = 0.0396$), which was particularly evident after dynamic conditioning (dynamic unseeded 35.7 ± 3.3% vs dynamic seeded 59.5 ± 6.8%; **Figure 6.7D**). The rupture strain is a measure of the maximum increase in length before the graft rupture, and therefore an increase in this is indicative of improved compliance. The thickness of the scaffold was initially measured just for calculation of mechanical properties; however, the data was also interesting as it demonstrated the thickening of cellularised conduits (two-way ANOVA, $p < 0.0001$), which was significantly enhanced by dynamic conditioning (two-way ANOVA, $p = 0.0039$). After 5 days static conditioning, cellularised CorMatrix was on average 70µm thicker than acellular grafts (**Figure 6.7E**). After a further 7 days dynamic conditioning, the cellularised graft thickness increased significantly (470 ± 8µm dynamic vs 406 ± 10µm static), with the average thickness 135µm greater than acellular grafts. These results corroborated previous data from H&E staining, which demonstrated the development of a <100µm cellular layer after static

conditioning that increased to 100-200μm thick after dynamic conditioning (**Figure 6.6**). As expected, there was no change in acellular graft thickness during conditioning.

Analysis of CM collected after static and dynamic conditioning identified presence of soluble collagen, which was not detected in unseeded grafts (two-way ANOVA, $p = 0.0457$; **Figure 6.7F**). This demonstrates that NG2 UCPs significantly alter the extracellular environment by producing collagen, which is a major structural component of vascular tissue.

Altogether, these results highlight the ability of UCPs to engraft and proliferate within the CorMatrix scaffold, changing the ECM protein content toward an elastic phenotype.

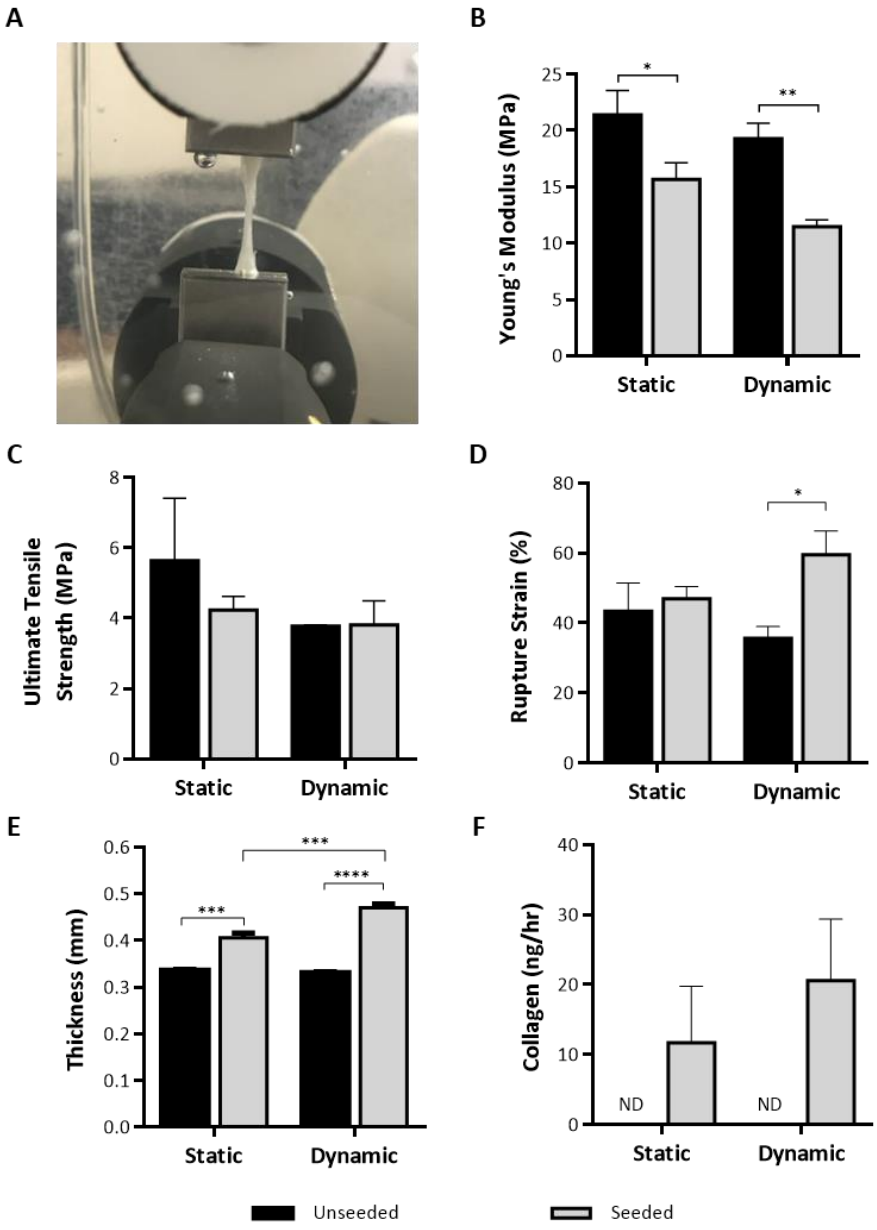

Figure 6.7: Analysis of NG2 UCP engineered graft properties. (A) Mechanical stretching of engineered graft. (B) Quantification of Young's Modulus. (C) Quantification of ultimate tensile strength. (D) Quantification of rupture strain. (E) Quantification of graft thickness. (F) Quantification of Pro-Collagen 1 a1 in CM. ND = not detectable. Static = 5 days static conditioning, dynamic = 5 days static plus 7 days dynamic conditioning. Data represent means (± S.E.M). Unseeded n = 3, and seeded n = 4. * $p<0.05$, ** $p<0.01$, *** $p<0.001$ and *** $p<0.0001$ as determined by two-way ANOVA followed by Tukey's or Sidak's post hoc test.

6.3.4. Feasibility of Cryopreserving Ready-made Grafts

To confirm if NG2 UCP functionalised grafts could be stored before surgery, cellularised CorMatrix samples were cryopreserved and cell response assessed upon thawing. After 5 days static conditioning, samples were either directly analysed or submerged in FBS + 10% DMSO, placed in a CoolCell freezing container at -80ºC for 24 hours, which ensures a consistent -1 ºC/min cooling rate, and transferred to liquid nitrogen for long-term storage. Following 7 days cryopreservation, seeded scaffolds were thawed and washed in medium before culturing for a further 5 days and analysing. Cell coverage was significantly reduced after cryopreservation; however, the density still remained at 20,000 cells/cm^2 (**Figure 6.8A**). Importantly, freezing had no obvious effect on the number of proliferative cells. A significant drop in cell viability was observed after freezing, which was expected due to the toxicity of DMSO and stress of cryopreservation; however, 80% of the cells were still viable (**Figure 6.8C**). Overall, these data indicated that despite signs of stress, cryopreservation of pre-seeded grafts is feasible.

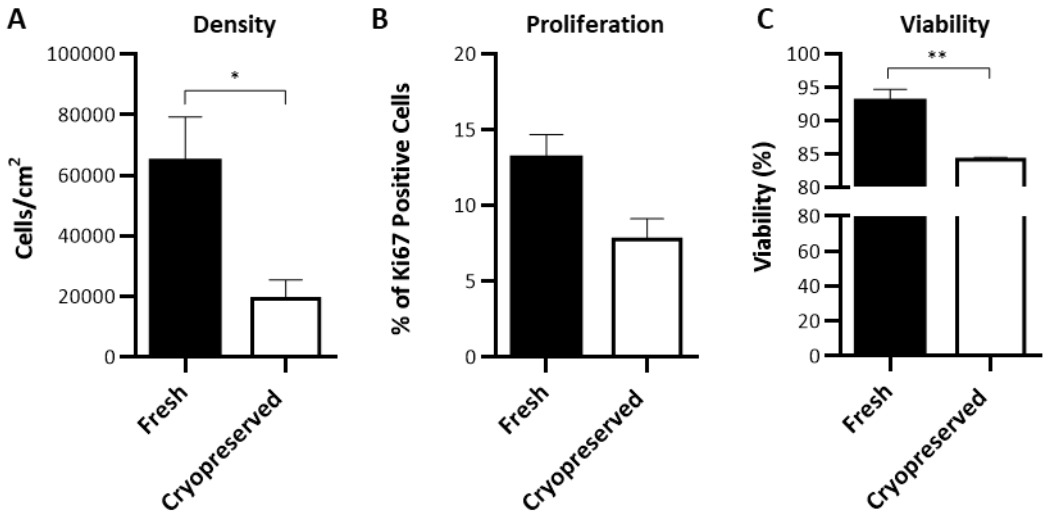

Figure 6.8: Analysis of graft robustness to cryopreservation. (A) Cell density pre- and post-cryopreservation. (B) Cell proliferation pre- and post-cryopreservation. (C) Cell viability pre- and post-cryopreservation. Data represent means (± S.E.M), n = 3. * $p<0.05$ and ** $p<0.01$ as determined by Student's t-test.

6.4. Discussion

In the previous chapters, NG2 UCPs were characterised to assess their applicability for neonatal vascular tissue engineering. Efficient isolation and expansion of phenotypically pure pericytes from discarded umbilical cord tissue was achieved. Functional characterisation demonstrated that NG2 UCPs possess angiogenic and endothelium supporting properties, along with the capacity to differentiate into VSMCs. Furthermore, *in vitro* analysis suggests that NG2 UCPs can remodel the extracellular environment and resist pathological processes such as calcification. Together, these data suggested that NG2 UCPs possess ideal properties for tissue engineering of vascular grafts that could address the limitations of current prostheses used for reconstruction of cardiac defects such as ToF; however, the feasibility of using these cells for functionalisation of acellular scaffolds had not been demonstrated. Here, through utilisation of tissue engineering principles and methods we have established in vitro proof of concept for NG2 UCP tissue engineered vascular grafts as a viable option for CHD repair.

The first step in development of the tissue engineered vascular graft was selection of a suitable scaffold that met the requirements set out in the introduction, namely adequate biocompatibility and mechanical properties. Fabrication of a custom-made scaffold is a very complex and time intensive process, which was outside the scope of this project, and therefore it was decided to use a well characterised material that possessed the desired properties. CorMatrix was identified as a suitable candidate for scaffold choice. CorMatrix comprises of decellularized porcine small intestinal submucosa, a 3D bioactive structure that supports host cell ingrowth, proliferation and differentiation, along with adequate biodegradability, mechanical and immunogenicity properties (Badylak et al., 2009; Mosala et al., 2016). The properties of CorMatrix have been extensively characterised and it has been used in more than one million patients, many of which involve cardiovascular surgery (Mosala et al., 2016). Indeed, in the last 10 years clinical studies have explored the feasibility of using CorMatrix for reconstruction of CHD (Quarti et al., 2011; Witt et al., 2013). Encouraging results were reported with no signs of calcification; however, the studies were limited by a small group size and short mean follow up time, and some inflammatory events have been observed (Mosala et al., 2016). Furthermore, evidence of growth and remodelling has not been substantiated (Woo et al., 2016). In fact, a recent study explored the remodelling capacity of CorMatrix through implantation of a valved conduit into the thoracic aorta of adult pigs (Nezhad et al., 2017). The authors demonstrated

that after 6 months, the graft had failed to remodel in an anatomical fashion, and signs of calcification were present.

Although acellular CorMatrix appears to possess limitations, functionalisation with cells may address these shortcomings by conferring the scaffold with anti-calcific properties and the ability to remodel. For example, as previously mentioned, CorMatrix lacks an elastin component, which is important for the functionality of vascular tissue. Cells that produce elastin may be able to overcome this disadvantage by remodelling the matrix with newly synthesised elastin. Indeed, data from the previous chapter has demonstrated that NG2 UCPs possess some calcification resistance and cam modify the ECM. Moreover, the feasibility of CorMatrix functionalisation using pericytes has been validated in previous *in vitro* and preclinical studies, indicating potential compatibility of NG2 UCPs and CorMatrix for vascular tissue engineering (Alvino et al., 2020; Avolio, Rodriguez-Arabaolaza, et al., 2015). Overall, as the properties of CorMatrix and behaviour of pericytes on this scaffold are well characterised, in addition to the fact that CorMatrix has been widely used for cardiovascular surgery, the decision was taken to use this material for graft production experiments.

Following the selection of a suitable scaffold, seeding conditions needed to be optimised and cell behaviour studied to confirm the compatibility of NG2 UCPs and CorMatrix. The physical properties of the scaffold, such as stiffness and topography, can influence cell viability and processes such as migration, differentiation, adhesion and proliferation (Levy-Mishali et al., 2009; Whang et al., 2016; Xing et al., 2019). For example, stiff materials such as tissue culture plastic are known to unnaturally increase cell proliferation and adhesion (Wells, 2008). In fact, tissue culture plastic is five times stiffer than CorMatrix (~100MPa vs ~20MPa), which could significantly modify cell behaviour (Alvino et al., 2020; Skardal et al., 2013). Consequently, it was important to confirm NG2 UCPs were still capable of attaching to CorMatrix and proliferating within the scaffold material whilst maintaining sufficient viability.

Previous studies had demonstrated the feasibility of seeding CorMatrix with pericytes using static seeding, and therefore this methodology was utilised for NG2 UCP seeding (Alvino et al., 2020; Avolio, Rodriguez-Arabaolaza, et al., 2015). In concurrence with these studies, after static seeding, NG2 UCPs demonstrated efficient attachment to the scaffold and maintained a high viability. NG2 UCPs cultured on CorMatrix did not reach the confluency of tissue plastic

cultured cells, which may be due to the induction in cell proliferation caused by stiffer materials such as tissue culture plastic (Wells, 2008; Xing et al., 2019).

Qualitative analysis of cell viability suggested most cells were viable after culture on CorMatrix, with no obvious differences between plastic and scaffold culture. Further analysis of cytotoxicity was completed by measuring LDH release. LDH is a cytosolic enzyme which is released into cell culture medium when the plasma membrane of a cell is damaged, and can therefore give an indication of cell stress (Kumar et al., 2018). In contrast with qualitative data, LDH levels in scaffold cultured cells were considerably higher than plastic cultured. A slight increase in LDH was expected due to the additional stress to cells caused by a change in culture conditions; however, the fold change in LDH release was surprisingly high. This result may be explained by the difference in substrate stiffness between tissue culture plastic and CorMatrix which is known to influence viability (Wells, 2008). For example, Levy-Mishali et al showed that decreasing the stiffness of poly(L-lactide)/polylactic-co-glycolic acid scaffolds resulted in a reduction in viability of cultured skeletal myoblasts (Levy-Mishali et al., 2009). However, if this was the case, there should have been more widespread staining of ethidium homodimer-1. Whilst there certainly appears to be a change in LDH after seeding cells on the scaffold, this difference may be accentuated by normalisation. LDH levels were normalised by the number of the cells seeded on the scaffold, which was calculated by counting average number of cells per field of a view and scaling this number according to scaffold seeding area. This meant that any floating cells or cells that attached to the underside of the scaffold or culture plastic underneath were not included in normalisation but would have contributed to LDH levels in the media. So that only the viability of scaffold seeded cells was considered, subsequent viability analysis was quantified by counting calcein AM and ethidium homodimer-1 positive cells instead of using the LDH assay.

For optimisation of seeding conditions, NG2 UCPs were seeded at three different densities. Avolio et al and Alvino et al previously demonstrated that 20,000 - 30,000 cardiac pericytes per cm^2 produced a homogenous cell layer on CorMatrix substrate, and therefore similar seeding densities were initially explored (Alvino et al., 2020; Avolio, Rodriguez-Arabaolaza, et al., 2015). Analysis revealed that 20,000 pericytes/cm^2 was sufficient to produce adequate scaffold coverage; however, increasing the density beyond this did not further improve confluency. Despite optimising seeding density, cellular distribution remained uneven, with some areas of CorMatrix highly populated and others with very few cells engrafted, which was

not seen in previous studies (Alvino et al., 2020; Avolio, Rodriguez-Arabaolaza, et al., 2015). To improve cell attachment, scaffolds were coated. Specifically, a fibronectin and collagen coating and FBS coating were used due to their ability to promote cellular adhesion and previous application in scaffold seeding (Hayman et al., 1985; Villalona et al., 2010). Scaffold coating did not affect cell coverage. Although coating the CorMatrix with FBS increased the average cell density, sparsely populated areas remained. It was thought that the uneven cell distribution might be due to two factors. Firstly, to limit the use of CorMatrix, which is an expensive material, optimisation experiments were scaled down to 96-well plate size scaffold sections, which did not provide enough space for a suspended crown set up of the CorMatrix. Instead, the matrix was positioned on the bottom of the well, which resulted in migration of cells from the scaffold to the plastic culture, where they have been shown to proliferate more. Secondly, the intrinsic properties of the scaffold, namely irregular topography, may influence cell behaviour. For example, ridges were detected in the scaffold that could affect cell migration. In hindsight, a higher seeding density may have addressed the irregular cell coverage. Despite data, and previous studies from our group, demonstrating that 20,000 cells/cm^2 was sufficient, other tissue engineering studies using CorMatrix as a scaffold required up to 250,000 cells/cm^2 to achieve adequate cell engraftment (Albertario et al., 2019; Alvino et al., 2020; Avolio, Rodriguez-Arabaolaza, et al., 2015; Ghorbel et al., 2019; Iacobazzi et al., 2020; Teebken et al., 2000). Of course, using a larger number of cells increases the time needed for cell expansion before graft production, which may not be appropriate depending on patient needs.

Following optimisation experiments, the feasibility of engineering clinical size NG2 UCP functionalised CorMatrix grafts was assessed. Using crowns to fix the CorMatrix suspended in medium resulted in an improved, largely homogenous, cell distribution; however, areas that had been gripped with forceps were sparsely populated and had an increased number of apoptotic cells. Furthermore, a drop in viability was observed after conduit stitching and dynamic conditioning, which indicated improvement in physical manipulation of the scaffold is warranted to maintain cell viability from static to dynamic conditions.

Interestingly, after stimulation under flow conditions, NG2 UCPs demonstrated organization perpendicular to the direction of flow. Although NG2 UCPs were seeded on the abluminal layer of the graft, and therefore not directly exposed to the flow, it is likely that the cells reacted to the cyclic strain induced by the pulsatile flow provided by the peristaltic pump. Indeed, flow-

induced cell alignment is well documented in cells of the vascular wall (A. A. Lee et al., 2002; Schrimpf et al., 2017). *In vivo*, VSMCs align circumferentially to provide blood vessels with mechanical integrity and compliance; however, this organisation is often not seen in engineered tissues (Agrawal et al., 2015; Bacakova, Travnickova, Filova, Matějka, et al., 2018). Furthermore, Agrawal et al suggested that development of vascular grafts exhibiting circumferential VSMC alignment could improve mechanical properties and overcome limitations with the compliance mismatch between engineered and native vessels (Agrawal et al., 2015). Consequently, the alignment of NG2 UCPs after dynamic conditioning may have important implications for functional development of the graft and demonstrated the importance of using bioreactors to provide biomechanical cues.

Immunohistochemical staining was used to confirm engraftment of cells and assess if the scaffold environment and dynamic conditioning affected cell phenotype. Indeed, previous studies have demonstrated that cyclic strain alone can induce spontaneous differentiation of bone marrow MSCs towards a contractile state, as evidenced by acquisition of αSMA expression (Dan et al., 2015). Analysis demonstrated that NG2 UCPs retained their original phenotype. The absence of αSMA indicates that additional stimuli and/or prolonged exposure to flow are required to encourage development of a smooth muscle layer. It was also revealed that the cells form a layer on the external surface of the CorMatrix scaffold rather than infiltrate into the matrix. Past studies using CorMatrix functionalised with WJ-MSCs or cardiac pericytes reported similar engraftment, indicating this was most likely due to the matrix architecture (Alvino et al., 2020; Iacobazzi et al., 2020). Whilst this lack of infiltration initially looked concerning, it is not necessarily a poor outcome. The purpose of cellularising the exterior surface of the CorMatrix conduit was to create an adventitial cellular layer capable of recruiting native vascular cells and repopulating the acellular scaffold through the therapeutic properties of NG2 UCPs.

Despite tissue culture plastic studies demonstrating that NG2 UCPs secrete significant amounts of elastin, no new elastin fibres were detected in the NG2 UCP seeded CorMatrix. Elastic fibres play an essential role in vascular wall mechanics such as vessel compliance (Kielty et al., 2007). Indeed, the lack of elastin synthesis has been suggested as a significant limitation to functionality of engineered grafts, and therefore this was a disappointing result (Patel et al., 2006). Moreover, acellular CorMatrix contains no elastin fibres and is made up of 90% collagen, whilst native vascular tissues contains up to 50% elastin, highlighting the need for

modification of protein composition (Badylak et al., 2009; Xu et al., 2014). The lack of elastic fibre production could be attributed to the composition of the CorMatrix scaffold. Previous studies have suggested that collagen based-scaffolds are unfavourable for elastin biosynthesis (Patel et al., 2006). In fact, this may explain why elastin was detected in plastic cultured NG2 UCPs but not scaffold cultured NG2 UCPs. Alternatively, the 12 days of culture may not have been sufficient for development of the elastic fibre complexes, which are important to confer the scaffold with elastic properties similar to native arterial tissue. Indeed, previous studies of cellularised CorMatrix grafts did not show conclusive elastic fibre deposition after in vitro conditioning; however, histological analysis following in vivo implantation demonstrated significant elastic fibre presence in comparison with acellular grafts (Alvino et al., 2020; Ghorbel et al., 2019; Iacobazzi et al., 2020).

Although no elastin fibres were found, evidence of scaffold remodelling was detected through the presence of soluble collagen (alpha-1 type I collagen) in the CM. Alpha-1 type I collagen is a major component of collagen type 1, and therefore its presence may indicate that the cells are actively remodelling the collagen in the CorMatrix scaffold through MMP mediated degradation (Henriksen et al., 2016). Furthermore, progressive collagen deposition on the cellularised side of the CorMatrix was detected along with an increased graft thickness. This was particularly evident after dynamic conditioning and coincided with the development of a multi-layered cellular distribution. In future studies, it would be interesting to know if the accumulation of collagen and formation of a multi-layered cell structure was induced through dynamic condition or if it was simply due to prolonged cell culture. Nevertheless, evidence of some remodelling is an important result as it may indicate a functional change and/or an ability to grow.

In accordance with visible remodelling of the extracellular environment, a considerable change in the mechanical properties of NG2 UCP functionalised CorMatrix grafts was detected. Although the cellularised graft still remained stiffer than native arterial tissue, the reduction in Young's modulus demonstrated a significant increase in elasticity from the acellular graft (Akhtar et al., 2011). It is interesting to note that NG2 UCP engineered CorMatrix grafts demonstrate enhanced elastic properties in comparison to CorMatrix grafts functionalized with cardiac pericytes, thymus MSCs, WJ-MSC, or MSC-derived VSMC before implantation (Alvino et al., 2020; Iacobazzi et al., 2020). Despite using similar conditioning times, the cellularised grafts did not show any improvement in Young's Modulus in comparison to

acellular grafts. It may be that the improved elastic behaviour is a result of superior NG2 UCP ECM remodelling properties. Indeed, in the previous chapter NG2 UCPs were shown to secrete more ECM proteins and induce higher collagenase activity than WJ-MSCs. Furthermore, MMP-1 presence, which may indicate remodelling, was detected in NG2 UCP grafts but not in previous studies using thymus MSCs or MSC-derived VSMCs (Albertario et al., 2019; Ghorbel et al., 2019).To validate this theory, in vitro characterisation of ECM remodelling properties is needed. Nonetheless, this decrease in Young's Modulus observed in NG2 UCP cellularised grafts represents an important change in elasticity more in line with native vessels, which is essential for normal function in a pulsatile circulatory system (Wagenseil et al., 2009).

Rupture strain of the graft was estimated by measuring the maximum elongation before breaking. As the graft was mechanically stretched circumferentially, this property is indicative of the maximum expansion/compliance of the conduit, which is essential for normal arterial function (Thenappan et al., 2016). In fact, the lack of vascular compliance in patients with pulmonary arterial hypertension is associated with increased risk of mortality, highlighting the importance of this property (Mahapatra et al., 2006). In accordance with changes in elasticity, NG2 UCP cellularised CorMatrix demonstrated a significant increase in rupture strain compared with acellular CorMatrix, although this was only observed after dynamic conditioning indicating the importance of this step. Similarly, this represented an improvement over cardiac pericyte cellularised CorMatrix grafts that had been dynamically conditioned for an equal amount of time (Alvino et al., 2020). It is worth noting that this is an estimate of rupture strain at the end of plastic deformation of the graft. Although this is definitely a useful measure of how much strain the graft can withstand before complete failure, it may not accurately represent the maximum strain before the conduit becomes dysfunctional. Indeed, blood vessels rely on elastic recoil to function, and therefore for future experiments it may also be beneficial to measure the strain at the end of the elastic deformation of the graft, which could indicate the maximum strain at which the graft can still return to its original dimensions and remain functional. Alternatively, an in vitro system capable of measuring burst pressure may be useful to provide a more in-depth analysis of the graft functionality. Although a change in rupture strain and elasticity was observed, the ultimate tensile strength remained the same, demonstrating that remodelling did not notably weaken the graft.

In addition to improvements in mechanical properties, cryopreservation studies demonstrated the feasibility of storing ready-made NG2 UCP engineered grafts. This could have important

implications for surgical intervention. As discussed in chapter 1, the optimum time for surgical correction of ToF can vary between 90 days and 11 months (Pigula et al., 1999; Van Arsdell et al., 2000). The robustness of NG2 UCP cellularised grafts to cryopreservation means that they can be manufactured soon after birth and stored until they required for surgery, which is dependent on patient needs.

Overall, these data demonstrate the feasibility of functionalising CorMatrix grafts with NG2 UCPs. NG2 UCPs promote moderate remodelling of the CorMatrix scaffold and significantly improve the mechanical performance of acellular CorMatrix, which is an FDA-approved material already widely used in cardiovascular reconstructive surgery of paediatric and adult patients.

7. General Discussion

7.1. Summary Discussion

In ToF, the most prevalent form of complex CHD, surgical intervention in the first year of life is usually required for repair of the defect (van der Ven et al., 2019). Repair is completed by patching the VSD and reconstructing the RVOT so that sufficient blow flow to the lungs is restored. Whilst closing the VSD is now relatively routine in congenital heart surgery, reconstruction of the RVOT is a more complex process, especially in patients with considerable pulmonary annular hypoplasia or atresia. These patients often require a pulmonary conduit or valved conduit to remove the obstruction (Downing et al., 2015). Current options for the conduits frequently fail due to adverse remodelling, for example calcification or thrombotic events, and/or lack of growth potential, which results in degeneration of the graft and the need for replacement (Kalfa et al., 2013; Sugiura et al., 2018). In fact, reoperation rate can be as high as 50%, with many patients requiring multiple surgical corrections, which severely impact quality of life (Berdat et al., 2004; van der Ven et al., 2019).

Tissue engineered vascular grafts may have the potential to overcome the limitations of current protheses used for reconstruction of cardiac defects by creating biological 'living' grafts, which can provide greater functionality and resistance to degenerative processes (Avolio, Caputo, et al., 2015; Mirensky et al., 2008). Indeed, previous work has provided a rationale for the use of human cardiac pericytes from the neonatal heart to engineer clinically available prosthetic grafts (Alvino et al., 2020; Avolio, Rodriguez-Arabaolaza, et al., 2015). However, isolation of this promising cell population is reliant upon tissue obtained during initial palliative surgery or an *ad hoc* invasive cardiac biopsy. In search of a more accessible source of pericytes, umbilical cord was explored, which is acknowledged to contain stromal cells and perivascular cells endowed with regenerative capacity. It was hypothesized that umbilical cord pericytes may possess the ideal properties for neonatal vascular tissue engineering applications. Pericytes are known to play a key role in vascular development, homeostasis and endothelium support through processes such as angiogenesis, differentiation and immunomodulation (Cathery et al., 2018). By isolating pericytes from an accessible tissue source such as the umbilical cord, it was thought these key properties could be harnessed to improve the functionality of tissue engineered vascular grafts used in paediatric surgery.

The umbilical cord reaches its final form by the 12th week of gestation, measuring approximately 50 – 60 cm long and consisting of a vein and two arteries embedded WJ, which is surrounded by an epithelial layer (Spurway et al., 2012). Previous studies have demonstrated this tissue contains MSCs which could be used for regenerative medicine; however, some evidence suggests that the therapeutic capacity of these cells is reduced by full term (Hong et al., 2013). Alternatively, this result may the product of the non-selective isolation method used for MSC purification, which may not be adequate to separate and expand the small number of progenitors contained within the bulk cell population of umbilical cord.

To enable generation of a reproducible purified pericyte population with progenitor activity, a cell specific isolation protocol was established. Initially, a methodology incorporating enzymatic digestion and CD31-/CD34+ MACs selection was used, which has previously been applied to purify adventitial pericytes from cardiac tissue and saphenous vein (Avolio, Rodriguez-Arabaolaza, et al., 2015; Campagnolo et al., 2010). A lack of successful isolations was attributed to evidence that the umbilical vessels, unlike other blood vessels of their size, lack a distinct vasa vasorum, which is the site CD31-/CD34+ pericytes were found in saphenous vein (Sexton et al., 1996). Subsequently, alternative isolation protocols were developed utilising different selection markers. These methods were performed in parallel to improve the chance of successful isolation, reducing delays to the project, but also allowing us to compare and contrast the protocols.

A novel isolation protocol was developed using explant outgrowth followed by NG2+/CD31- selection. Explant outgrowth was utilised to improve initial cell yield and negate the harmful effect of enzymatic digestion (Hendijani, 2017; Yoon et al., 2013), whilst NG2 selection was chosen due to its general association as a pericyte marker and evidence from Crisan et al., which indicates NG2 has a high specificity for pericytes in the umbilical artery (Crisan et al., 2012). In parallel, isolation of CD146+/CD31- pericytes was attempted using a protocol adapted from Tsang et al. (Tsang et al., 2013). Furthermore, the initial CD31-/CD34+ isolation protocol was utilised on placenta, which was obtained later in the study, to see if this population inhabited this particular tissue. Pericytes selected using these antigenic markers have previously shown enhanced regenerative potential, and therefore it would be interesting to

evaluate if these cells possessed advantageous properties in comparison to the other pericyte isolations (Alvino et al., 2018; R. Katare et al., 2011; R. G. Katare et al., 2013).

All isolation strategies were effective and histological analysis demonstrated their localisation in the tissue. An assessment of phenotype and in vitro growth confirmed that both populations of umbilical cord pericytes represented a consistent pure population which could be efficiently expanded in vitro; however, this was not the case for placenta pericytes. Whilst CD34 PLPs did possess some characteristics of pericytes previously isolated using the same protocol, namely the absence of CD146 expression (Avolio, Rodriguez-Arabaolaza, et al., 2015; Campagnolo et al., 2010), there was inconsistency in phenotype and irregular cell growth, which was indicative of a heterogenous cell source. Interestingly, all isolated cell lines expressed pluripotency markers NANOG, OCT4 and SOX2, which suggests a level of plasticity that was not seen in MSCs previously isolated from full term cord (Hong et al., 2013). This was in line with the suggestion that selective cell isolation is able to capture progenitor cells more efficiently, although more work on gene expression and differentiation potential is needed to confirm this.

To assess the ability of isolated pericytes to facilitate the development of vascular tissue, the VSMC differentiation capacity and angiogenic properties of the cells were explored. All pericytes demonstrated successful differentiation towards a contractile phenotype, with upregulation of VSMC associated markers such as calponin and transgelin; however, a mature phenotype, as seen in cardiac pericytes, was not achieved (Avolio, Rodriguez-Arabaolaza, et al., 2015). This result was not entirely unexpected as a mature VSMC phenotype is difficult to achieve in vitro (Ayoubi et al., 2017; Dan et al., 2015; Qiu et al., 2014). Nonetheless, this may indicate that cardiac pericytes possess a superior capacity for vascular differentiation, which is important to establish functional tissue layers.

One of the most difficult challenges for tissue engineering is development of vascularised tissue. Tissue thicker than 1mm often degenerates before perfusion of host vasculature due to inadequate supply of oxygen and nutrient to cells, so it is essential to promote angiogenesis in avascular engineered tissues (Chang et al., 2017). A prominent strategy for promoting this process relies on seeding engineered constructs with pro-angiogenic cells to encourage vessel sprouting (Mastrullo et al., 2020). To establish whether pericytes could be used for this purpose, the angiogenic properties were evaluated. All three pericyte types secreted an array

of growth factors important for the development and stability of vasculature, namely ANGPT-1, VEGF, HGF and MCP-1. In general, under normoxia the cells exhibited a secretome that indicated a stabilising nature, with high levels of ANGPT-1, a factor important for vessel stability, and low levels of potent angiogenesis stimulating factor VEGF (Gowdak et al., 2018). Under reduced oxygen levels, more representative of avascular tissue engineered constructs, the balance of these factors was altered as evidenced by a significant upregulation of VEGF and downregulation of ANGPT-1. In correlation with growth factor release, media collected from hypoxic conditioned cord pericytes induced significant endothelial tube formation in a co culture assay, which is a useful model indicative of angiogenic activity (Hetheridge et al., 2011), whereas under normoxic conditions only modest tube formation was observed. This balanced behaviour is important to ensure angiogenic activity is tightly regulated and only induced when necessary. Interestingly, CD34 PLPs did not significantly influence endothelial tube formation. This may be due to an imbalance in growth factor secretion, such as the extremely high release of HGF relative to other factors, or another unexplored growth factor.

Together, the data on isolation efficiency, VSMC differentiation and angiogenic activity indicated that NG2 UCPs were the most promising cell source for vascular tissue engineering, fulfilling our criteria of a readily available pure autologous cell source with angiogenic and vascular differentiation potential. Only marginal differences were detected between NG2 UCPs and CD146 UCPs, suggesting that these may have been similar umbilical cord pericyte populations that were just purified using different antigenic markers. Nevertheless, NG2 UCPs presented an interesting cell source for neonatal vascular tissue engineering, which possessed distinct advantages over other cell sources explored for similar applications, such as cardiac pericytes and MSCs. For example, although cardiac pericytes appear to have a higher degree of plasticity, they are inferior to NG2 UCPs with regards to paracrine endothelial influence, and also availability given they require surgical access to cardiac tissue (Avolio, Rodriguez-Arabaolaza, et al., 2015). Likewise, WJ-MSCs match NG2 UCPs for their availability and VSMC capacity but provide less endothelial influence, most likely due to an absence of VEGF secretion (Arutyunyan et al., 2016; Widowati et al., 2017). The enhanced promigratory and proangiogenic properties observed in NG2 UPCs are not only key for promoting vascularisation of the tissue, but may also be improve endothelialisation of engineered grafts and reduce thrombotic events by enhancing trans-anastomotic ingrowth and transmural capillarisation (Pennel et al., 2018; Zilla et al., 2020). Indeed, studies by Albertario et al and

Sugiura both concluded that cellularised grafts mainly regenerate tissue through paracrine activity as the seeded cells disappeared from the graft after implantation (Albertario et al., 2019; Sugiura et al., 2016). Nonetheless, without in vivo studies to corroborate the in vitro characterisation, these assertions cannot be validated.

Characterisation of NG2 UCPs ability to integrate and remodel the graft environment was achieved by quantifying production of extracellular proteins and enzymes. Whilst native arteries undergo dynamic composition alterations through regulation of ECM protein expression and metalloprotease mediated degradation, this functionality is lost in acellular constructs, leading to graft degeneration and growth limitation (Jacob et al., 2001; Z. Ma et al., 2020). It was shown that NG2 UCPs produce significant amounts of both elastin and collagen, which are the main components of the arterial wall and important for mechanical stability and physiological vessel function (Xu et al., 2014). The high elastin production relative to MSCs is particularly interesting given that a lack of elastin synthesis in engineered grafts is a major barrier to clinical success and acellular grafts such as CorMatrix are mainly composed of collagen (Mosala et al., 2016; Patel et al., 2006). This result may indicate that NG2 UCPs could reconstitute acellular grafts with new ECM composed of elastin, improving the mechanical properties such as elasticity. To balance the production of ECM components, NG2 UCPs produce an array of MMPs and TIMPs, including an abundance of extracellular MMP-1, which is used as a remodelling marker (Albertario et al., 2019; Ghorbel et al., 2019). These proteolytic enzymes and inhibitors enable the degradation of collagen based matrices and may even contribute to the angiogenic activity of NG2 UCPs through facilitating pericyte vessel detachment amongst other processes (Oxford et al., 2019; Rundhaug, 2005). It would be interesting to study the ECM composition and enzymatic activity in more detail, including the relative contribution of glycoproteins, types of collagen and specific MMPs to see how these compare with native arterial tissue; however, time constraints of the project have limited the analysis. Nevertheless, if the behaviour of NG2 UCPs observed in vitro is replicated in a graft environment then they may have the capacity to remodel the acellular graft and confer growth potential, which is a major limitation to current prostheses (Pashneh-Tala et al., 2015).

The behaviour of NG2 UCPs under hyperphosphatemia was explored to assess their resistance to calcification processes. Calcification is a common reason for graft failure and the risk is elevated in children with CHD (Avolio, Caputo, et al., 2015; Jover et al., 2018; Kalfa et al., 2013). Consequently, understanding the cellular response to an inductive environment may

give an indication of the cell's suitability for neonatal vascular tissue engineering. NG2 UCPs demonstrated a clear resistance to calcification relative to MSCs, highlighting them as an ideal cell type for graft development. It would be interesting to investigate in further studies whether these cells have the capacity to confer the graft with anti-calcific properties as observed when functionalising heart valves with adventitial pericytes (Jover et al., 2021).

The final objective of this project involved confirming the feasibility of using NG2 UCPs and CorMatrix scaffolds to create a biological graft with optimal properties. Analysis of cell distribution demonstrated a largely uniform engraftment on top of the scaffold, although some areas where the conduit had been gripped were sparsely populated and had an increased number of apoptotic cells. After exposing the cells to flow, representative of the in vivo environment, the cell layer became thicker and aligned perpendicular to the flow direction similar to native VSMCs (A. A. Lee et al., 2002), which could improve the mechanical performance of the graft (Agrawal et al., 2015).

Evidence of extracellular remodelling was observed through collagen deposits located on the cellularised surface of the scaffold and soluble collagen which was released into the media. Although elastin deposition was observed under plastic culture, no elastic fibres were detected through histological analysis of the graft. It was believed that this may be due to inadequate time for fibre development, as previous studies using a similar model failed to demonstrate elastic fibre presence in vitro, but following in vivo implantation observable fibres had formed (Alvino et al., 2020; Ghorbel et al., 2019; Iacobazzi et al., 2020). Despite this result, functionalisation of acellular CorMatrix grafts did improve the mechanical properties. Namely, the graft elasticity and rupture were significantly increased. This was an exciting result as these properties are essential for normal arterial function (Thenappan et al., 2016; Wagenseil et al., 2009). Furthermore, previous studies demonstrated relatively little difference between acellular and cellularised grafts characterised in vitro (Alvino et al., 2020; Iacobazzi et al., 2020). This may be a result of superior ECM remodelling capabilities, as it was already shown that NG2 UCPs secrete more elastin and MMP activity than WJ-MSCs; however, this behaviour remains to be explored in other sources of pericytes. Nevertheless, evidence of remodelling and a subsequent change in properties suggest these grafts may be able to adapt to the in vivo environment and resist degenerative processes that result in graft replacement.

Overall, these data indicate that NG2 UCPs are an exciting cell source for neonatal vascular tissue engineering with distinct advantages over alternative cell types, namely WJ-MSCs and cardiac pericytes, due to their ease of isolation, homogenous phenotype and therapeutic properties. NG2 UCP-engineered grafts appear superior to acellular CorMatrix grafts, which are already FDA-approved and routinely used in surgery, highlighting their applicability for cardiac reconstruction in malformations such as ToF. Furthermore, although the lack of in vivo work does not facilitate measurement of parameters such as graft growth and endothelialisation, and therefore limits comparison to the grafts with growth potential developed by Ghorbel et al and Syedain et al (Ghorbel et al., 2019; Syedain et al., 2016), the in vitro testing demonstrated that NG2 UCP functionalised CorMatrix grafts possessed remodelling capabilities and improved mechanical properties in comparison with alternative cell types developed using a similar model. If the improvements seen in vitro can be realised in vivo, then NG2 UCP engineered grafts may have the potential to address the limitations of current prostheses.

7.1. Limitations and Future Perspectives

The most significant limitation to this study was the absence of in vivo experiments. Despite the in vitro characterisation of cells demonstrating that cord pericytes, namely NG2 UCPs, possessed exciting therapeutic potential, the relevance of these results could not be confirmed through an animal model. For example, NG2 UCPs demonstrated an enhanced promigratory and angiogenic influence over ECs in plastic culture relative to other cell sources. These properties are integral for graft survival through promoting vascularisation and endothelialisation. Indeed, Ghorbel et al demonstrated enhanced luminal endothelium formation and adventitial capillarization in cellularised grafts, which they suggested was due to paracrine signalling (Ghorbel et al., 2019). The in vitro characterisation of NG2 UCPs indicates that they may positively influence these processes; however, without an in vivo model this cannot be substantiated. Likewise, the data collected on ECM production, MMP activity and calcification resistance is exciting, but further exploration is warranted to verify if this enables non-pathological graft remodelling. Future work should address this limitation by incorporating NG2 UCP-engineered CorMatrix grafts into a preclinical animal study

representative of ToF, such as the pulmonary artery implantation swine model previously employed (Alvino et al., 2020; Ghorbel et al., 2019). This would allow us to identify if the therapeutic properties of NG2 UCPs discovered in vitro translate to an improved graft in vivo, capable of addressing the limitations of the current surgical practice.

As highlighted in the discussion sections, the breadth of this study meant that some specific aspects could not be explored in the detail warranted. For example, the immunomodulation properties of pericytes were discussed in chapter one; however, this aspect was not explored through in vitro characterisation. Further work using flow cytometry could confirm whether NG2 UCPs express a similar immunogenic profile to the placental pericytes studied by Maier et al, which demonstrated low basal expression of HLA-DR and T-cell stimulatory molecules CD80 and CD86, in combination with high levels of inhibitory molecules such as PD-1 ligand (Maier et al., 2011). A simple T-cell proliferation assay could also be incorporated to validate any immune response regulation. Furthermore, whilst autologous cell sources are assumed to be poorly immunogenic, the procedure of in vitro culture and expansion can introduce contaminants. As discussed by Pachler et al. during the development of a GMP compliant protocol for MSC culture, use of xeno-based reagents during culture such as FBS can introduce viruses or alter cells to induce an immune response following clinical application (Mackensen et al., 2000; Pachler et al., 2017). To address this, future work should test the feasibility of adapting the cell isolation and culture protocol to include xeno-free reagents. The recent paper by Iacobazzi et al. demonstrated this can be done without significantly affecting cell phenotype or behaviour (Iacobazzi et al., 2020)

Another interesting aspect to consider is the how the in vitro cell culture environment can influence cell functionality. Specifically, there is a large discrepancy in the partial pressure of gases such as oxygen in vivo and in vitro. The physiological oxygen levels experienced by cells in vivo range from ~3 – 13%, whilst in vitro the standard culture levels are 21% (Chapple et al., 2016). Changes in oxygen levels can modulate cell function, meaning that the behaviour of cells in vitro may not be representative of their behaviour once transferred to the in vivo environment. For example, Chapple showed that endothelial cells adapted to 5% oxygen instead of in vitro oxygen levels presented altered redox defences through bach1 regulation of Nuclear Factor-E2-Related Factor 2-dependent genes HO-1 and NQO1 (Chapple et al., 2016). HO-1 plays a significant role in vascular inflammation (Araujo et al., 2012). Cells or grafts characterised under standard in vitro oxygen levels may display differential regulation of genes

such as this once transplanted in vivo, which may trigger changes in cell functionality and unwanted vascular events. Similarly, changes in the partial pressure of oxygen have been suggested as a trigger for terminal differentiation of bone marrow MSCs (Keeley et al., 2019). To address this issue, future work should consider the expansion of cells and development of vascular grafts under physiologically relevant oxygen levels, moving away from the traditional hyperoxic conditions used in standard in vitro culture.

For the development of the tissue engineered vascular graft, CorMatrix was used as the scaffold. This collagen-based scaffold made from decellularized porcine small intestinal submucosa was chosen due to its well characterised properties, which support cell ingrowth, and the fact it has been FDA approved and routinely used in cardiovascular surgery (Mosala et al., 2016). This was beneficial for two main reasons. Firstly, it meant that the contribution of the cells to the graft properties could be easily evaluated, and secondly, using an FDA approved material would accelerate clinical translation. Despite this, the scaffold material is not perfect, with some reports of inflammation and degeneration post implantation (Woo et al., 2016). Given more time, other options would have been explored. Indeed, natural biomaterials such as fibrinogen, collage and alginate have shown exciting potential for cardiovascular tissue engineering applications (Majid et al., 2020). These can be tailored to form custom three-dimensional porous structures that may overcome the limitations of CorMatrix, whilst retaining a high level of biocompatibility. Ideally, a completely autologous based graft could be produced with properties tailored for the particular application. In fact, a number of studies have explored the possibility of using decellularized WJ for cell culture and tissue engineering applications (Dan et al., 2017; Jadalannagari et al., 2017; Li et al., 2019). The WJ contains a combination of naturally occurring biomaterials and growth factors that may make it and ideal scaffold. Indeed, Dan et al demonstrated that WJ ECM could be used as a coating on vascular grafts to increase cell adherence and proliferation. Utilising concepts from this study and a novel method by Pati et al to produce decellularized ECM bioink, we have begun a preliminary investigation into the feasibility of developing a WJ based bioink for 3D printing of a scaffold (Pati et al., 2014). This would require considerable future development but could pave the way for the generation of an entirely autologous NG2 UCP engineered vascular graft. Another interesting scaffold possibility is to explore manufacturing techniques such as electrospinning to create custom hybrid scaffolds with detailed microstructures and highly tailorable properties, in addition to excellent biocompatibility. Indeed, recent work from our group has demonstrated

the potential of using a combination of 3D printed polylactic-co-glycolic acid and electro-spun gelatin nanofibers for vascular tissue engineering (Carrabba et al., 2020). The bioactive properties of the scaffold were capable of promoting infiltration by host cells and reparative angiogenesis in an in vivo mouse model. Given the time to explore alternative scaffolds, it would also be particularly exciting to assess pericyte behaviour after culture on the different types of scaffolds in parallel. As previously mentioned, the scaffold properties such as stiffness can influence cell behaviour. The angiogenic properties and phenotype of the pericytes may be altered in response to the mechanical and chemical stimuli of the scaffold. Additionally, the anti-calcification properties of the pericytes could be explored and compared between different scaffolds.

In addition to development of a tailored scaffold, further graft complexity could be added by producing a layered conduit with spatially distribution of different vascular cell types. Research into tissue engineering of vascular grafts has mostly focused on either acellular strategies or scaffolds that incorporate just one or two cell types, often EC luminal seeding and VSMC abluminal seeding (Nakayama et al., 2015; Pashneh-Tala et al., 2015; Song et al., 2018), whilst the native vascular wall is composed of numerous cell types organised into distinct layers (Mazurek et al., 2017). Greater effort to mimic this complexity could yield more successful results. For example, in vitro analysis demonstrated that NG2 UCPs were capable of differentiating towards a VSMC phenotype and promoting endothelial tube formation. Both these characteristics could be included in future graft development. Firstly, following static seeding of the scaffold with NG2 UCPs, the cells could be differentiated to form a smooth muscle layer. ECs and non-differentiated NG2 UCPs could then be seeded on top of this layer, using a similar methodology to the co-culture method employed for angiogenic characterisation to form a vascularised adventitial layer reminiscent of the vasa vasorum. A pre-vascularised construct could facilitate rapid perfusion through integration with patient vasculature soon after implantation, whilst a smooth muscle layer may improve the mechanical properties of the graft, such as elasticity. Although the mechanical improvements in mechanical properties could be evaluated using the current in vitro system, detailed analysis would also require a in vivo study as suggested above.

In summary, the work presented here has identified an exciting cell source for vascular tissue engineering and evidenced that these cells can be used to improve currently used clinically approved vascular grafts. This proof of concept is a key step in translation of tissue engineering

approach from the lab to the clinic; however, there are some significant aspects mentioned above that I would explore next given further time. Firstly, an in vivo study is required to demonstrate the in vitro behaviour and therapeutic potential of the cells and graft can be replicated in a physiological environment. Following this, I would complete a more thorough analysis of scaffold options and compare how the properties such as calcification resistance and angiogenesis are affected. Finally, I would seek to develop a more complex graft, with multiple cell types spatially distributed to mimic the layered structure of native vascular tissue more closely.

7.2. Conclusion

This study aimed to evaluate the feasibility of isolating phenotypically pure pericytes from the umbilical cord to enable generation of autologous tissue engineered grafts with superior properties to the current prostheses used for correction of ToF.

To address this aim, a variety of different isolation strategies were explored, resulting in the expansion of three different pericyte lines from umbilical cord and placenta tissue; NG2 UCPs, CD146 UCPs and CD34 PLPs. Characterisation of these cell types revealed VSMC differentiation capabilities as well as endothelium supporting properties. Comparison of cell characteristics demonstrated that NG2 UCPs possessed the highest purity along with enhanced therapeutic properties relative to other cell sources such as WJ-MSCs. Further analysis of this cell type uncovered ECM remodelling capabilities and resistance to calcification. In vitro development of a pericyte engineered graft demonstrated the feasibility of using NG2 UCPs to functionalise and improve the properties of acellular CorMatrix scaffolds, which are routinely used in correction of CHD.

In chapter one, the requirements of an optimal graft for neonatal vascular tissue engineering were set out as follows: availability, calcification resistance, compliance, customisable, durability, growth potential, mechanical integrity, non-immunogenic, and non-thrombotic. The graft developed in this study is readily available and customisable, having been composed of an accessible cell source and a commercialised scaffold which can be easily manipulated into shape. Moreover, the functionalised graft demonstrated improved compliance and mechanical properties. Whilst some aspects of the graft could not be tested in vitro, namely growth potential, calcification resistance, immunogenicity and thrombosis induction, the properties of

NG2 UCPs observed in vitro suggest these cells may support non-pathological growth and endothelium development. An in vivo study is warranted to confirm the validity of in vitro analysis.

References

Abbaszadeh, H., Ghorbani, F., Derakhshani, M., Movassaghpour, A. A., Yousefi, M., Talebi, M., & Shamsasenjan, K. (2020). Regenerative potential of Wharton's jelly-derived mesenchymal stem cells: A new horizon of stem cell therapy. *Journal of Cellular Physiology*. https://doi.org/10.1002/jcp.29810

Abbott, N. J. (2000). Inflammatory Mediators and Modulation of Blood–Brain Barrier Permeability. *Cellular and Molecular Neurobiology*, *20*(2), 131–147. https://doi.org/10.1023/A:1007074420772

Agrawal, A., Lee, B. H., Irvine, S. A., An, J., Bhuthalingam, R., Singh, V., Low, K. Y., Chua, C. K., & Venkatraman, S. S. (2015). *Smooth Muscle Cell Alignment and Phenotype Control by Melt Spun Polycaprolactone Fibers for Seeding of Tissue Engineered Blood Vessels*. *2015*.

Ährlund-Richter, L., De Luca, M., Marshak, D. R., Munsie, M., Veiga, A., & Rao, M. (2009). Isolation and Production of Cells Suitable for Human Therapy: Challenges Ahead. *Cell Stem Cell*, *4*(1), 20–26. https://doi.org/10.1016/j.stem.2008.11.012

Akhtar, R., Sherratt, M. J., Cruickshank, J. K., & Derby, B. (2011). Characterizing the elastic properties of tissues. *Materials Today*, *14*(3), 96–105. https://doi.org/10.1016/S1369-7021(11)70059-1

Akwii, R. G., Sajib, M. S., Zahra, F. T., & Mikelis, C. M. (2019). Role of Angiopoietin-2 in Vascular Physiology and Pathophysiology. *Cells*, *8*(5), 471. https://doi.org/10.3390/cells8050471

Albertario, A., Swim, M. M., Ahmed, E. M., Iacobazzi, D., Yeong, M., Madeddu, P., Ghorbel, M. T., & Caputo, M. (2019). Successful Reconstruction of the Right Ventricular Outflow Tract by Implantation of Thymus Stem Cell Engineered Graft in Growing Swine. *JACC: Basic to Translational Science*, *4*(3), 364–384. https://doi.org/10.1016/j.jacbts.2019.02.001

Allen, B. S., El-zein, C., Cuneo, B., Cava, J. P., Barth, M. J., & Ilbawi, M. N. (2002).

Pericardial Tissue Valves and Gore-Tex Conduits as an Alternative for Right Ventricular Outflow Tract Replacement in Children. *4975*(02).

Allt, G., & Lawrenson, J. G. (2001). Pericytes: Cell Biology and Pathology. *Cells Tissues Organs*, *169*(1), 1–11. http://www.karger.com/DOI/10.1159/000047855

Alsop, A. T., Pence, J. C., Weisgerber, D. W., Harley, B. A. C., & Bailey, R. C. (2014). Photopatterning of vascular endothelial growth factor within collagen-glycosaminoglycan scaffolds can induce a spatially confined response in human umbilical vein endothelial cells. *Acta Biomaterialia*, *10*(11), 4715–4722. https://doi.org/10.1016/j.actbio.2014.07.002

Alvino, V. V., Fernández-Jiménez, R., Rodriguez-Arabaolaza, I., Slater, S., Mangialardi, G., Avolio, E., Spencer, H., Culliford, L., Hassan, S., Sueiro Ballesteros, L., Herman, A., Ayaon-Albarrán, A., Galán-Arriola, C., Sánchez-González, J., Hennessey, H., Delmege, C., Ascione, R., Emanueli, C., Angelini, G. D., … Madeddu, P. (2018). Transplantation of Allogeneic Pericytes Improves Myocardial Vascularization and Reduces Interstitial Fibrosis in a Swine Model of Reperfused Acute Myocardial Infarction. *Journal of the American Heart Association*, *7*(2), e006727. https://doi.org/10.1161/JAHA.117.006727

Alvino, V. V., Kilcooley, M., Thomas, A. C., Carrabba, M., Fagnano, M., Cathery, W., Avolio, E., Iacobazzi, D., Ghorbel, M., Caputo, M., & Madeddu, P. (2020). In Vitro and In Vivo Preclinical Testing of Pericyte-Engineered Grafts for the Correction of Congenital Heart Defects. *Journal of the American Heart Association*, *9*(4). https://doi.org/10.1161/JAHA.119.014214

Amable, P. R., Vinicius, M., Teixeira, T., Bizon, R., & Carias, V. (2014). *Protein synthesis and secretion in human mesenchymal cells derived from bone marrow , adipose tissue and Wharton ' s jelly*. 1–13. https://doi.org/10.1186/scrt442

Amos, P. J., Cagavi Bozkulak, E., & Qyang, Y. (2011). Methods of cell purification: A critical juncture for laboratory research and translational science. *Cells Tissues Organs*, *195*(1–2), 26–40. https://doi.org/10.1159/000331390

Anja, H., Stefanie, K., Karin, W., Dieter, M., G., A. H., & Ulrike, F. (2004). Expression of Angiopoietin-2 in Endothelial Cells Is Controlled by Positive and Negative Regulatory Promoter Elements. *Arteriosclerosis, Thrombosis, and Vascular Biology*, *24*(10), 1803–

1809. https://doi.org/10.1161/01.ATV.0000140819.81839.0e

Ansari, A. S., Yazid, M. D., Qisya, N., Veronica, A., Razali, R. A., Saim, A. Bin, Bt, R., & Idrus, H. (2018). Osteogenic Induction of Wharton ' s Jelly-Derived Mesenchymal Stem Cell for Bone Regeneration : A Systematic Review. *Stem Cells International*. https://doi.org/10.1155/2018/2406462

Araujo, J., Zhang, M., & Yin, F. (2012). Heme Oxygenase-1, Oxidation, Inflammation, and Atherosclerosis . In *Frontiers in Pharmacology* (Vol. 3, p. 119). https://www.frontiersin.org/article/10.3389/fphar.2012.00119

Arenz, C., Laumeier, A., Lütter, S., Blaschczok, H. C., Sinzobahamvya, N., Haun, C., Asfour, B., & Hraska, V. (2013). Is there any need for a shunt in the treatment of tetralogy of fallot with one source of pulmonary blood flow? *European Journal of Cardio-Thoracic Surgery*, *44*(4), 648–654. https://doi.org/10.1093/ejcts/ezt124

Armiñán, A., Gandía, C., Bartual, M., García-Verdugo, J. M., Lledó, E., Mirabet, V., Llop, M., Barea, J., Montero, J. A., & Sepúlveda, P. (2008). Cardiac Differentiation Is Driven by NKX2.5 and GATA4 Nuclear Translocation in Tissue-Specific Mesenchymal Stem Cells. *Stem Cells and Development*, *18*(6), 907–918. https://doi.org/10.1089/scd.2008.0292

Armulik, A., Genové, G., & Betsholtz, C. (2011). Pericytes: Developmental, Physiological, and Pathological Perspectives, Problems, and Promises. *Developmental Cell*, *21*(2), 193–215. https://doi.org/10.1016/j.devcel.2011.07.001

Arpino, V., Brock, M., & Gill, S. E. (2015). The role of TIMPs in regulation of extracellular matrix proteolysis. *Matrix Biology*, *44–46*, 247–254. https://doi.org/10.1016/j.matbio.2015.03.005

Arutyunyan, I., Fatkhudinov, T., Kananykhina, E., Usman, N., Elchaninov, A., Makarov, A., Bolshakova, G., Goldshtein, D., & Sukhikh, G. (2016). Role of VEGF-A in angiogenesis promoted by umbilical cord-derived mesenchymal stromal / stem cells : in vitro study. *Stem Cell Research & Therapy*, 1–13. https://doi.org/10.1186/s13287-016-0305-4

Attwell, D., Mishra, A., Hall, C. N., O'Farrell, F. M., & Dalkara, T. (2016). What is a

pericyte? *Journal of Cerebral Blood Flow & Metabolism*, *36*(2), 451–455. https://doi.org/10.1177/0271678X15610340

Avolio, E., Caputo, M., & Madeddu, P. (2015). Stem cell therapy and tissue engineering for correction of congenital heart disease. *Frontiers in Cell and Developmental Biology*, *3*(June), 1–17. https://doi.org/10.3389/fcell.2015.00039

Avolio, E., Rodriguez-Arabaolaza, I., Spencer, H. L., Riu, F., Mangialardi, G., Slater, S. C., Rowlinson, J., Alvino, V. V., Idowu, O. O., Soyombo, S., Oikawa, A., Swim, M. M., Kong, C. H. T., Cheng, H., Jia, H., Ghorbel, M. T., Hancox, J. C., Orchard, C. H., Angelini, G., … Madeddu, P. (2015). Expansion and characterization of neonatal cardiac pericytes provides a novel cellular option for tissue engineering in congenital heart disease. *Journal of the American Heart Association*, *4*(6), e002043. https://doi.org/10.1161/JAHA.115.002043

Ayoubi, S., Sheikh, S. P., & Eskildsen, T. V. (2017). Human induced pluripotent stemcell-derived vascular smooth muscle cells: Differentiation and therapeutic potential. *Cardiovascular Research*, *113*(11), 1282–1293. https://doi.org/10.1093/cvr/cvx125

Baba, K., Mikhailov, A., & Sankai, Y. (2021). Dynamic flow priming programs allow tuning up the cell layers properties for engineered vascular graft. *Scientific Reports*, *11*(1), 14666. https://doi.org/10.1038/s41598-021-94023-9

Bacakova, L., Travnickova, M., Filova, E., Matejka, R., Stepanovska, J., Musilkova, J., Zarubova, J., & Molitor, M. (2018). Vascular Smooth Muscle Cells (VSMCs) in Blood Vessel Tissue Engineering: The Use of Differentiated Cells or Stem Cells as VSMC Precursors. *Intech Open*.

Bacakova, L., Travnickova, M., Filova, E., Matějka, R., Stepanovska, J., Musilkova, J., Zarubova, J., & Molitor, M. (2018). The Role of Vascular Smooth Muscle Cells in the Physiology and Pathophysiology of Blood Vessels. *Intech Open*.

Badylak, S. F., Freytes, D. O., & Gilbert, T. W. (2009). Extracellular matrix as a biological scaffold material: Structure and function. *Acta Biomaterialia*, *5*(1), 1–13. https://doi.org/10.1016/j.actbio.2008.09.013

Bajpai, V. K., & Andreadis, S. T. (2012). Stem Cell Sources for Vascular Tissue Engineering

and Regeneration. *Tissue Engineering Part B: Reviews*, *18*(5), 405–425. https://doi.org/10.1089/ten.teb.2011.0264

Baksh, D., Yao, R., & Tuan, R. S. (2007). Comparison of Proliferative and Multilineage Differentiation Potential of Human Mesenchymal Stem Cells Derived from Umbilical Cord and Bone Marrow. *Stem Cells*, *25*(6), 1384–1392. https://doi.org/10.1634/stemcells.2006-0709

Balabanov, R., Washington, R., Wagnerova, J., & Dore-Duffy, P. (1996). CNS microvascular pericytes express macrophage-like function, cell surface integrin alpha M, and macrophage marker ED-2. *Microvasc Res*, *52*(2), 127–142. https://doi.org/10.1006/mvre.1996.0049

Bandopadhyay, R., Orte, C., Lawrenson, J. G., Reid, A. R., De Silva, S., & Allt, G. (2001). Contractile proteins in pericytes at the blood-brain and blood-retinal barriers. *Journal of Neurocytology*, *30*(1), 35–44. https://doi.org/10.1023/A:1011965307612

Batteux, C., Haidar, M. A., & Bonnet, D. (2019). 3D-Printed Models for Surgical Planning in Complex Congenital Heart Diseases : A Systematic Review. *Frontiers in Pediatrics*, *7*(February), 1–8. https://doi.org/10.3389/fped.2019.00023

Beazley-Long, N., Durrant, A. M., Swift, M. N., & Donaldson, L. F. (2018). The physiological functions of central nervous system pericytes and a potential role in pain. *F1000Research*, *7*(0). https://doi.org/10.12688/f1000research.13548.1

Berdat, P. A., Immer, F., Pfammatter, J., & Carrel, T. (2004). *Reoperations in adults with congenital heart disease : analysis of early outcome*. *93*, 239–245. https://doi.org/10.1016/j.ijcard.2003.04.005

Bergers, G., & Song, S. (2005). The role of pericytes in blood-vessel formation and maintenance. *Neuro-Oncology*, *7*(4), 452–464. https://doi.org/10.1215/S1152851705000232

Birbrair, A, Zhang, T., Wang, Z. M., Messi, M. L., Enikolopov, G. N., Mintz, A., & Delbono, O. (2013). Skeletal muscle neural progenitor cells exhibit properties of NG2-glia. *Exp Cell Res*, *319*(1), 45–63. https://doi.org/10.1016/j.yexcr.2012.09.008

Birbrair, Alexander, Borges, I. da T., Gilson Sena, I. F., Almeida, G. G., da Silva Meirelles,

L., Gonçalves, R., Mintz, A., & Delbono, O. (2017). How Plastic Are Pericytes? *Stem Cells and Development*, *26*(14), 1013–1019. https://doi.org/10.1089/scd.2017.0044

Birbrair, Alexander, Zhang, T., Wang, Z.-M., Messi, M. L., Mintz, A., & Delbono, O. (2015). Pericytes at the intersection between tissue regeneration and pathology: Figure 1. *Clinical Science*, *128*(2), 81–93. https://doi.org/10.1042/CS20140278

Bjornard, K., Riehle-colarusso, T., Gilboa, S. M., & Correa, A. (2013). Patterns in the Prevalence of Congenital Heart Defects , Metropolitan Atlanta , 1978 to 2005. *Birth Defects Research Part A - Clinical and Molecular Teratology*, *97*(2), 87–94. https://doi.org/10.1002/bdra.23111

Blasi, A., Martino, C., Balducci, L., Saldarelli, M., Soleti, A., Navone, S. E., Canzi, L., Cristini, S., Invernici, G., Parati, E. A., & Alessandri, G. (2011). *Dermal fibroblasts display similar phenotypic and differentiation capacity to fat-derived mesenchymal stem cells , but differ in anti-inflammatory and angiogenic potential*. 1–14. https://doi.org/10.1186/2045-824X-3-5

Blocki, A., Wang, Y., Koch, M., Peh, P., Beyer, S., Law, P., Hui, J., & Raghunath, M. (2013). Not All MSCs Can Act as Pericytes: Functional In Vitro Assays to Distinguish Pericytes from Other Mesenchymal Stem Cells in Angiogenesis. *Stem Cells and Development*, *22*(17), 2347–2355. https://doi.org/10.1089/scd.2012.0415

Blue, G. M., Kirk, E. P., Sholler, G. F., Harvey, R. P., & Winlaw, D. S. (2012). Congenital heart disease: current knowledge about causes and inheritance. *Clinical Focus*, *197*(August), 155–159. https://doi.org/10.5694/mja12.10811

Boyd, R., Parisi, F., & Kalfa, D. (2019). State of the Art : Tissue Engineering in Congenital Heart Surgery. *Seminars in Thoracic and Cardiovascular Surgery*, 1–11. https://doi.org/10.1053/j.semtcvs.2019.05.023

Brudno, Y., Ennett-shepard, A. B., Chen, R. R., Aizenberg, M., & Mooney, D. J. (2013). Enhancing microvascular formation and vessel maturation through temporal control over multiple pro-angiogenic and pro-maturation factors. *Biomaterials*, *34*(36), 9201–9209. https://doi.org/10.1016/j.biomaterials.2013.08.007

Cabrera-pérez, R., Monguió-tortajada, M., Gámez-valero, A., Rojas-márquez, R., Borràs, F.

E., Roura, S., & Vives, J. (2019). *Osteogenic commitment of Wharton ' s jelly mesenchymal stromal cells : mechanisms and implications for bioprocess development and clinical application*. *3*, 1–11.

Cai, A., Hardt, M., Schneider, P., Schmid, R., Lange, C., Dippold, D., Schubert, D. W., Boos, A. M., Weigand, A., Arkudas, A., Horch, R. E., & Beier, J. P. (2018). Myogenic differentiation of primary myoblasts and mesenchymal stromal cells under serum-free conditions on PCL-collagen I-nanoscaffolds. *BMC Biotechnology*, *18*(1), 75. https://doi.org/10.1186/s12896-018-0482-6

Cai, X., Lin, Y., Friedrich, C. C., Neville, C., Pomerantseva, I., Sundback, C. A., Sharma, P., Zhang, Z., Vacanti, J. P., Hauschka, P. V., & Grottkau, B. E. (2009). Bone marrow derived pluripotent cells are pericytes which contribute to vascularization. *Stem Cell Reviews and Reports*, *5*(4), 437–445. https://doi.org/10.1007/s12015-009-9097-6

Campagnolo, P., Cesselli, D., Al Haj Zen, A., Beltrami, A. P., Kränkel, N., Katare, R., Angelini, G., Emanueli, C., & Madeddu, P. (2010). Human adult vena saphena contains perivascular progenitor cells endowed with clonogenic and proangiogenic potential. *Circulation*, *121*(15), 1735–1745. https://doi.org/10.1161/CIRCULATIONAHA.109.899252

Campagnolo, P., Gormley, A. J., Chow, L. W., Guex, A. G., Parmar, P. A., Puetzer, J. L., Steele, J. A. M., Breant, A., Madeddu, P., & Stevens, M. M. (2016). Pericyte Seeded Dual Peptide Scaffold with Improved Endothelialization for Vascular Graft Tissue Engineering. *Advanced Healthcare Materials*, *5*(23), 3046–3055. https://doi.org/10.1002/adhm.201600699

Carmeliet, P., & Jain, R. K. (2011). Molecular mechanisms and clinical applications of angiogenesis. *Nature*, *473*(7347), 298–307. https://doi.org/10.1038/nature10144

Carrabba, M., Jover, E., Fagnano, M., Thomas, A. C., Avolio, E., Richardson, T., Carter, B., Vozzi, G., Perriman, A. W., & Madeddu, P. (2020). Fabrication of New Hybrid Scaffolds for in vivo Perivascular Application to Treat Limb Ischemia. *Frontiers in Cardiovascular Medicine*, *7*(November), 1–17. https://doi.org/10.3389/fcvm.2020.598890

Carrabba, M., & Madeddu, P. (2018). Current Strategies for the Manufacture of Small Size

Tissue Engineering Vascular Grafts. *Frontiers in Bioengineering and Biotechnology*, *6*, 41. https://doi.org/10.3389/fbioe.2018.00041

Carrabba, M., Maria, C. De, Oikawa, A., Reni, C., Rodriguez-Arabaolaza, I., Spencer, H., Slater, S., Avolio, E., Dang, Z., Spinetti, G., Madeddu, P., & Vozzi, G. (2016). Design, fabrication and perivascular implantation of bioactive scaffolds engineered with human adventitial progenitor cells for stimulation of arteriogenesis in peripheral ischemia. *Biofabrication*, *8*(1), 15020. https://doi.org/10.1088/1758-5090/8/1/015020

Cathery, W., Faulkner, A., Maselli, D., & Madeddu, P. (2018). Concise Review: The Regenerative Journey of Pericytes Toward Clinical Translation. *Stem Cells*, *36*(9), 1295–1310. https://doi.org/10.1002/stem.2846

ÇELEBİ SALTIK, B., & GÖKÇINAR YAĞCI, B. (2017). Expansion of human umbilical cord blood hematopoietic progenitors with cord vein pericytes. *Turkish Journal of Biology*, *41*, 49–57. https://doi.org/10.3906/biy-1510-49

Chambers, I., Colby, D., Robertson, M., Nichols, J., Lee, S., Tweedie, S., & Smith, A. (2003). *Functional Expression Cloning of Nanog , a Pluripotency Sustaining Factor in Embryonic Stem Cells*. *113*, 643–655.

Chang, W. G., & Niklason, L. E. (2017). A short discourse on vascular tissue engineering. *Npj Regenerative Medicine*, *2*(1), 7. https://doi.org/10.1038/s41536-017-0011-6

Chapple, S. J., Keeley, T. P., Mastronicola, D., Arno, M., Vizcay-Barrena, G., Fleck, R., Siow, R. C. M., & Mann, G. E. (2016). Bach1 differentially regulates distinct Nrf2-dependent genes in human venous and coronary artery endothelial cells adapted to physiological oxygen levels. *Free Radical Biology and Medicine*, *92*, 152–162. https://doi.org/10.1016/j.freeradbiomed.2015.12.013

Chen, J., Luo, Y., Hui, H., Cai, T., Huang, H., Yang, F., Feng, J., Zhang, J., & Yan, X. (2017). CD146 coordinates brain endothelial cell–pericyte communication for blood–brain barrier development. *Proceedings of the National Academy of Sciences*, *114*(36), E7622–E7631. https://doi.org/10.1073/pnas.1710848114

Chen, W. C. W., Baily, J. E., Corselli, M., Díaz, M. E., Sun, B., Xiang, G., Gray, G. A., Huard, J., Péault, B., Diaz, M. E., Sun, B., Xiang, G., Gray, G. A., Huard, J., & Peault,

B. (2015). Human myocardial pericytes: multipotent mesodermal precursors exhibiting cardiac specificity. *Stem Cells*, *33*(2), 557–573. https://doi.org/10.1002/stem.1868

Choi, M., Lee, H., Naidansaren, P., Kim, H., Eunju, O., Cha, J., Ahn, H., In, P., Shin, J., & Ae, Y. (2013). Proangiogenic features of Wharton ' s jelly-derived mesenchymal stromal / stem cells and their ability to form functional vessels. *International Journal of Biochemistry and Cell Biology*, *45*(3), 560–570. https://doi.org/10.1016/j.biocel.2012.12.001

Chopra, H., Hung, M. K., Kwong, D. L., Zhang, C. F., & Pow, E. H. N. (2018). Insights into endothelial progenitor cells: Origin, classification, potentials, and prospects. *Stem Cells International*, *2018*. https://doi.org/10.1155/2018/9847015

Corselli, M, Crisan, M., Murray, I. R., West, C. C., Scholes, J., Codrea, F., Khan, N., & Peault, B. (2013). Identification of perivascular mesenchymal stromal/stem cells by flow cytometry. *Cytometry A*, *83*(8), 714–720. https://doi.org/10.1002/cyto.a.22313

Corselli, Mirko, Chen, C.-W., Sun, B., Yap, S., Rubin, J. P., & Péault, B. (2012). The Tunica Adventitia of Human Arteries and Veins As a Source of Mesenchymal Stem Cells. *Stem Cells and Development*, *21*(8), 1299–1308. https://doi.org/10.1089/scd.2011.0200

Corselli, Mirko, Crisan, M., Murray, I. R., West, C. C., Scholes, J., Codrea, F., Khan, N., & Bruno, P. (2013). Identification of Perivascular Mesenchymal Stromal / Stem Cells by Flow Cytometry. *Cytometry Part A*, *00A*, 1–7. https://doi.org/10.1002/cyto.22313

Cox, T. R., & Erler, J. T. (2011). Remodeling and homeostasis of the extracellular matrix: Implications for fibrotic diseases and cancer. *DMM Disease Models and Mechanisms*, *4*(2), 165–178. https://doi.org/10.1242/dmm.004077

Crisan, M., Chen, C.-W., Corselli, M., Andriolo, G., Lazzari, L., & Péault, B. (2009). Perivascular Multipotent Progenitor Cells in Human Organs. *Annals of the New York Academy of Sciences*, *1176*(1), 118–123. https://doi.org/10.1111/j.1749-6632.2009.04967.x

Crisan, M., Corselli, M., Chen, W. C. W., & Péault, B. (2012). Perivascular cells for regenerative medicine. *J Cell Mol Med*, *16*(12), 2851–2860. https://doi.org/10.1111/j.1582-4934.2012.01617.x

Crisan, M., Yap, S., Casteilla, L., Chen, C. W., Corselli, M., Park, T. S., Andriolo, G., Sun, B., Zheng, B., Zhang, L., Norotte, C., Teng, P. N., Traas, J., Schugar, R., Deasy, B. M., Badylak, S., Buhring, H. J., Giacobino, J. P., Lazzari, L., … Péault, B. (2008). A Perivascular Origin for Mesenchymal Stem Cells in Multiple Human Organs. *Cell Stem Cell*, *3*(3), 301–313. https://doi.org/10.1016/j.stem.2008.07.003

Dan, P., Velot, É., Decot, V., & Menu, P. (2015). The role of mechanical stimuli in the vascular differentiation of mesenchymal stem cells. *Journal of Cell Science*, *128*(14), 2415–2422. https://doi.org/10.1242/jcs.167783

Dan, P., Velot, É., Francius, G., Menu, P., & Decot, V. (2017). Human-derived extracellular matrix from Wharton's jelly: An untapped substrate to build up a standardized and homogeneous coating for vascular engineering. *Acta Biomaterialia*, *48*, 227–237. https://doi.org/10.1016/j.actbio.2016.10.018

Davenport, A. P., Hyndman, K. A., Dhaun, N., Southan, C., Kohan, D. E., Pollock, J. S., & Pollock, D. M. (2016). Endothelin. *Pharmacological Reviews*, *68*, 357–418.

de Souza, L. E. B., Malta, T. M., Kashima Haddad, S., & Covas, D. T. (2016). Mesenchymal Stem Cells and Pericytes: To What Extent Are They Related? *Stem Cells and Development*, *25*(24), 1843–1852. https://doi.org/10.1089/scd.2016.0109

De Visscher, G., Mesure, L., Meuris, B., Ivanova, A., & Flameng, W. (2012). Improved endothelialization and reduced thrombosis by coating a synthetic vascular graft with fibronectin and stem cell homing factor SDF-1α. *Acta Biomaterialia*, *8*(3), 1330–1338. https://doi.org/10.1016/j.actbio.2011.09.016

Dellavalle, A., Sampaolesi, M., Tonlorenzi1, R., Tagliafico, E., Sacchetti, B., Perani, L., Innocenzi, A., Galvez, B. G., Messina, G., Morosetti, R., Li, S., Belicchi, M., Peretti, G., Chamberlain, J. S., Wright, W. E., Torrente, Y., Ferrari, S., Bianco, P., Cossu, G., … Cossu, G. (2007). Pericytes of human skeletal muscle are myogenic precursors distinct from satellite cells. *Nature Cell Biology*, *9*(3), 255–267. https://doi.org/10.1038/ncb1542

Dias Moura Prazeres, P. H., Sena, I. F. G., Borges, I. da T., de Azevedo, P. O., Andreotti, J. P. P. P., de Paiva, A. E., de Almeida, V. M., de Paula Guerra, D. A., Pinheiro dos Santos, G. S., Mintz, A., Delbono, O., & Birbrair, A. (2017). Pericytes are

heterogeneous in their origin within the same tissue. *Developmental Biology*, *427*(1), 6–11. https://doi.org/10.1016/j.ydbio.2017.05.001

Dimarino, A. M., Caplan, A. I., & Bonfield, T. L. (2013). Mesenchymal stem cells in tissue repair. *Frontiers in Immunology*, *4*, 201. https://doi.org/10.3389/fimmu.2013.00201

Dimberg, A., & Sund, M. (2014). *Cancer Angiogenesis and Vasculogenesis* (L. M. McManus & R. N. B. T.-P. of H. D. Mitchell (eds.); pp. 403–411). Academic Press. https://doi.org/https://doi.org/10.1016/B978-0-12-386456-7.01908-0

Dixit, R., Narasimhan, C., Balekundri, V. I., Agrawal, D., Kumar, A., & Mohapatra, B. (2018). Functionally significant, novel GATA4 variants are frequently associated with Tetralogy of Fallot. *Human Mutation*, *39*(12), 1957–1972. https://doi.org/10.1002/humu.23620

Dolk, H., Loane, M., & Garne, E. (2011). Congenital heart defects in Europe: prevalence and perinatal mortality, 2000 to 2005. *Circulation*, *123*(8), 841–849. https://doi.org/10.1161/CIRCULATIONAHA.110.958405

Domev, H., Milkov, I., Itskovitz-Eldor, J., & Dar, A. (2014). Immunoevasive Pericytes From Human Pluripotent Stem Cells Preferentially Modulate Induction of Allogeneic Regulatory T Cells. *Stem Cells Translational Medicine*, *3*(10), 1169–1181. https://doi.org/10.5966/sctm.2014-0097

Dominici, M., Le Blanc, K., Mueller, I., Slaper-Cortenbach, I., Marini, F. C., Krause, D. S., Deans, R. J., Keating, A., Prockop, D. J., & Horwitz, E. M. (2006). Minimal criteria for defining multipotent mesenchymal stromal cells. The International Society for Cellular Therapy position statement. *Cytotherapy*, *8*(4), 315–317. https://doi.org/10.1080/14653240600855905

Downing, T. E., & Kim, Y. Y. (2015). Tetralogy of Fallot. General Principles of Management. *Cardiology Clinics*, *33*(4), 531–541. https://doi.org/10.1016/j.ccl.2015.07.002

Drews, J. D., Miyachi, H., & Shinoka, T. (2017). Tissue-engineered vascular grafts for congenital cardiac disease: Clinical experience and current status. *Trends in Cardiovascular Medicine*, *27*(8), 521–531. https://doi.org/10.1016/j.tcm.2017.06.013

Duan, B. (2017). State-of-the-Art Review of 3D Bioprinting for Cardiovascular Tissue Engineering. *Annals of Biomedical Engineering*, *45*(1), 195–209. https://doi.org/10.1007/s10439-016-1607-5

Eaker, S., Armant, M., Brandwein, H., Burger, S., Campbell, A., Carpenito, C., Clarke, D., Fong, T., Karnieli, O., Niss, K., Van't Hof, W., & Wagey, R. (2013). Concise Review: Guidance in Developing Commercializable Autologous/Patient-Specific Cell Therapy Manufacturing. *STEM CELLS Translational Medicine*, *2*(11), 871–883. https://doi.org/10.5966/sctm.2013-0050

Edwards, S. S., Zavala, G., Martı, S., Egan, J. T., & Vegf-a, Á. (2014). *Functional analysis reveals angiogenic potential of human mesenchymal stem cells from Wharton ' s jelly in dermal regeneration*. 851–866. https://doi.org/10.1007/s10456-014-9432-7

Eilken, H. M., Diéguez-Hurtado, R., Schmidt, I., Nakayama, M., Jeong, H.-W., Arf, H., Adams, S., Ferrara, N., & Adams, R. H. (2017). Pericytes regulate VEGF-induced endothelial sprouting through VEGFR1. *Nature Communications*, *8*(1), 1574. https://doi.org/10.1038/s41467-017-01738-3

Erikssen, G., LiestØl, K., Seem, E., Birkeland, S., Saatvedt, K. J., Hoel, T. N., DØhlen, G., Skulstad, H., Svennevig, J. L., Thaulow, E., & Lindberg, H. L. (2015). Achievements in congenital heart defect surgery : A prospective, 40-year study of 7038 patients. *Circulation*, *131*(4), 337–346. https://doi.org/10.1161/CIRCULATIONAHA.114.012033

Fahed, A. C., Gelb, B. D., Seidman, J. G., & Seidman, C. E. (2013). Genetics of congenital heart disease: The glass half empty. *Circulation Research*, *112*(4), 707–720. https://doi.org/10.1161/CIRCRESAHA.112.300853

Farup, J., De Lisio, M., Rahbek, S. K., Bjerre, J., Vendelbo, M. H., Boppart, M. D., & Vissing, K. (2015). Pericyte response to contraction mode-specific resistance exercise training in human skeletal muscle. *Journal of Applied Physiology*, *119*(10), 1053–1063. https://doi.org/10.1152/japplphysiol.01108.2014

Ferreira, J. R., Teixeira, G. Q., Santos, S. G., Barbosa, M. A., Almeida-Porada, G., & Gonçalves, R. M. (2018). Mesenchymal Stromal Cell Secretome: Influencing Therapeutic Potential by Cellular Pre-conditioning . In *Frontiers in Immunology*

(Vol. 9, p. 2837). https://www.frontiersin.org/article/10.3389/fimmu.2018.02837

Flanagan, T. C., Cornelissen, C., Koch, S., Tschoeke, B., Sachweh, S., Schmitz-rode, T., & Jockenhoevel, S. (2007). *The in vitro development of autologous fibrin-based tissue-engineered heart valves through optimised dynamic conditioning*. *28*, 3388–3397. https://doi.org/10.1016/j.biomaterials.2007.04.012

Forbes, S., Bond, A. R., Thirlwell, K. L., Burgoyne, P., Samuel, K., Noble, J., Borthwick, G., Colligan, D., McGowan, N. W. A., Lewis, P. S., Fraser, A. R., Mountford, J. C., Carter, R. N., Morton, N. M., Turner, M. L., Graham, G. J., & Campbell, J. D. M. (2020). Human umbilical cord perivascular cells improve human pancreatic islet transplant function by increasing vascularization. *Science Translational Medicine*, *12*(526), eaan5907. https://doi.org/10.1126/scitranslmed.aan5907

Foster, K., Sheridan, J., Veiga-Fernandes, H., Roderick, K., Pachnis, V., Adams, R., Blackburn, C., Kioussis, D., & Coles, M. (2008). Contribution of Neural Crest-Derived Cells in the Embryonic and Adult Thymus. *The Journal of Immunology*, *180*(5), 3183–3189. https://doi.org/10.4049/jimmunol.180.5.3183

Gabe, I. T., Gault, J. H., Ross, J., Mason, D. T., Mills, C. J., Schillingford, J. P., & Braunwald, E. (1969). Measurement of instantaneous blood flow velocity and pressure in conscious man with a catheter-tip velocity probe. *Circulation*, *40*(5), 603–614. https://doi.org/10.1161/01.CIR.40.5.603

Geenen, I. L. A., Molin, D. G. M., van den Akker, N. M. S., Jeukens, F., Spronk, H. M., Schurink, G. W. H., & Post, M. J. (2015). Endothelial cells (ECs) for vascular tissue engineering: venous ECs are less thrombogenic than arterial ECs. *Journal of Tissue Engineering and Regenerative Medicine*, *9*(5), 564–576. https://doi.org/10.1002/term.1642

Geevarghese, A., & Herman, I. M. (2014). Pericyte-endothelial crosstalk: Implications and opportunities for advanced cellular therapies. *Translational Research*. https://doi.org/10.1016/j.trsl.2014.01.011

Gerhardt, H., Golding, M., Fruttiger, M., Ruhrberg, C., Lundkvist, A., Abramsson, A., Jeltsch, M., Mitchell, C., Alitalo, K., Shima, D., & Betsholtz, C. (2003). VEGF guides angiogenic sprouting utilizing endothelial tip cell filopodia. *Journal of Cell Biology*,

161(6), 1163–1177. https://doi.org/10.1083/jcb.200302047

Gerrah, R., Turner, M. E., Gottlieb, D., Quaegebeur, J. M., & Bacha, E. (2015). Repair of Tetralogy of Fallot in Children Less Than 4 kg Body Weight. *Pediatric Cardiology*, *36*(7), 1344–1349. https://doi.org/10.1007/s00246-015-1163-z

Ghafarzadeh, M., Namdari, M., & Eatemadi, A. (2016). Stem cell therapies for congenital heart disease. *Biomedicine and Pharmacotherapy*, *84*, 1163–1171. https://doi.org/10.1016/j.biopha.2016.10.055

Ghorbel, M. T., Jia, H., Swim, M. M., Iacobazzi, D., Albertario, A., Zebele, C., Holopherne-Doran, D., Hollander, A., Madeddu, P., & Caputo, M. (2019). Reconstruction of the pulmonary artery by a novel biodegradable conduit engineered with perinatal stem cell-derived vascular smooth muscle cells enables physiological vascular growth in a large animal model of congenital heart disease. *Biomaterials*, *217*(February), 119284. https://doi.org/10.1016/j.biomaterials.2019.119284

Giachelli, C. M. (1999). Ectopic calcification: Gathering hard facts about soft tissue mineralization. *American Journal of Pathology*, *154*(3), 671–675. https://doi.org/10.1016/S0002-9440(10)65313-8

Gökçinar-Yagci, B., Özyüncü, Ö., & Çelebi-Saltik, B. (2016). Isolation, characterisation and comparative analysis of human umbilical cord vein perivascular cells and cord blood mesenchymal stem cells. *Cell and Tissue Banking*, *17*(2), 345–352. https://doi.org/10.1007/s10561-015-9542-5

Gokcinar-Yagci, B., Uckan-Cetinkaya, D., & Celebi-Saltik, B. (2015). Pericytes: Properties, functions and applications in tissue engineering. *Stem Cell Reviews and Reports*, *11*(4), 549–559. https://doi.org/10.1007/s12015-015-9590-z

Golob, M. J., Tabima, D. M., Wolf, G. D., Johnston, J. L., Forouzan, O., Mulchrone, A. M., Kellihan, H. B., Bates, M. L., & Chesler, N. C. (2017). Pulmonary arterial strain- and remodeling-induced stiffening are differentiated in a chronic model of pulmonary hypertension. *Journal of Biomechanics*, *55*, 92–98. https://doi.org/https://doi.org/10.1016/j.jbiomech.2017.02.003

Gomez-salazar, M., Gonzalez-galofre, Z. N., Casamitjana, J., & Martin, I. (2020). *Five*

Decades Later , Are Mesenchymal Stem Cells Still Relevant ? 8(February), 148. https://doi.org/10.3389/fbioe.2020.00148

Gowdak, L. H. W., & Krieger, J. E. (2018). Vascular Growth Factors, Progenitor Cells, and Angiogenesis. In *Endothelium and Cardiovascular Diseases: Vascular Biology and Clinical Syndromes* (pp. 49–62). https://doi.org/10.1016/B978-0-12-812348-5.00005-2

Gui, L., Dash, B. C., Luo, J., Qin, L., Zhao, L., Yamamoto, K., Hashimoto, T., Wu, H., Dardik, A., Tellides, G., Niklason, L. E., & Qyang, Y. (2016). Implantable tissue-engineered blood vessels from human induced pluripotent stem cells. *Biomaterials*, *102*, 120–129. https://doi.org/10.1016/j.biomaterials.2016.06.010

Hall, A. P. (2006). Review of the pericyte during angiogenesis and its role in cancer and diabetic retinopathy. *Toxicol Pathol*, *34*(6), 763–775. https://doi.org/10.1080/01926230600936290

Hall, C. N., Reynell, C., Gesslein, B., Hamilton, N. B., Mishra, A., Sutherland, B. A., Oâ Farrell, F. M., Buchan, A. M., Lauritzen, M., & Attwell, D. (2014). Capillary pericytes regulate cerebral blood flow in health and disease. *Nature*, *508*(1), 55–60. https://doi.org/10.1038/nature13165

Hayman, E. G., Pierschbacher, M. D., Suzuki, S., & Ruoslahti, E. (1985). Vitronectin—A major cell attachment-promoting protein in fetal bovine serum. *Experimental Cell Research*, *160*(2), 245–258. https://doi.org/https://doi.org/10.1016/0014-4827(85)90173-9

He, W., Nieponice, A., Soletti, L., Hong, Y., Gharaibeh, B., Crisan, M., Usas, A., Peault, B., Huard, J., Wagner, W. R., & Vorp, D. A. (2010). Pericyte-based human tissue engineered vascular grafts. *Biomaterials*, *31*(32), 8235–8244. https://doi.org/10.1016/j.biomaterials.2010.07.034

Heil, M., Eitenmüller, I., Schmitz-Rixen, T., & Schaper, W. (2006). Arteriogenesis versus angiogenesis: Similarities and differences. *Journal of Cellular and Molecular Medicine*, *10*(1), 45–55. https://doi.org/10.1111/j.1582-4934.2006.tb00290.x

Henaine, R., Roubertie, F., Vergnat, M., & Ninet, J. (2012). Valve replacement in children: A challenge for a whole life. *Archives of Cardiovascular Diseases*, *105*(10), 517–528.

https://doi.org/10.1016/j.acvd.2012.02.013

Hendijani, F. (2017). *Explant culture : An advantageous method for isolation of mesenchymal stem cells from human tissues*. *October 2016*, 1–14. https://doi.org/10.1111/cpr.12334

Henriksen, K., & Karsdal, M. A. (2016). Type I Collagen. In *Biochemistry of Collagens, Laminins and Elastin*. Elsevier Inc. https://doi.org/10.1016/B978-0-12-809847-9.00001-5

Hetheridge, C., Mavria, G., & Mellor, H. (2011). Uses of the in vitro endothelial–fibroblast organotypic co-culture assay in angiogenesis research. *Biochemical Society Transactions*, *39*(6), 1597–1600. https://doi.org/10.1042/BST20110738

Hilenski, L. L., & Griendling, K. K. (2012). Vascular Smooth Muscle. In *Vascular Medicine: A Companion to Braunwald's Heart Disease: Second Edition* (Second Edi). Elsevier Inc. https://doi.org/10.1016/B978-1-4377-2930-6.00003-3

Holst, K. A., Dearani, J. A., Burkhart, H. M., Connolly, H. M., Warnes, C. A., Li, Z., & Schaff, H. V. (2011). *Risk Factors and Early Outcomes of Multiple Reoperations in Adults With Congenital Heart Disease*. https://doi.org/10.1016/j.athoracsur.2011.03.102

Holst, K. A., Said, S. M., Nelson, T. J., Cannon, B. C., & Dearani, J. A. (2017). Current Interventional and Surgical Management of Congenital Heart Disease: Specific Focus on Valvular Disease and Cardiac Arrhythmias. *Circulation Research*, *120*(6), 1027–1044. https://doi.org/10.1161/CIRCRESAHA.117.309186

Hong, S., Maghen, L., Kenigsbcerg, S., Teichert, A., Rammeloo, A. W., Shlush, E., Szaraz, P., Pereira, S., Lulat, A., Xiao, R., & Yie, S. (2013). *Ontogeny of Human Umbilical Cord Perivascular Cells : 22*(17), 1–15. https://doi.org/10.1089/scd.2012.0552

Howard, D., Buttery, L. D., Shakesheff, K. M., & Roberts, S. J. (2008). Tissue engineering: Strategies, stem cells and scaffolds. *Journal of Anatomy*, *213*(1), 66–72. https://doi.org/10.1111/j.1469-7580.2008.00878.x

Hu, P., Zhang, W., Xin, H., Deng, G., Bankston, A. S., & Deng, G. (2016). *Single Cell Isolation and Analysis*. *4*(October), 1–12. https://doi.org/10.3389/fcell.2016.00116

Hur, J., Yoon, C. H., Kim, H. S., Choi, J. H., Kang, H. J., Hwang, K. K., Oh, B. H., Lee, M.

M., & Park, Y. B. (2004). Characterization of Two Types of Endothelial Progenitor Cells and Their Different Contributions to Neovasculogenesis. *Arteriosclerosis, Thrombosis, and Vascular Biology*, *24*(2), 288–293. https://doi.org/10.1161/01.ATV.0000114236.77009.06

Iacobazzi, D., Rapetto, F., Albertario, A., Swim, M. M., Narayan, S., Skeffington, K., Salih, T., Alvino, V. V., Madeddu, P., Ghorbel, M. T., & Caputo, M. (2020). Wharton's Jelly-Mesenchymal Stem Cell-Engineered Conduit for Pediatric Translation in Heart Defect. *Tissue Engineering. Part A*. https://doi.org/10.1089/ten.TEA.2020.0088

Jacob, M. P., Badier-Commander, C., Fontaine, V., Benazzoug, Y., Feldman, L., & Michel, J. B. (2001). Extracellular matrix remodeling in the vascular wall. *Pathologie Biologie*, *49*(4), 326–332. https://doi.org/10.1016/S0369-8114(01)00151-1

Jacobs, J. P., Mavroudis, C., Quintessenza, J. A., Chai, P. J., Pasquali, S. K., Hill, K. D., Vricella, L. A., Jacobs, M. L., Dearani, J. A., & Cameron, D. (2014). Reoperations for pediatric and congenital heart disease: an analysis of the Society of Thoracic Surgeons (STS) congenital heart surgery database. *Seminars in Thoracic and Cardiovascular Surgery. Pediatric Cardiac Surgery Annual*, *17*(1), 2–8. https://doi.org/10.1053/j.pcsu.2014.01.006

Jadalannagari, S., Converse, G., McFall, C., Buse, E., Filla, M., Villar, M. T., Artigues, A., Mellot, A. J., Wang, J., Detamore, M. S., Hopkins, R. A., & Aljitawi, O. S. (2017). Decellularized Wharton's Jelly from human umbilical cord as a novel 3D scaffolding material for tissue engineering applications. *PLoS ONE*, *12*(2), 1–23. https://doi.org/10.1371/journal.pone.0172098

Jaing, T.-H. (2014). Umbilical cord blood: a trustworthy source of multipotent stem cells for regenerative medicine. *Cell Transplantation*, *23*(4–5), 493–496. https://doi.org/10.3727/096368914X678300

Jia, W., Gungor-Ozkerim, P. S., Zhang, Y. S., Yue, K., Zhu, K., Liu, W., Pi, Q., Byambaa, B., Dokmeci, M. R., Shin, S. R., & Khademhosseini, A. (2016). Direct 3D bioprinting of perfusable vascular constructs using a blend bioink. *Biomaterials*. https://doi.org/10.1016/j.biomaterials.2016.07.038

Jin, H. J., Kwon, J. H., Kim, M., Bae, Y. K., Choi, S. J., Oh, W., Yang, Y. S., & Jeon, H. B.

(2016). Downregulation of Melanoma Cell Adhesion Molecule (MCAM/CD146) Accelerates Cellular Senescence in Human Umbilical Cord Blood-Derived Mesenchymal Stem Cells. *STEM CELLS Translational Medicine*, *5*(4), 427–439. https://doi.org/10.5966/sctm.2015-0109

Jo, M.-K. M., & Michael, S. (2014). Vasa Vasorum in Normal and Diseased Arteries. *Circulation*, *129*(24), 2557–2566. https://doi.org/10.1161/CIRCULATIONAHA.113.007189

Jobin, P. G., Butler, G. S., & Overall, C. M. (2017). New intracellular activities of matrix metalloproteinases shine in the moonlight. *BBA - Molecular Cell Research*, *1864*(11), 2043–2055. https://doi.org/10.1016/j.bbamcr.2017.05.013

Jover, E., Fagnano, M., Angelini, G., & Madeddu, P. (2018). Cell Sources for Tissue Engineering Strategies to Treat Calcific Valve Disease. *Frontiers in Cardiovascular Medicine*, *5*(November). https://doi.org/10.3389/fcvm.2018.00155

Jover, E., Fagnano, M., Cathery, W., Slater, S., Pisanu, E., Gu, Y., Avolio, E., Bruno, D., Baz-Lopez, D., Faulkner, A., Carrabba, M., Angelini, G., & Madeddu, P. (2021). Human adventitial pericytes provide a unique source of anti-calcific cells for cardiac valve engineering: Role of microRNA-132-3p. *Free Radical Biology and Medicine*. https://doi.org/https://doi.org/10.1016/j.freeradbiomed.2021.01.029

Ju, Y. M., Ahn, H., Arenas-Herrera, J., Kim, C., Abolbashari, M., Atala, A., Yoo, J. J., & Lee, S. J. (2017). Electrospun vascular scaffold for cellularized small diameter blood vessels: A preclinical large animal study. *Acta Biomaterialia*, *59*, 58–67. https://doi.org/https://doi.org/10.1016/j.actbio.2017.06.027

Jung, S., & Kleinheinz, J. (2013). *Angiogenesis — The Key to Regeneration*. https://doi.org/10.5772/55542

Kalaszczynska, I., & Ferdyn, K. (2015). Wharton's jelly derived mesenchymal stem cells: Future of regenerative medicine? Recent findings and clinical significance. *BioMed Research International*, *2015*. https://doi.org/10.1155/2015/430847

Kalfa, D., Ph, D., & Bacha, E. (2013). *New Technologies for Surgery of the Congenital Cardiac Defect*. *4*(3). https://doi.org/10.5041/RMMJ.10119

Kandalam, V., Basu, R., Moore, L., Fan, D., Wang, X., Jaworski, D. M., Oudit, G. Y., & Kassiri, Z. (2011). *Lack of Tissue Inhibitor of Metalloproteinases 2 Leads to Exacerbated Left Ventricular Dysfunction and Adverse Extracellular Matrix Remodeling in Response to Biomechanical Stress*. 2094–2105. https://doi.org/10.1161/CIRCULATIONAHA.111.030338

Karwowski, W., Naumnik, B., Szczepanski, M., & Mysliwiec, M. (2012). The mechanism of vascular calcification – a systematic review. *Medical Science Monitor*, *18*(1), 1–11.

Katare, R. G., & Madeddu, P. (2013). Pericytes from human veins for treatment of myocardial ischemia. *Trends in Cardiovascular Medicine*, *23*(3), 66–70. https://doi.org/10.1016/j.tcm.2012.09.002

Katare, R., Riu, F., Mitchell, K., Gubernator, M., Campagnolo, P., Cui, Y., Fortunato, O., Avolio, E., Cesselli, D., Beltrami, A. P., Angelini, G., Emanueli, C., & Madeddu, P. (2011). Transplantation of human pericyte progenitor cells improves the repair of infarcted heart through activation of an angiogenic program involving micro-RNA-132. *Circulation Research*, *109*(8), 894–906. https://doi.org/10.1161/CIRCRESAHA.111.251546

Keeley, T. P., & Mann, G. E. (2019). Defining physiological normoxia for improved translation of cell physiology to animal models and humans. *Physiological Reviews*, *99*(1), 161–234. https://doi.org/10.1152/physrev.00041.2017

Kenny, D. (2018). *Interventional Cardiology for Congenital Heart Disease*. *48*(5), 350–364.

Kielty, C. M., Stephan, S., Sherratt, M. J., Williamson, M., & Shuttleworth, C. A. (2007). Applying elastic fibre biology in vascular tissue engineering. *Philosophical Transactions of the Royal Society B: Biological Sciences*, *362*(1484), 1293–1312. https://doi.org/10.1098/rstb.2007.2134

Kiess, M. (2016). History and evolution of the treatment of adult congenital heart disease. *BC Medical Journal*, *58*(september), 368–372.

Kinsey, R., Williamson, M. R., Chaudhry, S., Mellody, K. T., McGovern, A., Takahashi, S., Shuttleworth, C. A., & Kielty, C. M. (2008). Fibrillin-1 microfibril deposition is dependent on fibronectin assembly. *Journal of Cell Science*, *121*(16), 2696–2704.

https://doi.org/10.1242/jcs.029819

Kloesel, B., Dinardo, J. A., & Body, S. C. (2016). Cardiac Embryology and Molecular Mechanisms of Congenital Heart Disease: A Primer for Anesthesiologists. *Anesthesia and Analgesia*, *123*(3), 551–569. https://doi.org/10.1213/ANE.0000000000001451

Knowles, R. L., Bull, C., Wren, C., & Dezateux, C. (2012). Mortality with congenital heart defects in England and Wales, 1959-2009: exploring technological change through period and birth cohort analysis. *Archives of Disease in Childhood*, *97*(10), 861–865. https://doi.org/10.1136/archdischild-2012-301662

Krautler, N. J., Kana, V., Kranich, J., Tian, Y., Perera, D., Lemm, D., Schwarz, P., Armulik, A., Browning, J. L., Tallquist, M., Buch, T., Oliveira-Martins, J. B., Zhu, C., Hermann, M., Wagner, U., Brink, R., Heikenwalder, M., & Aguzzi, A. (2012). Follicular dendritic cells emerge from ubiquitous perivascular precursors. *Cell*, *150*(1), 194–206. https://doi.org/10.1016/j.cell.2012.05.032

Kumar, P., Nagarajan, A., & Uchil, P. D. (2018). Analysis of Cell Viability by the Lactate Dehydrogenase Assay. *Cold Spring Harbor Protocols*, *2018*(6). https://doi.org/10.1101/pdb.prot095497

Kunisaki, Y., Merad, M., & Frenette, P. S. (2013). Nestin+ Pericytes In The Fetal Liver Are Necessary To Maintain HSCs. *Blood*, *122*(21), 583 LP – 583. http://www.bloodjournal.org/content/122/21/583.abstract

Kunz, J., Krause, D., Kremer, M., & Dermietzel, R. (1994). The 140-kDa Protein of Blood-Brain Barrier-Associated Pericytes Is Identical to Aminopeptidase N. *Journal of Neurochemistry*, *62*(6), 2375–2386. https://doi.org/10.1046/j.1471-4159.1994.62062375.x

Kurobe, H., Maxfield, M. W., Breuer, C. K., & Shinoka, T. (2012). *Concise Review : Tissue-Engineered Vascular Grafts for Cardiac Surgery : Past , Present , and Future*. 566–571.

Kuttappan, S., Mathew, D., Jo, J. ichiro, Tanaka, R., Menon, D., Ishimoto, T., Nakano, T., Nair, S. V., Nair, M. B., & Tabata, Y. (2018). Dual release of growth factor from nanocomposite fibrous scaffold promotes vascularisation and bone regeneration in rat

critical sized calvarial defect. *Acta Biomaterialia*, *78*, 36–47. https://doi.org/10.1016/j.actbio.2018.07.050

Langer, R., & Vacanti, J. P. (1993). - ARTICLES Tissue Engineering. *Science*, *260*(May), 920–926. https://doi.org/10.1126/science.8493529

Laredo, F., Plebanski, J., & Tedeschi, A. (2019). Pericytes: Problems and Promises for CNS Repair . In *Frontiers in Cellular Neuroscience* (Vol. 13, p. 546). https://www.frontiersin.org/article/10.3389/fncel.2019.00546

Lee, A. A., Graham, D. A., Ratcliffe, A., & Karlon, W. J. (2002). *Fluid Shear Stress-Induced Alignment of Cultured Vascular Smooth Muscle Cells*. *124*(February 2002), 37–43. https://doi.org/10.1115/1.1427697

Lee, K., Kaplan, D. L., Lovett, M., Ph, D., Lee, K., Ph, D., Edwards, A., Ph, D., Kaplan, D. L., & Ph, D. (2009). *Vascularization Strategies for Tissue Engineering Vascularization Strategies for Tissue Engineering*. *15*(July). https://doi.org/10.1089/ten.TEB.2009.0085

Lev, M., & Eckner, F. A. (1964). The Pathologic Anatomy of Tetralogy of Fallot and Its Variations. *Diseases of the Chest*, *45*(3), 251–261. https://doi.org/10.1378/chest.45.3.251

Levy-Mishali, M., Zoldan, J., & Levenberg, S. (2009). Effect of scaffold stiffness on myoblast differentiation. *Tissue Engineering. Part A*, *15*(4), 935–944. https://doi.org/10.1089/ten.tea.2008.0111

Li, D., Chiu, G., Lipe, B., Hopkins, R. A., Lillis, J., Ashton, J. M., Paul, S., & Aljitawi, O. S. (2019). Decellularized Wharton jelly matrix: A biomimetic scaffold for ex vivo hematopoietic stem cell culture. *Blood Advances*, *3*(7), 1011–1026. https://doi.org/10.1182/bloodadvances.2018019315

Lin, Y., Guo, X., Zhao, B., Liu, J., Da, M., Wen, Y., Hu, Y., Ni, B., Zhang, K., Yang, S., Xu, J., Dai, J., Wang, X., Xia, Y., Ma, H., Jin, G., Yu, S., Liu, J., Keavney, B. D., … Hu, Z. (2015). Association analysis identifies new risk loci for congenital heart disease in Chinese populations. *Nature Communications*, *6*. https://doi.org/10.1038/ncomms9082

Liu, Y., Chen, S., Zühlke, L., Black, G. C., Choy, M. K., Li, N., & Keavney, B. D. (2019). Global birth prevalence of congenital heart defects 1970-2017: Updated systematic

review and meta-analysis of 260 studies. *International Journal of Epidemiology*, *48*(2), 455–463. https://doi.org/10.1093/ije/dyz009

Livak, K. J., & Schmittgen, T. D. (2001). Analysis of Relative Gene Expression Data Using Real-Time Quantitative PCR and the 2−ΔΔCT Method. *Methods*, *25*(4), 402–408. https://doi.org/https://doi.org/10.1006/meth.2001.1262

Lozito, T. P., & Tuan, R. S. (2010). Mesenchymal Stem Cells Inhibit Both Endogenous and Exogenous MMPs via Secreted TIMPs. *Cellular Physiology*, *April*, 385–396. https://doi.org/10.1002/jcp.22344

Lu, P., Takai, K., Weaver, V. M., & Werb, Z. (2011). Extracellular matrix degradation and remodeling in development and disease. *Cold Spring Harbor Perspectives in Biology*, *3*(12), a005058. https://doi.org/10.1101/cshperspect.a005058

Ma, X., He, Z., Li, L., Liu, G., Li, Q., Yang, D., Zhang, Y., & Li, N. (2017). Development and in vivo validation of tissue-engineered, small-diameter vascular grafts from decellularized aortae of fetal pigs and canine vascular endothelial cells. *Journal of Cardiothoracic Surgery*, *12*(1), 101. https://doi.org/10.1186/s13019-017-0661-x

Ma, Z., Mao, C., Jia, Y., Fu, Y., & Kong, W. (2020). Extracellular matrix dynamics in vascular remodeling. *American Journal of Physiology. Cell Physiology*, *319*(3), C481–C499. https://doi.org/10.1152/ajpcell.00147.2020

Mackensen, A., Dräger, R., Schlesier, M., Mertelsmann, R., & Lindemann, A. (2000). Presence of IgE antibodies to bovine serum albumin in a patient developing anaphylaxis after vaccination with human peptide-pulsed dendritic cells. *Cancer Immunology, Immunotherapy*, *49*(3), 152–156. https://doi.org/10.1007/s002620050614

Mahapatra, S., Nishimura, R. A., Sorajja, P., Cha, S., & McGoon, M. D. (2006). Relationship of Pulmonary Arterial Capacitance and Mortality in Idiopathic Pulmonary Arterial Hypertension. *Journal of the American College of Cardiology*, *47*(4), 799–803. https://doi.org/https://doi.org/10.1016/j.jacc.2005.09.054

Maier, C. L., & Pober, J. S. (2011). Human placental pericytes poorly stimulate and actively regulate allogeneic CD4 T cell responses. *Arteriosclerosis, Thrombosis, and Vascular Biology*, *31*(1), 183–189. https://doi.org/10.1161/ATVBAHA.110.217117

Maier, C. L., Shepherd, B. R., Yi, T., & Pober, J. S. (2010). Explant outgrowth, propagation and characterization of human pericytes. *Microcirculation*, *17*(5), 367–380. https://doi.org/10.1111/j.1549-8719.2010.00038.x

Majid, Q. A., Fricker, A. T. R., Gregory, D. A., Davidenko, N., Hernandez Cruz, O., Jabbour, R. J., Owen, T. J., Basnett, P., Lukasiewicz, B., Stevens, M., Best, S., Cameron, R., Sinha, S., Harding, S. E., & Roy, I. (2020). Natural Biomaterials for Cardiac Tissue Engineering: A Highly Biocompatible Solution. *Frontiers in Cardiovascular Medicine*, *7*(October), 1–32. https://doi.org/10.3389/fcvm.2020.554597

Malda, J., Rouwkema, J., Martens, D. E., Le Comte, E. P., Kooy, F. K., Tramper, J., Van Blitterswijk, C. A., & Riesle, J. (2004). Oxygen Gradients in Tissue-Engineered PEGT/PBT Cartilaginous Constructs: Measurement and Modeling. *Biotechnology and Bioengineering*, *86*(1), 9–18. https://doi.org/10.1002/bit.20038

Mallis, P., Papapanagiotou, A., Katsimpoulas, M., Kostakis, A., Siasos, G., Kass, E., Stavropoulos-Giokas, C., & Michalopoulos, E. (2020). Efficient differentiation of vascular smooth muscle cells from Wharton's Jelly mesenchymal stromal cells using human platelet lysate: A potential cell source for small blood vessel engineering. *World Journal of Stem Cells*, *3*, 203–221.

Mantakaki, A., Fakoya, A. O. J., & Sharifpanah, F. (2018). Recent advances and challenges on application of tissue engineering for treatment of congenital heart disease. *PeerJ*, *6*, e5805. https://doi.org/10.7717/peerj.5805

Mastrullo, V., Cathery, W., Velliou, E., Madeddu, P., & Campagnolo, P. (2020). Angiogenesis in Tissue Engineering: As Nature Intended? *Frontiers in Bioengineering and Biotechnology*, *8*(March), 1–13. https://doi.org/10.3389/fbioe.2020.00188

Mayshar, Y., Ben-David, U., Lavon, N., Biancotti, J.-C., Yakir, B., Clark, A. T., Plath, K., Lowry, W. E., & Benvenisty, N. (2010). Identification and classification of chromosomal aberrations in human induced pluripotent stem cells. *Cell Stem Cell*, *7*(4), 521–531. https://doi.org/10.1016/j.stem.2010.07.017

Mazurek, R., Dave, J. M., Chandran, R. R., Misra, A., Sheikh, A. Q., & Greif, D. M. (2017). Vascular cells in blood vessel wall development and disease Renata. *Advances in Pharmacology*, *78*, 323–350. https://doi.org/doi:10.1016/bs.apha.2016.08.001.

McCORD, M. C., VAN ELK, J., & BLOUNT, S. G. J. (1957). Tetralogy of Fallot; clinical and hemodynamic spectrum of combined pulmonary stenosis and ventricular septal defect. *Circulation*, *16*(5), 736–749. https://doi.org/10.1161/01.cir.16.5.736

Mcdonald, D. M., Bailie, J. R., Archer, D. B., & Chakravarthy, U. (1995). *Characterization of Endothelin A (ET A) and Endothelin B (ET B) Receptors in Cultured Bovine Retinal Pericytes*. *36*(6).

Meijer, F. M. M., Kies, P., Jongbloed, M. R. M., Hazekamp, M. G., Koolbergen, D. R., Blom, N. A., de Roos, A., Schalij, M. J., & Vliegen, H. W. (2019). Excellent durability of homografts in pulmonary position analysed in a predefined adult group with tetralogy of Fallot†. *Interactive CardioVascular and Thoracic Surgery*, *28*(2), 279–283. https://doi.org/10.1093/icvts/ivy242

Mesotten, L., Maes, A., Hambÿe, A. S., Everaert, H., Van Den Maegdenbergh, V., Franken, P., & Mortelmans, L. (1998). Nuclear cardiology, Part I: Anatomy and function of the normal heart. *Journal of Nuclear Medicine Technology*, *26*(1), 4–8.

Mirensky, T. L., & Breuer, C. K. (2008). *The Development of Tissue-Engineered Grafts for Reconstructive Cardiothoracic Surgical Applications*. *63*(5).

Miyoshi, H., & Adachi, T. (2014). Topography design concept of a tissue engineering scaffold for controlling cell function and fate through actin cytoskeletal modulation. *Tissue Engineering. Part B, Reviews*, *20*(6), 609–627. https://doi.org/10.1089/ten.TEB.2013.0728

Montemurro, T., Andriolo, G., Montelatici, E., Weissmann, G., Crisan, M., Colnaghi, M. R., Rebulla, P., Mosca, F., Péault, B., & Lazzari, L. (2011). Differentiation and migration properties of human foetal umbilical cord perivascular cells: Potential for lung repair. *Journal of Cellular and Molecular Medicine*, *15*(4), 796–808. https://doi.org/10.1111/j.1582-4934.2010.01047.x

Mosala, Z., Poncelet, A., Kerchove, L. De, Gianello, P., & Fervaille, C. (2016). *Small intestinal submucosa extracellular matrix (CorMatrix ®) in cardiovascular surgery : a systematic review*. *22*(February), 839–850. https://doi.org/10.1093/icvts/ivw020

Murfee, W. L., Skalak, T. C., & Peirce, S. M. (2005). Differential arterial/venous expression

of NG2 proteoglycan in perivascular cells along microvessels: identifying a venule-specific phenotype. *Microcirculation*, *12*(2), 151–160. https://doi.org/10.1080/10739680590904955

Murphy, C. M., Haugh, M. G., & O'Brien, F. J. (2010). The effect of mean pore size on cell attachment, proliferation and migration in collagen-glycosaminoglycan scaffolds for bone tissue engineering. *Biomaterials*, *31*(3), 461–466. https://doi.org/10.1016/j.biomaterials.2009.09.063

Nakagomi, T., Kubo, S., Nakano-Doi, A., Sakuma, R., Lu, S., Narita, A., Kawahara, M., Taguchi, A., & Matsuyama, T. (2015). Brain Vascular Pericytes Following Ischemia Have Multipotential Stem Cell Activity to Differentiate Into Neural and Vascular Lineage Cells. *STEM CELLS*, *33*(6), 1962–1974. https://doi.org/10.1002/stem.1977

Nakayama, K. H., Hou, L., & Huang, N. F. (2014). Role of extracellular matrix signaling cues in modulating cell fate commitment for cardiovascular tissue engineering. *Advanced Healthcare Materials*, *3*(5), 628–641. https://doi.org/10.1002/adhm.201300620

Nakayama, K. H., Joshi, P. A., Lai, E. S., Gujar, P., Joubert, L.-M., Chen, B., & Huang, N. F. (2015). Bilayered vascular graft derived from human induced pluripotent stem cells with biomimetic structure and function. *Regenerative Medicine*, *10*(6), 745–755. https://doi.org/10.2217/rme.15.45

Navarro, R., Compte, M., Álvarez-Vallina, L., & Sanz, L. (2016). Immune regulation by pericytes: Modulating innate and adaptive immunity. *Frontiers in Immunology*, *7*(NOV), 1–10. https://doi.org/10.3389/fimmu.2016.00480

Nees, S., Weiss, D. R., Senftl, A., Knott, M., Forch, S., Schnurr, M., Weyrich, P., & Juchem, G. (2012). Isolation, bulk cultivation, and characterization of coronary microvascular pericytes: the second most frequent myocardial cell type in vitro. *AJP: Heart and Circulatory Physiology*, *302*(1), H69–H84. https://doi.org/10.1152/ajpheart.00359.2011

Nees, Stephan, Weiss, D. R., & Juchem, G. (2013). Focus on cardiac pericytes. *Pflugers Archiv European Journal of Physiology*, *465*(6), 779–787. https://doi.org/10.1007/s00424-013-1240-1

Neff, L. P., Tillman, B. W., Yazdani, S. K., Machingal, M. A., Yoo, J. J., Soker, S., Bernish, B. W., Geary, R. L., & Christ, G. J. (2011). Vascular smooth muscle enhances functionality of tissue-engineered blood vessels in vivo. *YMVA*, *53*(2), 426–434. https://doi.org/10.1016/j.jvs.2010.07.054

Neidenbach, R., Niwa, K., Oto, O., Oechslin, E., Aboulhosn, J., Celermajer, D., Schelling, J., Pieper, L., Sanftenberg, L., Oberhoffer, R., De Haan, F., Weyand, M., Achenbach, S., Schlensak, C., Lossnitzer, D., Nagdyman, N., Von Kodolitsch, Y., Kallfelz, H. C., Pittrow, D., … Kaemmerer, H. (2018). Improving medical care and prevention in adults with congenital heart disease—reflections on a global problem—part I: Development of congenital cardiology, epidemiology, clinical aspects, heart failure, cardiac arrhythmia. *Cardiovascular Diagnosis and Therapy*, *8*(6), 705–715. https://doi.org/10.21037/cdt.2018.10.15

Nezhad, Z. M., Poncelet, A., Kerchove, L. De, Fervaille, C., Banse, X., Bollen, X., Dehoux, J., Khoury, G. El, & Gianello, P. (2017). *CorMatrix valved conduit in a porcine model : long-term remodelling and biomechanical characterization †*. *24*(September 2016), 90–98. https://doi.org/10.1093/icvts/ivw314

Novosel, E. C., Kleinhans, C., & Kluger, P. J. (2011). Vascularization is the key challenge in tissue engineering. *Advanced Drug Delivery Reviews*, *63*(4), 300–311. https://doi.org/10.1016/j.addr.2011.03.004

Nwadozi, E., Rudnicki, M., & Haas, T. L. (2020). Metabolic Coordination of Pericyte Phenotypes: Therapeutic Implications. *Frontiers in Cell and Developmental Biology*, *8*(February), 1–16. https://doi.org/10.3389/fcell.2020.00077

O'Brien, F. J. (2011). Biomaterials & scaffolds for tissue engineering. *Materials Today*, *14*(3), 88–95. https://doi.org/10.1016/S1369-7021(11)70058-X

Okano, H., Nakamura, M., Yoshida, K., Okada, Y., Tsuji, O., Nori, S., Ikeda, E., Yamanaka, S., & Miura, K. (2013). Steps toward safe cell therapy using induced pluripotent stem cells. *Circulation Research*, *112*(3), 523–533. https://doi.org/10.1161/CIRCRESAHA.111.256149

Oxford, J. T., Reeck, J. C., & Hardy, M. J. (2019). Extracellular Matrix Degradation and Remodeling in Development and Disease. *International Journal of Molecular Sciences*,

20(1). https://doi.org/10.3390/ijms20010205

Özen, I., Deierborg, T., Miharada, K., Padel, T., Englund, E., Genové, G., & Paul, G. (2014). Brain pericytes acquire a microglial phenotype after stroke. *Acta Neuropathologica*, *128*(3), 381–396. https://doi.org/10.1007/s00401-014-1295-x

Ozerdem, U., Grako, K. A., Dahlin-Huppe, K., Monosov, E., & Stallcup, W. B. (2001). NG2 proteoglycan is expressed exclusively by mural cells during vascular morphogenesis. *Developmental Dynamics*, *222*(2), 218–227. https://doi.org/10.1002/dvdy.1200

Pachler, K., Lener, T., Streif, D., Dunai, Z. A., Desgeorges, A., Feichtner, M., Öller, M., Schallmoser, K., Rohde, E., & Gimona, M. (2017). A Good Manufacturing Practice–grade standard protocol for exclusively human mesenchymal stromal cell–derived extracellular vesicles. *Cytotherapy*, *19*(4), 458–472. https://doi.org/https://doi.org/10.1016/j.jcyt.2017.01.001

Pashneh-Tala, S., MacNeil, S., & Claeyssens, F. (2015). The Tissue-Engineered Vascular Graft—Past, Present, and Future. *Tissue Engineering Part B: Reviews*, *22*(1), ten.teb.2015.0100. https://doi.org/10.1089/ten.teb.2015.0100

Patel, A., Fine, B., Sandig, M., & Mequanint, K. (2006). Elastin biosynthesis: The missing link in tissue-engineered blood vessels. *Cardiovascular Research*, *71*(1), 40–49. https://doi.org/10.1016/j.cardiores.2006.02.021

Pati, F., Jang, J., Ha, D. H., Won Kim, S., Rhie, J. W., Shim, J. H., Kim, D. H., & Cho, D. W. (2014). Printing three-dimensional tissue analogues with decellularized extracellular matrix bioink. *Nature Communications*, *5*, 1–11. https://doi.org/10.1038/ncomms4935

Pattabhi, S., Martinez, J. S., & Keller, T. C. S. (2015). Decellularized ECM effects on human mesenchymal stem cell stemness and differentiation. *Differentiation*, *88*(4–5), 131–143. https://doi.org/10.1016/j.diff.2014.12.005

Paul, G., Özen, I., Christophersen, N. S., Reinbothe, T., Bengzon, J., Visse, E., Jansson, K., Dannaeus, K., Henriques-Oliveira, C., Roybon, L., Anisimov, S. V., Renström, E., Svensson, M., Haegerstrand, A., & Brundin, P. (2012). The adult human brain harbors multipotent perivascular mesenchymal stem cells. *PLoS ONE*, *7*(4). https://doi.org/10.1371/journal.pone.0035577

Pavel, M., Renna, M., Park, S. J., Menzies, F. M., Ricketts, T., Füllgrabe, J., Ashkenazi, A., Frake, R. A., Lombarte, A. C., Bento, C. F., Franze, K., & Rubinsztein, D. C. (2018). Contact inhibition controls cell survival and proliferation via YAP/TAZ-autophagy axis. *Nature Communications*. https://doi.org/10.1038/s41467-018-05388-x

Peehl, D. M., & Sellers, R. G. (1998). *Basic FGF , EGF , and PDGF Modify TGFB - Induction of Smooth Muscle Cell Phenotype in Human Prostatic Stromal Cells*. *134*(January), 125–134.

Pennel, T., Bezuidenhout, D., Koehne, J., Davies, N. H., & Zilla, P. (2018). Transmural capillary ingrowth is essential for confluent vascular graft healing. *Acta Biomaterialia*, *65*, 237–247. https://doi.org/10.1016/j.actbio.2017.10.038

Pfister, F., Przybyt, E., Harmsen, M. C., & Hammes, H. P. (2013). Pericytes in the eye. *Pflugers Archiv European Journal of Physiology*, *465*(6), 789–796. https://doi.org/10.1007/s00424-013-1272-6

Pigula, F. A., Khalil, P. N., Mayer, J. E., Del Nido, P. J., & Jonas, R. A. (1999). Repair of tetralogy of Fallot in neonates and young infants. *Circulation*, *100*(19 SUPPL.). https://doi.org/10.1161/01.cir.100.suppl_2.ii-157

Plunkett, N., & Brien, F. J. O. (2011). Bioreactors in tissue engineering. *Technol Health Care*, *19*, 55–69. https://doi.org/10.3233/THC-2011-0605

Post, A., Wang, E., & Cosgriff-Hernandez, E. (2019). A Review of Integrin-Mediated Endothelial Cell Phenotype in the Design of Cardiovascular Devices. *Annals of Biomedical Engineering*, *47*(2), 366–380. https://doi.org/10.1007/s10439-018-02171-3

Proudfoot, D., Skepper, J. N., Hegyi, L., Farzaneh-Far, A., Shanahan, C. M., & Weissberg, P. L. (2001). The role of apoptosis in the initiation of vascular calcification. *Zeitschrift Fur Kardiologie*, *90*(SUPPL. 3), 43–46. https://doi.org/10.1007/s003920170041

Qiu, J., Zheng, Y., Hu, J., Liao, D., Gregersen, H., Deng, X., Fan, Y., & Wang, G. (2014). Biomechanical regulation of vascular smooth muscle cell functions: From in vitro to in vivo understanding. *Journal of the Royal Society Interface*, *11*(90). https://doi.org/10.1098/rsif.2013.0852

Quarti, A., Nardone, S., Colaneri, M., Santoro, G., & Pozzi, M. (2011). Preliminary

experience in the use of an extracellular matrix to repair congenital heart diseases. *Interactive CardioVascular and Thoracic Surgery*, *13*, 569–572. https://doi.org/10.1510/icvts.2011.280016

Raja, S. G., & Pozzi, M. (2004). Growth of Pulmonary Autograft after Ross Operation in Pediatric Patients. *Asian Cardiovascular and Thoracic Annals*, *12*(4), 285–290. https://doi.org/10.1177/021849230401200402

Ramsauer, M., Kunz, J., Krause, D., & Dermietzel, R. (1998). Regulation of a blood-brain barrier-specific enzyme expressed by cerebral pericytes (pericytic aminopeptidase N/pAPN) under cell culture conditions. *Journal of Cerebral Blood Flow and Metabolism : Official Journal of the International Society of Cerebral Blood Flow and Metabolism*, *18*(11), 1270–1281. https://doi.org/10.1097/00004647-199811000-00014

Rensen, S. S. M., Doevendans, P. A. F. M., & Eys, G. J. J. M. Van. (2007). *Regulation and characteristics of vascular smooth muscle cell phenotypic diversity*. *15*(3), 100–108.

Ribatti, D., Nico, B., & Crivellato, E. (2011). The role of pericytes in angiogenesis. *Int J Dev Biol*, *55*(3), 261–268. https://doi.org/10.1387/ijdb.103167dr

Richards, M., & Mellor, H. (2016). *Chapter 10 In Vitro Coculture Assays of Angiogenesis*. *1430*, 159–166. https://doi.org/10.1007/978-1-4939-3628-1

Rizzino, A. (2009). Sox2 and Oct-3/4: A Versatile Pair of Master Regulators that Orchestrate the Self-renewal and Pluripotency of Embryonic Stem Cells by Functioning as Molecular Rheostats. *Wiley Interdiscip Rev Syst Biol Med*, *4*(4), 1–16. https://doi.org/10.1002/wsbm.12.Sox2

Roberts, B. W. C., Mason, D. T., Morrow, A. G., & Braunwald, E. (1968). Calcific Pulmonic Stenosis. *Circulation*, *37*(6), 973–978.

Rodda, D. J., Chew, J., Lim, L., Loh, Y., Wang, B., Ng, H., & Robson, P. (2005). *Transcriptional Regulation of Nanog by OCT4 and SOX2 *. 280*(26), 24731–24737. https://doi.org/10.1074/jbc.M502573200

Roos-Hesselink, J. W., Kerstjens-Frederikse, W. S., Meijboom, F. J., & Pieper, P. G. (2005). Inheritance of congenital heart disease. *Netherlands Heart Journal : Monthly Journal of the Netherlands Society of Cardiology and the Netherlands Heart Foundation*, *13*(3),

88–91. https://pubmed.ncbi.nlm.nih.gov/25696460

Ross, J. M. (1998). *Chapter II. 1 - Cell-Extracellular Matrix Interactions* (C. W. Patrick, A. G. Mikos, L. V McIntire, & R. S. B. T.-F. in T. E. Langer (eds.); pp. 15–27). Pergamon. https://doi.org/https://doi.org/10.1016/B978-008042689-1/50004-2

Ruel, M., Kulik, A., Lam, B. K., Rubens, F. D., Hendry, P. J., Masters, R. G., Bédard, P., & Mesana, T. G. (2005). Long-term outcomes of valve replacement with modern prostheses in young adults☆. *European Journal of Cardio-Thoracic Surgery*, *27*(3), 425–433. https://doi.org/10.1016/j.ejcts.2004.12.002

Rundhaug, J. E. (2005). Matrix metalloproteinases and angiogenesis. *Journal of Cellular and Molecular Medicine*, *9*(2), 267–285. https://doi.org/10.1111/j.1582-4934.2005.tb00355.x

Russell, K. C., Phinney, D. G., Lacey, M. R., Barrilleaux, B. L., Meyertholen, K. E., & O'Connor, K. C. (2010). In vitro high-capacity assay to quantify the clonal heterogeneity in trilineage potential of mesenchymal stem cells reveals a complex hierarchy of lineage commitment. *Stem Cells*, *28*(4), 788–798. https://doi.org/10.1002/stem.312

Rutkovskiy, A., Malashicheva, A., Sullivan, G., Bogdanova, M., Kostareva, A., Stensløkken, K. O., Fiane, A., & Vaage, J. (2017). Valve interstitial cells: The key to understanding the pathophysiology of heart valve calcification. *Journal of the American Heart Association*, *6*(9), 1–23. https://doi.org/10.1161/JAHA.117.006339

Saeedi, P., Halabian, R., & Imani Fooladi, A. A. (2019). A revealing review of mesenchymal stem cells therapy, clinical perspectives and Modification strategies. *Stem Cell Investigation*, *6*, 34–34. https://doi.org/10.21037/sci.2019.08.11

Sakuma, R., Kawahara, M., Nakano-Doi, A., Takahashi, A., Tanaka, Y., Narita, A., Kuwahara-Otani, S., Hayakawa, T., Yagi, H., Matsuyama, T., & Nakagomi, T. (2016). Brain pericytes serve as microglia-generating multipotent vascular stem cells following ischemic stroke. *J Neuroinflammation*, *13*(1), 57. https://doi.org/10.1186/s12974-016-0523-9

Salibe-Filho, W., Araujo, T. L. S., G. Melo, E., B. C. T. Coimbra, L., Lapa, M. S., Acencio,

M. M. P., Freitas-Filho, O., Capelozzi, V. L., Teixeira, L. R., Fernandes, C. J. C. S., Jatene, F. B., Laurindo, F. R. M., & Terra-Filho, M. (2020). Shear stress-exposed pulmonary artery endothelial cells fail to upregulate HSP70 in chronic thromboembolic pulmonary hypertension. *PLOS ONE*, *15*(12), e0242960. https://doi.org/10.1371/journal.pone.0242960

Sánchez, P. F., Brey, E. M., & Briceño, J. C. (2018). Endothelialization mechanisms in vascular grafts. *Journal of Tissue Engineering and Regenerative Medicine*, *12*(11), 2164–2178. https://doi.org/10.1002/term.2747

Sarugaser, R., Ennis, J., Stanford, W. L., & Davies, J. E. (2009). Isolation, Propagation, and Characterization of Human Umbilical Cord Perivascular Cells (HUCPVCs). In *Methods in Molecular Biology* (Vol. 482, pp. 269–279). https://doi.org/10.1007/978-1-59745-060-7

Sarugaser, R., Lickorish, D., Baksh, D., Hosseini, M. M., & Davies, J. E. (2005). Human Umbilical Cord Perivascular (HUCPV) Cells: A Source of Mesenchymal Progenitors. *Stem Cells*, *23*(2), 220–229. https://doi.org/10.1634/stemcells.2004-0166

Sathy, B. N., Mony, U., Menon, D., Baskaran, V. K., Mikos, A. G., & Nair, S. (2015). Bone tissue engineering with multilayered scaffolds - Part I: An approach for vascularizing engineered constructs in vivo. *Tissue Engineering - Part A*, *21*(19–20), 2480–2494. https://doi.org/10.1089/ten.tea.2015.0098

Schmidt, D., Stock, U. A., & Hoerstrup, S. P. (2007). Tissue engineering of heart valves using decellularized xenogeneic or polymeric starter matrices. *Philosophical Transactions of the Royal Society of London. Series B, Biological Sciences*, *362*(1484), 1505–1512. https://doi.org/10.1098/rstb.2007.2131

Scholl, F. G., Boucek, M. M., Chan, K. C., Valdes-Cruz, L., & Perryman, R. (2010). Preliminary Experience With Cardiac Reconstruction Using Decellularized Porcine Extracellular Matrix Scaffold: Human Applications in Congenital Heart Disease. *World Journal for Pediatric and Congenital Heart Surgery*, *1*(1), 132–136. https://doi.org/10.1177/2150135110362092

Scholzen, T., & Gerdes, J. (2000). The Ki-67 protein: From the known and the unknown. *Journal of Cellular Physiology*, *182*(3), 311–322. https://doi.org/10.1002/(SICI)1097-

4652(200003)182:3<311::AID-JCP1>3.0.CO;2-9

Schrimpf, C., Koppen, T., Duffield, J. S., Böer, U., David, S., Ziegler, W., Haverich, A., Teebken, O. E., & Wilhelmi, M. (2017). TIMP3 is Regulated by Pericytes upon Shear Stress Detection Leading to a Modified Endothelial Cell Response. *European Journal of Vascular and Endovascular Surgery*, *54*(4), 524–533. https://doi.org/https://doi.org/10.1016/j.ejvs.2017.07.002

Schugar, R. C., Chirieleison, S. M., Wescoe, K. E., Schmidt, B. T., Askew, Y., Nance, J. J., Evron, J. M., Peault, B., & Deasy, B. M. (2009). High harvest yield, high expansion, and phenotype stability of CD146 mesenchymal stromal cells from whole primitive human umbilical cord tissue. *Journal of Biomedicine and Biotechnology*, *2009*. https://doi.org/10.1155/2009/789526

Seliktar, D., Black, R. A., Vito, R. P., & Nerem, R. M. (2000). Dynamic Mechanical Conditioning of Collagen-Gel Blood Vessel Constructs Induces Remodeling In Vitro. *Annals of Biomedical Engineering*, *28*, 351–362.

Sexton, A. J., Turmaine, M., Cai, W. Q., & Burnstock, G. (1996). A study of the ultrastructure of developing human umbilical vessels. *J. Anat*, *188*, 75–85.

Sharma, U., Pal, D., & Prasad, R. (2014). Alkaline phosphatase: An overview. *Indian Journal of Clinical Biochemistry*, *29*(3), 269–278. https://doi.org/10.1007/s12291-013-0408-y

Shen, C., Lie, P., Miao, T., Yu, M., Lu, Q., Feng, T., Li, J., Zu, T., Liu, X., & Li, H. (2015). *Conditioned medium from umbilical cord mesenchymal stem cells induces migration and angiogenesis*. 20–30. https://doi.org/10.3892/mmr.2015.3409

Shepro, D. (1993). Pericyte physiology. *The Faseb Journal*, *7*(11), 1031–1038.

Shi, S., & Gronthos, S. (n.d.). *Perivascular Niche of Postnatal Mesenchymal Stem Cells in Human Bone Marrow and Dental Pulp.*

Shoji, T., & Shinoka, T. (2018). *Tissue engineered vascular grafts for pediatric cardiac surgery*. *7*(6), 188–195. https://doi.org/10.21037/tp.2018.02.01

Sidney, L. E., Branch, M. J., Dunphy, S. E., Dua, H. S., & Hopkinson, A. (2014). Concise review: Evidence for CD34 as a common marker for diverse progenitors. *Stem Cells*,

32(6), 1380–1389. https://doi.org/10.1002/stem.1661

Silverman, L. I., Flanagan, F., Rodriguez-Granrose, D., Simpson, K., Saxon, L. H., & Foley, K. T. (2019). Identifying and Managing Sources of Variability in Cell Therapy Manufacturing and Clinical Trials. *Regenerative Engineering and Translational Medicine*, *5*(4), 354–361. https://doi.org/10.1007/s40883-019-00129-y

Sjöstedt, S., Rooth, G., & Caligara, F. (1960). The oxygen tension of the blood in the umbilical cord and the intervillous space. *Archives of Disease in Childhood*, *35*(184), 529–533. https://doi.org/10.1136/adc.35.184.529

Skardal, A., Mack, D., Atala, A., & Soker, S. (2013). Substrate elasticity controls cell proliferation, surface marker expression and motile phenotype in amniotic fluid-derived stem cells. *Journal of the Mechanical Behavior of Biomedical Materials*, *17*, 307–316. https://doi.org/10.1016/j.jmbbm.2012.10.001

Smith, R. J., Nasiri, B., Kann, J., Yergeau, D., Bard, J. E., Swartz, D. D., & Andreadis, S. T. (2020). Endothelialization of arterial vascular grafts by circulating monocytes. *Nature Communications*, *11*(1). https://doi.org/10.1038/s41467-020-15361-2

Smith, R. J., Yi, T., Nasiri, B., Breuer, C. K., & Andreadis, S. T. (2019). Implantation of VEGF-functionalized cell-free vascular grafts: Regenerative and immunological response. *FASEB Journal*, *33*(4), 5089–5100. https://doi.org/10.1096/fj.201801856R

Song, H.-H. G., Rumma, R. T., Ozaki, C. K., Edelman, E. R., & Chen, C. S. (2018). Vascular Tissue Engineering: Progress, Challenges, and Clinical Promise. *Cell Stem Cell*, *22*(3), 340–354. https://doi.org/10.1016/j.stem.2018.02.009

Spencer, H. L., Jover, E., Cathery, W., Avolio, E., Rodriguez-arabaolaza, I., Thomas, A. C., Alvino, V. V, Sala-newby, G., Dang, Z., Fagnano, M., Reni, C., Rowlinson, J., Vono, R., Spinetti, G., Beltrami, A. P., Gargioli, C., Caporali, A., Angelini, G., & Madeddu, P. (2019). Role of TPBG (Trophoblast Glycoprotein) Antigen in Human Pericyte Migratory and Angiogenic Activity. *Arteriosclerosis, Thrombosis, and Vascular Biology*, 1113–1124. https://doi.org/10.1161/ATVBAHA.119.312665

Spurway, J., Logan, P., & Pak, S. (2012). The development, structure and blood flow within the umbilical cord with particular reference to the venous system. *Australasian Journal*

of Ultrasound in Medicine, *15*(3), 97–102. https://doi.org/10.1002/j.2205-0140.2012.tb00013.x

Stallcup, W. B. (2017). NG2 proteoglycan enhances brain tumor progression by promoting beta-1 integrin activation in both Cis and Trans Orientations. *Cancers*, *9*(4), 1–15. https://doi.org/10.3390/cancers9040031

Stark, K., Eckart, A., Haidari, S., Tirniceriu, A., Lorenz, M., Von Brühl, M. L., Gärtner, F., Khandoga, A. G., Legate, K. R., Pless, R., Hepper, I., Lauber, K., Walzog, B., & Massberg, S. (2013). Capillary and arteriolar pericytes attract innate leukocytes exiting through venules and "instruct" them with pattern-recognition and motility programs. *Nature Immunology*, *14*(1), 41–51. https://doi.org/10.1038/ni.2477

Staton, C. A., Reed, M. W. R., & Brown, N. J. (2009). A critical analysis of current in vitro and in vivo angiogenesis assays. *International Journal of Experimental Pathology*, *90*(3), 195–221. https://doi.org/10.1111/j.1365-2613.2008.00633.x

Stefańska, K., Ożegowska, K., Hutchings, G., Popis, M., Moncrieff, L., Dompe, C., Janowicz, K., Pieńkowski, W., Gutaj, P., Shibli, J. A., Prado, W. M., Piotrowska-Kempisty, H., Mozdziak, P., Bruska, M., Zabel, M., Kempisty, B., & Nowicki, M. (2020). Human Wharton's Jelly—Cellular Specificity, Stemness Potency, Animal Models, and Current Application in Human Clinical Trials. In *Journal of Clinical Medicine* (Vol. 9, Issue 4). https://doi.org/10.3390/jcm9041102

Sugiura, T., Hibino, N., Breuer, C. K., & Shinoka, T. (2016). Tissue-engineered cardiac patch seeded with human induced pluripotent stem cell derived cardiomyocytes promoted the regeneration of host cardiomyocytes in a rat model. *Journal of Cardiothoracic Surgery*, *11*(1), 163. https://doi.org/10.1186/s13019-016-0559-z

Sugiura, T., Matsumura, G., Miyamoto, S., Miyachi, H., Breuer, C. K., & Shinoka, T. (2018). Tissue-engineered Vascular Grafts in Children With Congenital Heart Disease: Intermediate Term Follow-up. *Seminars in Thoracic and Cardiovascular Surgery*, *30*(2), 175–179. https://doi.org/10.1053/j.semtcvs.2018.02.002

Sun, R., Liu, M., Lu, L., Zheng, Y., & Zhang, P. (2015). Congenital Heart Disease: Causes, Diagnosis, Symptoms, and Treatments. *Cell Biochemistry and Biophysics*, *72*(3), 857–860. https://doi.org/10.1007/s12013-015-0551-6

Suvarnapathaki, S., Wu, X., Lantigua, D., Nguyen, M. A., & Camci-Unal, G. (2019). Breathing life into engineered tissues using oxygen-releasing biomaterials. *NPG Asia Materials*, *11*(1). https://doi.org/10.1038/s41427-019-0166-2

Suzuki, S., Namiki, J., Shibata, S., Mastuzaki, Y., & Okano, H. (2010). The neural stem/progenitor cell marker nestin is expressed in proliferative endothelial cells, but not in mature vasculature. *Journal of Histochemistry and Cytochemistry*, *58*(8), 721–730. https://doi.org/10.1369/jhc.2010.955609

Syedain, Z., Reimer, J., Lahti, M., Berry, J., Johnson, S., & Tranquillo, R. T. (2016). Tissue engineering of acellular vascular grafts capable of somatic growth in young lambs. *Nature Communications*, *7*, 1–9. https://doi.org/10.1038/ncomms12951

Tallawi, M., Rosellini, E., Barbani, N., Cascone, M. G., Rai, R., Saint-pierre, G., & Boccaccini, A. R. (2015). *Strategies for the chemical and biological functionalization of scaffolds for cardiac tissue engineering : a review*.

Tang, Y., Yang, X., Friesel, R. E., Vary, C. P. H., & Liaw, L. (2011). *Mechanisms of TGF-B -Induced Differentiation in Human Vascular Smooth Muscle Cells*. 485–494. https://doi.org/10.1159/000327776

Tawfik, O., Rao, D., Nothnick, W. B., Graham, A., Mau, B., & Fan, F. (2014). Transgelin, a Novel Marker of Smooth Muscle Differentiation, Effectively Distinguishes Endometrial Stromal Tumors from Uterine Smooth Muscle Tumors. *Int J Gynecol Obstet Reprod Med Res*, *1*(1), 26–31.

Teebken, O. E., Bader, A., Steinhoff, G., & Haverich, A. (2000). *Tissue Engineering of Vascular Grafts : Human Cell Seeding of Decellularised Porcine Matrix*. *386*, 381–386. https://doi.org/10.1053/ejvs.1999.1004

Teichert, M., Milde, L., Holm, A., Stanicek, L., Gengenbacher, N., Savant, S., Ruckdeschel, T., Hasanov, Z., Srivastava, K., Hu, J., Hertel, S., Bartol, A., Schlereth, K., & Augustin, H. G. (2017). Pericyte-expressed Tie2 controls angiogenesis and vessel maturation. *Nature Communications*, *8*(May), 16106. https://doi.org/10.1038/ncomms16106

Thenappan, T., Prins, K. W., Pritzker, M. R., Scandurra, J., Volmers, K., & Weir, E. K. (2016). The Critical Role of Pulmonary Arterial Compliance in Pulmonary

Hypertension. *Annals of the American Thoracic Society*, *13*(2). https://doi.org/10.1513/AnnalsATS.201509-599FR

Thottappillil, N., & Nair, P. D. (2015). Scaffolds in vascular regeneration: current status. *Vascular Health and Risk Management*, *11*, 79–91. https://doi.org/10.2147/VHRM.S50536

Tomlinson, M. J., Tomlinson, S., Yang, X. B., & Kirkham, J. (2013). Cell separation: Terminology and practical considerations. *Journal of Tissue Engineering*, *4*(1), 204173141247269. https://doi.org/10.1177/2041731412472690

Triedman, J. K., & Newburger, J. W. (2016). Trends in congenital heart disease. *Circulation*, *133*(25), 2716–2733. https://doi.org/10.1161/CIRCULATIONAHA.116.023544

Trost, A., Schroedl, F., Lange, S., Rivera, F. J., Tempfer, H., Korntner, S., Stolt, C. C., Wegner, M., Bogner, B., Kaser-Eichberger, A., Krefft, K., Runge, C., Aigner, L., & Reitsamer, H. A. (2013). Neural crest origin of retinal and choroidal pericytes. *Investigative Ophthalmology and Visual Science*, *54*(13), 7910–7921. https://doi.org/10.1167/iovs.13-12946

Tsang, W. P., Shu, Y., Kwok, P. L., Zhang, F., Lee, K. K. H., Tang, M. K., Li, G., Chan, K. M., Chan, W. Y., & Wan, C. (2013). CD146+ Human Umbilical Cord Perivascular Cells Maintain Stemness under Hypoxia and as a Cell Source for Skeletal Regeneration. *PLoS ONE*, *8*(10), 1–13. https://doi.org/10.1371/journal.pone.0076153

Tschoeke, B., Flanagan, T. C., Cornelissen, A., Koch, S., Roehl, A., Sriharwoko, M., Sachweh, J. S., Gries, T., Schmitz-Rode, T., & Jockenhoevel, S. (2008). Development of a composite degradable/nondegradable tissue-engineered vascular graft. *Artificial Organs*, *32*(10), 800–809. https://doi.org/10.1111/j.1525-1594.2008.00601.x

Tu, Z., Li, Y., Smith, D. S., Sheibani, N., Huang, S., Kern, T., & Lin, F. (2011). Retinal pericytes inhibit activated T cell proliferation. *Investigative Ophthalmology and Visual Science*, *52*(12), 9005–9010. https://doi.org/10.1167/iovs.11-8008

Van Arsdell, G. S., Maharaj, G. S., Tom, J., Rao, V. K., Coles, J. G., Freedom, R. M., Williams, W. G., & McCrindle, B. W. (2000). What is the Optimal Age for Repair of Tetralogy of Fallot? *Circulation*, *102*(suppl_3), Iii-123-Iii–129.

https://doi.org/10.1161/circ.102.suppl_3.III-123

Van Der Bom, T., Zomer, A. C., Zwinderman, A. H., Meijboom, F. J., Bouma, B. J., & Mulder, B. J. M. (2011). The changing epidemiology of congenital heart disease. *Nature Reviews Cardiology*, *8*(1), 50–60. https://doi.org/10.1038/nrcardio.2010.166

van der Ven, J. P. G., van den Bosch, E., Bogers, A. J. C. C., & Helbing, W. A. (2019). *Current outcomes and treatment of tetralogy of Fallot*. *8*, 1–15.

Van Dijk, C. G. M., Nieuweboer, F. E., Pei, J. Y., Xu, Y. J., Burgisser, P., Van Mulligen, E., El Azzouzi, H., Duncker, D. J., Verhaar, M. C., & Cheng, C. (2015). The complex mural cell: Pericyte function in health and disease. *International Journal of Cardiology*, *190*(1), 75–89. https://doi.org/10.1016/j.ijcard.2015.03.258

van Royen, N., G.D., G., H., Z., S., E., C., G., J., L., & R.H., S. (2001). Stimulation of arteriogenesis; a new concept for the treatment of arterial occlusive disease. *Cardiovascular Research*, *49*(3), 543–553. https://doi.org/10.1016/S0008-6363(00)00206-6

Verbeek, M. M., Otte-Höller, I., Wesseling, P., Ruiter, D. J., & de Waal, R. M. (1994). Induction of alpha-smooth muscle actin expression in cultured human brain pericytes by transforming growth factor-beta 1. *The American Journal of Pathology*, *144*(2), 372–382.

Verheugt, C. L., Uiterwaal, C. S. P. M., Van Der Velde, E. T., Meijboom, F. J., Pieper, P. G., Van Dijk, A. P. J., Vliegen, H. W., Grobbee, D. E., & Mulder, B. J. M. (2010). Mortality in adult congenital heart disease. *European Heart Journal*, *31*(10), 1220–1229. https://doi.org/10.1093/eurheartj/ehq032

Vicente-Manzanares, M., Ma, X., Adelstein, R. S., & Horwitz, A. R. (2009). Non-muscle myosin II takes centre stage in cell adhesion and migration. *Nature Reviews Molecular Cell Biology*, *10*(11), 778–790. https://doi.org/10.1038/nrm2786

Villalona, G. A., Udelsman, B., Duncan, D. R., McGillicuddy, E., Sawh-Martinez, R. F., Hibino, N., Painter, C., Mirensky, T., Erickson, B., Shinoka, T., & Breuer, C. K. (2010). Cell-seeding techniques in vascular tissue engineering. *Tissue Engineering - Part B: Reviews*, *16*(3), 341–350. https://doi.org/10.1089/ten.teb.2009.0527

Volz, K. S., Jacobs, A. H., Chen, H. I., Poduri, A., McKay, A. S., Riordan, D. P., Kofler, N., Kitajewski, J., Weissman, I., & Red-Horse, K. (2015). Pericytes are progenitors for coronary artery smooth muscle. *ELife*, *4*, 1–22. https://doi.org/10.7554/eLife.10036

Vono, R., Fuoco, C., Testa, S., Pirró, S., Maselli, D., McCollough, D. F., Sangalli, E., Pintus, G., Giordo, R., Finzi, G., Sessa, F., Cardani, R., Gotti, A., Losa, S., Cesareni, G., Rizzi, R., Bearzi, C., Cannata, S., Spinetti, G., … Madeddu, P. (2016). Activation of the pro-oxidant PKCβIIp66Shc Signaling pathway contributes to pericyte dysfunction in skeletal muscles of patients with diabetes with critical limb Ischemia. *Diabetes*, *65*(12), 3691–3704. https://doi.org/10.2337/db16-0248

Wagenseil, J. E., Ciliberto, C. H., Knutsen, R. H., Levy, M. A., Kovacs, A., & Mecham, R. P. (2009). Reduced vessel elasticity alters cardiovascular structure and function in newborn mice. *Circulation Research*, *104*(10), 1217–1224. https://doi.org/10.1161/CIRCRESAHA.108.192054

Wang, F., Li, Y., Shen, Y., Wang, A., Wang, S., & Xie, T. (2013). The functions and applications of RGD in tumor therapy and tissue engineering. *International Journal of Molecular Sciences*, *14*(7), 13447–13462. https://doi.org/10.3390/ijms140713447

Wang, N., Deng, Y., Liu, A., Shen, N., Wang, W., Du, X., Tang, Q., Li, S., Odeh, Z., Wu, T., & Lin, H. (2017). Novel Mechanism of the Pericyte-Myofibroblast Transition in Renal Interstitial Fibrosis: Core Fucosylation Regulation. *Scientific Reports*, *7*(1), 16914. https://doi.org/10.1038/s41598-017-17193-5

Wang, Y., Hu, J., Jiao, J., Liu, Z., Zhou, Z., Zhao, C., Chang, L., Chen, Y. E., Ma, P. X., & Yang, B. (2014). Engineering vascular tissue with functional smooth muscle cells derived from human iPS cells and nano fi brous scaffolds. *Biomaterials*, *35*(32), 8960–8969. https://doi.org/10.1016/j.biomaterials.2014.07.011

Wang, Z., Oron, E., Nelson, B., Razis, S., & Ivanova, N. (2012). Distinct lineage specification roles for NANOG, OCT4, and SOX2 in human embryonic stem cells. *Cell Stem Cell*, *10*(4), 440–454. https://doi.org/10.1016/j.stem.2012.02.016

Weiss, M. L., & Troyer, D. L. (2006). *Stem Cells in the Umbilical Cord*. *00*, 155–162.

Wells, R. G. (2008). *The Role of Matrix Stiffness in Regulating Cell Behavior*. 1394–1400.

https://doi.org/10.1002/hep.22193

Whang, M., & Kim, J. (2016). Synthetic hydrogels with stiffness gradients for durotaxis study and tissue engineering scaffolds. *Tissue Engineering and Regenerative Medicine*, *13*(2), 126–139. https://doi.org/10.1007/s13770-016-0026-x

Widowati, W., Laksmitawati, D., Sumitro, S., & Widodo, M. A. (2017). Interleukins and VEGF secretome of human wharton's Jelly mesenchymal stem cells-conditioned medium (hwjmscs-CM) in different passages and oxygen tensions. *Bioscience Research*, *November*.

Williams, J. K., & Heistad, D. D. (1996). Structure and function of vasa vasorum. *Trends in Cardiovascular Medicine*, *6*(2), 53–57. https://doi.org/10.1016/1050-1738(96)00008-4

Winkler, E. A., Bell, R. D., & Zlokovic, B. V. (2011). Central nervous system pericytes in health and disease. *Nat Neurosci*, *14*(11), 1398–1405. https://doi.org/10.1038/nn.2946

Witt, R. G., Raff, G., Gundy, J. Van, Rodgers-ohlau, M., & Si, M. (2013). Short-term experience of porcine small intestinal submucosa patches in paediatric cardiovascular surgery. *European Journal of Cardio-Thoracic Surgery*, *44*(January), 72–76. https://doi.org/10.1093/ejcts/ezs638

Wolner, E., Rieder, E., Kasimir, M.-T., Silberhumer, G., Seebacher, G., Wolner, E., Simon, P., & Weigel, G. (2004). Decellularization protocols of porcine heart valves differ importantly in efficiency of cell removal and susceptibility of the matrix to recellularization with human vascular cells. *The Journal of Thoracic and Cardiovascular Surgery*, *127*(2), 399–405. https://doi.org/10.1016/j.jtcvs.2003.06.017

Woo, J. S., Fishbein, M. C., & Reemtsen, B. (2016). Histologic examination of decellularized porcine intestinal submucosa extracellular matrix (CorMatrix) in pediatric congenital heart surgery. *Cardiovascular Pathology*, *25*(1), 12–17. https://doi.org/10.1016/j.carpath.2015.08.007

Wren, C., Birrell, G., & Hawthorne, G. (2003). Cardiovascular malformations in infants of diabetic mothers. *Heart (British Cardiac Society)*, *89*(10), 1217–1220. https://doi.org/10.1136/heart.89.10.1217

Wu, M., Rementer, C., & Giachelli, C. M. (2013). Vascular calcification: An update on

mechanisms and challenges in treatment. *Calcified Tissue International*, *93*(4), 365–373. https://doi.org/10.1007/s00223-013-9712-z

Wynne, B., Chiao, C., & Clinton Webb, R. (2009). Vascular smooth muscle cell signaling mechanisms for contraction to angiotensin II and endothelin-1. *Journal of the American Society of Hypertension*, *3*(2), 84–95. https://doi.org/10.1016/j.jash.2008.09.002.Vascular

Xie, C., Ouyang, L., Chen, J., Zhang, H., Luo, P., Wang, J., & Huang, H. (2019). The emerging role of mesenchymal stem cells in vascular calcification. *Stem Cells International*, *2019*(1). https://doi.org/10.1155/2019/2875189

Xie, L., Zeng, X., Hu, J., & Chen, Q. (2015). Characterization of Nestin, a Selective Marker for Bone Marrow Derived Mesenchymal Stem Cells. *Stem Cells International*, *2015*. https://doi.org/10.1155/2015/762098

Xin, X., Yang, S., Ingle, G., Zlot, C., Rangell, L., Kowalski, J., Schwall, R., Ferrara, N., & Gerritsen, M. E. (2001). Hepatocyte growth factor enhances vascular endothelial growth factor-induced angiogenesis in vitro and in vivo. *American Journal of Pathology*, *158*(3), 1111–1120. https://doi.org/10.1016/S0002-9440(10)64058-8

Xing, F., Li, L., Zhou, C., Long, C., Wu, L., Lei, H., Kong, Q., Fan, Y., Xiang, Z., & Zhang, X. (2019). Regulation and Directing Stem Cell Fate by Tissue Engineering Functional Microenvironments : Scaffold Physical and Chemical Cues. *Stem Cells International*.

Xu, J., & Shi, G. (2014). Vascular wall extracellular matrix proteins and vascular diseases. *BBA - Molecular Basis of Disease*, *1842*(11), 2106–2119. https://doi.org/10.1016/j.bbadis.2014.07.008

Yamazaki, T., & Mukouyama, Y. (2018). Tissue Specific Origin , Development , and Pathological Perspectives of Pericytes. *Frontiers in Cardiovascular Medicine*, *5*(June), 1–6. https://doi.org/10.3389/fcvm.2018.00078

Yamazaki, T., Nalbandian, A., Uchida, Y., Li, W., Arnold, T. D., Kubota, Y., Yamamoto, S., Ema, M., & Mukouyama, Y. (2017). TISSUE MYELOID PROGENITORS DIFFERENTIATE INTO PERICYTES THROUGH TGF-β SIGNALING IN DEVELOPING SKIN VASCULATURE. *Cell Reports*, *18*(12), 2991–3004.

https://doi.org/10.1016/j.celrep.2017.02.069

Yannarelli, G., Dayan, V., Pacienza, N., Lee, C.-J., Medin, J., & Keating, A. (2013). Human Umbilical Cord Perivascular Cells Exhibit Enhanced Cardiomyocyte Reprogramming and Cardiac Function after Experimental Acute Myocardial Infarction. *Cell Transplantation*, *22*(9), 1651–1666. https://doi.org/10.3727/096368912X657675

Yau, J. W., Teoh, H., & Verma, S. (2015). Endothelial cell control of thrombosis. *BMC Cardiovascular Disorders*, *15*, 130. https://doi.org/10.1186/s12872-015-0124-z

Yianni, V., & Sharpe, P. T. (2018). Molecular Programming of Perivascular Stem Cell Precursors. *Stem Cells (Dayton, Ohio)*, *36*(12), 1890–1904. https://doi.org/10.1002/stem.2895

Yoder, M. C. (2015). Differentiation of pluripotent stem cells into endothelial cells. *Current Opinion in Hematology*, *22*(3), 252–257. https://doi.org/10.1097/MOH.0000000000000140

Yoon, J. H., Roh, E. Y., Shin, S., Jung, N. H., Song, E. Y., Chang, J. Y., Kim, B. J., & Jeon, H. W. (2013). *Comparison of Explant-Derived and Enzymatic Digestion-Derived MSCs and the Growth Factors from Wharton ' s Jelly*. *2013*.

Zannettino, A. C. W., Paton, S., Arthur, A., Khor, F., Itescu, S., Gimble, J. M., & Gronthos, S. (2008). Multipotential human adipose-derived stromal stem cells exhibit a perivascular phenotype in vitro and in vivo. *Journal of Cellular Physiology*, *214*(2), 413–421. https://doi.org/10.1002/jcp.21210

Zhang, Y., Yu, Y., & Ozbolat, I. T. (2013). Direct bioprinting of vessel-like tubular microfluidic channels. *Journal of Nanotechnology in Engineering and Medicine*, *4*(2), 1–7. https://doi.org/10.1115/1.4024398

Zhao, J., Griffin, M., Cai, J., Li, S., Bulter, P. E. M., & Kalaskar, D. M. (2016). Bioreactors for tissue engineering: An update. *Biochemical Engineering Journal*, *109*, 268–281. https://doi.org/10.1016/j.bej.2016.01.018

Zilla, P., Deutsch, M., Bezuidenhout, D., Davies, N. H., & Pennel, T. (2020). Progressive Reinvention or Destination Lost ? Half a Century of Cardiovascular Tissue Engineering. *Frontiers in Cardiovascular Medicine*, *7*(September), 1–32.

https://doi.org/10.3389/fcvm.2020.00159

Zimmerman, M. S., Smith, A. G. C., Sable, C. A., Echko, M. M., Wilner, L. B., Olsen, H. E., Atalay, H. T., Awasthi, A., Bhutta, Z. A., Boucher, J. L. A., Castro, F., Cortesi, P. A., Dubey, M., Fischer, F., Hamidi, S., Hay, S. I., Hoang, C. L., Hugo-Hamman, C., Jenkins, K. J., … Kassebaum, N. J. (2020). Global, regional, and national burden of congenital heart disease, 1990–2017: a systematic analysis for the Global Burden of Disease Study 2017. *The Lancet Child and Adolescent Health*, *4*(3), 185–200. https://doi.org/10.1016/S2352-4642(19)30402-X

Appendix A: Flow Cytometry Fluorophore Spectrum and Novocyte Excitation Channels

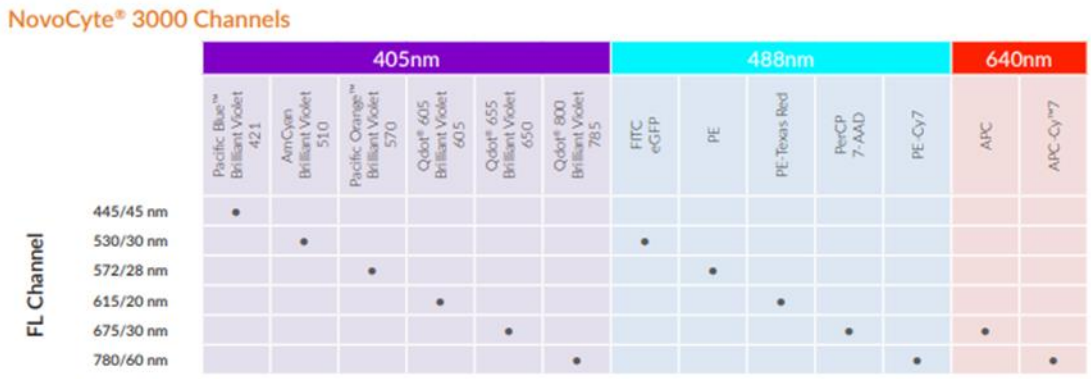

Excitation Wavelength = 488nm, Fluorophores FITC, PE, PE-Cy7, PerCP-Cy5.5

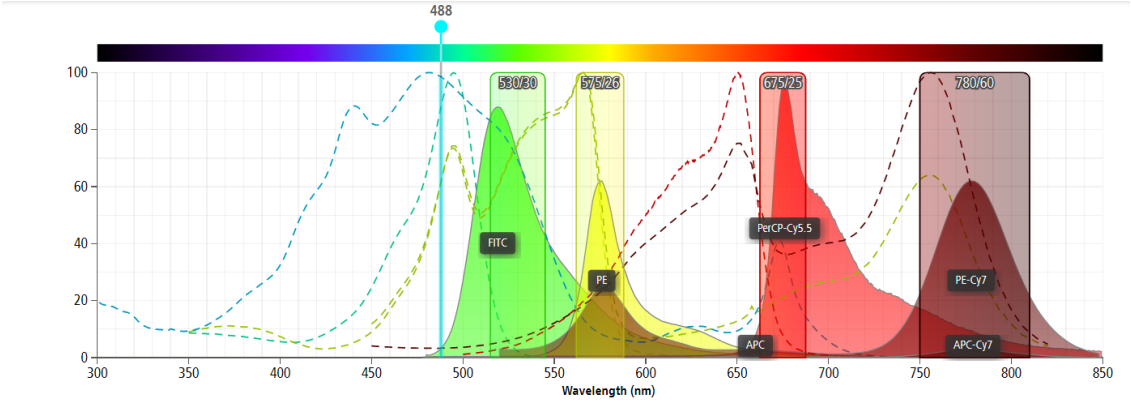

	Fluorochrome	%Max	Ex	Em	Filters	FITC	PE	PerCP...	PE-Cy7	APC	APC-C...
1	FITC	88.0	☑	☑	530/30	47.4%	0.4%	0.3%	1.8%	x	x
2	PE	61.6	☑	☑	575/26	10.6%	55.9%	0.3%	12.6%	x	x
3	PerCP-Cy5.5	98.4	☑	☑	675/25	x	1.9%	34.3%	1.2%	31.2%	3.0%
4	PE-Cy7	61.8	☑	☑	780/60	x	x	11.9%	60.5%	x	15.8%
5	APC	1.1	☑	☑	675/25	x	1.9%	34.3%	1.2%	31.2%	3.0%
6	APC-Cy7	3.3	☑	☑	780/60	x	x	11.9%	60.5%	x	77.6%

Excitation Wavelength = 640nm, Fluorophores APC, APC-Cy7

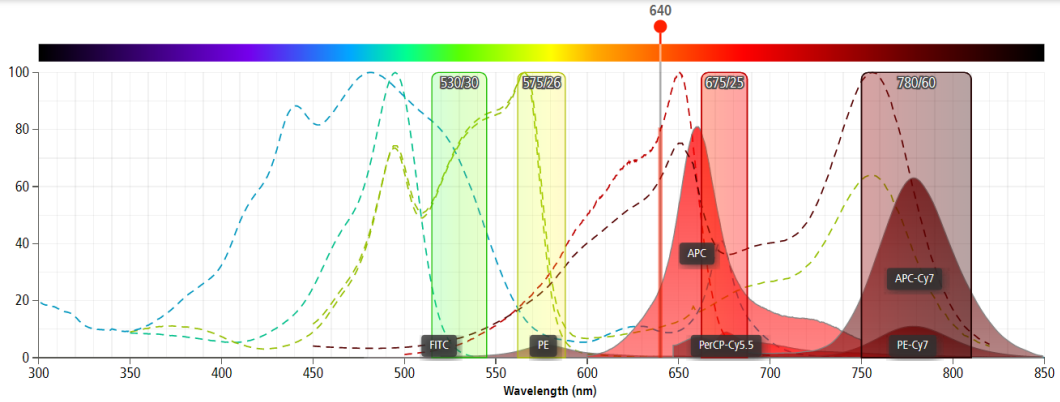

	Fluorochrome	%Max	Ex	Em	Filters	FITC	PE	PerCP...	PE-Cy7	APC	APC-C...
1	FITC	0.0	☑	☑	530/30	47.4%	0.4%	0.3%	1.8%	x	x
2	PE	0.4	☑	☑	575/26	10.6%	55.9%	0.3%	12.6%	x	x
3	PerCP-Cy5.5	9.2	☑	☑	675/25	x	1.9%	34.3%	1.2%	31.2%	3.0%
4	PE-Cy7	10.7	☑	☑	780/60	x	x	11.9%	60.5%	x	77.6%
5	APC	80.7	☑	☑	675/25	x	1.9%	34.3%	1.2%	31.2%	3.0%
6	APC-Cy7	62.9	☑	☑	780/60	x	x	11.9%	60.5%	x	77.6%

Appendix B: Full Vector Information

Vector Information

pLVX-Puro Vector Information

PT4002-5
Catalog No. 632164

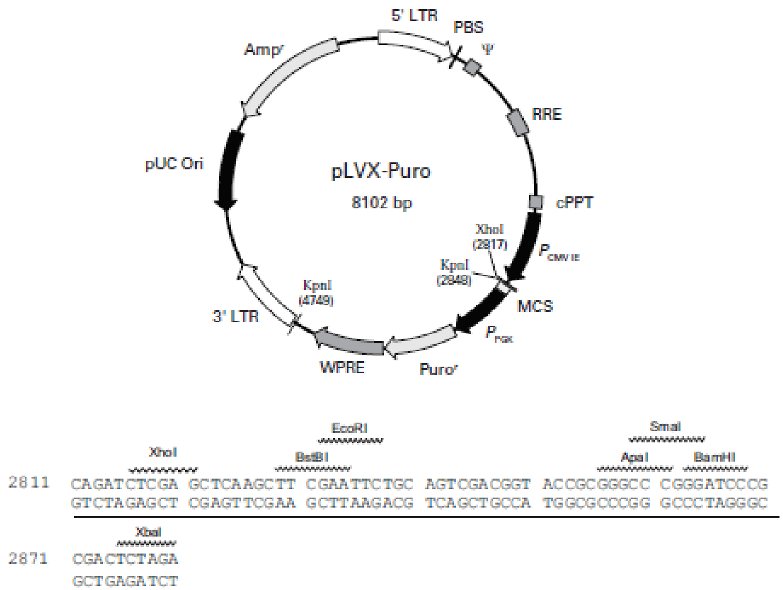

pLVX-Puro Vector Map and Multiple Cloning Site (MCS).

Description

pLVX-Puro is an HIV-1-based, lentiviral expression vector. Lentiviral particles derived from the vector allow you to express your gene of interest in virtually any cell type, even primary cells. Expression of your gene is driven by the constitutively active human cytomegalovirus immediate early promoter ($P_{CMV IE}$), located just upstream of the multiple cloning site (MCS), allowing constitutive, high level expression of your protein of interest.

pLVX-Puro contains all of the viral processing elements necessary for the production of replication-incompetent lentivirus, as well as elements to improve viral titer, transgene expression, and overall vector function. The woodchuck hepatitis virus posttranscriptional regulatory element (WPRE) promotes RNA processing events and enhances nuclear export of viral and transgene RNA (1), leading to increased viral titers from packaging cells, and enhanced expression of your gene of interest in target cells. In addition, the vector includes a Rev-response element (RRE), which further increases viral titers by enhancing the transport of unspliced viral RNA out of the nucleus (2). Finally, pLVX-Puro also contains a central polypurine tract (cPPT) element that increases nuclear importation of the viral genome during target cell infection, resulting in improved vector integration and more efficient transduction (3).

In addition to lentiviral elements, pLVX-Puro contains a puromycin resistance gene (Puro^r) under the control of the murine phosphoglycerate kinase (PGK) promoter (P_{PGK}) for the selection of stable transductants. The vector also contains a pUC origin of replication and an *E. coli* ampicillin resistance gene (Amp^r) for propagation and selection in bacteria.

(PR073568; published 01 July 2010)

Clontech

United States/Canada
800.662.2566
Asia Pacific
+1.650.919.7300
Europe
+33.(0)1.3904.6880
Japan
+81.(0)77.543.6116

Clontech Laboratories, Inc.
A Takara Bio Company
1290 Terra Bella Ave.
Mountain View, CA 94043
Technical Support (US)
E-mail: tech@clontech.com
www.clontech.com

Use

pLVX-Puro constitutively expresses your gene of interest from $P_{CMV\,IE}$ when transduced into target cells. Before the vector can be transduced into cells, however, it must be transfected into 293T packaging cells with our Lenti-X™ HTX Packaging System (Cat. Nos. 631247 and 631249). This packaging system allows you to safely produce high titer, infectious, replication-incompetent, VSV-G pseudotyped lentiviral particles that can infect a wide range of cell types, including non-dividing and primary cells (4).

Location of Features

- 5' LTR: 1–635
- PBS (primer binding site): 636–653
- Ψ (packaging signal): 685–822
- RRE (Rev-response element): 1303–1536
- cPPT (central polypurine tract): 2028–2151
- $P_{CMV\,IE}$ (human cytomegalovirus immediate early promoter): 2185–2788
- MCS (multiple cloning site): 2816–2880
- P_{PGK} (phosphoglycerate kinase promoter): 2882–3390
- Puro^r (puromycin resistance gene): 3411–4010
- WPRE (woodchuck hepatitis virus posttransctiptional regulatory element): 4024–4615
- 3' LTR: 4819–5455
- pUC origin of replication: 5925–6595 (complementary)
- Amp^r (ampicillin resistance gene (β-lactamase): 6740–7736 (complementary)

Selection of Stable Transfectants

- Selectable marker: plasmid confers resistance to puromycin.

Propagation in *E. coli*

- Suitable host strains: DH5α™ and other general purpose strains.
- Selectable marker: plasmid confers resistance to ampicillin (100 µg/ml) in *E. coli* hosts.
- *E. coli* replication origin: pUC
- Copy number: high

Notes:

The vector sequence was compiled from information in the sequence databases, published literature, and other sources, together with partial sequences obtained by Clontech. This vector has not been completely sequenced.

The viral supernatants produced by this lentiviral vector could contain potentially hazardous recombinant virus. Due caution must be exercised in the production and handling of recombinant lentivirus. Appropriate NIH, regional, and institutional guidelines apply.

References

1. Zufferey, R. *et al.* (1999) *J. Virol.* **73**(4):2886–2892.
2. Cochrane, A.W. *et al.* (1990) *Proc. Natl. Acad. Sci. USA* **87**(3):1198–1202.
3. Zennou, V. *et al.* (2000) *Cell* **101**(2):173–185.
4. Wu, X. *et al.* (2000) *Mol. Ther.* **2**(1):47–55.

Notice to Purchaser

Clontech products are to be used for research purposes only. They may not be used for any other purpose, including, but not limited to, use in drugs, *in vitro* diagnostic purposes, therapeutics, or in humans. Clontech products may not be transferred to third parties, resold, modified for resale, or used to manufacture commercial products or to provide a service to third parties without written approval of Clontech Laboratories, Inc.

Clontech has a license to sell products containing WPRE, under the terms described below. Any use of WPRE outside of Clontech's product or the product's intended use, requires a license as detailed below. Before using the product containing WPRE, please read the following license agreement. If you do not agree to be bound by its terms, contact Clontech within 10 days for authorization to return the unused product containing WPRE and to receive a full credit.
Patents: The WPRE technology is covered by one or more of the following U.S. Patents and corresponding patent claims outside the U.S.: 6,136,597; 6,284,469; 6,312,912; 6,287,814, issued to The Salk Institute for Biological Studies
Individual License Agreement: Clontech grants you a non-exclusive license to use the enclosed product containing WPRE in its entirety for its intended use. The product is being transferred to you in furtherance of, and reliance on, such license. Any use of WPRE outside of Clontech's product or the product's intended use, requires a license from the Salk Institute for Biological Studies.
Termination of License: This license agreement is effective until terminated. You may terminate it at any time by destroying all products containing WPRE in your control. It will also terminate automatically if you fail to comply with the terms and conditions of the license agreement. You shall, upon termination of the license agreement, destroy all products containing WPRE in your control, and so notify Clontech in writing. This License shall be governed in its interpretation and enforcement by the laws of the State of California.
Contact for WPRE Licensing: The Salk Institute for Biological Studies, 10010 North Torrey Pines Road, La Jolla, CA 92037, Attn.: Office of Technology Management, Phone: 858.453.4100 ext. 1275, Fax: 858.546.8093

This product and its use are the subject of U.S. Pat. No. 6,682,907 The purchase of this product conveys to the buyer the non-transferable right to use the purchased amount of the product and components of the product in research conducted by the buyer (whether the buyer is an academic or for-profit entity). The buyer cannot disclose information, sell or otherwise transfer this product, its components or materials made using this product or its components to a third party or otherwise use this product or its components or materials made using this product or its components for any commercial purposes. If the buyer is not willing to accept the limitations of this limited use statement, Clontech is willing to accept return of the product with a full refund. For information on purchasing a license to the DNA-Flap technology for purposes other than research, contact the Transfer of Technology Office, Institut Pasteur, 28 rue du Docteur Roux, 75 724 Paris Cedex 15 (www.pasteur.fr).

DH5α™ and DH10B™ are trademarks of Life Technologies Corporation.